NOTICE

The quality of this microfiche is heavily dependent upon the quality of the original thesis submitted for microfilming. Every effort has been made to ensure the highest quality of reproduction possible.

If pages are missing, contact the university which granted the degree.

Some pages may have indistinct print especially if the original pages were typed with a poor typewriter ribbon or if the university sent us a poor photocopy.

Previously copyrighted materials (journal articles, published tests, etc.) are not filmed.

Reproduction in full or in part of this film is governed by the Canadian Copyright Act, R.S.C. 1970, c. C-30. Please read the authorization forms which accompany this thesis.

THIS DISSERTATION
HAS BEEN MICROFILMED
EXACTLY AS RECEIVED

AVIS

La qualité de cette microfiche dépend grandement de la qualité de la thèse soumise au microfilmage. Nous avons tout fait pour assurer une qualité supérieure de reproduction.

S'il manque des pages, veuillez communiquer avec l'université qui a conféré le grade.

La qualité d'impression de certaines pages peut laisser à désirer, surtout si les pages originales ont été dactylographiées à l'aide d'un ruban usé ou si l'université nous a fait parvenir une photocopie de mauvaise qualité.

Les documents qui font déjà l'objet d'un droit d'auteur (articles de revue, examens publiés, etc.) ne sont pas microfilmés.

La reproduction, même partielle, de ce microfilm est soumise à la Loi canadienne sur le droit d'auteur, SRC 1970, c. C-30. Veuillez prendre connaissance des formules d'autorisation qui accompagnent cette thèse.

LA THÈSE A ÉTÉ
MICROFILMÉE TELLE QUE
NOUS L'AVONS REÇUE

IMAGE PROCESSING OF GEOLOGICAL DATA

by

Andrea Gabriele Fabbri

A thesis submitted to the School of Graduate Studies and Research in partial fulfillment of the requirements for the degree of Ph. D. in Geology

UNIVERSITY OF OTTAWA

OTTAWA, CANADA, 1981

to Finella

IMAGE PROCESSING OF GEOLOGICAL DATA

ABSTRACT

This thesis proposes to study geological maps and microscopic images of thin sections of rocks by methods of image processing. Such methods, which include pattern recognition and image analysis, are used for extracting information from two-dimensionally distributed data in computer form called pictures or images.

Although our visual system is well suited for qualitative interpretations of pictures, our innate ability to carry out quantitative measurements "at a glance" is extremely coarse. For a computer the situation is the opposite: accurate measurements and extensive computations are quite easily programmable while the identification of what to measure may be difficult or even impossible in the light of the present knowledge. For this reason, the so called "interactive methods" can be very succesful. The data processing is simply shared between the man and the computer, each doing what is easy.

In order to support the claim made that image processing and pattern recognition can be useful in geology, an

interactive package of Fortran programs was assembled which is called GIAPP, a geological image analysis program package for estimating geometrical probabilities. The package was developed particularly for geological applications in the areas of statistical mineral resources estimation, stereology, and image analysis by mathematical morphology.

When, in patterns systematically quantified from maps, we can identify conditions favourable to the occurrence of mineralizations (or other ancillary events) the geometric probabilities associated with these patterns can be combined with the probabilities associated with the distribution of mineral occurrences. This concept is our base for developing predictive models. Microscopic images of rock material can also be transformed into computer images and considered like micromaps which cover very small geological areas. Particular attention is given to the extraction and analysis of black and white, "binary", images because their quantitative characteristics involve geometrical properties of "objects" and relationships among objects which can be expressed as geometrical probabilities and can be easily measured by a computer.

The thesis spans three different aspects of geological image processing: the philosophical approach in geology, the programming of image processing software, and several practical applications of increasing complexity including

one pattern recognition experiment. The study is aimed at applications of the dimension and character of conventional real-life geological studies, and also at relatively large images of about one million picture elements.

A description is given of geological images, of their usage, of how to digitize images as line drawings, of a small computer dedicated to image processing, and of the software package GIAPP, which enables the geologist to perform both image digitization and processing entirely by himself. A review is made of the original studies of computer processing of binary images by electronic engineers in pattern recognition during the past twenty years. Simple examples of binary geological images are used to introduce concepts of parallel processing and processors, and mathematical morphology concepts for image analysis: i. e., logical operations between binary images and transformations of binary images by structuring elements. Those operations and transformations can be computed with a degree of parallellism on general purpose computers if the binary images are in a "compressed" state in which to every picture element only one "bit" of the computer word corresponds in order to store the black or the white color.

A case history application is made to the study of regional mineral resources in an area in Canada for which a set of large images in registration with one another is

used. Particular attention is given to map digitization, preprocessing of the digitized images, and extraction of environments related to uranium mineralization. Two thin sections of metamorphic rocks, a granulite and an amphibolite, are analyzed for quantitative characterization of the crystals by the study of their profiles, stereological properties, and for comparing the performance of an image analyzer dedicated instrument (a Quantimet 720) with that of the software programmed in GIAPP on a minicomputer. Finally an experiment is made of truly automatic processing, i. e., pattern recognition: the counting of alpha particle tracks from autoradiographs of radioactive minerals. This last application exemplifies how complex it is for a machine to "recognize" and count features which our visual system, the eyes and the brain, perceive "at a glance".

Many more problems are available in the geological domain which are particularly well suited for image processing, especially so when the data are characteristically obtained at discrete locations and can be represented in map form or in the form of a digitized photograph and other imagery. Throughout the thesis, the visual aspect is stressed by inserting many illustrations in harmony with the interactive nature of the methods used and also with the Chinese proverb: "A picture is worth a thousand words". The subject lies at the triple point of geology, computer

science, and geometric probability; the aim is to familiarize the geologist with the image processing approach by way of example. Reviews of related geological applications, a user's guide to interactive sessions of GIAPP's programs, and operational flowcharts are provided.

LE TRAITEMENT DES IMAGES DE DONNEES GEOLOGIQUES

RESUME

On se propose dans la présenté thèse de faire une étude de cartes géologiques et de microimages de minces sections de roches en faisant appel à des méthodes d'imagerie. De telles méthodes, dont la reconnaissance des formes et l'analyse des images, sont utilisées pour extraire de l'information de données à distribution bidimensionnelle sous forme informatique; autrement dit, elles servent à saisir de l'information contenue dans des images.

L'appareil oculaire de l'homme est extrêmement bien adaptée à l'interprétation qualitative des images mais sa capacité à l'évaluation quantitative rapide d'une image est très limitée. Pour l'ordinateur, l'inverse est vrai: il est facile de programmer un calculateur pour qu'il prenne des mesures précises et effectue de longs calculs mais la reconnaissance de l'object à mesurer est d'une extrême difficulté, voire impossible, dans l'état actuel des connaissances. Pour cette raison, les méthodes dites interactives peuvent donner des résultats fructueux. Le traitement des données est tout simplement partagé entre l'homme et

l'ordinateur, chacun accomplissant ce qui lui est le plus facile.

Pour montrer l'utilité du traitement des images et de la reconnaissance des formes en géologie, on a mis au point un ensemble de programmes interactifs en Fortran, le GIAPP, qui permet l'analyse des images géologiques et l'évaluation des probabilités géométriques. Le GIAPP est plus particulièrement adapté aux utilisations géologiques dans les domaines de l'évaluation statistique des ressources en minéraux, à la stéréologie et à l'analyse des images par morphologie mathématique.

Lorsque, dans de formations quantifiées systématiquement à partir de cartes, il est possible de reconnaître des conditions favorables à la présence de minéralisations (ou d'autres manifestations secondaires), on peut associer les probabilités géométriques de ces formations aux probabilités de la distribution des gisements de minéraux. Cette notion d'association de deux probabilités est à la base de nos modèles de prévision. Des microimages d'échantillons de roche peuvent aussi être transformées en images numériques et par la suite être interprétées comme des microcartes de régions géologiques très petites. Une attention particulière est donnée à l'extraction et à l'analyse des images "binaires" noir et blanc car leurs caractéristiques quantitatives mettent en jeu de propriétés géométriques des

"objects" est des relations entre ces objects qu'il est possible d'exprimer en termes de probabilités géométriques et de mesurer facilement au moyen d'un ordinateur.

La thèse porte sur trois aspects différents du traitement des images géologiques: l'approche philosophique de la géologie, la programmation du logiciel de traitement des images, et enfin plusieurs utilisations pratiques de complexité croissante pour la résolution de problèmes de géologie, notamment une expérience de reconnaissance des formes. L'étude a pour but de dégager des applications de la dimension et du caractère des études géologiques classiques et aussi du traitement d'images relativement grandes composées d'environ un million d'éléments d'image.

On donne une description des images géologiques, on précise leurs utilisations et on explique comment sont numérisées des images comme des dessins de trait. On décrit aussi le petit ordinateur spécialisé pour le traitement des images ainsi que le logiciel GIAPP permettant au géologue de faire entièrement lui-même la numérisation et le traitement des images. On livre ensuite un résumé des résultats des premières études de traitement par ordinateur d'images numériques faites par des ingénieurs électroniciens dans le domaine de la reconnaissance des formes au cours des vingt dernières années. Des exemples simples d'images géologiques binaries servent à présenter les notions de traitement

parallèle, les ordinateurs ainsi que les notions de morphologie mathématique de l'analyse des images, c'est-à-dire les notions des opérations logiques entre les images binaires et de transformation de ces images par éléments structurants. Ces opérations et méthodes de transformation peuvent être programmées avec un haut degré de parallélisme sur des ordinateurs polyvalents si les images binaires sont "comprimées", c'est-à-dire si à tout élément d'image ne correspond qu'un seul bit du mot ordinateur pour le stockage de l'information "blanc" ou "noir".

On applique les principes à l'étude des ressources régionales en minéraux d'une région du Canada por laquelle on utilise des grandes images liées les unes aux autres. On accorde une attention particulière à la numérisation des cartes, au prétraitement des images numérisées et à l'extraction de données environnmentales relatives à des minéralisations d'uranium. Deux minces sections de roches métamorphiques, une granulite et une amphibolite, sont analysées pour établir la caractérisation quantitative des cristaux par étude de leurs profils et de leurs propriétés stéréologiques et pour comparer la performance d'un appareil spécialisé d'analyse d'image (un Quantimet 720) à celle du logiciel GIAPP implanté sur mini-ordinateur. Enfin, on expérimente un traitement entièrement automatique, soit la reconnaissance des formes: le comptage des traces de

particules alpha à partir d'autoradiographies de minéraux radioactifs. Cette application illustre combien il est complexe pour une machine de "reconnaître" et de caractériser des phénomènes que l'oeil et le cerveau de l'homme perçoivent "d'un coup d'oeil".

De nombreux autres problèmes se posant en géologie sont particulièrement bien adaptés au traitement des images, notamment quand les données sont caractéristiquement obtenue à des endroits discrets et qu'elles se prêtent à une représentation sous forme de carte, de photographie numérisée ou d'image quelconque. Dans la thèse, on souligne l'aspect visuel de la méthode en donnant de nombreuses illustrations représentatives de sa nature interactive, fidèle au proverbe qui dit qu'une image vaut mille mots. Le sujet est à la triple croisée de la géologie, de l'informatique et de la probabilistique géométrique. Le but visé est de familiariser le géologue, au moyen d'exemples, avec le traitement des images. A ce titre, on trouve dans la thèse une revue des applications géologiques connexes, une guide de l'utilisateur aux programmes interactifs GIAPP ainsi que des organigrammes opérationnels.

TABLE OF CONTENTS

LIST OF TABLES

LIST OF ILLUSTRATIONS

ACKNOWLEDGEMENTS

This work would not have been possible without the support of the Geological Survey of Canada (G.S.C.) my employer, and the assistance provided by the Electrical Engineering Division of the National Research Council of Canada (N.R.C.) where I have spent ~~four~~ years as "guest worker".

Many people have aided my efforts on this thesis. Foremost, Dr. Ralph Kretz and Dr. Frits P. Agterberg, my supervisors at the University of Ottawa, whose guidance is gratefully acknowledged. Also to be thanked are Dr. Tonis Kasvand and the staff of the Computer Graphics Section, Electrical Engineering Division of N.R.C., who provided facilities and means to this end. Special thanks are extended to Dr. William Petruk, Canada Centre for Mineral and Energy Technology, CANMET, who has provided useful suggestions and insight for several stereological applications.

1. Introduction

1.1 Geological questions as statistical problems

In the natural sciences the student is confronted with a real world of phenomena which frequently may seem continuous in time and physical properties. His task is to get familiar with them, by collecting observations over an area, a volume, or a time interval. The planning of these observations may be random at first, or can follow guidelines from previous knowledge which also may have been acquired by others, elsewhere. With the accumulation of observations, systematic patterns of similar observations that seem to correspond to phenomena observed in different places, provide the tools for organizing the collection of observations in comprehensible and reusable descriptions.

Because no natural phenomenon can be described entirely, its classification and the measurement of its properties is seldom a clearly definable task. In general the student resorts to assigning a certain degree of trust to each observation, and by comparing several observations with each other, he is likely to increase his confidence about phenomena occurring at smaller scales. In this process the student slowly progresses from elementary observations,

through intuition and cumulating knowledge to statistical statements. These statements represent part of the properties of the phenomena studied and must be viewed in terms of the sampling schemes employed.

In time some geological questions have been formulated in terms of mathematical models to which statistical tests could be applied. Many problems have become equally geological and statistical, and a new discipline termed "mathematical geology" was established about 15 years ago. However, several fundamental statistical questions in geology are older than that, as became apparent in the work of the mineralogist M. A. Delesse who, as early as 1848, indicated that the relative volumes of minerals in rocks could be measured from random sections. A recent overview of statistical applications and of their historical development in the study of spatial patterns in the earth sciences was made by Agterberg (1978), and Merriam (1981).

Modal analysis, quantitative stratigraphic correlation, analysis of vectorial data, trend analysis, statistical simulation, numerical classification, and mathematical morphology are just some of the subjects that have become integral parts of geology, as the compass and the field notes, in almost any geological specialty, whenever practical applications are required. The approach followed in this study is proposing that pattern-recognition techniques may

represent a powerful tool in many geological applications in which spatial patterns play an important role.

1.2 Bringing the image into the picture: image analysis and pattern recognition of geological maps

A great number of geological studies cover an area of given dimensions which can be sampled at different levels of detail. Time and financial constraints as well as other logistic limitations, tend to delimit drastically the level of detail of any study. For this reason the statistical impact of a study will be limited by the scale which has been chosen. Given the scale and the consequent sampling intervals, the geological observations can be represented in map form, where the different map units subdivide all representable features and portray their spatial attributes such as dimension, distribution and orientation, and also the interrelationship between the various features. Frequently, not all available types of observations can be represented on one single map, and several maps covering the same area have to be prepared. Different themes are developed for special purposes, such as lithology, structures, economic geology or geophysics, geochemistry, and engineering geology.

Each map unit has its set of properties, some of which can be important for describing particular geological aspects. It then becomes important to be able to capture these properties in a systematic manner, so that computations can be made easily for statistical estimates of the attributes of the map units.

Geological maps contain a great amount of information: in general not all the information stored in a map is used in most geological studies, but a selection is made of the relevant features to consider. Seldom is this selection systematic or dictated by quantitatively strict criteria. The methods employed in this study form an attempt to bring geological images "into the picture", therefore extending computations and interpretations to the geometrical attributes of geological representations.

Geological maps can be transformed into computer images for picture processing. Their attributes can be measured automatically, and from such measures it is possible to recognize patterns of relationships which may contribute to explain geological phenomena in quantitative terms.

Microscopic images of rock material also can be transformed into computer images and considered as micromaps which cover small geological areas.

1.3 Digitization and computer processing

Picture or image processing, pattern recognition, scene analysis are some of the names used to describe methods of extracting information from, usually, two-dimensionally distributed data. Normally such data are termed pictures or images. Our own visual system, the eyes and the brain, is extremely well suited for qualitative interpretations of pictures. Our innate ability to carry out quantitative measurements "at a glance", however, is extremely coarse. For a computer the situation is the opposite: accurate measurements and extensive computations are easily programmable whereas the identification of what to measure may be difficult or even impossible to program in the light of the present knowhow. For this reason, the so called "interactive methods" can be successful. The data processing load is simply shared between the man and the computer, each doing what is "easiest".

The number and variety of computerized picture processing methods is large, so large that only the relevant approaches have been summarized briefly in a recent volume on the subject by Rosenfeld and Kak (1976). Typically in image processing, the entire image is processed for the information rather than only applying statistical estimation tech-

niques to the image of a sample.

Pictures can be analyzed by computers only in digitized form: the computer memory stores the digital representation of pictures in the form of arrays of numbers, in which for each two-dimensional address a grey level or density value is associated which is in point-to-point correspondence with small areas on the original picture material. These arrays are the data sets on which programmed algorithms compute measures of the different parameters which describe the patterns contained in the picture. A description of a picture involves properties of the picture or of its parts, and relationships among the parts. Geometrical properties, for example, do not depend on the picture grey levels, but only on the sets of picture points that belong to given picture parts.

The digitization of picture data can be accomplished in several ways. Two usual methods are: (a) scanning by optical or mechanical devices, or (b) digitizing of contours by x-y digitizers. In this study, both techniques are applied. A flying spot scanner was used for 35 mm transparencies of black and white tracings of map unit boundaries, and an image analyzer was used to study black and white transparencies of maps; a graphic tablet was employed for digitizing boundaries of crystal grains from the tracings of rock textures and boundaries from map patterns.

Computer processing is accomplished with a program package developed in FORTRAN after a model interactive image processing system programmed by Dr. T. Kasvand at the Electrical Engineering Division of the National Research Council of Canada. The system designed especially for the analysis of geological images was termed GIAPP : Geological Image Analysis Program Package for estimating geometrical probabilities. The system is intended for a general purpose computer with a FORTRAN processor, in order to facilitate the usage of image-processing techniques by geologists to study map or microscopic images in terms of their geometrical attributes which can be estimated statistically. For this reason methods of mathematical morphology, geometrical probability, and image processing have been considered in the design.

The package consists of: file handling, interactive conversation, picture display, image digitization, and editing routines, in addition to algorithms for measuring parameters of images by many methods from different fields.

1.4 Statement of purpose of the study

This dissertation project was initiated in order to provide geologists with techniques for the analysis of

geological maps which capture the geometrical configuration of features and offer the choice of differing sampling schemes according to model requirements. These techniques are: (a) based on the quantification of images by a software-dependent flying spot scanner which allows control of raster geometrical configuration, and also on the usage of a graphic tablet, and (b) fully relying on computer programming for the analysis of image data interactively.

Computer algorithms have been developed which are on line with techniques and statistical methods developed in several different disciplines. This was done in order to make the software more general and flexible because the fields considered overlap to a great extent as to the type of problems being studied but not as to the methods applied.

Many instruments at present are available for image analysis. Generally they are built according to a modular concept, and have consisted until recently mostly of hardware. They are expensive, and their acquisition and usage can be justified only with production work. It is likely that soon, with the increased availability of cheaper computer memory and microprocessors, the manufacturers will add programmable computers to these instruments making it possible to use more complex and satisfactory image-processing methods than what is done at present. For research study, where experiments are performed only on

limited numbers of images ,however, computer processing, even with a medium-size or a small computer, offers more flexibility of approach and lighter capital costs. This is so if an available computer is used and the software is provided. For this reason an interactive image-processing computer package was programmed for the analysis of geological images. The package duplicates in part what those instruments can do, and in part it expands their capabilities. The logic followed by the various algorithms in the package is documented fully and it complies with the statistical theories developed in mathematical morphology for texture analysis. In addition the package contains several picture processing algorithms which expand the theory and applications of textural studies.

Much geological sampling of microscopic and macroscopic images may be bound by rigid preset schemes, as for example point counting for modal analysis or for map data quantification. The measurements made in this manner are in general time consuming and seldom is repeated sampling made possible. The scope of this study is to input images into computers in order to make more satisfactory measurements on them. The problem of both improving and accelerating input preparation, for example for images which are directly produced by a microscope, is complex and essentially material dependent: this is not considered in this study. Method

development through computer programming is the basic target of the study, which is related directly to important geological applications. The applications undertaken have been chosen because they are different in type, therefore they emphasize the adaptive character of the software development and the applicability of methods of image analysis which have broader application outside the purely geological domain.

The geological applications considered here are as follows: geometrical probabilities associated to geological and geophysical maps, textures in drafts from thin sections of metamorphic rocks, feature extraction from micrographs of alpha tracks, and extension of theory and applications on general texture problems. In general the results of these approaches will be in the form of images which can be displayed graphically in order to aid both communication and understanding of the various steps in computer processing.

2. Digitization and processing of images

2.1 Introduction

Digital images are best processed by computers interactively. Interactive processing is done in steps in which an image is transformed and then displayed in order to allow the operator to decide which further transformations may be required. The processing is essentially picture dependent, and human interaction is needed until enough is known about a picture that an automatic pattern recognition process can be designed. In general a picture is digitized first, then it undergoes various types of preprocessing transformations for image enhancement and feature extraction. Finally the picture is processed for recognition and classification.

This chapter describes briefly the computer equipment used for digitization, processing and display of image data.

2.2 A computer system dedicated to interactive image processing

In the development of the techniques for this project,

the electronic equipment used is a computer system intended for general research in image processing. The system forms part of the Computer Graphics Laboratory of the Electrical Engineering Division of The National Research Council of Canada in Ottawa. The electronic equipment in the laboratory can be classified broadly into the following five classes: (1) computer and peripherals, (2) interactive devices, (3) display devices, (4) digitization devices, and (5) recording devices. In this broad classification, however, we must keep in mind that the instruments grouped under one class may perform the roles of some other classes.

2.2.1 Computer and peripherals

A small general purpose computer, Modcomp II, with a read/write memory of 64 K (thousand) 16 bit words, two one million words disks and two 800 bpi (bits per inch) tape drives , was used for processing images. The peripheral I/O (input/output) devices consist of: a card reader, a Versatec dot matrix printer, a teletype, an on-line random addressable flying spot scanner, a memory type Tektronix 611 CRT (cathod ray tube) with a special operator console, and a Summagraphics graphic tablet digitizer. The computer and the peripherals are diagrammatically shown in Figure 2.1.

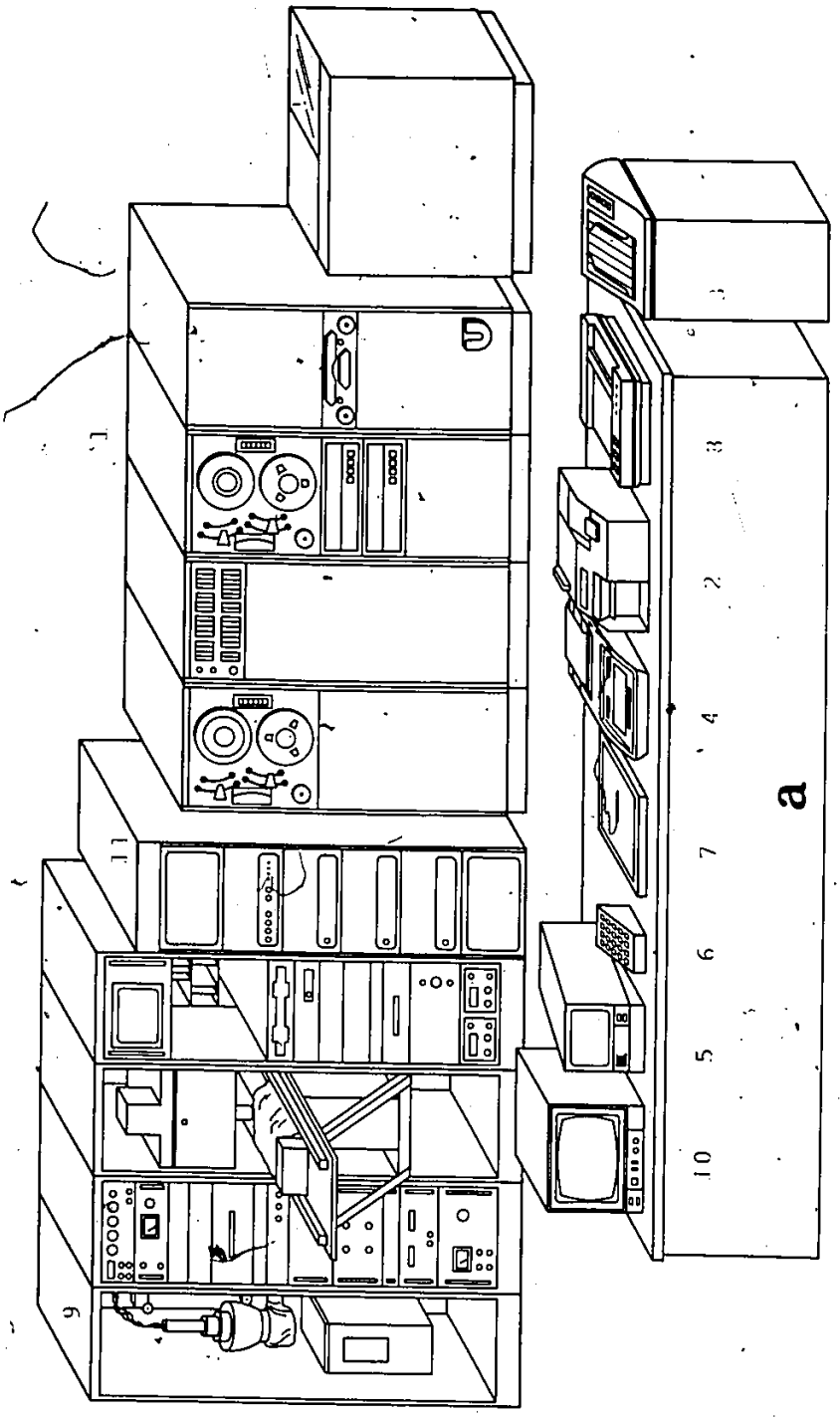

1. Modcomp II computer; 2. Card reader; 3. Versatec dot matrix printer; 4. Teletype; 5. Memory type Tektronix 611 CRT, with 6. Special operator console; 7. Summagraphics graphic tablet digitizer; 8. X-Y plotter; 9. Online. random addressable flying spot scanner; 10. Conrac color CRT, connected to 11. Norpak image buffer.

Figure 2.1: The Modcomp II computer and the peripheral equipment dedicated to general purpose image processing at the Computer Graphics Laboratory (a) and the interconnections of the various devices (b).

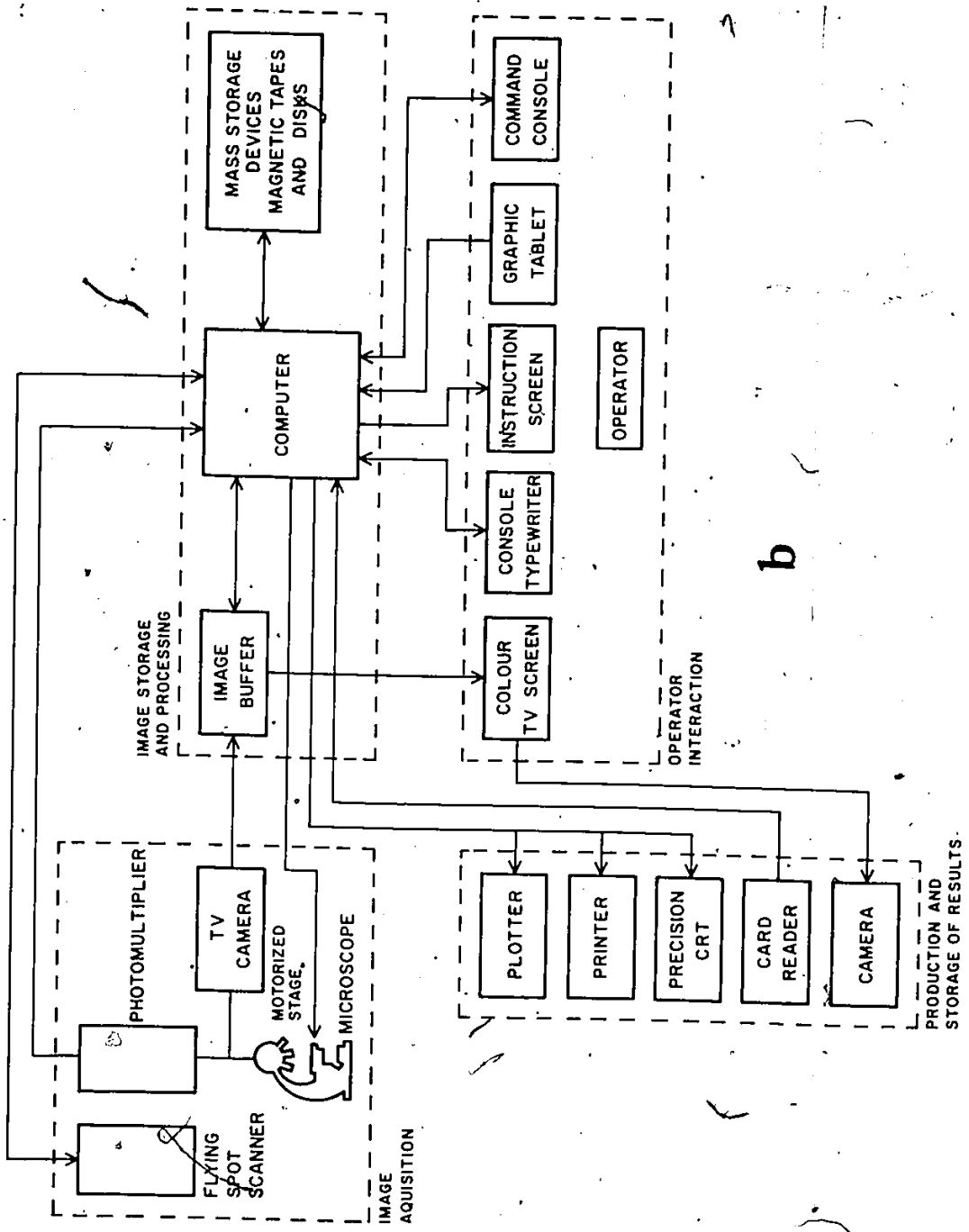

Figure 2.1: Concluded.

2.2.2 Interaction devices

The interaction equipment consists of a teletype and a special operator console connected to the Tektronix 611. The operator console is a pushbutton board consisting of 18 pushbuttons with indicator lights, six potentiometers with indicator lights for analog signal input and six additional indicator lights for general purposes. The illumination level of the console light is controlled entirely via FORTRAN callable routines.

2.2.3 Display devices

The display equipment consists of the Tektronix 611 memory type CRT which allows the display of four grey levels for an array of 4096 x 4096 points, a Versatec dot matrix printer/plotter for black and white only, for an array of 1024 x 746 dots per 8.5 x 11 inches per page, and a Conrac color television which displays arrays of 640 x 512 points.

2.2.4 Digitization devices

The digitization equipment consists of an on-line random addressable flying spot scanner, manufactured by Litton Co., for 35 mm transparencies, which has a resolution of 4096 x 4096 addressable positions over an area of 25 x 25 mm; and of a Summagraphics graphic tablet with a resolution of 1500 x 1500 positions over an area of approximately 14 x 14 inches. FORTRAN callable routines allow to control both digitizers.

Essentially a flying spot scanner, which can be used for both input and output of pictorial data, is a CRT which allows acces to any point in a two-dimensional data plane. It has 64 levels of light intensity at each point and can handle a maximum matrix size of 4096 x 4096 points. Input comes from a transparent film and output can be obtained using a standard camera. Since the flying spot scanner is just about at computer speed, it can be used as a random access memory.

On the graphic tablet lines can be traced manually by using a specialized stylus. The tablet and the stylus system is connected to the computer which receives and stores the x-y coordinates of the stylus while the operator traces the lines on the tablet.

2.2.5 Recording devices

The recording equipment used for picture data consists of two magnetic tape drives (many pictures are stored serially and in bulk), two disk drives (scratch, few pictures can be stored both in parallel or serially), and of course of the various display units. In the computer memory only part of one or more images can be stored for truly random access. Also a special memory was added to the system: it is called image buffer or frame buffer and can store an entire colour picture of 640 x 512 pixels, for random access. This buffer was built by Norpak Ltd. in Ottawa.

2.3 Methods of digitization of images

The quantification of two-dimensional images can be accomplished by digitization, which generally is termed quantization. It consists of a procedure for assigning to raster points of given coordinates numerical values proportional to the "grey level" (optical density, transmittance, reflectance, etc.) of the unit element of observation. In digital processing the picture samples must be quantized: thus the range of values in the samples must be divided into intervals and all the values within an interval must be represented by a single level. Generally the samples are

obtained by using an array of points.

Optical digitization is generally made by a variety of instruments termed scanners (microdensitometers, flying spot scanners, image analyzers) which break the image into a large number of raster units, each representing the tone or density in the immediate neighborhood of a point in a regular geometric array. In practice this array (pixel configuration in the structure of image data) is termed a raster and is either square or hexagonal.

A square raster as shown in Figure 2.2a is obtained by spacing the pixels so that they occupy the corners of a regular square grid. The unit distance between adjacent pixels in the direction of the grid is 1, whereas in the diagonal directions is $\sqrt{2}$. In the hexagonal raster, shown in Figure 2.2b, the pixels occupy the corners of a network of equilateral triangles. The unit distance between adjacent pixels is always 1; it can be measured along the three directions of the network. In this configuration the

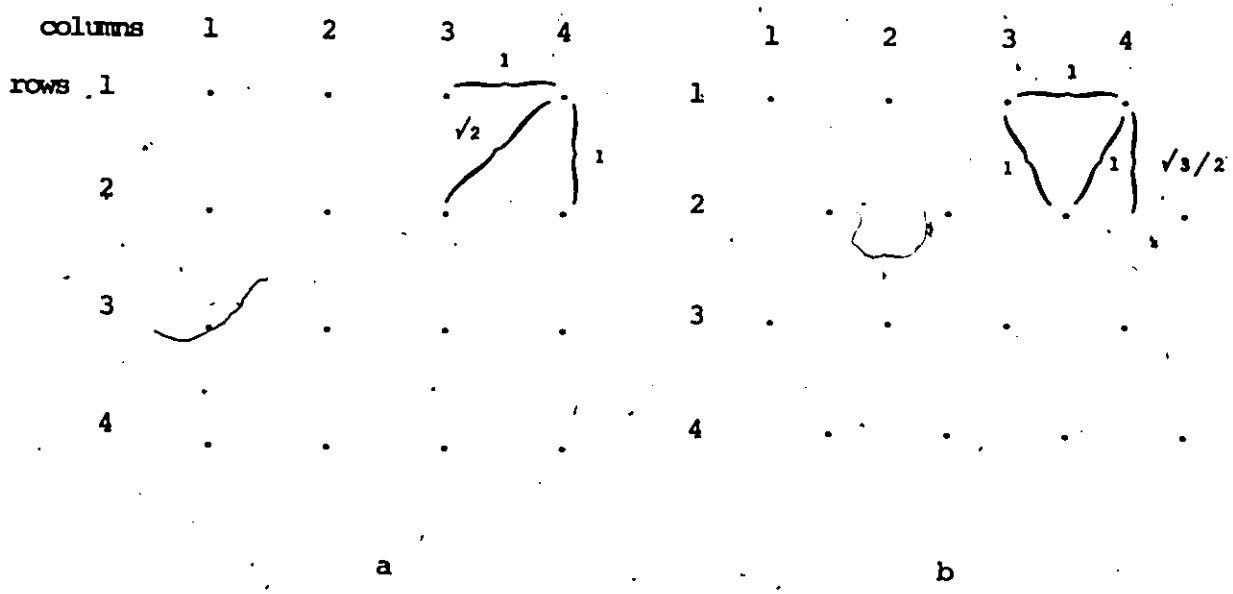

Figure 2.2: Diagrammatic structure of square (a) and hexagonal (b) raster configuration of pixels.

distance between adjacent rows is $\sqrt{3} / 2$.

If the raster is regular, it is not necessary to record geometrical addresses because they are implicit in the position of each observation in the series. Tone or density (grey level) of each raster point must be expressed as one of a list of limited number of digital characters. For black and white material it is sufficient that each observation shows only that the point was in the black and not in the white, i.e. in the binary 1 and not in the 0. For more complex structures, a separate character is required for each of the grey levels. If these are not uniformly spaced in the available tone range, several extra characters will be required. Such multiple level record will be treated as the source of several binary images, each representing one of the "phases" to be measured. Phase is here intended to be the set of points which includes all particles of a single type (here grey-level range, i.e. colour). This concept is important because it allows the analysis of complex structures to be treated as a set of binary problems. This treatment allows a computer equipped with Boolean operators to process an image at a faster rate than when each image point is processed as a numerical character.

A flying spot scanner is a fairly sophisticated expensive piece of equipment which allows raster scanning. However, there are many alternative instruments. The drum scanner

and the flat-bed scanner are two widely used raster input devices as alternative to the flying spot scanner. In the drum scanner a picture is mounted on a cylinder which spins on its axis. In the flat bed scanner a picture is mounted on a flat moving platform. A beam of light is reflected off or transmitted through the surface of the picture into a photocell.

2.4 Methods of image processing

Computer methods for image processing in general assume that the data to be processed have a particular arrangement. To clarify this concept it may be useful to consider image processing as opposite to computer graphics. According to the standard practice, image processing refers to operations that transform images into other images in order to obtain information about them and about the objects in them; image recognition is the mapping of images into non image description. Because problems are picture dependent, we do not know in advance what question to ask the computer about the picture, or which measurements to make. Images are stored and accessed directly as large matrices of values and the computer programs do not understand the images nor their parts. It is often said in image processing that images are

stored explicitly.

Different from both of these is computer graphics which is concerned primarily with computer synthesis and manipulation of images that are specified by descriptions. The various fundamental parts or objects belonging to the images must be known beforehand. A carefully designed and efficient data-base system is needed to manipulate pictures. Images are stored implicitly, i.e. synthesized into particular descriptions understood by the computer programs. The information, therefore, is coded and sparse. The amount of memory used is generally low, but the data must be arranged so that the needed information can be found without much searching and computation. Some fundamental parts of computer graphics information or data bases are coded as edges, polygons and various pointers to these, generally structured in particular sequences, in order to be most efficient for well-defined purposes.

In general picture processing or image processing is employed for the following reasons which also constitute the basic historical requirements for it: (a) picture digitization and coding, (b) picture enhancement and restoration, and (c) picture segmentation and description or pattern recognition. For these purposes pictures are stored as regular arrays or matrices of values each corresponding to an individual picture element or pixel which in turn is in

point-to-point correspondence with a point or better with a small area in the input material. Because usually these arrays can be large, e.g. 1000x1000 = 1 million pixels, images are stored into magnetic tapes or disks, rather than directly in the computer memory .

In the present system the picture data are represented as matrices of integer or one bit binary numbers of up to 1024x1024 elements. These are stored row by row in a sequential manner. Each row of picture data represents one logical record.

Grey-level pictures are digitized so that each computer word stores the grey-level value (generally an integer number) at a given position. A binary picture has only two values of grey level, 0 or 1, which can be considered as black and white respectively. Binary, 0-1 data , are compressed so that to each 0-1 pixel, there corresponds an "OFF"-"ON" bit status. This is done in order to economize in memory storage and to expedite I/O and some types of computations as we will see later.

Picture processing by a general purpose timeshared computer can produce satisfactorily the desired results with a relatively modest programming effort. Such computers generally are available everywhere, but the processing is bound to take considerable amounts of computer time. The general-purpose computer is thus ideal as a research tool, but not

adequate for routine production of results.

In processing of binary images, one word in the computer now can contain many picture elements, and in a modern computer all the bits within a computer word are processed in parallel when at least (Boolean) logical operations are involved; a degree of parallellism is obtained which is proportional to the word length within the computer. Thus certain binary operations can be speeded up considerably.

A variety of special "hard-wired" image processing devices has been on the market for some time (Hougardy, 1975). These devices, generally termed "image analyzers" are fast but the operation repertoire is very limited. Due to increased importance of picture processing, "pipe-lined" and "parallel" processing computers are becoming available which also can be programmed in a manner analogous to the ordinary general-purpose computers (Preston et al., 1979). Such computers, however, are expensive.

The approach followed in this thesis is directed towards a poor-man's solution in a time shared computer: a usual situation in which we are paying in computing time and not in hardware. The rich-man's solution is a special-purpose computer. This is now a problem at which the image processing community is active. Soon special image processing "chips" will be available (integrated circuits) which will be working in a so-called "pipeline fashion" at

approximately television speeds. It seems likely that geology as well as other disciplines such as remote sensing or signal processing, will take increasingly more advantage of the progress in image processing technology.

2.5 Techniques for the display of image data

Many aspects of picture processing are clearly related to the perception of pictures by humans. The results of the transformations computed can in general be appreciated best in pictorial form as displays obtainable on various display devices. On a television screen we can have a refreshed type of display: the image can be stored on a so-called image buffer or frame buffer, and then displayed continuously with many different grey levels and also colours. We can use a memory type CRT device, y levels and also colors. We can use a memory type CRT device, where the storage of the image occurs on the phosphorous surface: here only 3 or 4 grey levels can be displayed for each single dot.

Displays can be done on paper by using various types of printers. When using a line printer, characters can be overprinted to obtain a few different grey levels. Much more powerful types of printers are the plotters and the dot printers. Plotters, either drum or flat bed plotters, have

the capability of several color ribbons. Different picture parts can be represented by contours, graphic patterns, various characters or drafted symbols. In dot printers each picture point can be represented by a square matrix of dots. For example a 3x3 matrix could be used, and by deleting dots, 10 different grey level effects are obtained from a single color of dots, generally black. Recently colors became a possibility in ink jet plotters, where three guns fire droplets of fast drying ink of the three basic colours (yellow, magenta and cyan) onto a special absorbing paper. The colours are overprinted during three passes, and the end results are pictures of different colours and intensities, similar to what is done in a color television.

2.6 Limitations in multiuser interactive processing

Many display devices can be available on a dedicated computer system, like the one used here. When only a graphic terminal is available, and this is connected to a time shared computer, some limitations must be considered for display and interaction. The graphic terminal screen and its keyboard have to be used in turn for both the interaction and the display of pictures. It becomes necessary, however, to use a permanent recording device such as a

camera or better a printer or hard copy unit which, whenever needed, will photographically copy what is displayed on the screen for documentation of the processing results and the sequence of the various computational steps.

The usage of magnetic tapes may not be permitted in an interactive time shared environment with many users, therefore only disk space may be available. Finally, because the memory space allowed in interactive mode is more limited than in batch mode, programs will have to be taylored to the allowed memory, i.e. structured for minimum space requirements into overlays or into segments. Running speeds also will have to be minimal. Particularly, a relatively fast rate of transmission for the line connecting the graphic terminal to the computer is to be preferred for the display of images, e.g. 4800 or 9600 bauds (characters per second). Failure to obtain these speeds, will limit the efficiency of picture display in the multiuser interactive environment.

3. GIAPP: Geological Image Analysis Program Package

3.1 Introduction

An interactive system of FORTRAN programs termed Geological Image Analysis Program Package, GIAPP in short form, has been designed as part of multidisciplinary efforts in the fields of pattern recognition and mathematical geology. Several methods of picture processing, mathematical morphology and stereology have been brought together in programming the package. As a tool for the study of geological images it is adaptable being written in FORTRAN with few machine-dependent routines. A version of the package which was adapted to a multiuser environment, uses only a Tektronix graphic terminal for picture display and interactive commands and messages. In essence, GIAPP offers the possibility to do image processing without having to use an image analyzer.

GIAPP was programmed for the following reasons: (a) to handle images of maps or micrographs as matrices of numbers for computation, (b) to quantify all the information that they contain, (c) to describe the morphology of each map unit or microscopic phase, (d) to study the spatial rela-

tionships between map units, and (e) to provide automatically inputs to multivariate analysis.

3.2 Summary of the capabilities of the package

The present capabilities of GIAPP are summarized in Table 3.1. Some of the terminology in the table was taken after Rosenfeld and Kak (1976) who provided a comprehensive overview of digital image processing. The programs have been developed first on a small computer dedicated to general image processing: a Modcomp II computer with 64 decimal K's of memory of 16 bit words, two tape drives and two disks. Initially the computer was interfaced with a flying spot scanner, a Tektronix 611 video display unit, a Versatec dot matrix printer, a card reader and a graphic tablet digitizer. Later a Norpak image buffer and a Conrac colour television were added to the system. Part of the package has been converted to a CDC Cyber 74 computer which allows 70 octal K's of memory of 60 bit words for interactive processing and the access to several disks. In this second version a Tektronix 4014/1 video graphic terminal and a hard copy unit connected to it are the only communication and display devices available.

TABLE 3.1

General description of the capabilities of GIAPP

GENERAL FEATURES	PROCESSING OF NON-COMPRESSED IMAGES	PROCESSING OF BINARY COMPRESSED IMAGES
-file searching, copying, erasing and reviewing -expansion and compression of binary data -handling of commentaries added to image data sets by each processing routine -processing of binary, labeled and grey level images for both square and hexagonal rasters -output of image data on magnetic tape of data transfer -creation of binary compressed images of boundaries from a graphic tablet -scanning by means of a flying spot scanner	-smoothing, filtering, thresholding and graphical displays -component labeling of binary images -line thinning -phase labeling -junction detection -extraction of binary data from labeled images -digital displays -other special purpose algorithms -false color displays	-logical operations on or between binary images -Minkowski operations by means of programmable structuring elements of any shape -two-dimensional auto- and cross-correlations -point and vector displays of binary images -editing of binary images -creation of binary images from data on cards or computed from interactive commands (masks, grids, tests)

3.3 Data management

GIAPP was designed to make maximum use of a limited computer memory: a read/write memory of 32 decimal K to 64 K words of 16 bits. On the Modcomp II computer 12 K's of memory are used by the operating system. The remaining 52 K's of memory are reserved for: (1) the controlling part of the program (here called "Supermaster"), (2) the integer and the real common areas, (3) one group of programs coveniently grouped into an overlay (here called "Master") and finally a scratch area. Parts (3) and (4) of the memory are occupied in turns by each particular overlay or Master during an interactive session.

Initially the programs are stored on a magnetic tape and have to be transferred to disk before each run. Upon starting, a system of overlays is entered from which there is no exit until the processing work is completed or it is manually interrupted by activating an external interrupt switch button. Each overlay is accessed and exited interactively by teletype commands. Optionally the controlling commands can be issued by means of computer cards which are read by the card reader. The generalized program structure is shown in figure 3.1.

Figure 3.1: The program structure of GIAPP. [1] :SENSW(1,0) is a function which uses a machine dependent routine which activates external control by the first of eight switch buttons on the CPU of the Modcomp II computer. [2] : "cool start" is an automatic procedure to read some information from, and to account for all image files (data sets) on the two magnetic tapes, to prepare the three disk partitions for images and to read both integer and floating point defaults from cards. [3] : The default values can later be changed before calling other programs.

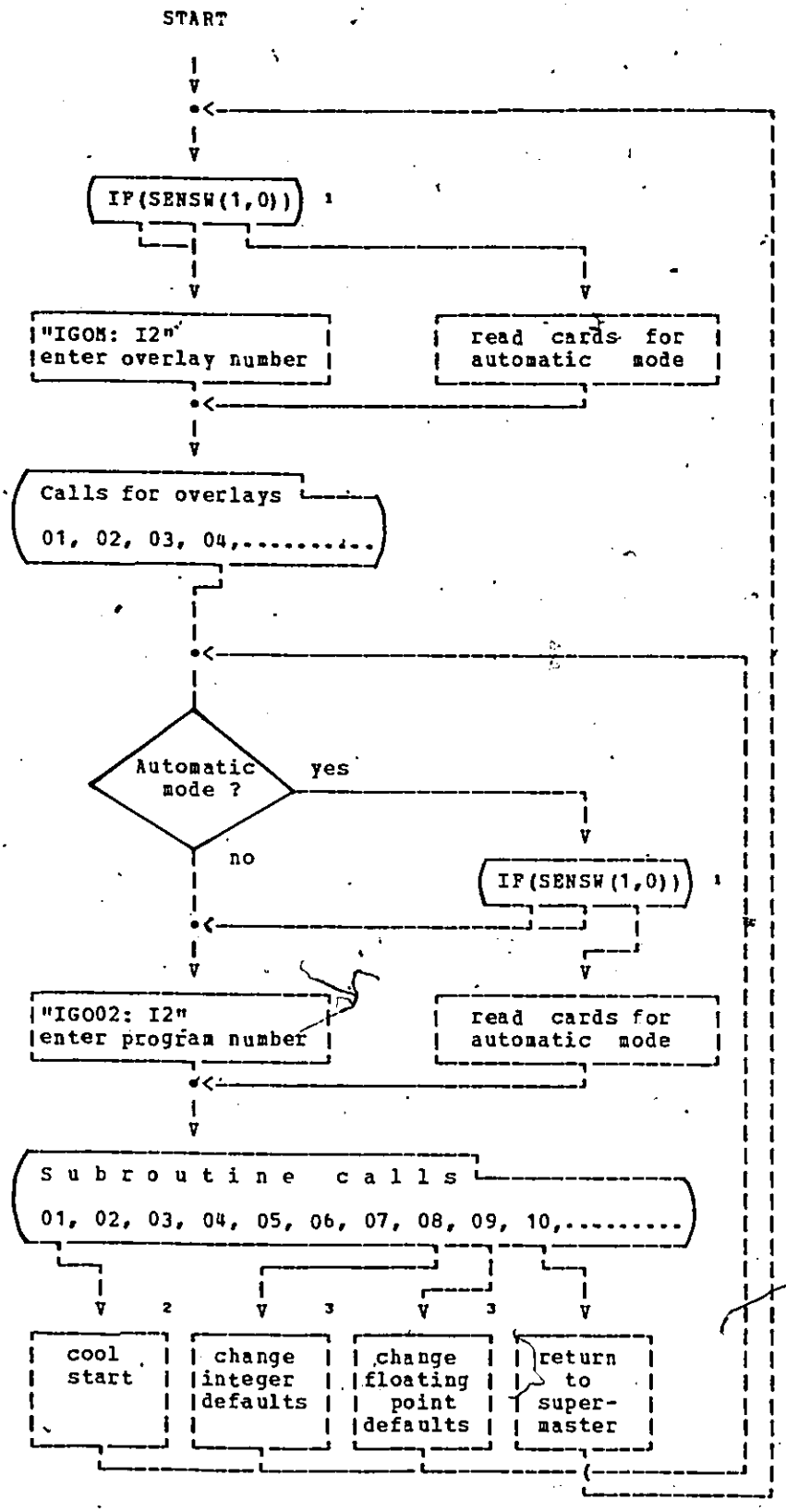

Figure 3.1: Concluded.

For the system a data set is a structured file of image data. As exemplified in Figure 3.2, a data set consists of: (1) a header record of 100 computer words, describing the picture sequential address, type and dimension, (2) a variable number of comment records of 100 computer words each, containing picture name and all names of the processing algorithms to which the picture was subjected, including the commentary of other pictures with which it was combined, (3) the picture data as a (m) x (n) array of integer numbers, in which m is the record length and n the number of records, and (4) an end-of-file mark.

Several pictures can be stored sequentially in any of the storage devices, tapes or disks, where each set of pictures is preceeded by a beginning-of-data record. The last data set is followed by an end-of-data record. Both the latter records are of 100 computer words each similar to the header record mentioned earlier. The package allows up to 5 independent I/O devices which are accessed entering the numbers between 100 and 599. Each physically independent unit can serve either as an input or an output storage device. A physical unit cannot, however, be used in more than one role at the same time. Because storage is sequential, only the last data set can be erased; a new data set can be added only next to the last data set.

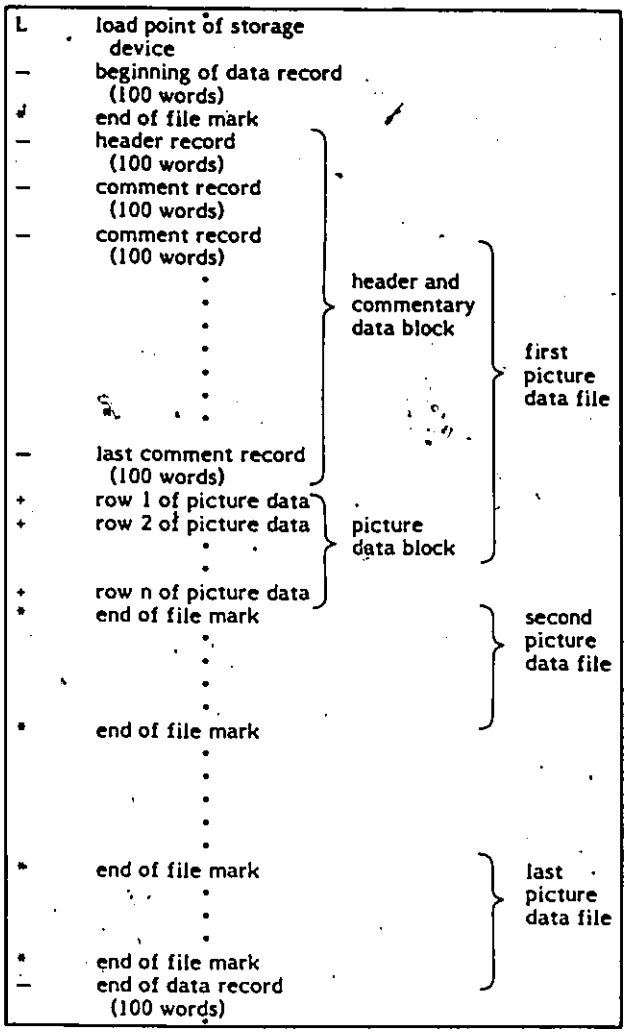

Figure 3.2: Physical structure of sequentially organized picture data in GIAPP.

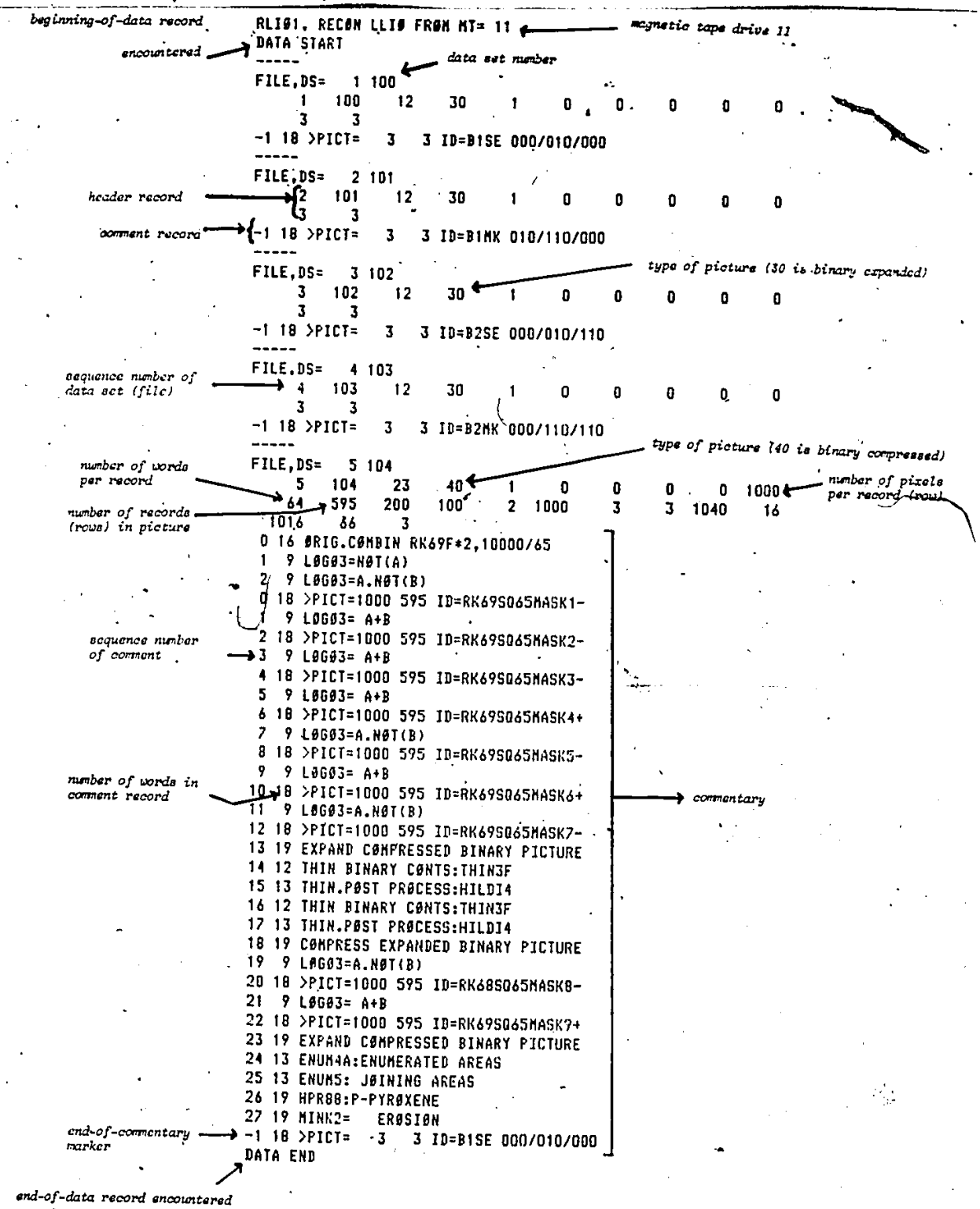

Figure 3.3 Example of printout during the "Cool Start" operation: header and commentary of GIAPP's picture data are listed as stored on a single magnetic tape on drive 11.

Figure 3.3 shows an example of printout of header and comments for several data sets stored on one single tape. The system attempts to be as useful as possible. At the beginning of a run in which one or more existing picture files are available, a procedure (called "Cool Start" in Figure 3.1) reads the headers of all the existing files and creates a table in memory which contains all the information for file availability (input or output data sets) on all 5 storage devices. If during a processing step the user tries to read a nonexistent data set or tries to overwrite existing data, the system simply generates error messages and returns control to the user, without ruining the picture data or aborting. As mentioned earlier, only the last picture on a physical device can be erased.

3.4 The conversational system

GIAPP is a self sufficient system which handles automatically storage and processing from several I/O devices (tapes or disks). This is possible via a very simple conversational language which is kept to a bare minimum by referring only to parameter addresses and to the corresponding values. The user is expected to specify three different classes of interaction: (1) define I/O picture numbers, (2)

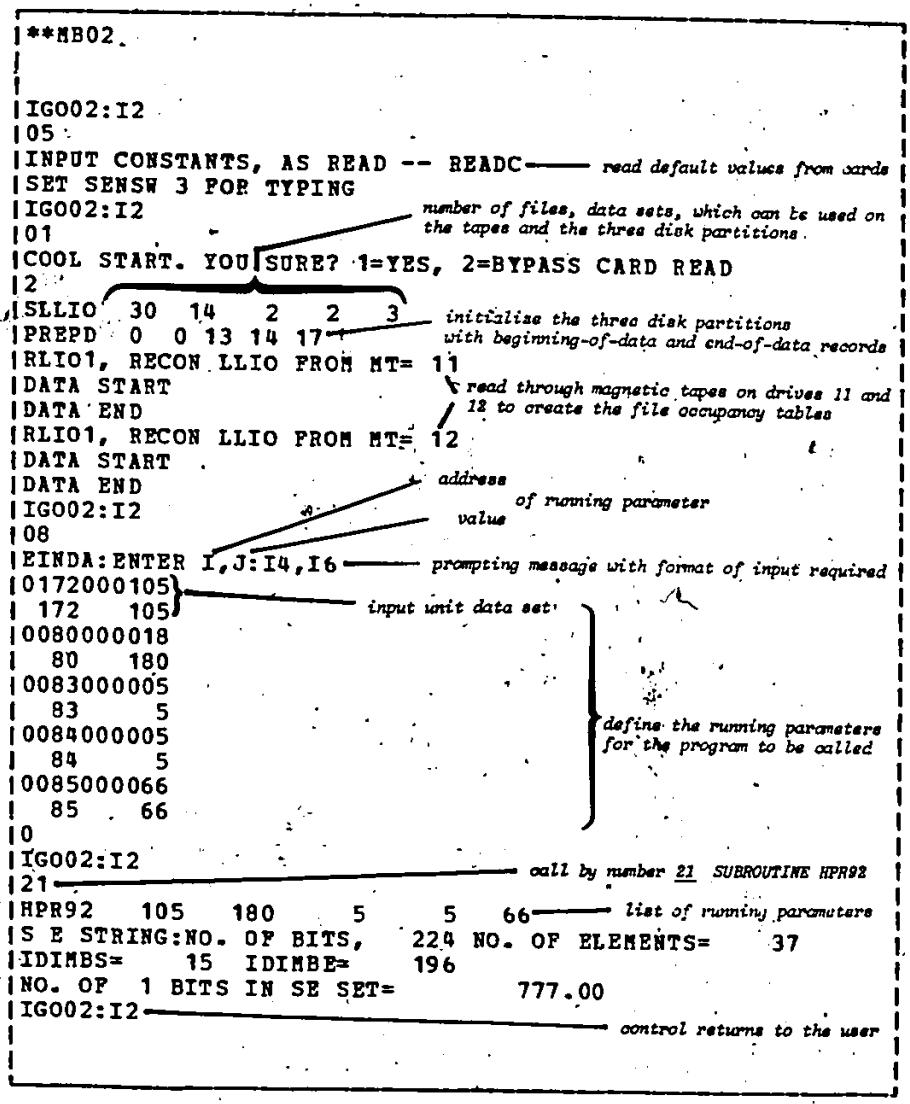

Figure 3.4: Example of conversation during a session of GIAPP.

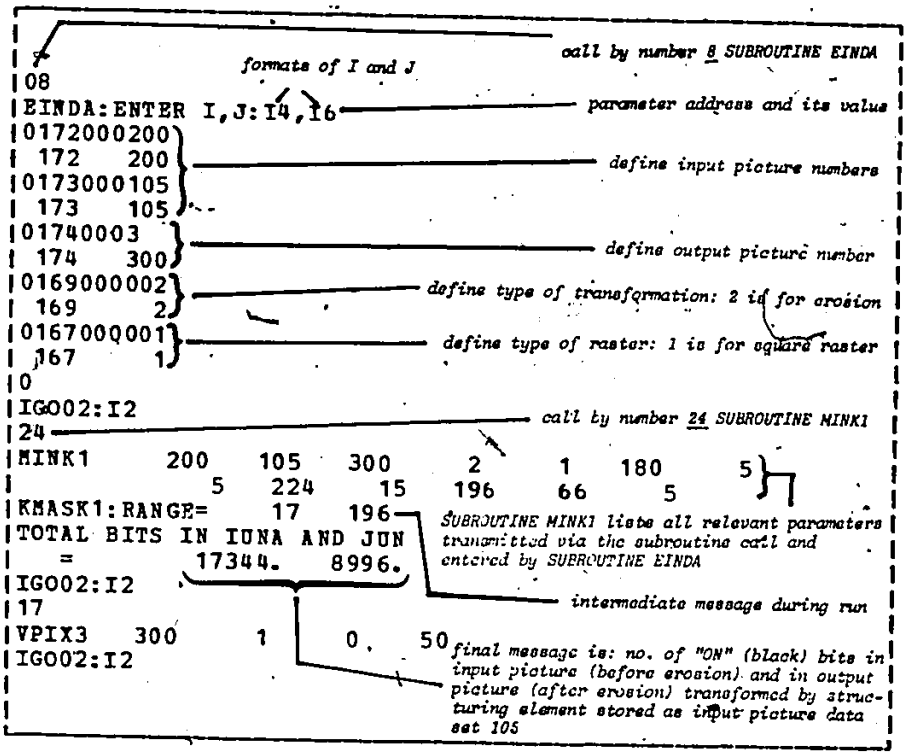

Figure 3.4: Concluded

define the running parameters for a given subprogram, and (3) call by number the particular program. When the program completes execution, the control returns to the user. If an error is detected, an error message is generated and again the control returns to the user.

A description of the programs and a list of their valid parameters and addresses and possible values must be used during the interaction. Some subprograms present various options to the user and require a response. These are explained in detail and in plain language by the programs during the interaction. The subprograms themselves are also called by numbers which are explained in the description. In GIAPP it is the responsibility of the user to know which label corresponds to which picture and to draw a flowchart of the processing. That flowchart and a copy of the text of the interactive conversation will enable to reconstruct the session at a later stage. Figure 3.4 shows an example of interactive conversation.

3.5 General structure of the processing algorithms

The optimization of processing speeds and the picture data organization depend on the nature of the picture processing algorithms. Most algorithms, however, process

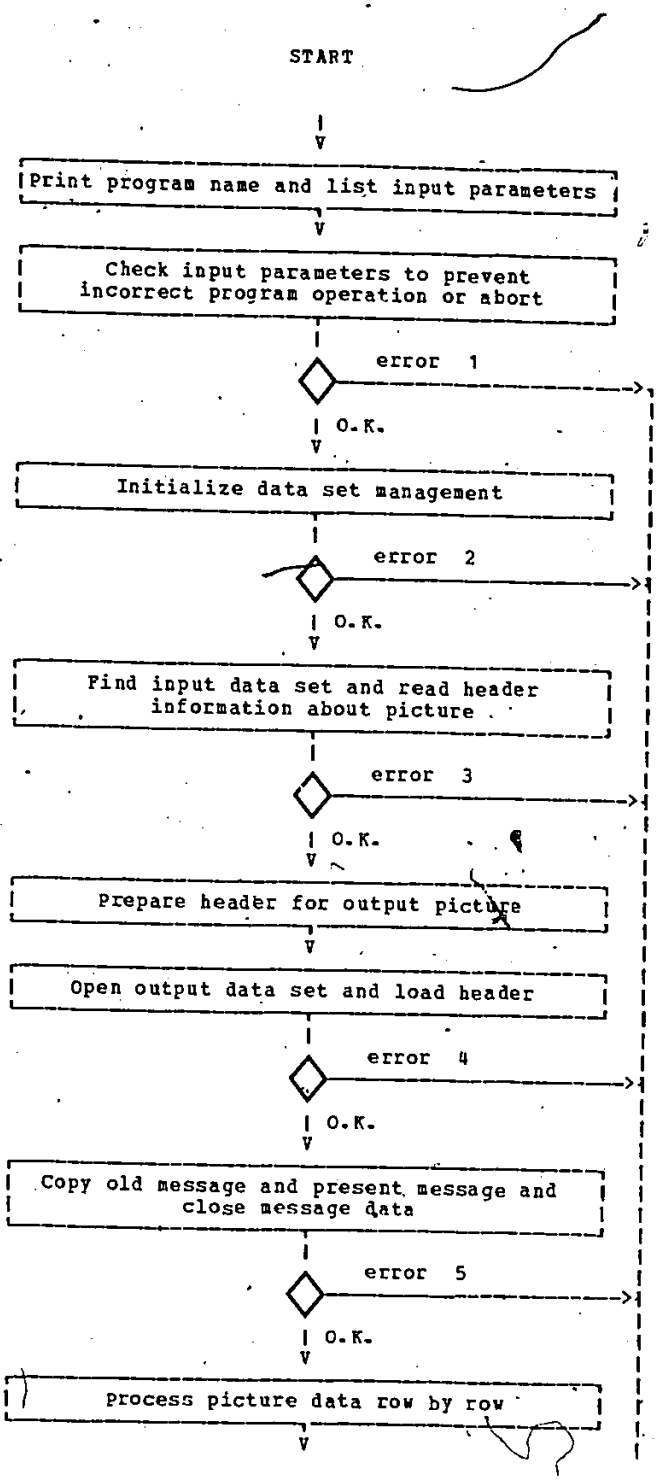

Figure 3.5: General structure of a processing algorithm in GIAPP.

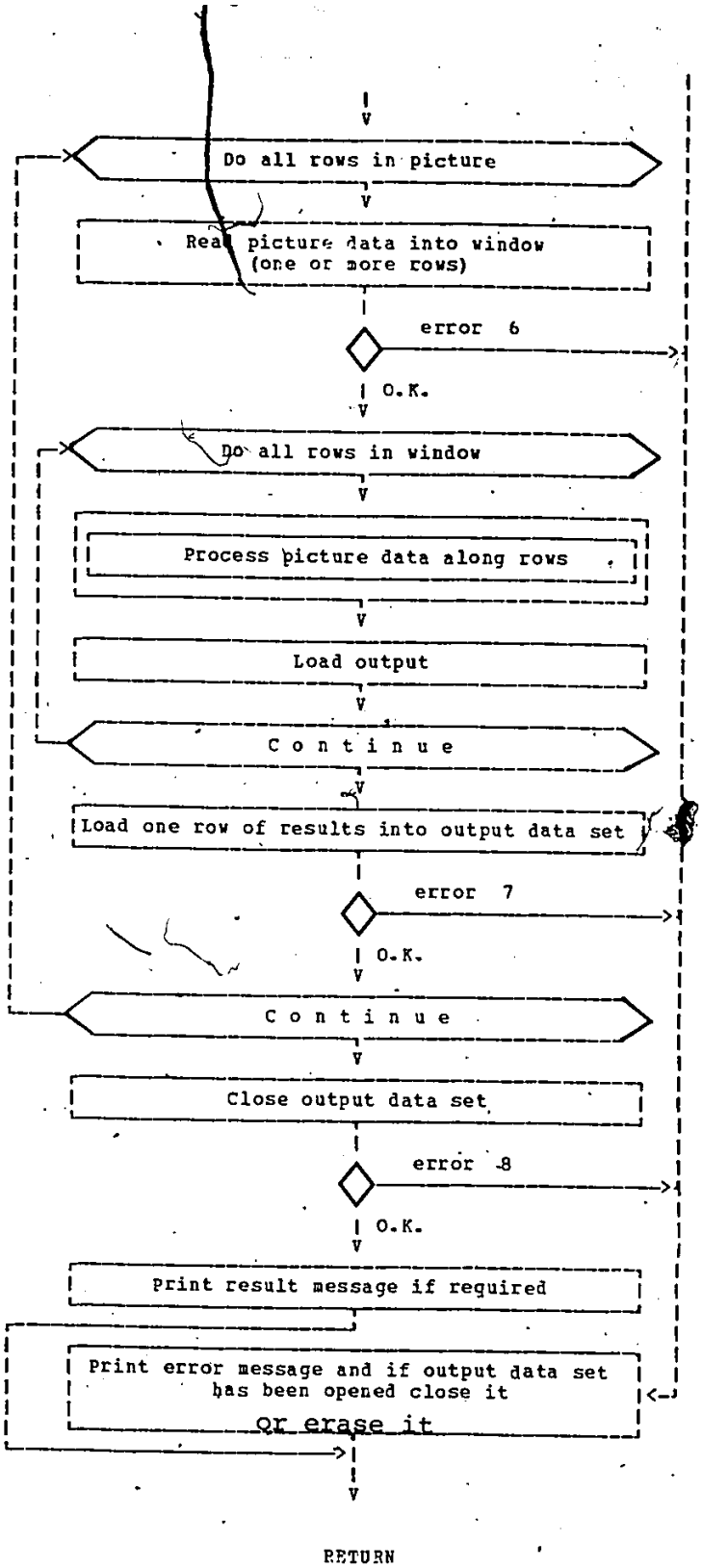

Figure 3.5: Concluded.

pictures in a systematic manner, starting at the top left corner of a picture and ending at the bottom right cor- ner. Therefore, the pictures can be stored as large two-dimensional matrices in which each element and a certain number of its intermediate neighbors or the corresponding elements in other picture matrices are used for computation. In order to minimize storage, only a strip across a picture is stored in core. The width of the strip corresponds to the number of raws of input picture data which are used by a given algorithm. The minimum strip consists of one raw of picture elements. Each raw of picture data represents a logical record. Figure 3.5 shows the schematic structure of a program, or processing algorithm. A complete listing of GIAPP's source programs will be available as a separate technical report (Fabbri, 1981).

3.6 Machine-dependent routines

Several machine dependent routines are used in the Modcomp II version of GIAPP. They have the following purposes: (a) file management, (b) debugging options activating printed messages, (c) bit manipulation and character manipulation, and (d) activating the peripheral equipment, such as the flying spot scanner, the graphic tablet digitiz-

er and the display devices. These routines are all Fortran callable but are machine specific. For this reason they will have to be rewritten or substituted for the particular equipment on which GIAPP may be transferred and converted to. A detailed description of these routines will be available as part of a separate technical report (Fabbri, 1981).

4. Organization of the processing algorithms of GIAPP

4.1 Introduction

The programs in GIAPP have been grouped into five classes as follows: (I) control of the flying spot scanner and processing of grey-level images; (II) digitization of line drawings by a graphic tablet, and editing of binary compressed images; (III) processing of binary images of boundaries to produce phase-labeled images and binary images of the different phases; (IV) processing and analysis of binary compressed images by means of structuring elements as defined in mathematical morphology; and (V) transfer of uncompressed image data outside the Modcomp II computer system.

Data-management programs for the automatic handling of image data with labeled file structure was mentioned earlier (see also Figure 3.2). These programs are used in the classes II, III and IV as sole file handling procedures; they are used in classes I and V as options. Class I handles unlabeled data sets, however it allows to create tape files - for both grey level images and binary compressed images obtained by thresholding, according to the

TABLE 4.1

Summary of the functions performed by the groups of programs in the five classes of SUPERMASTERS in GIAPP

SUPERMASTER	MASTER	FUNCTIONS
I	01	Scanning on a Flying Spot Scanner, display of the results of the scans, creation of grey level images, study and display of grey levels, thresholding of grey level images, and creation of binary compressed images as labeled data sets for subsequent processing
	02	Selection of subpictures from large original images, point operations on pixels for grey level images
II	03	Graphic tablet programs for digitizing line drawings, creation of files of vectors from a graphic tablet, transformation of vectors into binary images, assemblage of subpictures (384 pixels x 384 pixels maximum) into large mosaics of binary compressed images of line drawings
	04	Assemblage of subpictures (512 pixels x 512 pixels maximum) into large mosaics of binary compressed images of line drawings
	05	Editing, via graphical displays, of binary compressed images
III	06	Line thinning of binary expanded images, component labeling of lines, junctions or areas within contours
	07	Pase labeling via interactive displays, creation of phase labeled images, extraction of binary compressed images of each phase
IV	08	Logical operations on or between binary compressed images, Minkowski operations or transformations by means of programmable structuring elements, displays of binary compressed images
	09	Auto- and cross-correlation of binary compressed images in two dimensions creation of correlation images
V	10	Output of binary expanded images, labeled images and grey level images for transfer in different BCD formats

labeled structure for the other classes. Class V accepts labeled data sets as input and creates unlabeled and differently formatted files as output on magnetic tapes for image transfer.

The same simple type of conversational structure is used in all programs throughout the five classes.

An overlay program structure is used in the first four classes of programs. This is done in order to reduce the storage requirements. Programs have been grouped together which perform related tasks in order to provide practical selections of algorithms for each session.

Table 4.1 summarizes the various tasks performed within the five classes of programs of GIAPP. A brief introduction of the data managemant programs which are called by each processing routine is provided in the next section. Table outlines of the different algorithms within each Master program will follow.

4.2 Data management and conversational programs

A relatively crude method of handling image data is used first within SUPERMASTER I. Tapes are unlabeled, and each image may consist of the rectangular array of pixel values (computer words) followed by an end-of-file mark. Two

optional calls are available for going back one end-of-file mark, and for going forward, past one end-of-file mark, respectively, on each of the two magnetic tapes that can be mounted on the two tape drives called MT11 and MT12 . Prior knowledge about the sequence of images and careful annotations during a session, are necessary in order to place the I/O devices in the proper positions relatively to the image files desired. Image dimensions - record length and number of records - in each image file are assumed to be known and entered interactively before the file is accessed. File elimination in this situation is simply done by overwriting the last file in a sequence with the new file being created or copied.

For file management in the labeled system, during the initial part of a session, programs are called for: (1) reading from cards default values of input parameters (integer or floating point values) and, optionally, to print them out on the terminal teletype; (2) initializing the disk partitions with beginning-of-data records and end-of-data records; (3) reading through headers and comments of all files on the two magnetic tapes to create in core a file occupancy table. Optionally headers and comments for each data set containing an image or a table of data, can be printed by this program on the Versatec printer as backup information; (4) if desired the data on all or part of the

occupancy table can be listed for control; (5) unlabeled tapes can be initialized (by a beginning-of-data record followed by an end-of-data record) for usage onthis labeled file handling system. This is done by separate special calls; (6) a general program for: going through the occupancy table, file searching, header reading for the desired data set, writing a new data set header information record, and overwriting an end-of-data record at the beginning of the last data set on the medium mounted on a given device (rubbing a file), is called by all processing routines. It can also be called separately by a special call for data set (file) erasing. This routine is also used to put an end-of-file mark at the end of each data set (to close a file); (7) the handling of the commentary blocks is done by a separate function which reads the image commentary and writes old and new commentaries on newly created image data sets. This routine is called soon after the one in (6) above; (8) finally a separate routine is called for copying a data set from one I/O device to another to take best advantage of the file space available for retention (tapes) or for scratch (disks).

Beside the default values loaded first from the card reader, the conversational part of the programs calls separately routines for changing integer input values and floating point values. Each Supermaster program will requ-

est, during interaction, an integer number as call command to enter a Master program. Each Master program then will request an integer number as input command to call a processing routine. This is done after each routine has completed its task.

4.3 Organizational flowcharts of the SUPERMASTERS

Figures 4.1 to 4.5 provide simplified organizational flowcharts of the SUPERMASTERS I to V, respectively. The practicality of the operational flow is self evident in the figures. A more detailed level of information about the programs and their routines is provided in the user's guide, instruction sheets, in Appendix B.

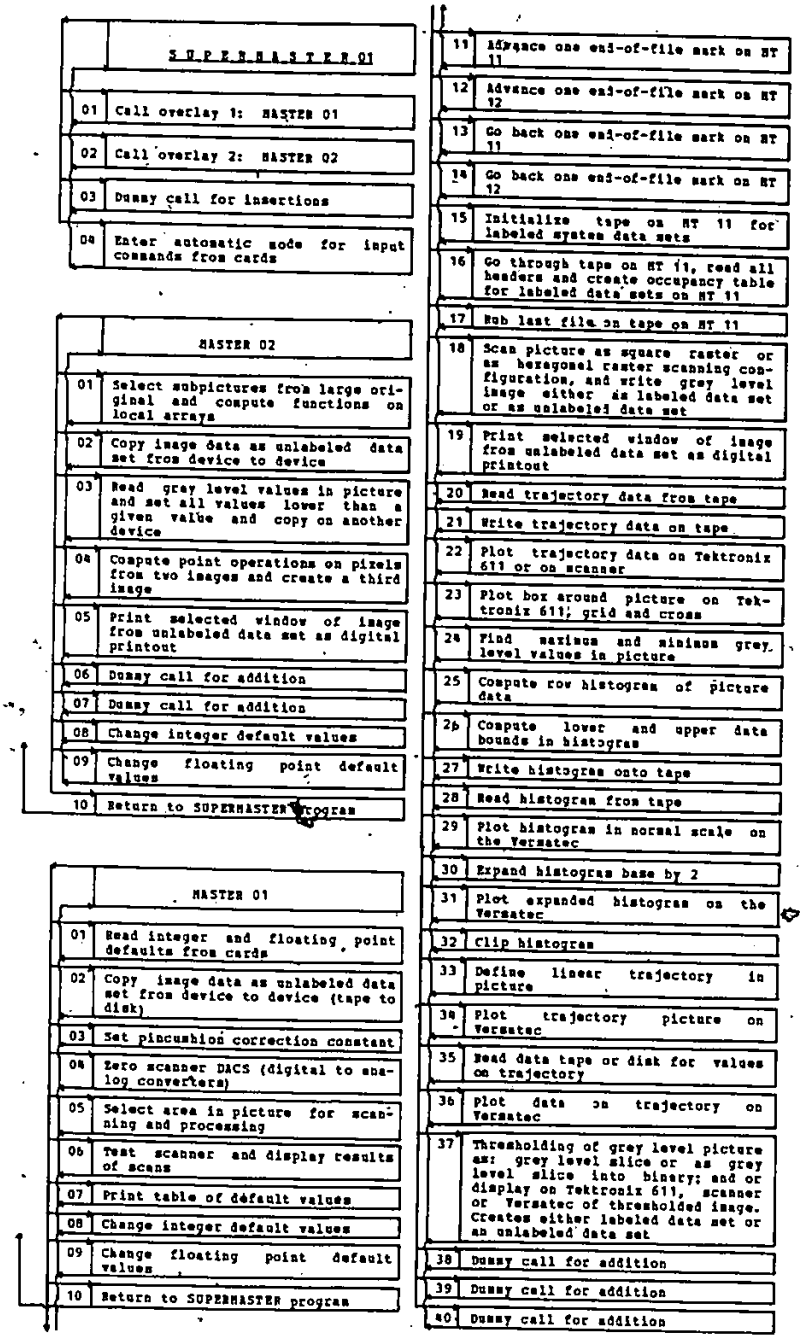

Figure 4.1: Organizational flowchart of "SUPERMASTER I" in GIAPP: scanning, thresholding and processing of grey level images.

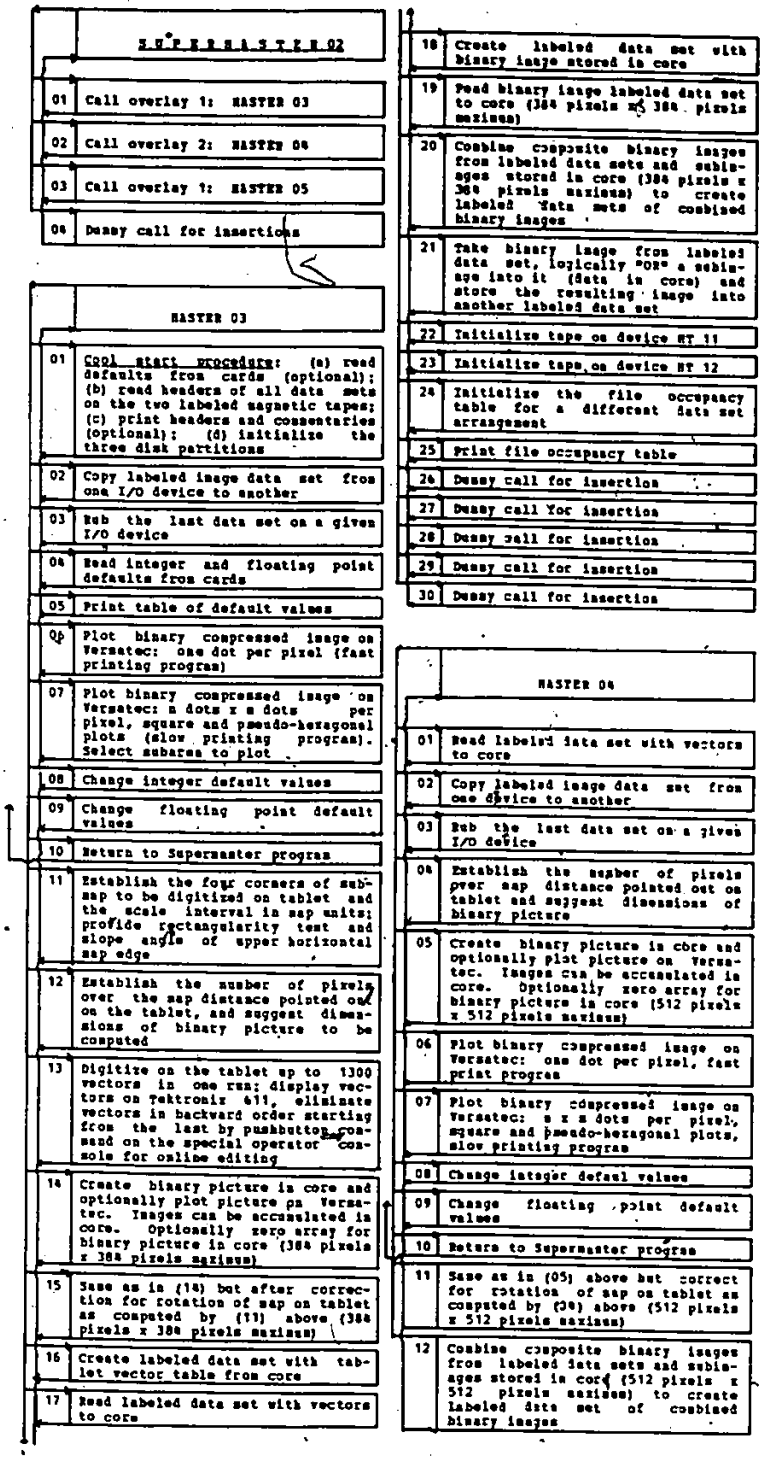

Figure 4.2: Organizational flowchart of "SUPERMASTER II" of GIAPP: graphic tablet subroutines for digitizing line drawings, editing and assemblage of mosaics of binary compressed images.

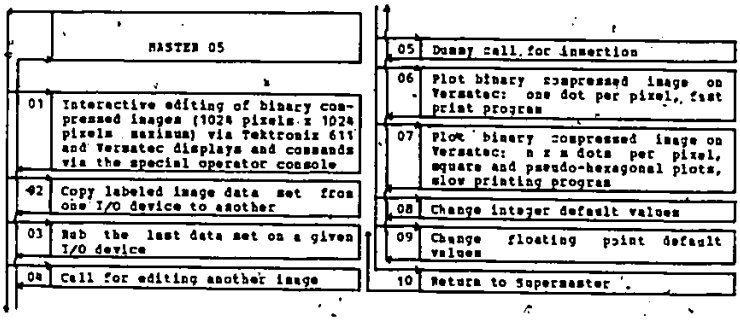

Figure 4.2: Concluded.

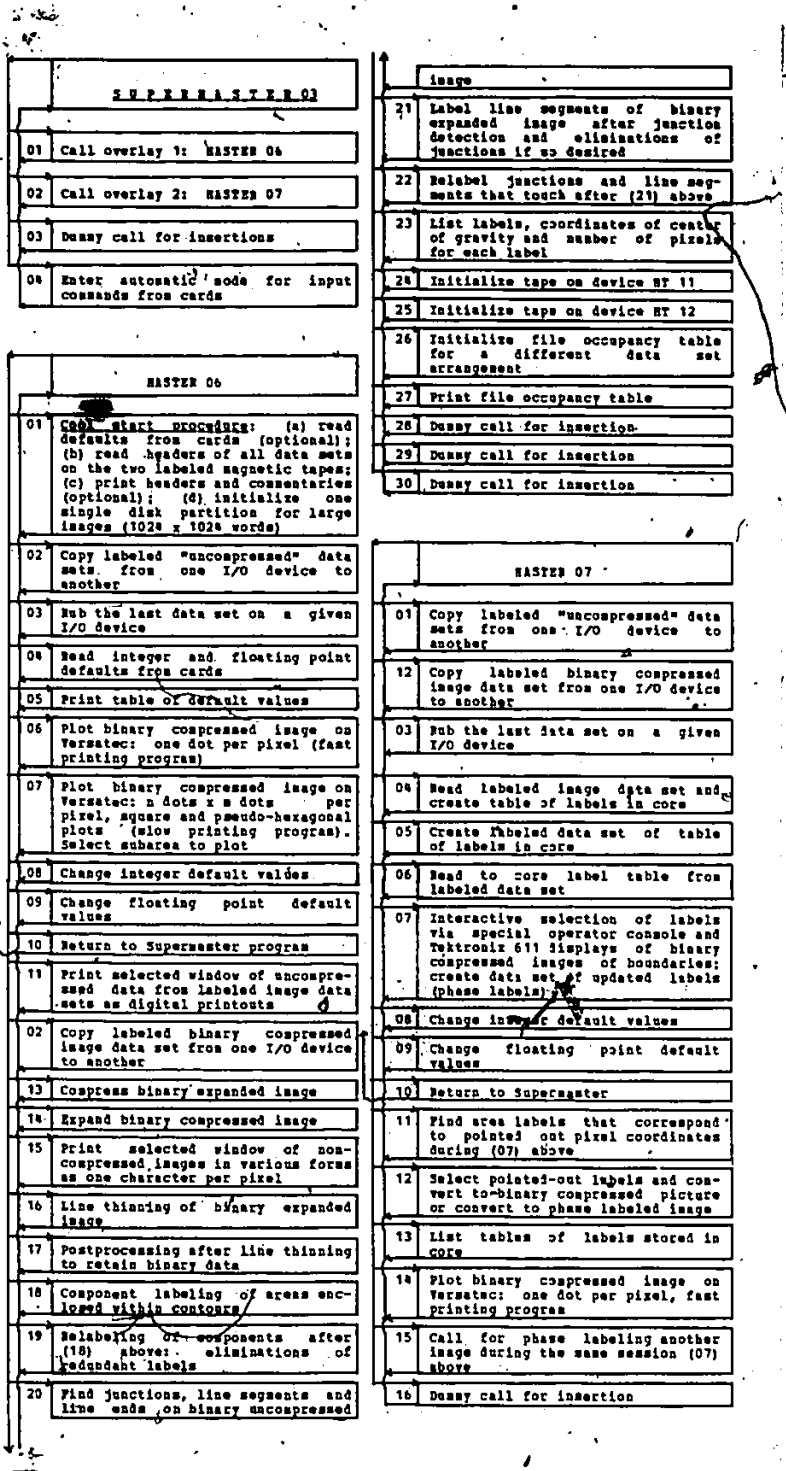

Figure 4.3: Organizational flowchart of "SUPERMASTER III" of GIAPP: line thinning of binary expanded images, component labeling of areas and of lines, phase labeling, and extraction of binary compressed and of phase labeled images from component-labeled images.

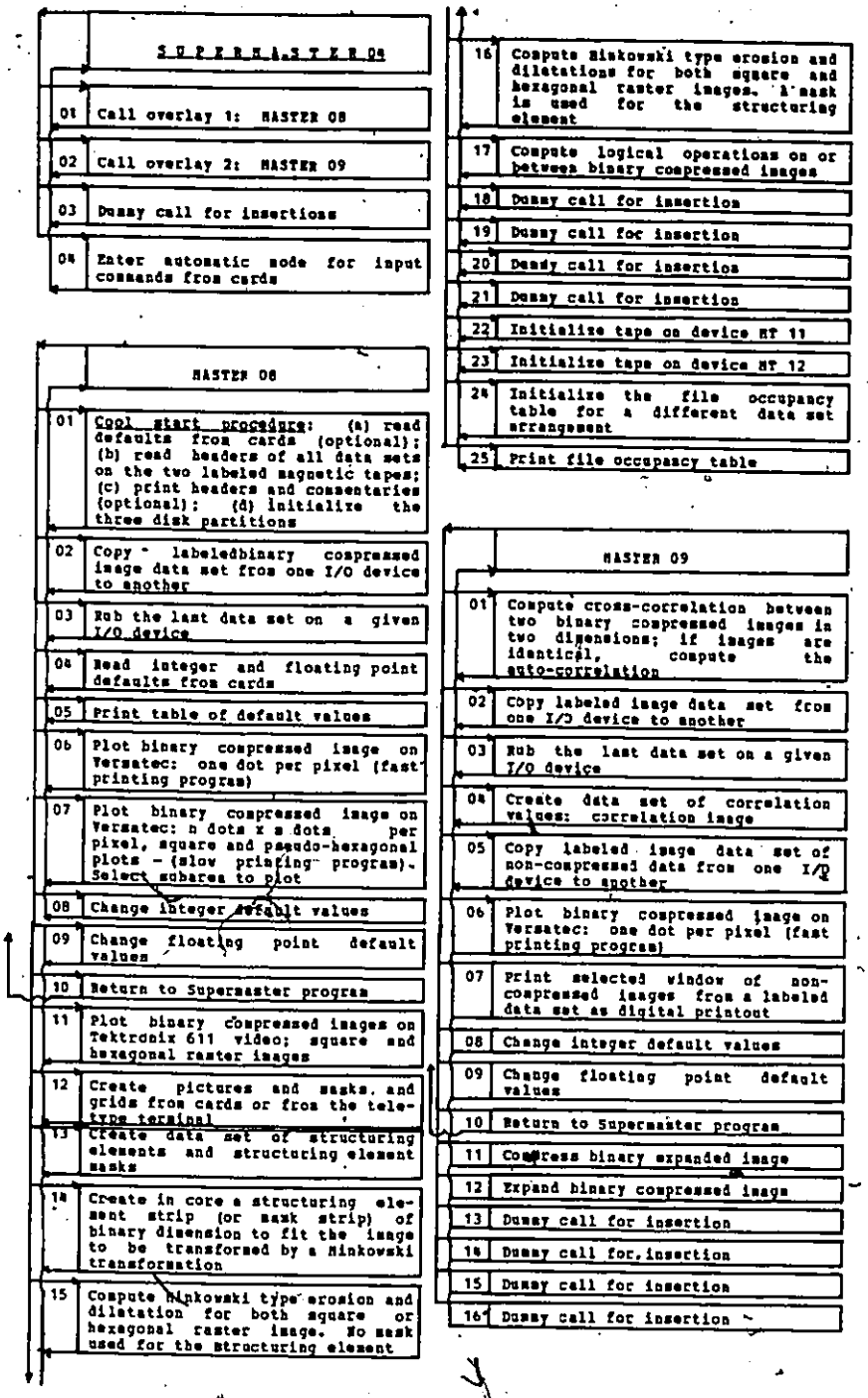

Figure 4.4: Organizational flowchart of "SUPERMASTER IV" of GIAPP: processing of binary compressed images.

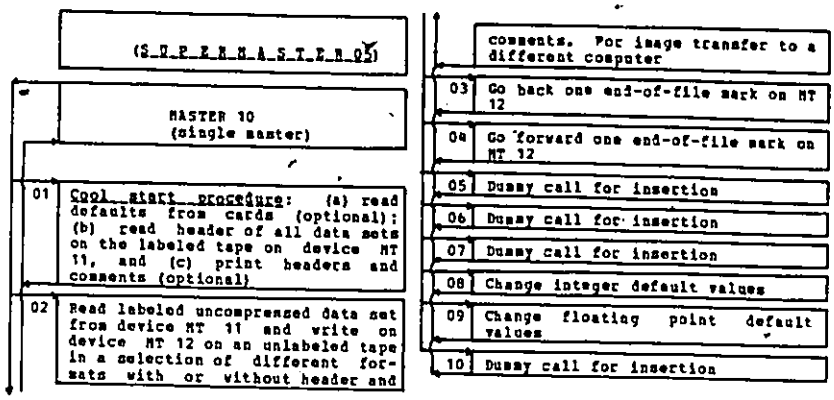

Figure 4.5: Organizational flowchart of "SUPERMASTER V" of GIAPP: output of image files in Binary Coded Decimal formats for transfering of data to other computing devices.

5. Transformations of binary images

5.1 Introduction

Experiments on simple images will be described at the end of this chapter. They exemplify the concepts which will be developed further on more complex practical applications on materials of geological nature. Mention is made first of the early approaches to the analysis of binary images by computer.

As previously described, in binary images there are only two grey levels, black (the objects) and white (the background). The description and quantitative characterization of binary images involve the geometrical properties of objects and relationships among objects. The set of these properties, however not necessarily limited to binary images, is termed texture. Methods for texture description in many different applications, have been developed in pattern recognition, stereology, and also in mathematical morphology. The approaches chosen in those fields had independent motivations , different statistical bases and physical applications. However, many of the solutions proposed for either practical or theoretical problems, have generated remarkable interdisciplinary overlaps.

After commenting briefly on these relationships, the software based approach for geological applications, proposed in this thesis, will be exemplified in terms of simulated parallel processing for a general purpose small computer.

5.2 Historical background on computer processing of binary images

The concept of applying television technology to quantitative image analysis followed closely the introduction of entertainment television . In the early fifties Roberts and Young (1952) introduced the flying spot scanner, an electronic digitizer which, entirely under computer control, produces digital images from transparencies. A first attempt to study pictures as sets of binary images by binary transformations, was made by Kirsh et al (1957) and Kirsh (1957) who developed some of the early ideas of Kovasznay and Joseph(1955). An organized approach to the analysis of binary images by computer was initiated by Moore (1968) in his description of a general purpose computer program for image analysis termed STRIP (Standard Taped Routines for Image Processing). He laid down the basis for the analysis of binary images as a relatively fast computer method for automated measurement of structures. After introducing the

concept of phase, which represents the set of all particles of a single kind within an image, he wrote:

> "The phase concept is important since it allows the analysis of complex structures to be treated as a series of binary problems. In each treatment it is necessary only to consider the pattern formed by the particles of a single phase, against a black background occupied by all the other phases. Such a simplified treatment permits a computer equipped with an adequate group of Boolean operations to process an image at a rate around 200 times faster than is attainable when processing each image point as a numerical character" (p. 277).

He further added:

> "The basic operations generally referred to as Boolean operations or Boolean algebra, are implemented mainly by the very simple expedient of disabling the "carry" mechanisms which normally inform the machine that 6 + 4 equals 10 rather than zero" (p. 294).

Thus images can be considered as compact arrays of bits, and operations between pictures are computed with relatively high speed. This capability is available on most general-purpose computers.

Moore described how sequences of logical transformations upon binary phase images, and "BIT OPerations" on them (Moore, 1968), can produce new images in which the number of pixels (or bits), which belong to the transformed objects, are closely related to the morphometric measures sought

after. By additional processing the various objects are identified and separated in the images, and statistics is computed for characterizing the distribution of a large number of parameters. In support of his approach, Moore was probably the first to document experiments in which processes simulated in time by sequences of binary transformations provided criteria for predicting the behaviour of the material analyzed.

Three main lines of work have developed since those early approaches to binary image processing. One, directly following Moore's work, dealt with the development of software, such as FORTRAN programs, and of bit-manipulation machine-language routines for general-purpose computers. A second line consisted of the designing of special hardware-built instruments connected to a television camera and monitor, which, in an interactive fashion, compute measures for selectively extracted binary patterns. The extraction is accomplished by semiautomatic grey-level slicing. A third line was the design of "parallel processors" and "pipeline processors", particularly fast computers for the analysis of grey-level images at real-time speeds. These complex and expensive computers allow processing of binary images as the simplest type of image data.

A recent software based approach to image processing, inspired after Moore's concepts, was considered by Rink

(1976a and 1976b). Versatility and relative independence from capital costs for special equipment were the argument in favour of the computationally slower approach.

Several specialized instruments, generally termed image analyzing systems or image analyzers, have been built for the automatic detection of binary patterns from various types of image material (ore microscopy, metallography, cytology etc.) and for making precision morphological measurements on the detected patterns. In general the image information is supplied by a wide range of input peripherals (optical microscopes, epidiascopes, slide or movie projectors, scanning electron microscopes, etc.) and passed onto the screen of a television camera. The electrical output from this camera passes into a closed-circuit television monitor to provide a television image and also to a detector unit where signals from the camera emanating from the features that need to be measured are discriminated and selected from the rest of the signal. The output from the detector, consisting of pulses from the detected features, also can be fed into the monitor, so that the operator can see which features he has detected, and into a computer which can be set to measure several geometrical properties (e.g., percentage area of a phase, number of detected features, their total projection and size distribution). Until recently the repertoire of measurements built as

hardware in these instruments was severely limited.

A first model of one of the most reliable of these instruments, the Quantimet A, became available in 1963 (Jesse, 1971). A more refined modular system, the Quantimet 720, was introduced in 1970 (Coles, 1971). A recent summary review of image-analyzing instruments was made by Hougardy (1976). Of particular interst was the model designed by Serra (1965,1967, and 1970) also described by Klein and Serra (1972). This model was constructed so that it could satisfy the statistical requirements of mathematical morphology theory. Later the Leitz company in Germany, built such an image analyzer which then was called TAS (Texture Analyzing System), and was described by Muller (1974), Serra and Muller (1974) and Serra (1974).

Most image analyzers underwent continuous developments and expansions which required redesign of the modules for the specific tasks and additions of new options for added programmability. Perhaps the most recent developments are programmable systems like "AT4" and "TAS second model" employed by Charmant and Coster (1978) in France. Beside having a rather extended programmability and being interfaced with large computers, these instruments have several memories for the storage of the detected images and their transformations. In practice an image analyzer is a costly instrument particularly well suited for routine

measurements.

In a parallel processor either the entire image or a large part of it are processed at once in a number of elementary steps. The processing is organized in parallel as opposed to sequential fashion (most computers are sequential machines) thus achieving optimal employment of the capabilities of the computer in time . The concept of a two-dimensional parallel computer with square module array was first introduced by Unger (1958,1959). The hexagonal array, instead,was proposed by McCormick (1963) as the "rhombic array", and hexagonal parallel pattern transformations designed by Golay (1969) and discussed further by Preston (1971). A first prototype of parallel processing system was described by Johnston (1970). At present "cellular logic" or also neighborhood logic, is the name given to a discipline in the field of computational geometry, which has ample applications in image processing, particularly in the design of parallel computers. Preston et al (1979) provide the state of the art in the subject. To quote the authors:

> "Cellular logic refers to an operation performed digitally on an array of data P(I,J) which is carried out so as to transform P(I,J) into a new array P'(I,J) wherein each element in the new array has a value determined only by the corresponding element in the original array along with the values of its nearest neighbors. The nearest neighbors configura-

> tion is called the "cell" and operations over arrays of identical cells are called "cellular logic". When one considers the implementation of celluler logic by an array of computers the logic and the memory associated with the cell define a processing element (PE). The array itself is then a cellular automaton (CA)." (p. 826).

While programming was extremely difficult on the first parallel computers, it has become easier on the latest models which are provided with high-level languages. Parallel computers, however, are expensive dedicated instruments.

After the interest during the fifties and the sixties in the development of image processing methods for the analysis of binary images, the subject was practically abandoned in pattern recognition during the seventies, if we make exception for special purpose practical applications, particularly related to the development of image analyzers.

As we will see in the next section, a renewed interest in the analysis of binary image information was generated partly because of the work for a theoretical background to geometrical probability concepts and applications, done by the French school of mathematical morphology. Also the work of stereologists in both the theoretical and practical aspects supported further the study of binary images.

The quotation by Preston et al (1979) was made here, because it summarizes well in image-processing terminology, a logic which has its equivalence in the theory of transfor-

mations by "structuring elements" proposed in mathematical morphology where the expression "hit or miss transformations" is frequently used.

5.3 On some relationships between pattern recognition, stereology, and mathematical morphology

Stereology is the field of exploration of the geometrical properties in three dimensions from two-dimensional sections or projections through solid materials. This field is interdisciplinary: it covers disciplines as far from each other as medicine, mineralogy, biology, metallurgy, mathematics, and statistics. During the past 25 years, the main interest of pattern recognition was in the development of automatic systems and machines. The instrumentation for data acquisition and preprocessing, some of the methods in artificial intelligence, statistical approaches to image processing and the development of picture languages, provided additional tools for the solution of stereological problems (Cheng, 1976; Chen, 1976). The different materials studied by stereologists, on the other hand, offered the opportunity and motivation for developing many applications of pattern recognition to a larger variety of everyday problems of practical utility. Common to both fields, according to Pavel (1976), is the aim of identifying

patterns from incomplete information. We can describe objects or images by primitive components and their composition, and also we can define them by their local or global topologically invariant properties. Recognition of a pattern is modeled as the detection of an equivalence with regard to a specific set of transformations, between the given objects and an element of a set of templates.

According to Serra (1976,1978), mathematical morphology theory can provide a background for extrapolation and prediction needed when a stereological model is needed for the interpretation of geometrical properties of a structure.

Bernroider (1978) pointed to probabilistic and computational geometry as a common methodological background between the various disciplines of quantitative structure analysis: stereology, image analysis and processing, pattern recognition and scene analysis. He suggested that a connection might exist of picture processing techniques, originally established in the U.S.A. over 20 years ago (Kovasznay and Joseph, 1955), with the "European School of Image Analysis and Stereology". This he considered of importance because the directions of structure analysis in the U.S.A. and Europe are different and seemed to be little aware of each other before 1977. Figure 5.1 after Bernroider (1978) portray this situation.

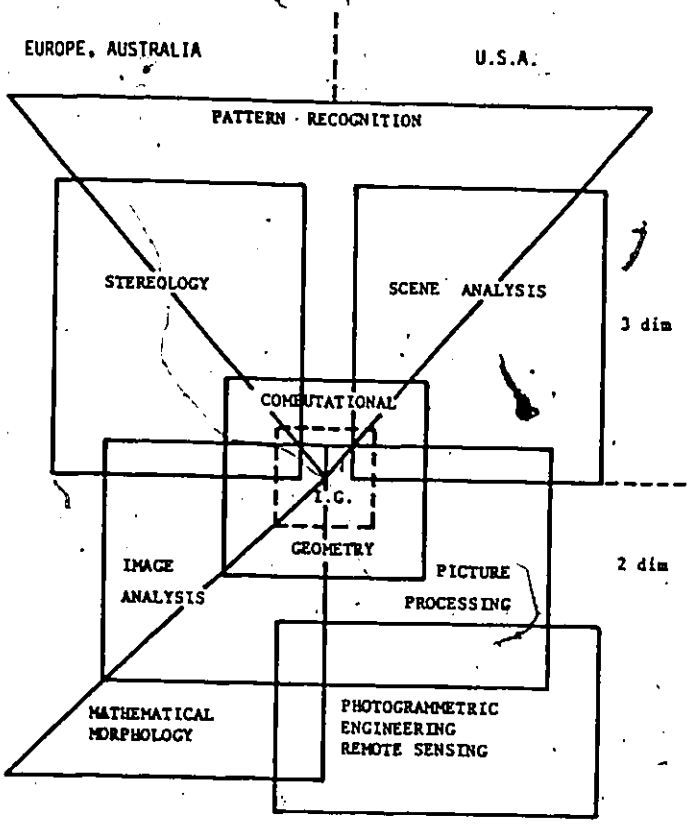

Figure 5.1: Schematic diagram which reflects the current situation regarding various branches in quantitative structural research according to Bernroider (1978, p. 155).

5.4 Logical operations on binary images

Boolean operations, Boolean algebra or logical operations are computed, for example, between two computer words at the bit level. If we consider computer words as sets, each of n bits (16, 32, 36 or 60, depending on the computer used) which can be either "ON" or "OFF" (0 or 1) status, we can obtain all the operations known in set theory by the symbols: $\cup$ (union), $\cap$ (intersection), ^{c} (complement) and their combinations. These operations are obtained in computer terminology, by the operands: .OR., .AND., and .NOT., respectively.

Let us take two computer words, and call them the sets A and B. We can write $A \cup B$, $A \cap B$, A^c, and B^c, which correspond to A.OR.B, A.AND.B, .NOT.A, and .NOT.B . Another operand which is sometimes used is .EXOR. (exclusive .OR.) for expressions like A.EXOR.B . For this we can use the symbol $\underline{\cup}$ in order to distinguish it from the union symbol $\cup$. This operation corresponds to the union of the nonoverlapping subsets of two sets : $(A \cap B^c) \cup (B \cap A^c) = A \underline{\cup} B$ for simplicity in expression.

The operands .AND., .OR., .EXOR., and .NOT., are machine dependent functions, callable in FORTRAN, which, if properly used can be parts of fast computations. In particular,

machine-language routines can be written for logical operations between sets or arrays of words, such as, for example, two rows of binary compressed images.

By making these operations between successive portions (words or set of words) of two images in corresponding subsequences of pixels, we can obtain logical operations between images at conveniently high speed. For example if A and B consist of 1024 x 1024 = 1048576 bits, on a 16 bit word computer, these can be stored in 64 x 1024 = 65536 words, and that many operations are needed to compute the picture resulting from a logical operation between A and B. In particular if routines are used for the operations between arrays of 1024 words, only 1024 calls to these routines will be needed for the operation between two images.

For illustration, figure 5.2 shows several logical operations between (and on) two artificial binary images A and B, each of 10 x 10 = 100 pixels in size. Ten operations which are more commonly used are as follows: (1) A.AND.B, (2) A.OR.B, (3) A.EXOR.B, (4) .NOT.A, (5) .NOT.(A.AND.B), (6) .NOT.(A.OR.B), (7) .NOT.(A.EXOR.B), (8) A.AND.(.NOT.B), (9) A.OR.(.NOT.B), and (10) A.EXOR.(.NOT.B) .

From the patterns in Figure 5.2 we can see how different relationships between two images can be expressed immediately by new images which are the result of logical

Figure 5.2: Several logical operations between (and on) two artificial binary images, sets A and B, each of 10 pixels x 10 pixels in size. The expressions below the images contain the following set symbols (and Fortran operators): $\cup$, union (.OR.), $\cap$, intersection (.AND.), ^{c}, complement (.NOT.), and $\dot{\cup}$, union of non-overlapping subsets (.EXOR.). Combinations of operations are also included, all of which are available in GIAPP as single operations. To the right of the logical expressions, the numbers are shown of the black pixels in the binary images.

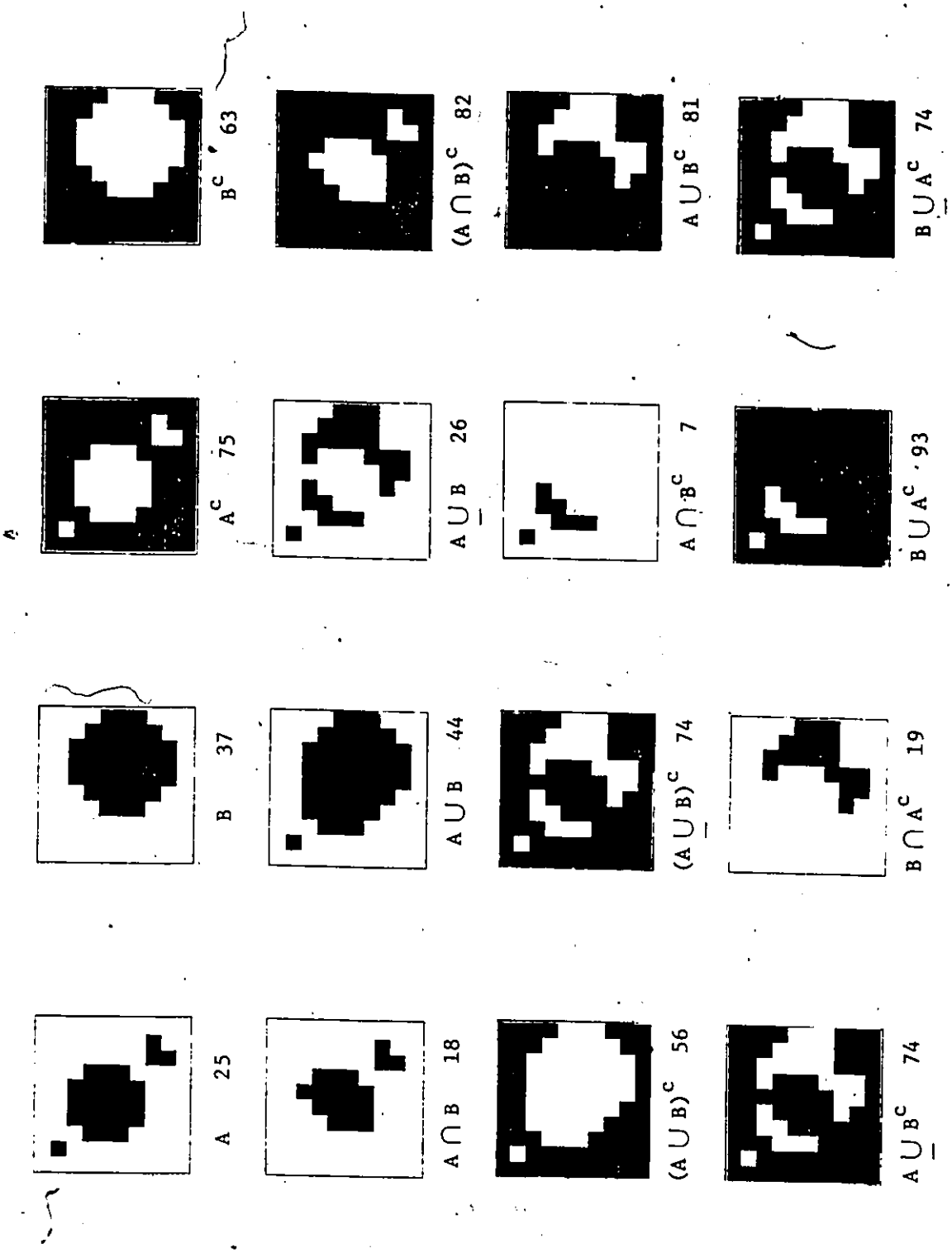

Figure 5.2: Concluded.

operations. Depending on the relationships between the two patterns compared, the results of some operations may be identical: this can be seen in Figure 5.2.

Logical operations can be combined with shifting (translation) operations in order to produce transformations which are used to characterize textures in binary images. Essentially, logical operations are parallel processes in which several bits (pixels) change their status at once in a single operation.

5.5 Structuring elements for the analysis of textures

According to concepts of mathematical morphology, if we consider binary images as sets of points in the picture space, we can compute operations and transformations which measure their geometrical attributes. This can be done, for example, by appropriately designed elementary sets of points which then are used as local operators.

A structuring element can be considered a set of pixels which is swept across every pixel of an image whose "ON"-"OFF" status is changed according to the degree of matching in its corresponding neighborhood. Several structuring elements, in the form of small binary images, can be seen in Figure 5.3. When the central pixel of the structuring elements happens to overlap a pixel in the image to be

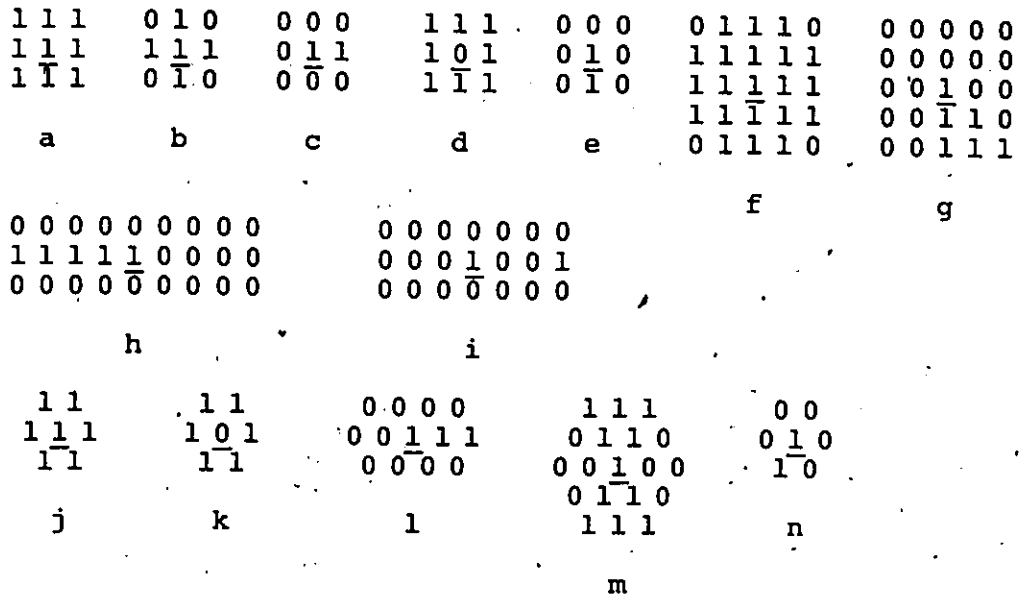

Figure 5.3: Some examples of structuring elements of square raster, (a) to (i), and of hexagonal raster, (j) to (n). Center pixels in structuring elements are underlined. Only the 1's identify the neighborhoods used in the transformations described by these structuring elements.

transformed, the surrounding pixels identify its neighborhood for local computations.

By means of structuring elements, several geometrical properties of binary images can be measured which are immediately transformable into geometrical probabilities.

In a square raster, for example, each element can be considered as surrounded by eight neighbors. Suppose that our structuring element B is a square array of 3 x 3 black pixels. Each pixel in a picture A is either black or white. By overlapping the structuring element with the pixels of the image we can make the pixel corresponding with the centre of the structuring element black if at least one of its neighbors is black. We call this operation a dilatation. We can write for the transformed image $C = \oplus B$, where the symbol $\oplus$ indicates a Minkowski addition as defined by Matheron (1975), and briefly reviewed by Watson (1975).

An opposite transformation of A can be obtained by making the pixels in the picture white if at least one of the pixels in the neighborhood is white. We call this operation an erosion. For the transformed image D we can write $D = A \ominus B$, where the symbol $\ominus$ indicates a Minkowski difference. These operations can be applied successively to the transformed images. We call opening of an image by a structuring element, an erosion followed by a dilatation.

Closing is a dilatation followed by an erosion. Extensive application background to these concepts can be found in Serra (1975,1976).

Figure 5.4 shows some transformations of a simple image A of 31 x 12 pixels by different structuring elements B_1 to B_4, in which the 1's represent the valid points of the neighborhoods to be considered for the transformations.

In general a transformation is evaluated according to the portion of pixels whose status has changed during the transformation. Logical operations between images befor and after the transformations produce binary images of all the pixels which have changed status. In this way expressions of single geometric attributes can be readily extracted and displayed.

All the transformations described in Figure 5.4 have been restricted to the following two cases: (1) "change status of pixel at the centre to 1 if at least a 1 matches with the structuring element" (dilatation), and (2) "change status of pixel at centre to 0 if at least a 1 mismatches with the structuring element" (erosion). The structuring elements used in Figure 5.4 were designed to be (m) x (n) arrays of binary pixels where (m) and (n) are odd integers ≥ 3. This was done in order to emphasize the similarity between structuring elements, binary neighborhoods and templates or small images. In particular the (m) x (n) structure is

Figure 5.4: Erosions and dilatation of a 32 pixels x 12 pixels artificial square raster binary image by different structuring elements B_1 to B_4. Structuring elements are shown below the transforms. White pixels in image A changed to black have been indicated by the symbol *; black pixels changed to white by the symbol +. Symbols 1 and . are for black and white pixels, respectively. Numbers of black pixels in each image or transform occur below to right of expression of transformation. In these structuring elements only the 1's identify the neighborhoods used in the transformations. The center pixels in the structuring elements are underlined.

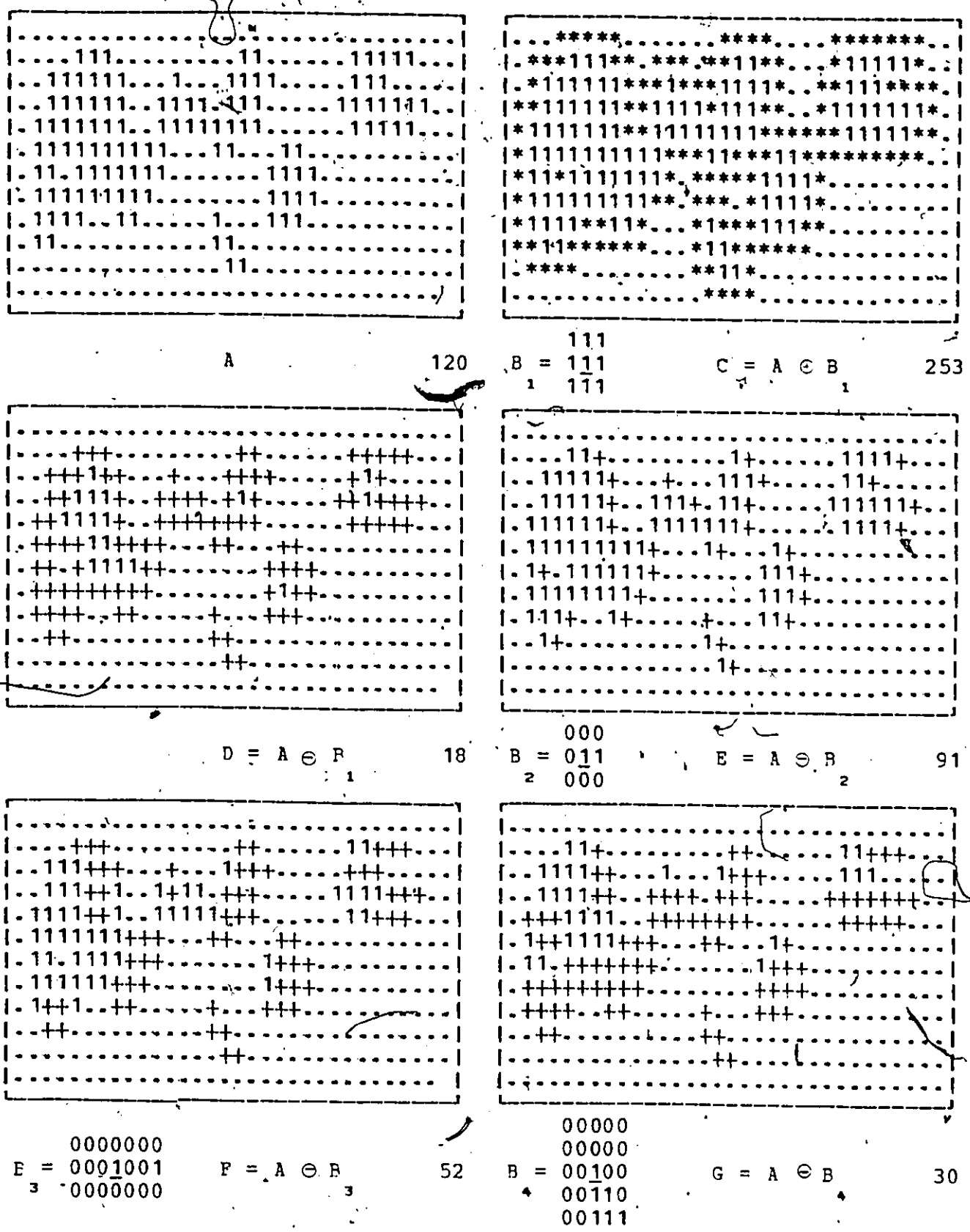

Figure 5.4: Concluded.

Figure 5.5: Erosions and dilatations of the same 32 pixels x 12 pixels square raster artificial binary image of Figure 5.4 by different structuring elements B_5 to B_{10}. Structuring elements are shown below the transforms. White pixels in image A changed to black have been indicated by the symbol *; black pixels changed to white by the symbol +. Symbols 1 and . are for black and white pixels, respectively. Numbers of black pixels in each image or transform occur below to the right of expression of transformation. In these structuring elements both the 1's and the 0's identify the neighborhoods used in the transformations (both 1's and 0's should coincide, i. e., match, with 1's and 0's in the image for computing the transformation). The center pixels in the structuring elements are underlined.

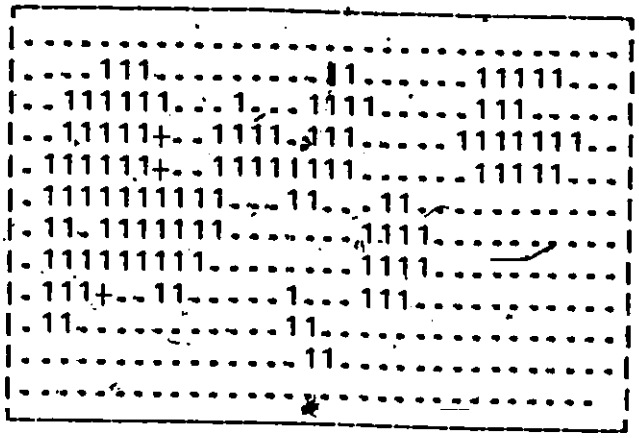

$B_5 = \underline{1}001$ $\quad H = A \ominus B_5$ $\quad 117$

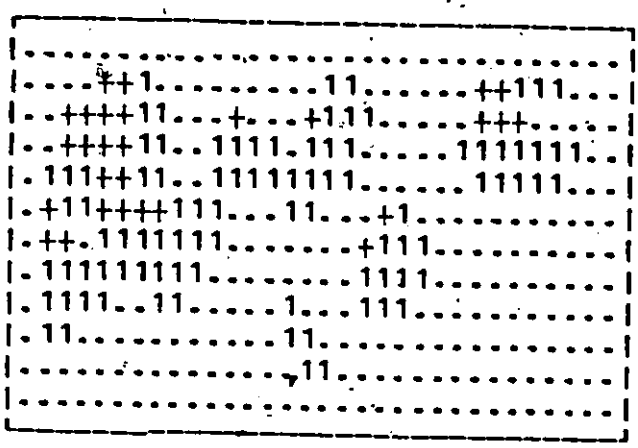

$B_6 = \begin{matrix}\underline{1}\\ \underline{11}\\ \underline{111}\end{matrix}$ $\quad I = A \ominus B_6$ $\quad 92$

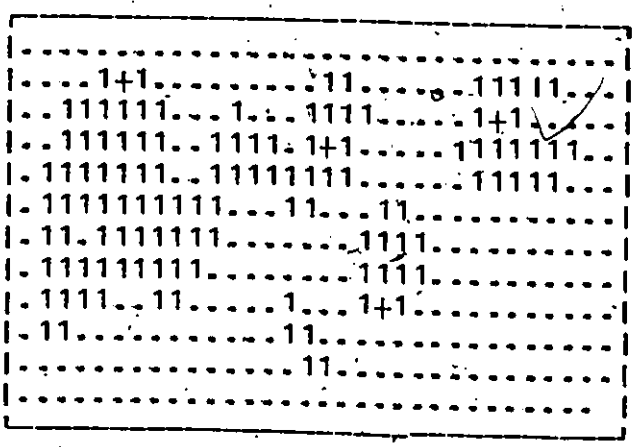

$B_7 = 01\underline{1}10$ $\quad J = A \ominus B_7$ $\quad 116$

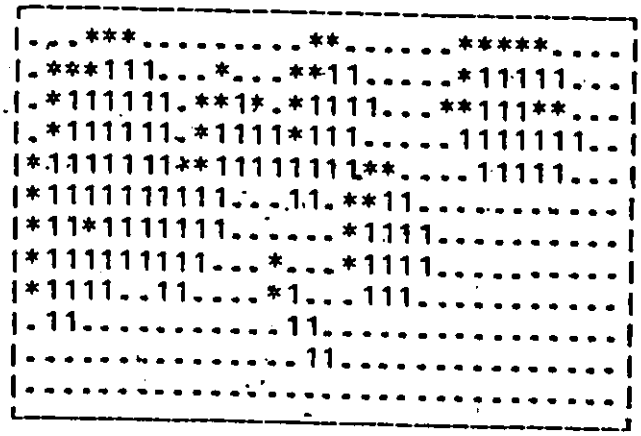

$B_8 = \underline{0}_1$ $\quad K = A \oplus B_8$ $\quad 165$

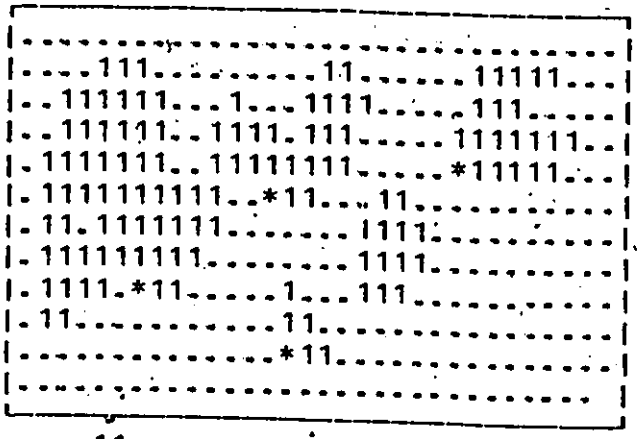

$B_9 = \begin{matrix}\underline{11}\\ \underline{01}\end{matrix}$ $\quad L = A \oplus B_9$ $\quad 124$

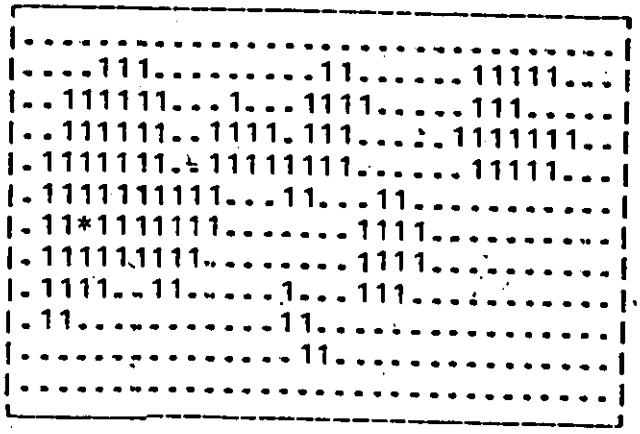

$B_{10} = \begin{matrix}\underline{1}\\ \underline{101}\\ \underline{1}\end{matrix}$ $\quad M = A \oplus B_{10}$ $\quad 121$

Figure 5.5: Concluded.

useful in programming the transformations with generalized structuring elements because the mapping of their centre pixel throughout an image is considerably simplified as we will see later on.

Transformations can be generalized further to cases in which the matches have to occur for the 0's as well as for the 1's. The logic for the transformations then changes to:"if matching is perfect for all valid 0's and 1's in the structuring element, the image pixel at its centre changes from 1 to 0 for an erosion (3), and changes from 0 to 1 for a dilatation (4)". For such transformations, however, erosions can be obtained when the structuring element has a 1 at its centre; for dilatations there must be a 0.

Figure 5.5 shows erosions and dilatations of the same image in Figure 5.3, by several structuring elements. Transformation rules (3) and (4) are used.

The programming approach chosen has been generalized for both the square and the hexagonal rasters. It is illustrative to consider few transformations of an artificial hexagonal image which have been described by Serra (1978). Figure 5.6 shows how Serra's transformations are obtained in the algorithms developed in GIAPP.

The examples shown in Figures 5.3 and 5.6 indicate transformations for which a structuring element is created as a small (m), x (n) binary image: it is the pattern within

Figure 5.6: Erosion of an artificial 14 pixels x 20 pixels hexagonal binary image by different hexagonal structuring elements B_1 to B_5. Structuring elements are shown below the transforms. Black pixels which turned into white pixels during the transformations are indicated by the symbol #. Symbols 1 and . are for black and white pixels, respectively. Number of black pixels in each image or transform occur below to the right of expressions for transformations. In the structuring elements representations, when the entire hexagonal neighborhoods are indicated, only the 1's identify the part of the neighborhoods used in the transformation, i. e., for B_1 and B_5; when only some pixels are considered in the neighborhoods but both 0's and 1's are used, only those are indicated (i. e., other pixels which surround them within the hexagonal neighborhoods are only used for "mapping" the center pixel). Center pixels in the structuring elements are underlined. This image was taken from Serra (1978).

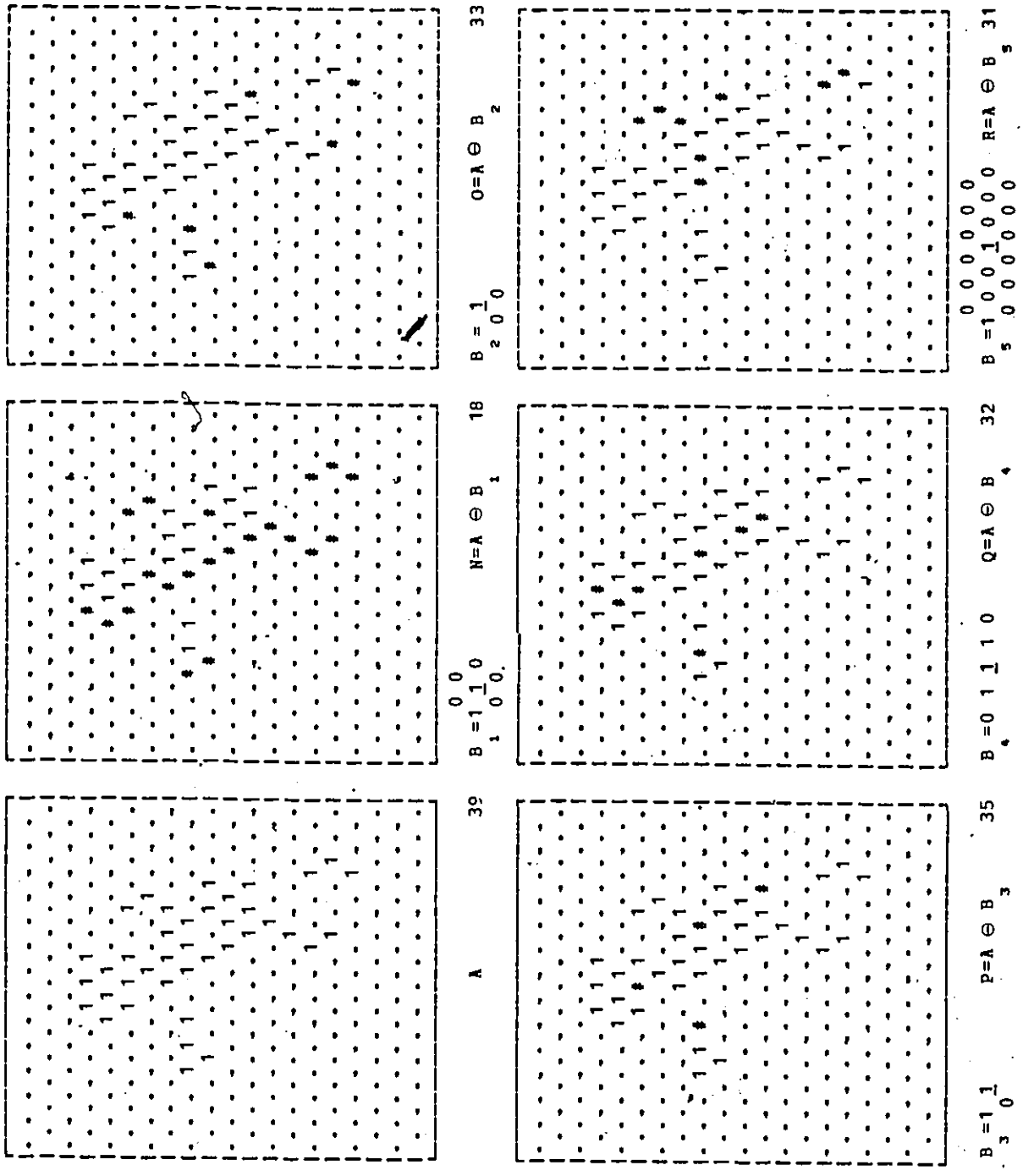

Figure 5.6: Concluded.

the structuring element that transforms another binary image according to the degree of matching locally occurring. This concept can be generalized further for different degrees of matching and also for non binary images, as is generally done in the technique of template matching by Rosenfeld and Kak (1976).

5.6 Parallel processing algorithms for Minkowski-type transformations of binary images on a minicomputer

A binary image has only two values of grey level: 0 or 1 which we can consider as white or black respectively. It can be obtained directly by mechanical digitization or by thresholding a grey level or by thresholding a grey-level image at a given value: lower values become 0's, higher values become 1's, or vice versa.

Binary data can be compressed so that to each 0-1 pixel an "OFF"-ON" bit status corresponds. This is done in order: (a) to economize in memory storage, (b) to expedite I/O and computations, and (c) to utilize efficiently logical and bit shift operators which exist on most computers.

As previously mentioned, in GIAPP all transformations are programmed in FORTRAN. Parallel processing, the contemporaneous transformation of the pixels of a binary image, is simulated for arrays of 1024 bits (1080 bits in the Cyber

computer), corresponding to individual rows of picture data. Logical operations between vectors of words (rows of image data), bit shift operations between vectors of 1024 bits (64 words), bit counting, bit status cecking, and bit status setting operations, are combined into programs for parallel processing of binary compressed images.

Four algorithms have been programmed in GIAPP for the following computations: (1) logical operations, (2) binary neighborhood transformations in which only matching or mismatching 1's are considered for both the square and the hexagonal images , (3) binary neighborhood transformations in which both the matching 0's and the matching 1's are considered, and (4) auto- and cross-correlation (geometrical covariance and cross-covariance). Simplified operational flowcharts for these four algorithms are shown in Figures 5.7, 5.8, 5.10, and 5.11. The operational flowcharts are self exlanatory, however, Figure 5.9 describes in detail the processing in "parallel" for computation (2) of Figure 5.8.

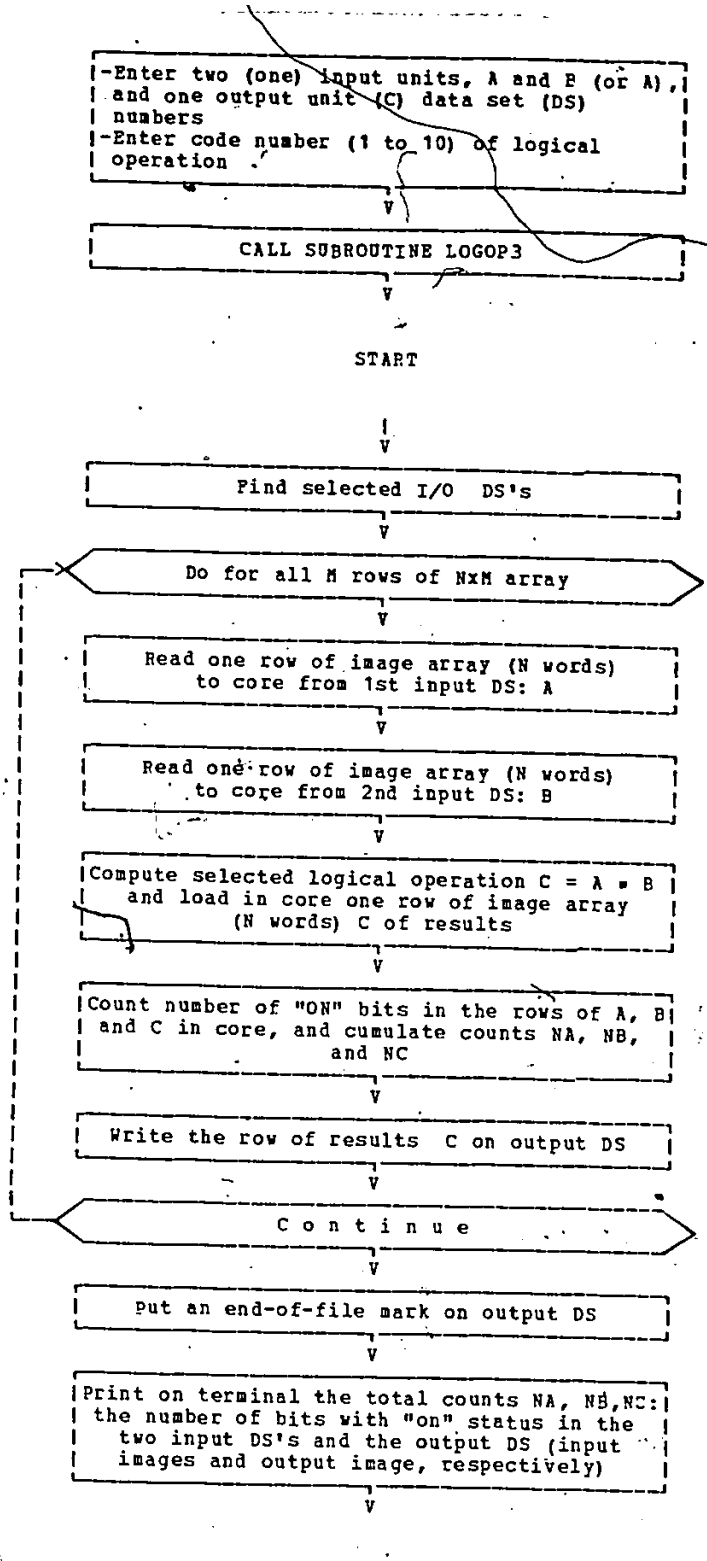

Figure 5.7: Generalized flowchart of an algorithm for logical operations between two binary compressed (one bit per pixel) images in GIAPP.

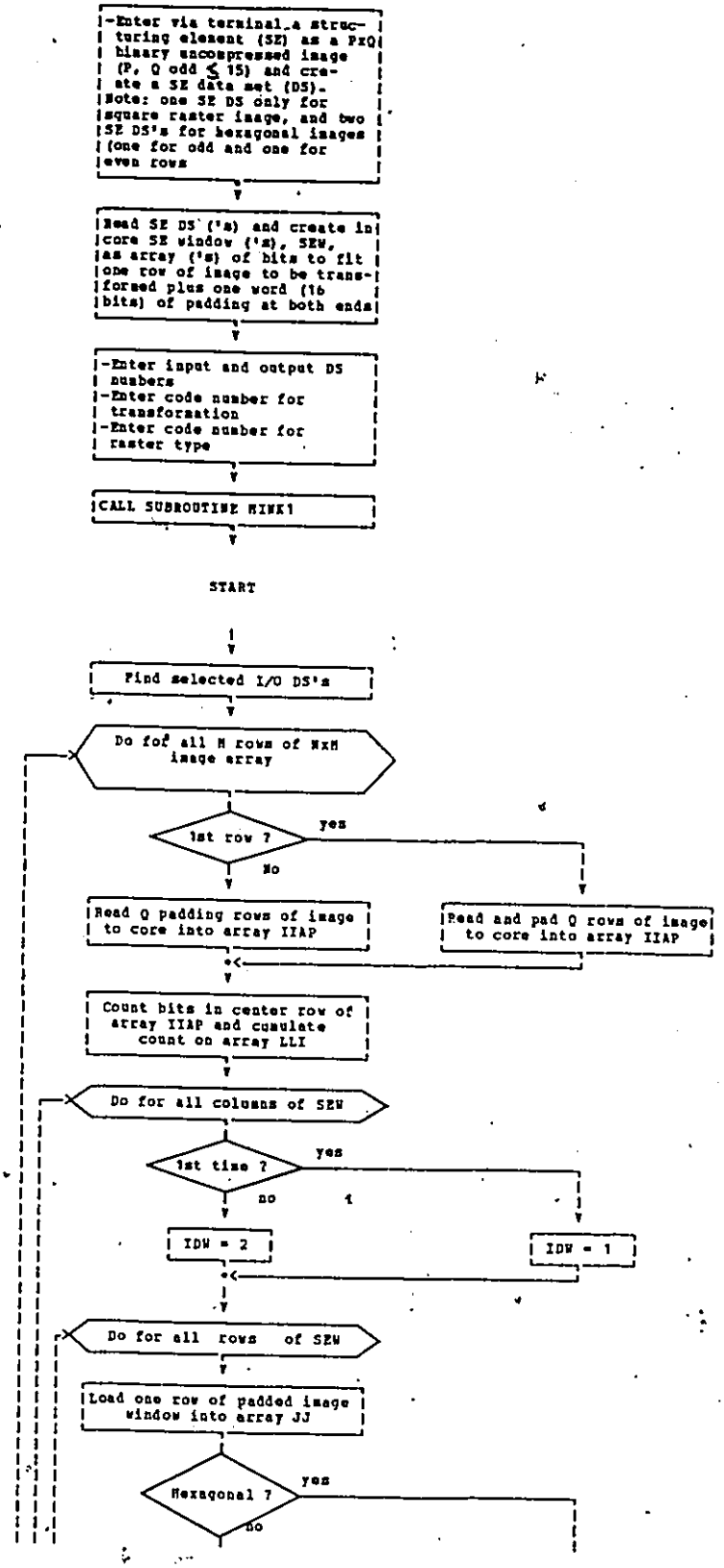

Figure 5.8: Generalized flowchart of an algorithm for structuring element binary (bit) transformations of binary compressed images in GIAPP: only matchings or mismatchings of binary 1's are considered in these transformations.

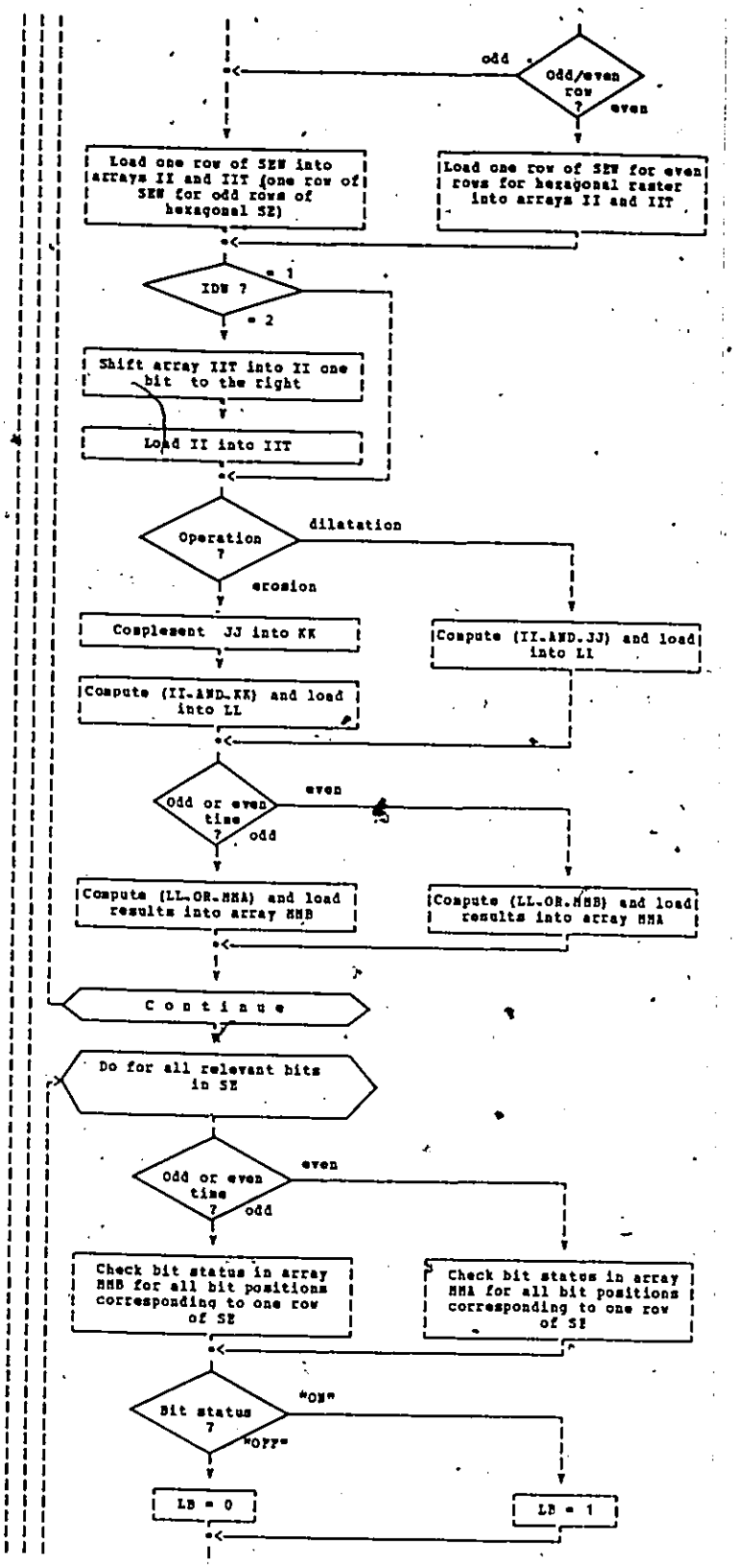

Figure 5.8: Continued.

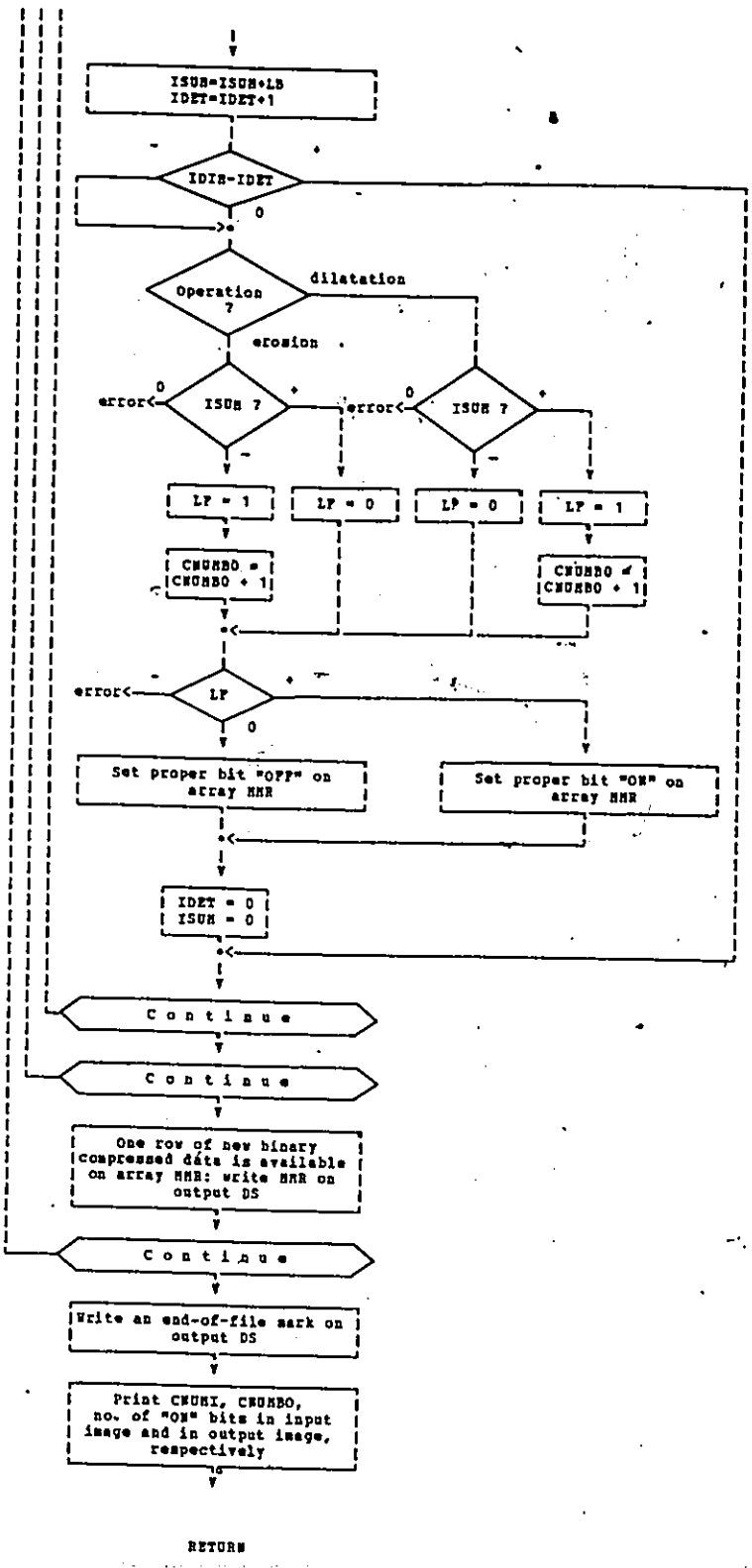

Figure 5.8: Concluded.

Figure 5.9: Example of "parallel" processing of a binary compressed image in GIAPP's SUBROUTINE MINK1 (described in Figure 5.8). The structuring element is expanded into structuring element windows to fit the image to be transformed. Both image and structuring element windows are "padded" (i. e., filled with 16 bits of binary 0 values at both left and right ends of each row. One row of padding is also added to the top and bottom of the image. Each row of structuring element window either shifted or unshifted is compared with the corresponding row of image window containing as many rows as there are in the structuring element window. The comparison with all rows of structuring element windows for shifts 0, 1, and 2, are computed and one row of output image is generated, before shifting the image window down the image one row. The processing continues until the last row of output image is completed. Both eroded image and dilatated image are displayed in the lower part of the illustration. The dimensions of the input and of the output images are 31 pixels x 12 pixels. The symbols 1 and . are used for indicating black and white pixels, respectively; this is so also for the structuring element and the structuring element windows where the center pixel is underlined. Only the 1's in the structuring element represented are used, in this case, for computing the two transformations. Comparison, i. e., the operation of .AND.'ing, is computed between two words at a time, each of 16 pixels (in reality this is done for two sets of 64 words at a time): this represents a degree of "parallellism", function of the word length (number of bits) of the computer. The processing can also be considered "pipelined", since the computations are structured row by row in order to optimize between processing time and available memory. I/O access time is minimized because advantage is taken of the machine-dipendent instruction set available for logical operations and also for bit shift operations for arrays of 64 words (i. e., 1024 bits).

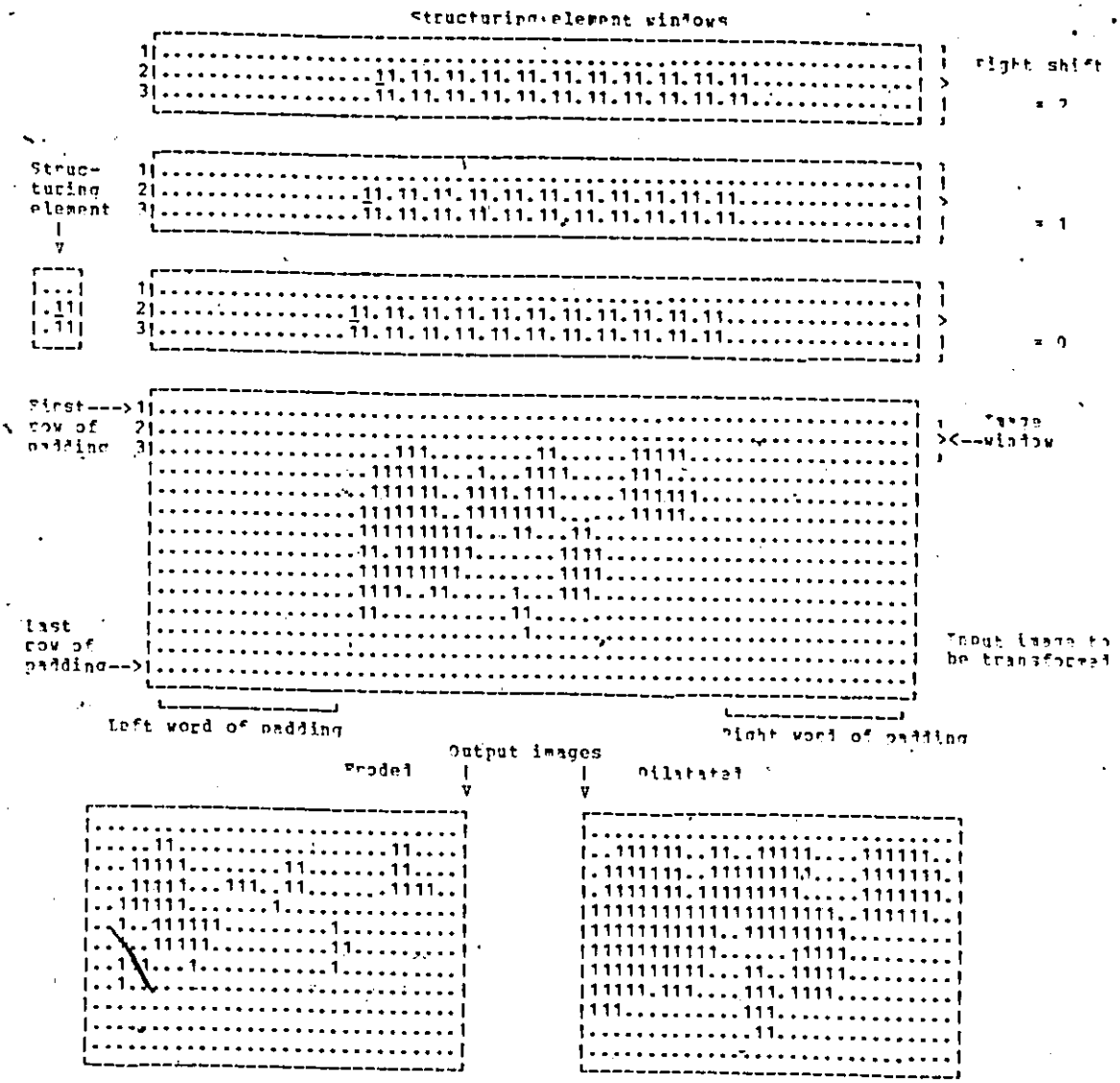

Figure 5.9: Concluded.

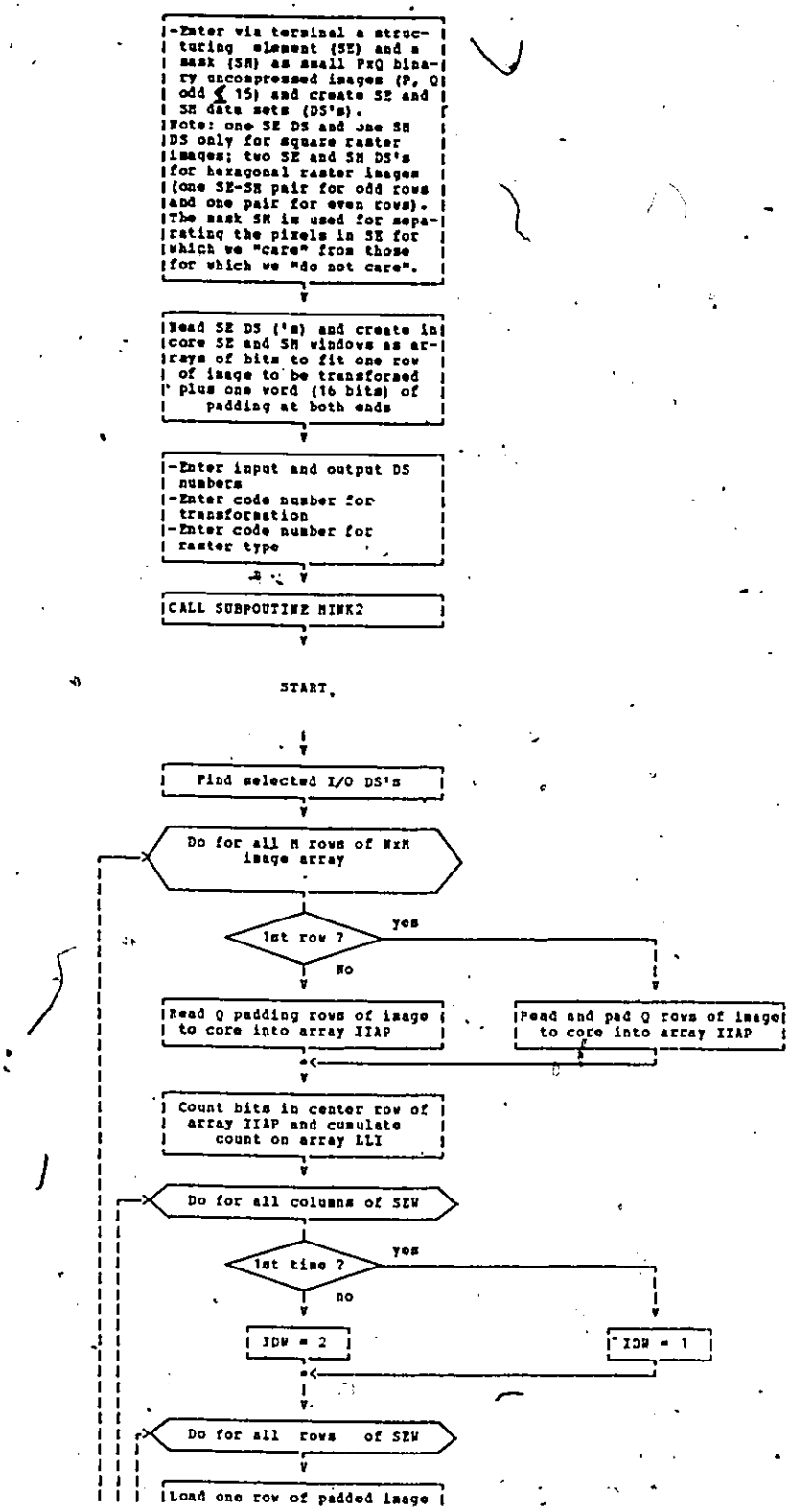

Figure 5.10: Generalized flowchart of an algorithm for structuring element binary (bit) transformations of binary compressed images in GIAPP: both matching and mismathching 1's and 0's are considered in these transformations.

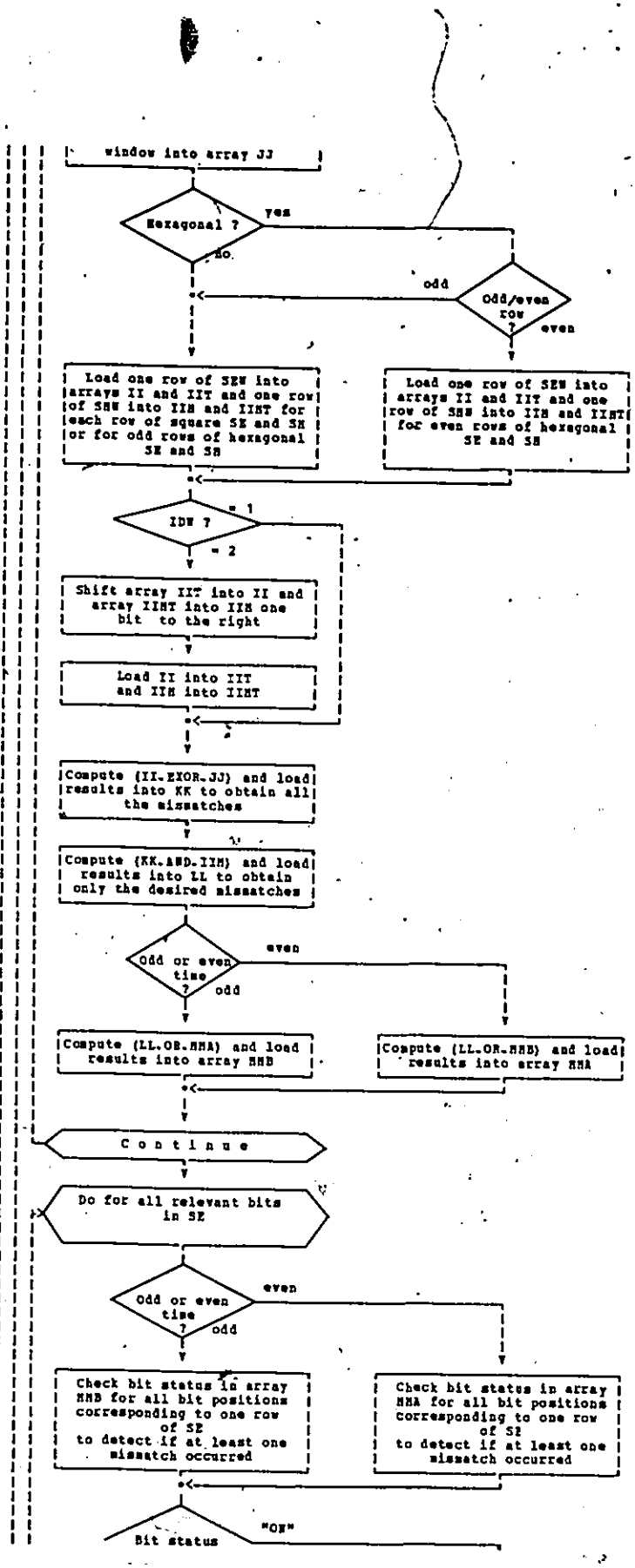

Figure 5.10: Continued.

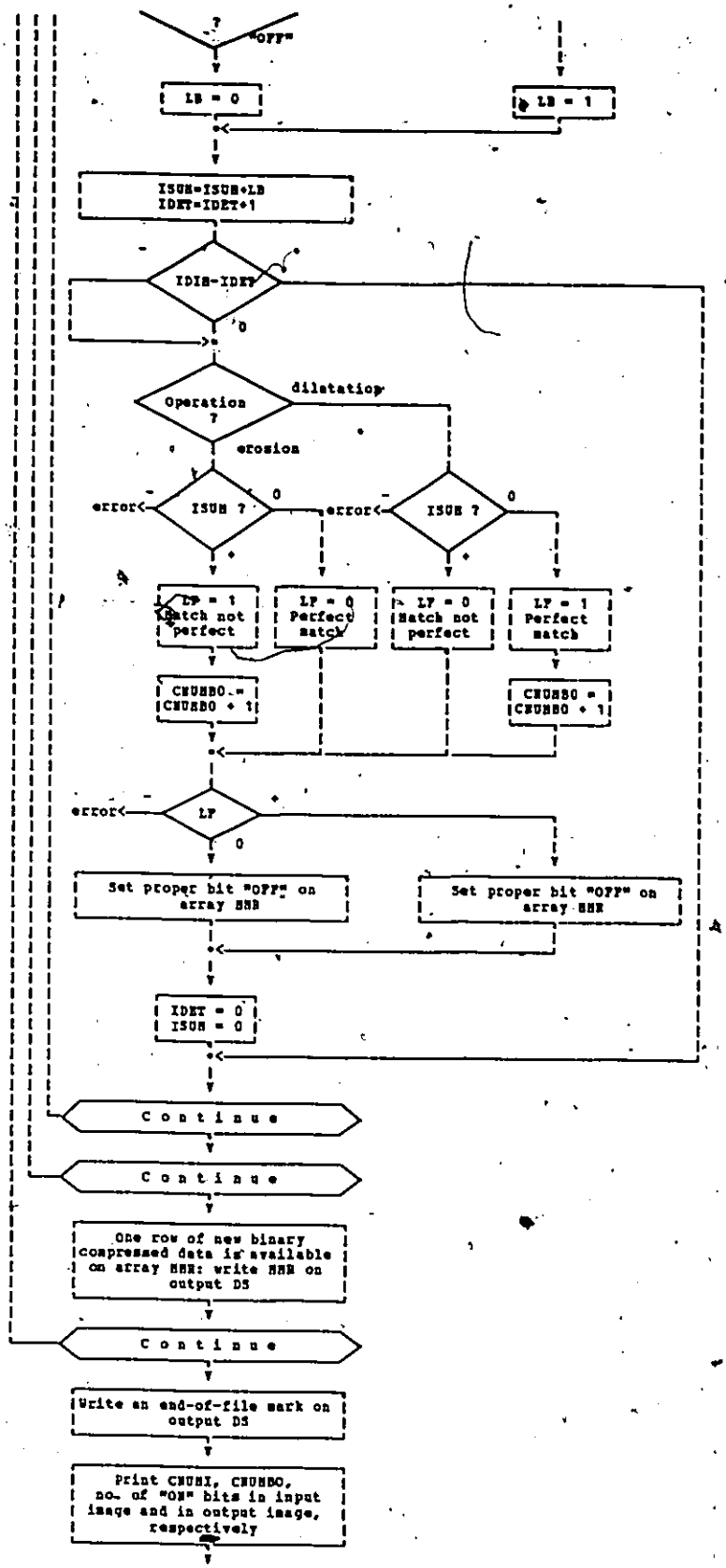

Figure 5.10: Concluded.

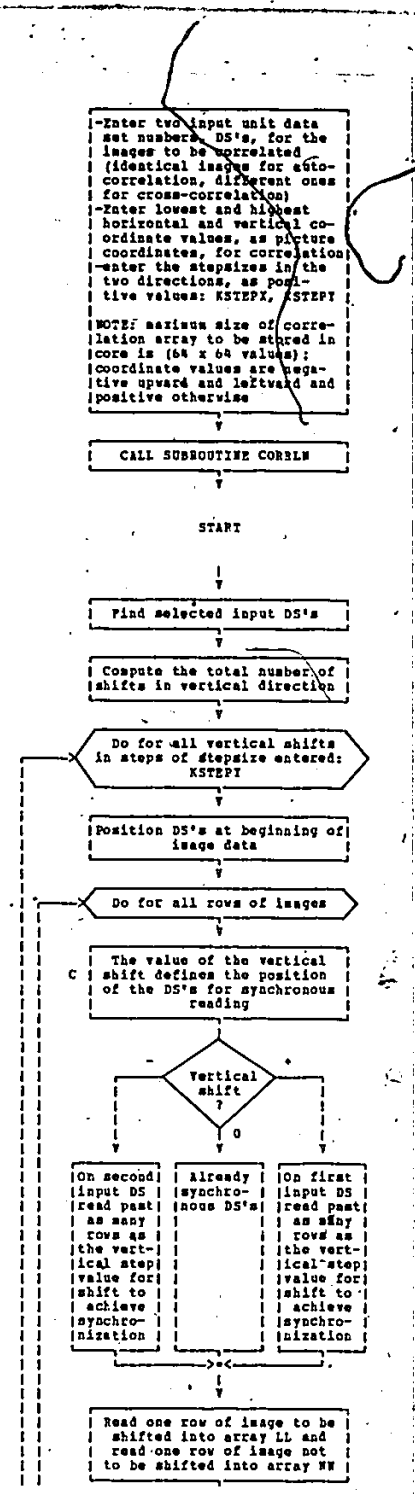

Figure 5.11: Generalized flowchart of an algorithm for computing the two-dimensional geometrical auto-covariance of a binary compressed image and the two-dimensional geometrical cross-covariance between two binary compressed images in GIAPP.

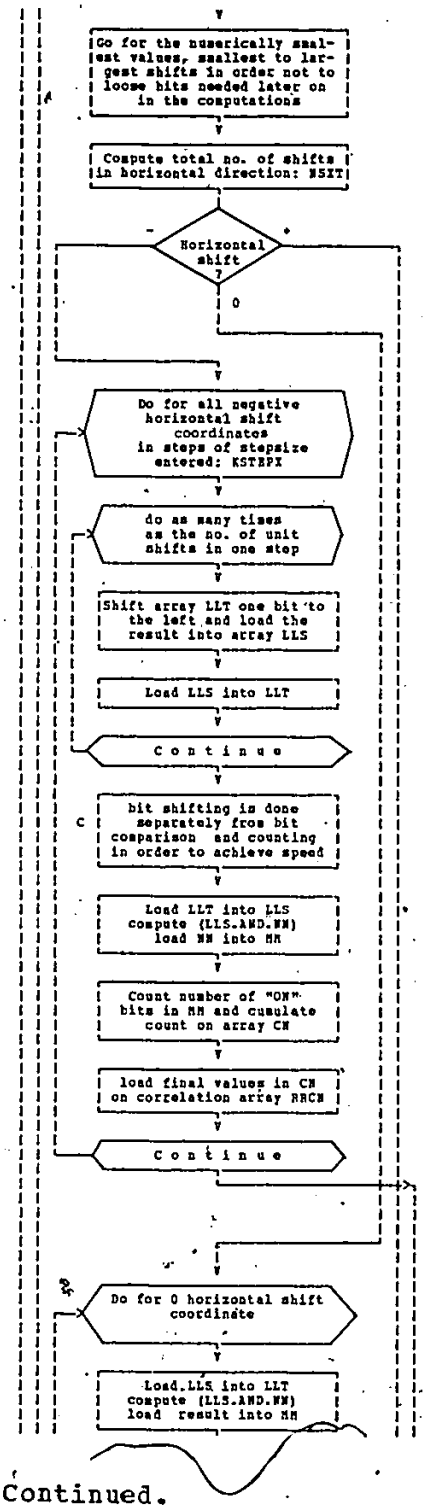

Figure 5.11: Continued.

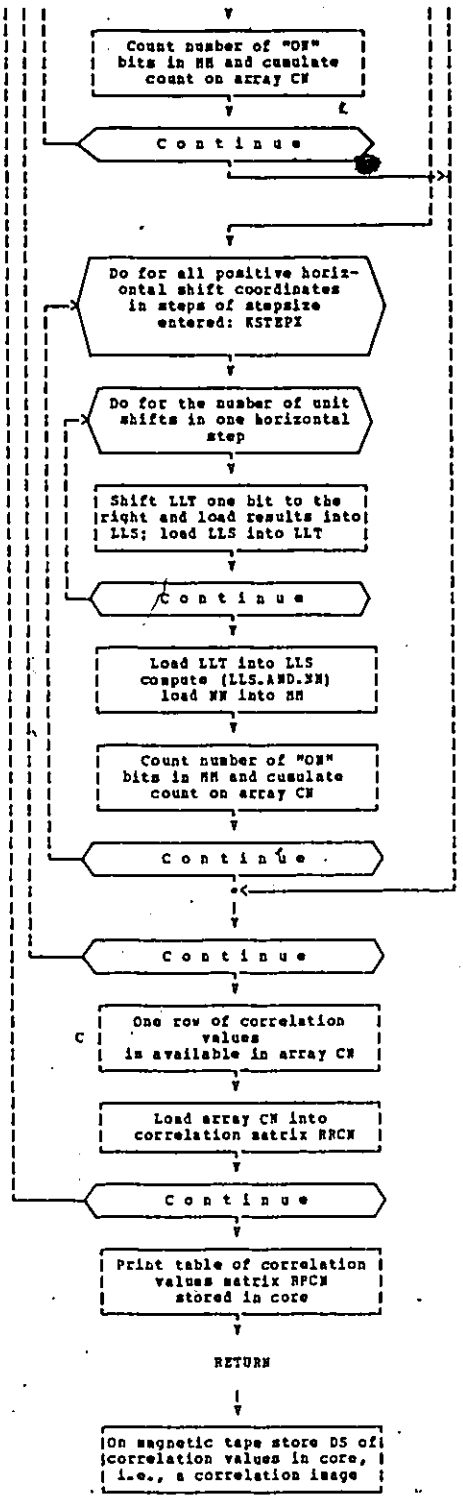

Figure 5.11: Concluded.

6. Some simple examples of processing geological data

6.1 Introduction

The experiments which will be treated in the following sections are of a descriptive nature: their aim is to introduce and explain the type of measurements and statistical estimates which are obtained from either large regional geological maps or microscopic images of rocks in thin sections. Concepts of spatial correlation of stratigraphic units quantified from geological maps and concepts of quantitative characterization of microtextures (texture analysis) will be illustrated by transformations of binary images obtained from a flying spot scanner or from a graphic tablet digitizer. According to mathematical morphology theory, geometrical characteristics of binary images can be measured by structuring elements, and thus transformed into quantitative descriptions or geometrical probabilities associated with the patterns in the images.

6.2 Study of a geological map pattern near Bathurst, New Brunswick

6.2.1 Introduction

The example to be discussed was selected initially in 1977 for a study on the quantitative stratigraphic correlation of rock units and other features represented on geological maps (Agterberg and Fabbri, 1978a). In 1979 this example was analyzed again by the author using some of the images previously studied by Agterberg and Fabbri (1978a) but obtaining a number of new results which also will be described here.

This study aims at the quantitative characterization and correlation of combinations of litho-stratigraphic units coded from geological maps. Geological maps and ancillary information, generally also in map form, are constructed for being of assistance in the following tasks: (1) in making interpretations, (2) in planning new surveys or searching strategies, and (3) in providing up-to-date syntheses on some geological processes for the prediction of other geological aspects.

Rock units on a map can be quantified with respect to a cell centered about an arbitrary point, and the average composition per cell can be determined as in Fabbri (1975). Mineral deposits tend to occur in regional environments of specific types. As exemplified by Agterberg et al (1972), it is useful to attempt to define these environments for systematic comparison to other environments in the same region.

Let us call "deposit cell" a random cell which contains one or more deposits of a specific type. We can compare the statistical population of the deposit cell with the population of the random cell. If the random cell is sufficiently small, it tends to contain only one rock type, and only one deposit. A geological map, then, can be quantified by subdividing it into a regular grid of many small cells, and assigning to each cell the rock types which occur at its center. Suppose that rock type i has n_i cells in a region and that n_{id} of these cells contain a deposit. Then the probability that a random cell in rock type i is a deposit cell is equal to n_{id}/n_i. In addition to this probability, we have to consider that the probability of occurrence of a deposit also may depend on the spatial pattern of litho-stratigraphic units at some distance, for example 10 km, from the deposits.

Let us consider a geological map as a set of map units, each representing the shape and distribution, in at least two dimensions, of the litho-stratigraphic units in the map. Over the entire surface of the geological map, each unit, distinguished by its color or graphical pattern, will occupy a given area. We can consider each map unit as a black pattern in a binary image (1-0 or black and white) in which the white background represents the area occupied by all other map units together. Suppose that a very small cell (a

square, a circle, a hexagon or an octagon) is placed at random over the map area. The probability that such a random cell will "hit" the pattern will be proportional to the area occupied by the pattern in the map; conversely the probability that our random cell will "miss" the pattern, will be proportional to the area occupied by all the other units together. If the cell is sufficiently small, it will fall entirely inside our pattern, or entirely outside it. When the cell is translated throughout the area to the intersections of a regular finely spaced grid, the area proportion of the pattern and the probability that our cell will hit the pattern will be expressed by the same value.

Let us consider the binary pattern for some ancillary data in map form, similar to the black point (pixel) distribution pattern of mineral deposits. The probability that our random cell will contain one deposit is a function of the cell size and the number and distribution of the points in the pattern. If our cell is so small that it can only contain one of the points at a time, and is translated in a regularly fashion as before, the area proportion of the blach point pattern in the map and the probability of hitting the point pattern with our cell probe will have the same value.

When, in patterns systematically quantified from maps, we can identify conditions favourable to the occurrence of

mineralizations (or other ancillary events) the geometric probabilities associated with these patterns can be combined with the probabilities associated with the distribution of mineral occurrences. This concept is our base for developing predictive methods. A relatively simple application of this concept is presented here.

6.2.2 The map pattern

The geology of the Bathurst area, New Brunswick, has been described by Skinner (1974). Forty known massive sulphide deposits from this area are related genetically to the occurrence of the acidic volcanic rocks of the Tetagouche Group of Middle-Late Ordovician age. These acidic volcanics were coded from 2 miles geological maps (scale 1:126720) from an experimental data base described in Fabbri, Divi, and Wong (1975). The pattern of acidic volcanics was drawn separately in black and white and photographed on a 35 mm color film. The film was later digitized on the flying spot scanner as a set of 18843 pixels on a square raster with a total of 324 x 320 = 103680 binary pixels. The spacing of the pixels is 259 m in the north-south and east-west directions. The resulting binary images (shown in Figure 6.1a) was obtained by thresholding of the grey-level image produced from the flying spot scanner. The square area

digitized corresponds to 84 x 83 km . The same pattern also was scanned according to a hexagonal raster configuration as a set of 22925 black pixels within an image of 313 x 349 = 109237 pixels spaced 256 m apart. Each pixel in this second image can be considered as a hexagon of 256 m of minimum diameter with its center at that distance from the center of any adjacent neighboring pixel. This image is shown in Figure 6.6a.

Figure 6.1: Erosions, dilatations of binary images of acidic volcanics in Bathurst area, New Brunswick. The original image A is shown in (a); there are 18843 black pixels in this image. The complement of A, A^c is shown in (b); there are 84837 black pixels in this image. Writing B for the operator set of 8-neighbor expansion, the transformed images are as follows. (c) $A \oplus B$; there are 23076 black pixels in this image. (d) $A \oplus 2B$; there are 27102 black pixels in this image. (e) $A \oplus 3B$; there are 29560 black pixels in this image. (f) $(A \oplus B) \cap A^c$; there are 5133 black pixels in this image. (g) $A \cap (A \ominus B)^c$; there are 5360 black pixels in this image. (h) $A \ominus B$; there are 13483 black pixels in this image. (i) $A \ominus 2B$; there are 9990 black pixels in this image. (j) $A \ominus 3B$; there are 7635 black pixels in this image. Dimensions of image are 84 km x 83 km, North direction points upwards.

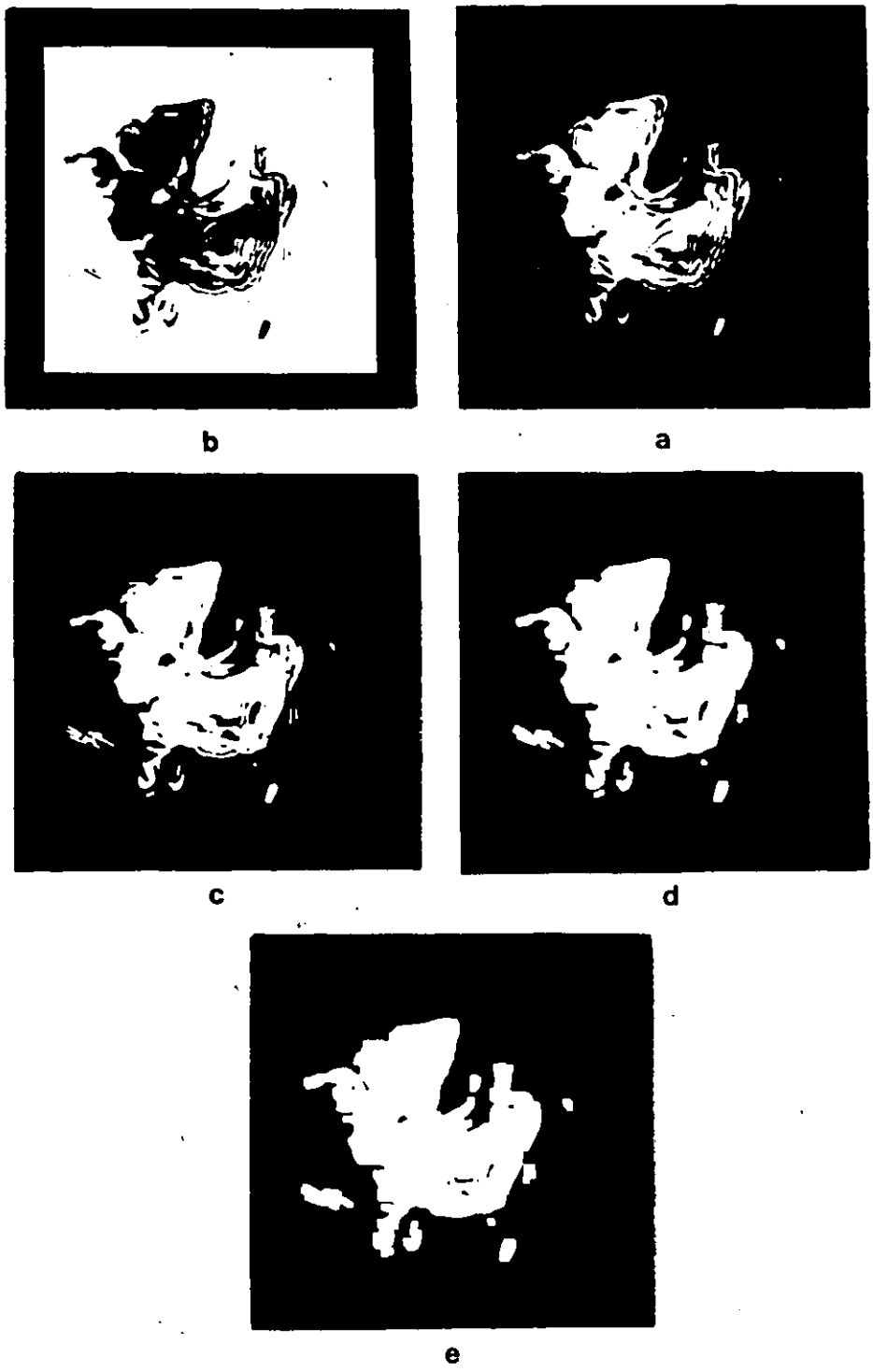

Figure 6.1: Continued

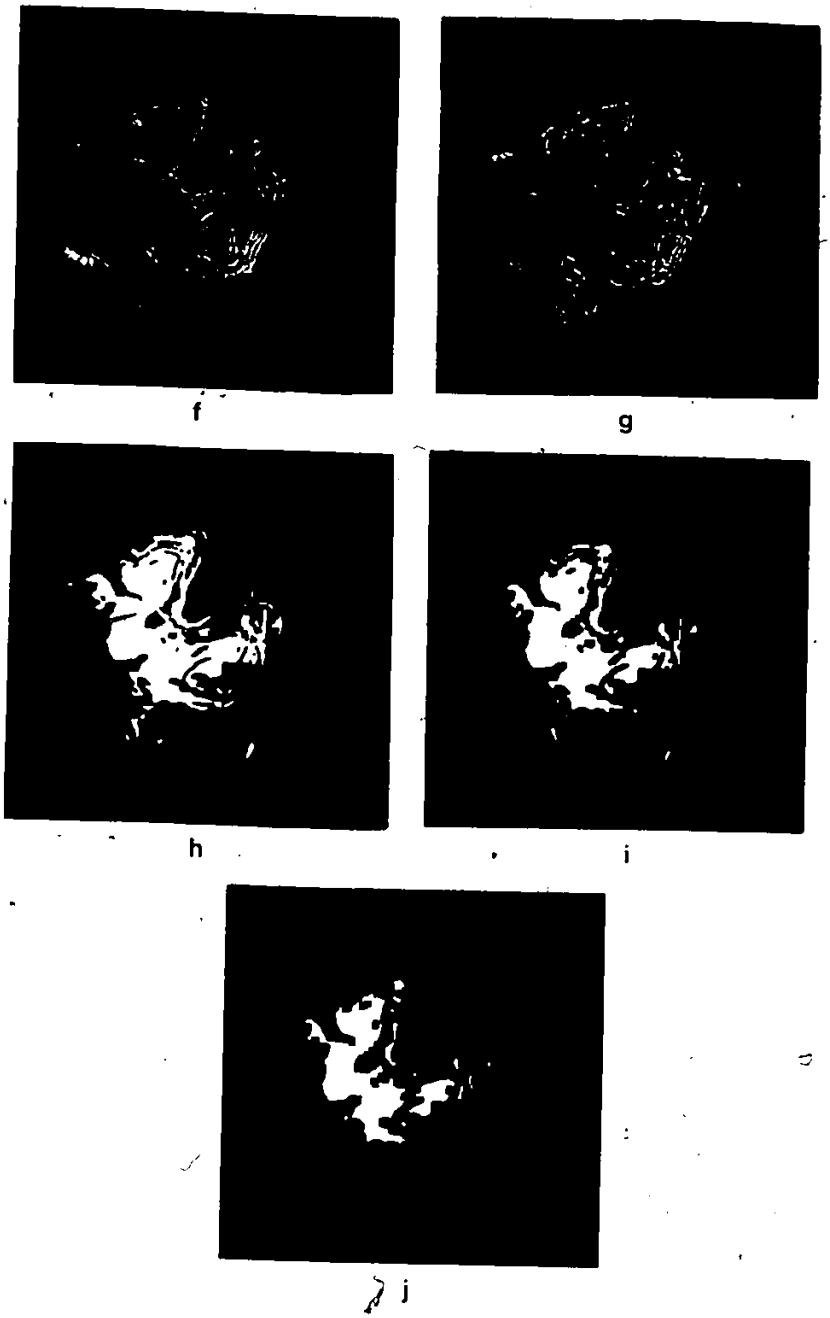

Figure 6.1: Concluded

According to Skinner (1974) the mapping of the Tetagouche Group is based on lithological units that have no stratigraphic significance because stratigraphy and structure of the Group have not yet been determined. These units are characterized by : (1) sedimentary rocks, (2) metabasalts, and (3) rhyolitic rocks. The rhyolitic unit is shown in Figures 6.1a and 6.6a. The rhyolitic rocks are interpreted by the author as the youngest part of the Group, surrounded by sedimentary rocks, the oldest part. The rhyolitic rocks, acidic volcanics, are possibly of ignimbritic (pyroclastic flow) origin.

6.2.3 Erosions and dilatations

In a square raster each pixel is surrounded by eight neighboring pixels. The eight pixels around any black pixel belonging to the image of Figure 6.1a, are either black or white. Suppose that they are changed into black pixels if they are white. This operation is termed 8-neighbor expansion (Rosenfeld and Kak, 1976) or dilatation. The result is a new image with 23976 pixels, shown in Figure 6.1c. The difference between the two images, Figures 6.1a and 6.1c, consists of 23976 - 18843 =5133 pixels and is shown in Figure 6.1f. A second dilatation gives the pattern of Figure 6.1d; a third dilatation produces the pattern of

Figure 6.1e. The reverse operation which consists of proceding from the image on Figure 6.1a to that of Figure 6.1h can be termed an 8-neighbor shrinking or erosion. Three successive erosions of the original image in Figure 6.1a, are shown in Figures 6.1h, 6.1i and 6.1j, respectively. The black pixels which turned to white in the first erosion are shown in Figure 6.1g.

In order to continue the discussion of these transformations, we can adopt the terminology of mathematical morphology as developed in Serra (1976) and Watson (1975). Suppose that the original image in Figure 6.1a is a set A with measure mes A. This measure is the area and can be expressed either as mes A = 18843 pixels or as mes A = 1264.01 km² (one pixel represents an area of 259 x 259 m). Let B be the operator set of the 8-neighbor square logic. B has an origin which is located at the center of the square described by the eight neighboring pixels.

The images of Figures 6.1c and 6.1d now can be represented as the Minkowski sums $(A \oplus B)$ and $(A \oplus 2B)$, respectively. In Agterberg and Fabbri (1978a) a set nB was defined by induction with $nB = ((n - 1) B) \oplus B$ for $n = 2, 3, \ldots$. It is seen readily that operating on A with the set nB is identical to applying the successive operations $A \oplus nB = (A \oplus (n - 1) B) \oplus B$ for $n = 2, 3, \ldots$. By using the concept of Minkowski subtraction, the patterns of Figures

6.1h, 6.1i and 6.1j can be written as $(A \ominus B)$, $(A \ominus 2B)$ and $(A \ominus 3B)$, respectively.

If the superscipt ^{c} denotes complement of a set with respect to the universal set T which consists of all the pixels in use, then the pattern in Figure 6.1b can be written A^c; the patterns of Figures 6.1f and 6.1g are $(A \oplus B) \cap A^c$, and $A \cap (A \ominus B)^c$, respectively.

6.2.4 Cross-correlations

A set C was formed by assigning each of the 40 volcanogenic massive sulphide deposits in the area to the picture points closest to it on the grid with 259 m spacing used for the binary images of Figure 6.1a. C consists of 40 black pixels which can be subjected to successive dilatations by use of B. The images, sets $(C \oplus 4B)$, $(C \oplus 9b)$ and $(C \oplus 19B)$ are shown in Figures 6.2a, 6.2b and 6.2c, respectively.

Because each pixel is representative for a cell of 259 m on a side, the length of a cell generated by n dilatations is equal to $(2n + 1) \times 259$ m. Hence the cells obtained by 4,9, and 19 dilatations of a single picture point are 2.33 km, 4.92 km and 10.10 km, respectively. The latter two cell sizes can be used to approximate (5 km x 5 km) cells and (10 km x 10 km) cells, respectively. The binary images of Figures 6.2a, 6.2b and 6.2c can be intersected with that of

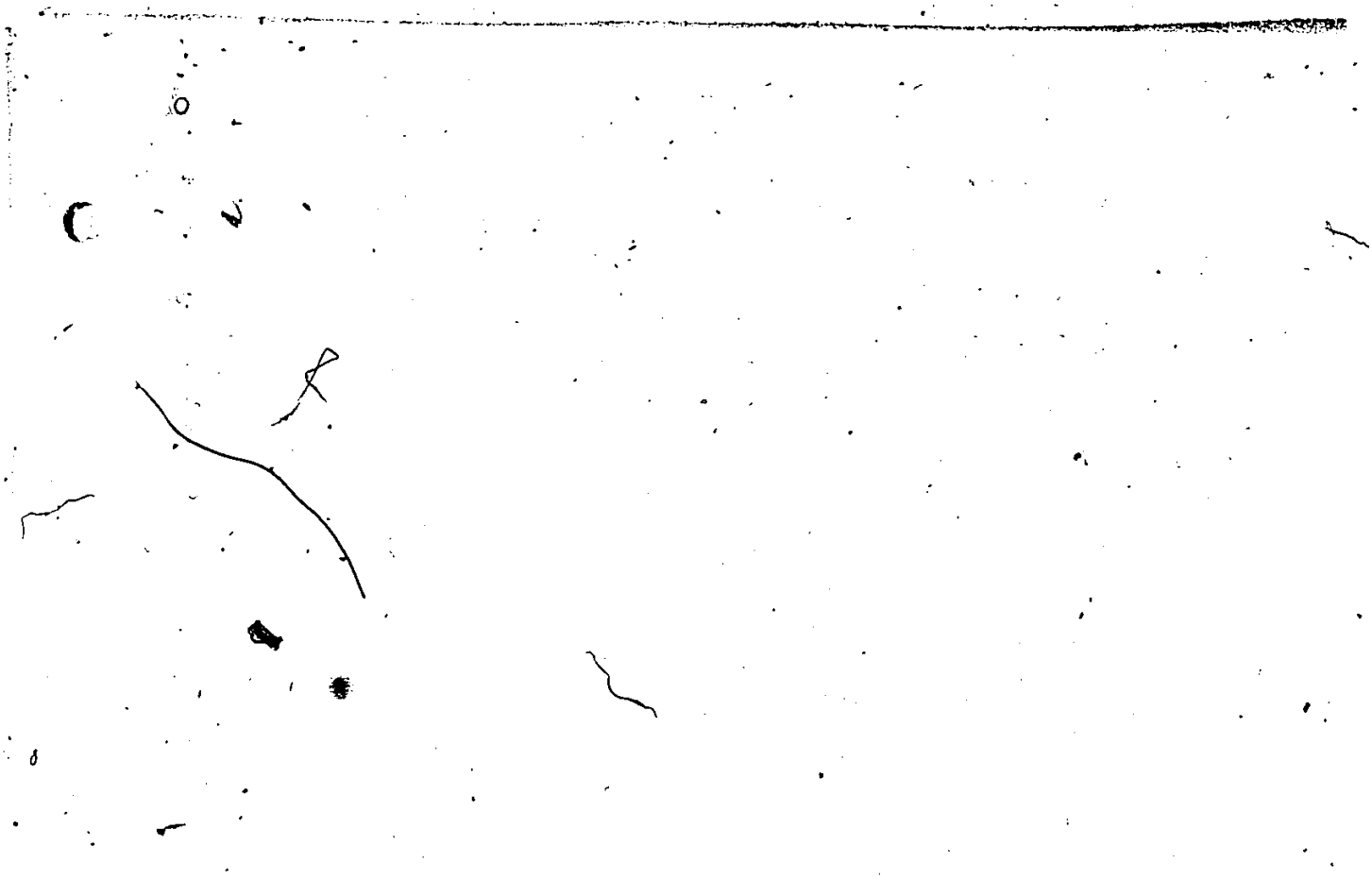

Figure 6.2: Dilatations of image set C for 40 deposit pixels and intersection of resulting sets with original image A in Figure 6.1a. (a) $C \oplus 4B$; there are 2342 black pixels in this image; (b) $A \cap (C \oplus 4B)$; there are 1512 black pixels in this image; (c) $C \oplus 9B$; there are 8390 black pixels in this image; (d) $A \cap (C \oplus 9B)$; there are 4501 black pixels in this image; (e) $C \oplus 19B$; there are 26654 black pixels in this image; and (f) $A \cap (C \oplus 19B)$; there are 12152 black pixels in this image.

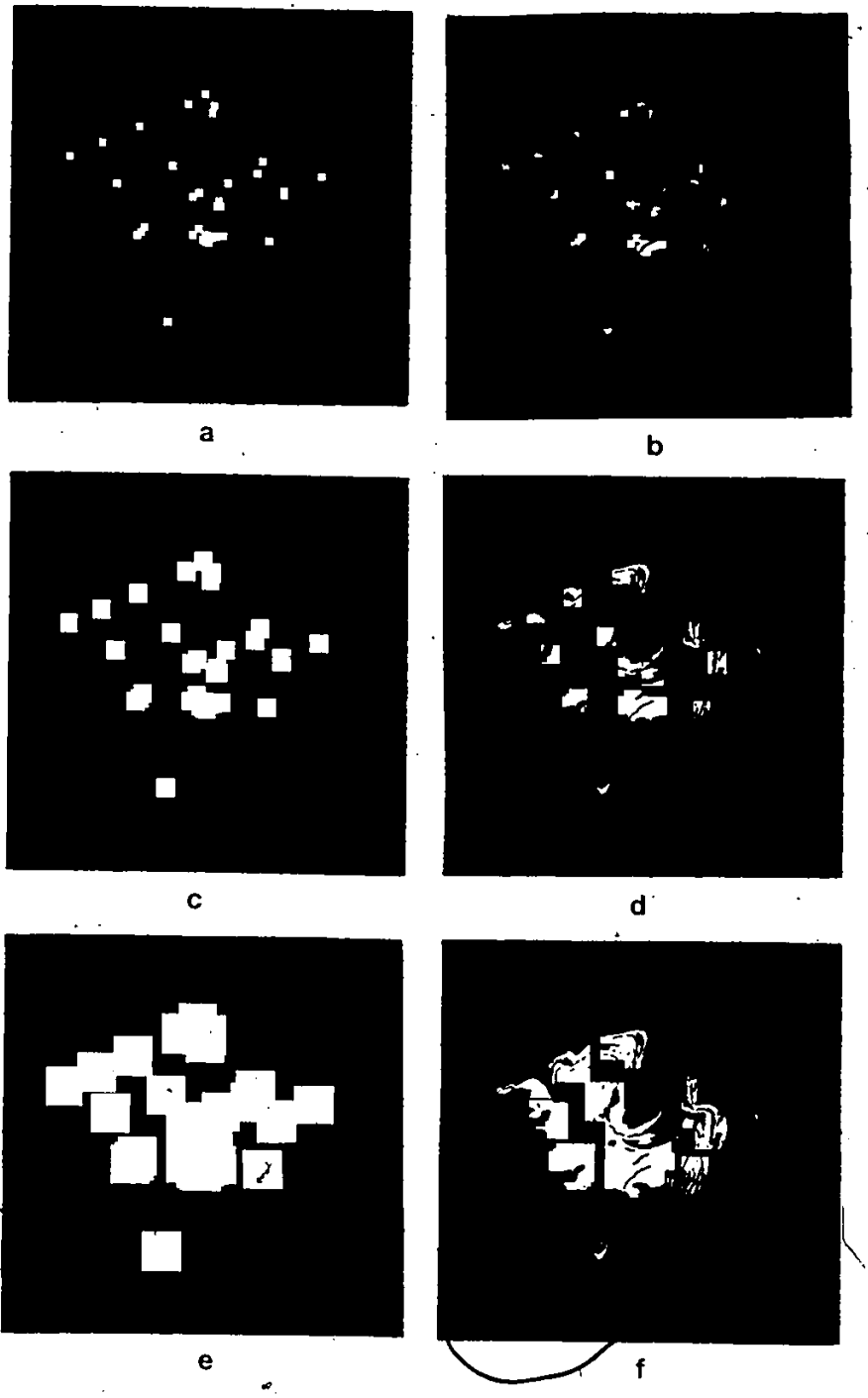

Figure 6.2: Concluded

Figure 6.1a. The resulting images, sets $(A \cap (C \oplus 4B))$, $(A \cap (C \oplus 9B))$ and $(A \cap (C \oplus 19B))$ are shown in figures 6.2d, 6.2e and 6.2f, respectively.

The erosion of Figure 6.1a can be continued from Figures 6.1h, 6.1i and 6.1j onward until not a single black pixel remains. Likewise, the dilatations can be continued from Figures 6.1c, 6.1d and 6.1e onward until most or all of the study area or image (set T) consists entirely of black pixels. The relative areas of the erosions and dilatations are shown in Figure 6.3. For dilatations each relative area can be interpreted as the probability P(nB) with

$$P(nB) = \text{mes } A \oplus nB \,/\, \text{mes } T \quad , \quad n = 1, 2, \ldots$$

that a random cell with side ((2n + 1) x 259) m contains one or more black pixels belonging to the original pattern of Figure 6.1a. The probability Q(nB) that a cell with size mes (C ⊕ nB) contains no acidic volcanics is equal to $Q(nB) = 1 - P(nB)$.

Likewise it is possible to measure the probability $P_d(nB)$ that a cell with side ((2n + 1) x 259) m is a deposit cell containing one or more deposits, as it is shown in Figure 6.4a, because

$$P_d(nB) = \text{mes } (C \oplus nB) \,/\, \text{mes } T \quad , \quad n = 1, 2, \ldots \; .$$

Another practical result is as follows. A correlation between sets A and C can be carried out by determining how

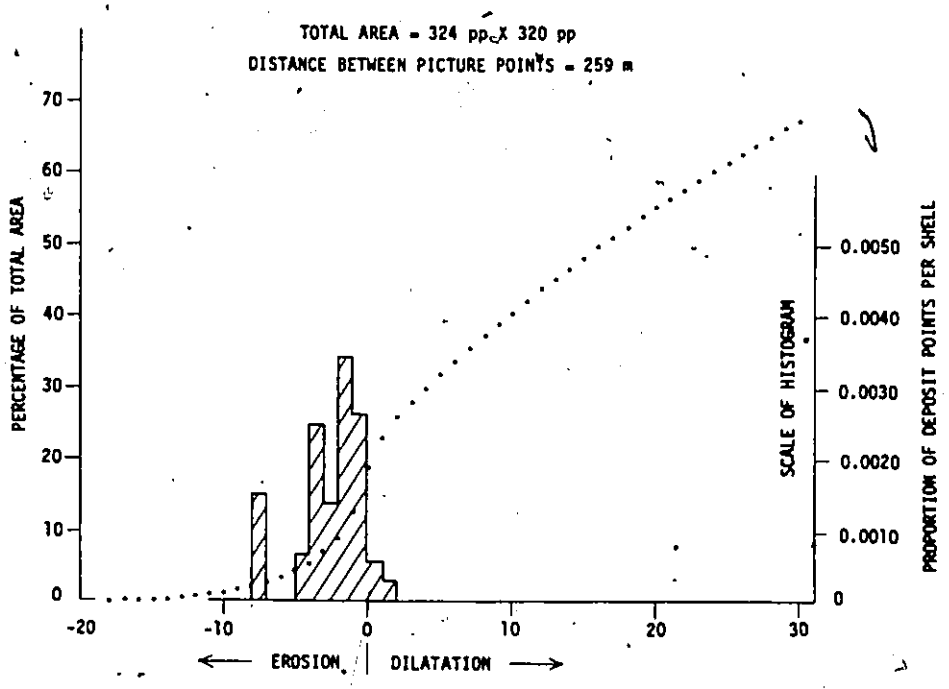

Figure 6.3: Percentage of total area occupied by the images obtained after successive erosions and dilatations. This histogram indicates probability that deposit pixel coincides with an arbitrary pixel in "shell added" after single dilatation or "removed" after single erosion.

many deposit points are contained in the separate shells added to, or subtracted from the original pattern of Figure 6.1a, by dilatation or erosion. The original pattern itself contains 36 deposit pixels or mes $(A \cap C) = 36$ pixels. The pattern of Figure 6.1g consists of 5360 black pixels and contains 14 deposit pixels. Hence the probability that an arbitrary pixel in this cell is a deposit pixel is equal to 14 / 5360 = 0.00261. This probability is one of the proportions for separate cells shown in the histogram of Figure 6.3. The image of Figure 6.1i consists of 9990 pixels and has mes $((A \oplus 2B) \cap C) = 10$ pixels. This indicates that 3602- 10 = 26 of the deposits (or 65%) occur in the zone identified as acidic volcanic rocks on the geological map, and within (2/2 x 259 m =) 733 m from a contact between acidic volcanics and other rock types on this map. This zone may be relatively favourable for the occurrence of massive sulphide deposits. The probability that a random pixel in the zone is a deposit cell amounts to 26 / (18843 - 9990) = 0.00294, which is about eight times greater than the probability (= 0.00039) that a random pixel in the entire study area is a deposit pixel. On the other hand, it is only about 1.5 times greater than the probability (= 0.00191) that an arbitrary pixel of the original binary image in Figure 6.1a is a deposit pixel.

As previously observed, 36 of the 40 deposit pixels (or

90%) coincide with the acidic volcanics, black pixels in Figure 6.1a. A more general form of this ratio for a cell of side ((2n + 1) x 259) m is:

$$M_{d_1} = \text{mes } (A \cap (C \oplus nB) \; / \; \text{mes } (C \oplus nB)$$

For the patterns shown in Figure 6.2, M_{d_1} amounts to: 0.646 (Figure 6.2d), 0.537 (Figure 6.2e), and 0.456 (Figure 6.2f). The ratio represents a weighted average proportion of acidic volcanics per cell for cells centered about the deposits. All these probabilities and ratios follow directly from Minkowski transformatioms of sets. Additionally by computing logical operations between the sets, binary images are produced which retain the spatial attributes which are hidden in the probability values.

6.2.5 Transformations by circular elements

In the Minkowski transformations discussed, the set B used was a 3 x 3 array of black pixels, representing a square. In some cases, particularly for computing measures related to distances in the two dimensions, the set B may be chosen so that it approximates as closely as possible a circle. In a square raster a circle can be approximated by a pseudo-octagon. Two pseudo-octagons are frequently used for this purpose, one whose area exceeds that of the circle

which has the same horizontal (or vertical) diameter, and a second whose area approximates by defect that of the circle of the same horizontal diameter. The first type of octagon, shown in Figure 6.4c, is contained within a 5 x 5 array of pixels: its horizontal and vertical sides have length of 2 pixels, its oblique sides have length of $\sqrt{2}$ pixels (1.4142). Its horizontal and vertical radius is 2.5 pixels. Transformations by this pseudo-octagon also can be obtained with two successive transformations by the two structuring elements of 4 and 8 neighbors also shown in Figure 6.4c. A second octagon is shown in Figure 6.4d. Its horizontal and vertical sides and its radius are of 2 and 3.5 pixels, respectively. Its oblique sides are of length $2\sqrt{2}$ (2.8284) pixels. Transformations by this pseudo-octagon can also be obtained with two successive transformations by two offset 11 neighbors sets (smaller octagons without a center pixel) also shown in Figure 6.4d.

For the hexagonal raster, like the one used to produce the hexagonally scanned image of Figure 6.6a, a good approximation to the circle is obtained with the hexagon: this is shown in Figure 6.4b. Figure 6.4 shows as open circles the area proportions of the set T occupied by the binary patterns of the 40 deposit pixels after several successive dilatations by means of square, octagonal and hexagonal sets B (structuring elements). Shown as solid

Figure 6.4: Probabilities that random cells, of different sizes and shapes approximating the circle, in the square raster and in the hexagonal raster configurations, contain one or more deposit pixels. The area proportions of the set T occupied by the binary image of the 40 deposit pixels are shown as open circles after several successive dilatations by a square (a), octagonal, (c) and (d), and hexagonal (b) sets B, the structuring elements. The area proportions are plotted against the horizontal diameters of the structuring elements; each point corresponds to a different successive dilatation. The vertical arrows point at the dilatations displayed in Figures 6.2 (square), 6.5 (octagons) and 6.6 (hexagons). The area proportions occupied by a hypothetical image of 40 black pixels such that the patterns of their dilatations do not overlap, is shown by solid squares. The solid circles indicate the theoretical area proportions of 40 non overlapping circles of diameters equal to the horizontal diameters of the sets B used for the dilatations. The structuring elements and the elementary sets which produce the octagons are shown above the area proportion diagrams. Additional descriptions are in text.

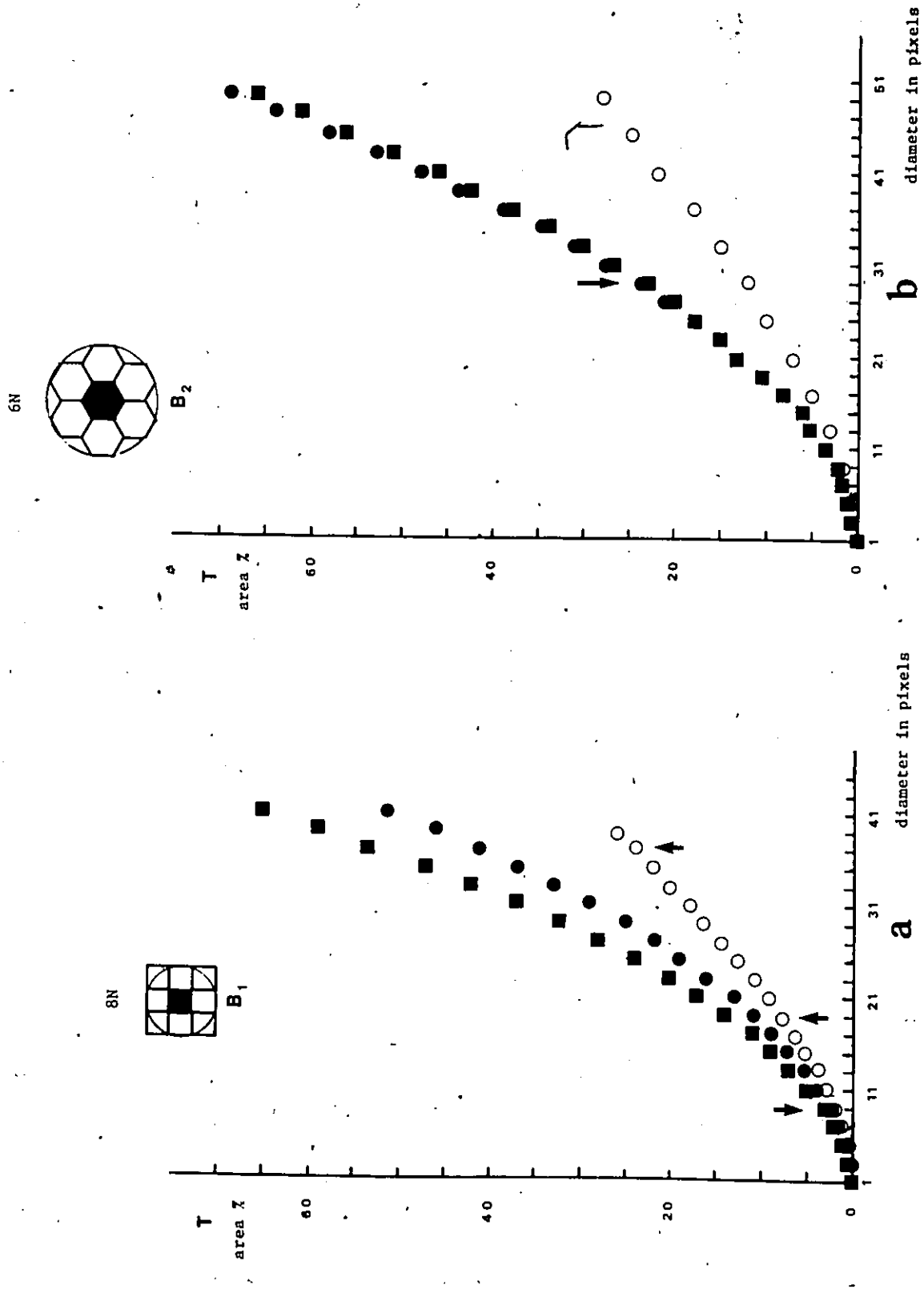

Figure 6.4: Continued

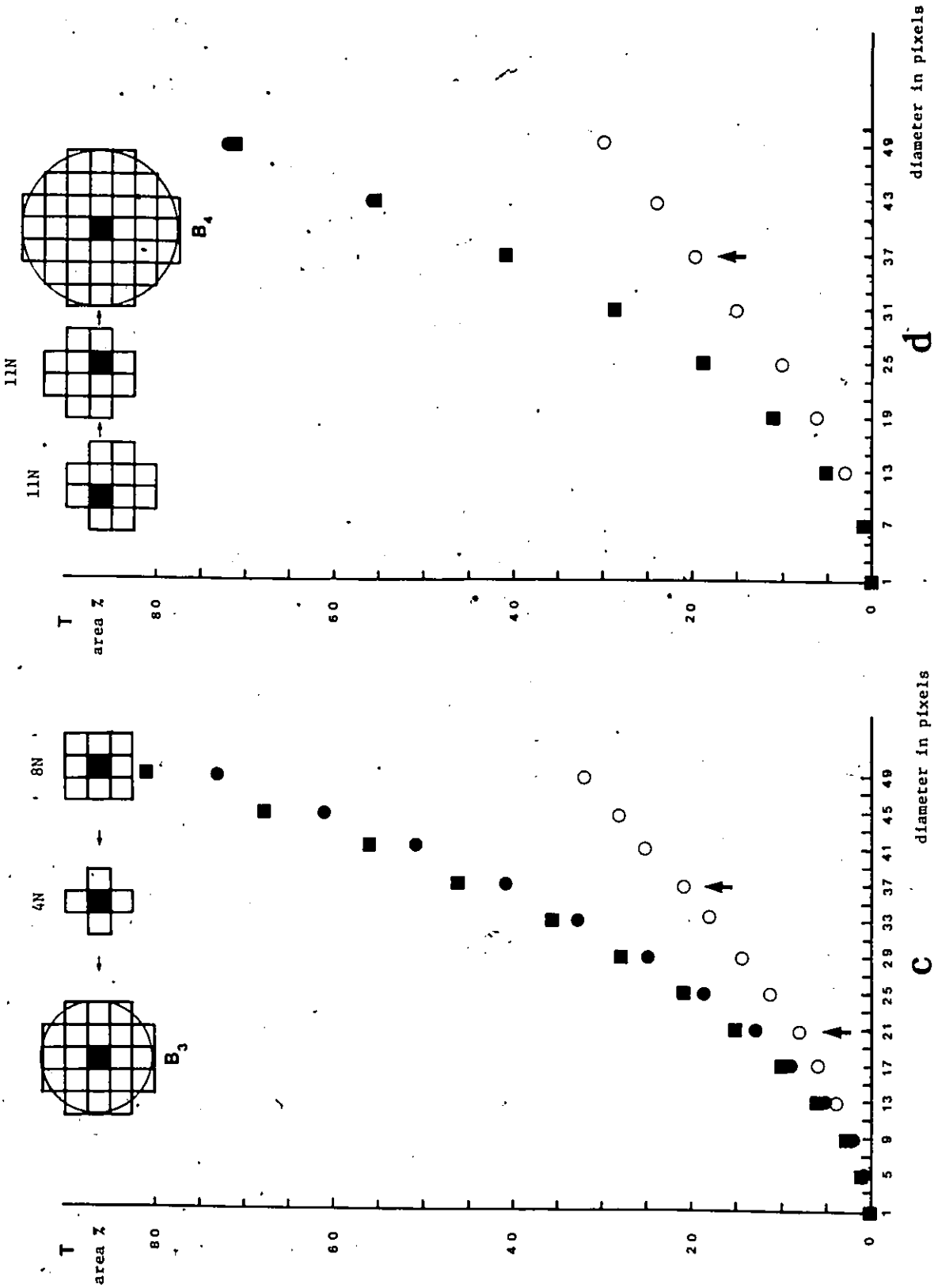

Figure 6.4: Concluded

squares are the areal proportions occupied by a pattern of 40 black pixels so that the patterns of their dilatations do not overlap. The functions of these proportions are compared with the theoretical area proportions, shown as solid circles, of 40 non overlapping circles of diameter equal to the horizontal diameters of the four sets B used. As can be seen in Figure 6.4a, for increasing dimensions, the area of the square exceeds that of the circle more than the area of the octagon in Figure 6.4c. A closer approximation within the range of dilatations considered, is obtained by the octagon in Figure 6.4d and the hexagon in Figure 6.4b.

The area proportions in Figure 6.4 can be interpreted as probabilities that the different shapes, approximating circles of various diameters, translated at random throughout the image containing the pattern of 40 deposit pixels, hit one of these. It also can be shown that the areas of octagons similar to the one in figure 6.4d and of hexagons, tend to depart from the areas of the corresponding circles with further increases in dimensions. The distribution pattern of the functions of the dilatations for our dot pattern, crosses in Figure 6.4, depends on the degree of clustering of the initial dot pattern, the initial number of dots and also on their location relatively to the edge of the image set T.

The horizontal and vertical diameters of the octagons in

Figure 6.4c and in Figure 6.4d, generated for n dilatations, are equal to ((4n + 1) x 259) m and to ((6n + 1) x 259) m, respectively. The results of 5 and 9 dilatations with the first octagon and of 6 dilatations with the second octagon correspond to diameters of 5439 m and 9583 m. The binary images on Figures 6.5a, 6.5b and 6.5c, corresponding to the above mentioned octagonal dilatations of the deposit pattern, can be intersected with the geological pattern of figure 6.1a. The resulting image sets $(A \cap (C \oplus 5B_3))$, $(A \cap (C \oplus 9B_3))$, and $(A \cap (C \oplus 6B_4))$, where B_3 and B_4 are the octagons of Figures 6.4c and 6.4d, respectively, are shown in Figures 6.5d, 6.5e and 6.5f. For these patterns M_{d_1} amounts to 0.530 (Figure 6.5d), 0.468 (Figure 6.5e) and 0.476 (Figure 6.5f). The intersection of the sets in Figure 6.5b with the complement of the set in Figure 6.5c is shown in Figure 6.5g in order to display the shape difference between the two types of pseudo-octagons which have the same horizontal diameter.

6.2.6 Hexagonal transformations

Figure 6.6a shows the pattern of hexagonally scanned Middle-Upper Ordovician volcanic rocks. Fourteen dilatations of the hexagonal pattern of 40 deposits produced the image of Figure 6.6b, the set (C ⊕ 14B) in which the minimum

Figure 6.5: Octagonal dilatations of image set C for 40 deposit pixels, intersection of the resulting sets with the original image A in Figure 6.1a, and comparison of the octagons. (a) $C \oplus 5B_3$; there are 8736 black pixels in this image; (b) $C \oplus 9B_3$; there are 22083 black pixels in this image; (c) $C \oplus 6B_4$; there are 20164 black pixels in this image; (d) $A \cap (C \oplus 5B_3)$; there are 4627 black pixels in this image; (e) $A \cap (C \oplus 9B_3)$; there are 10334 black pixels in this image; (f) $A \cap (C \oplus 6B_4)$; there are 9593 black pixels in this image; and (g) $(C \oplus 9B_3) \cap (C \oplus 6B_4)$; there are 1919 black pixels in this image which represents a comparison between dilatations of C by the two different pseudo-octagons when they have the same horizontal diameter.

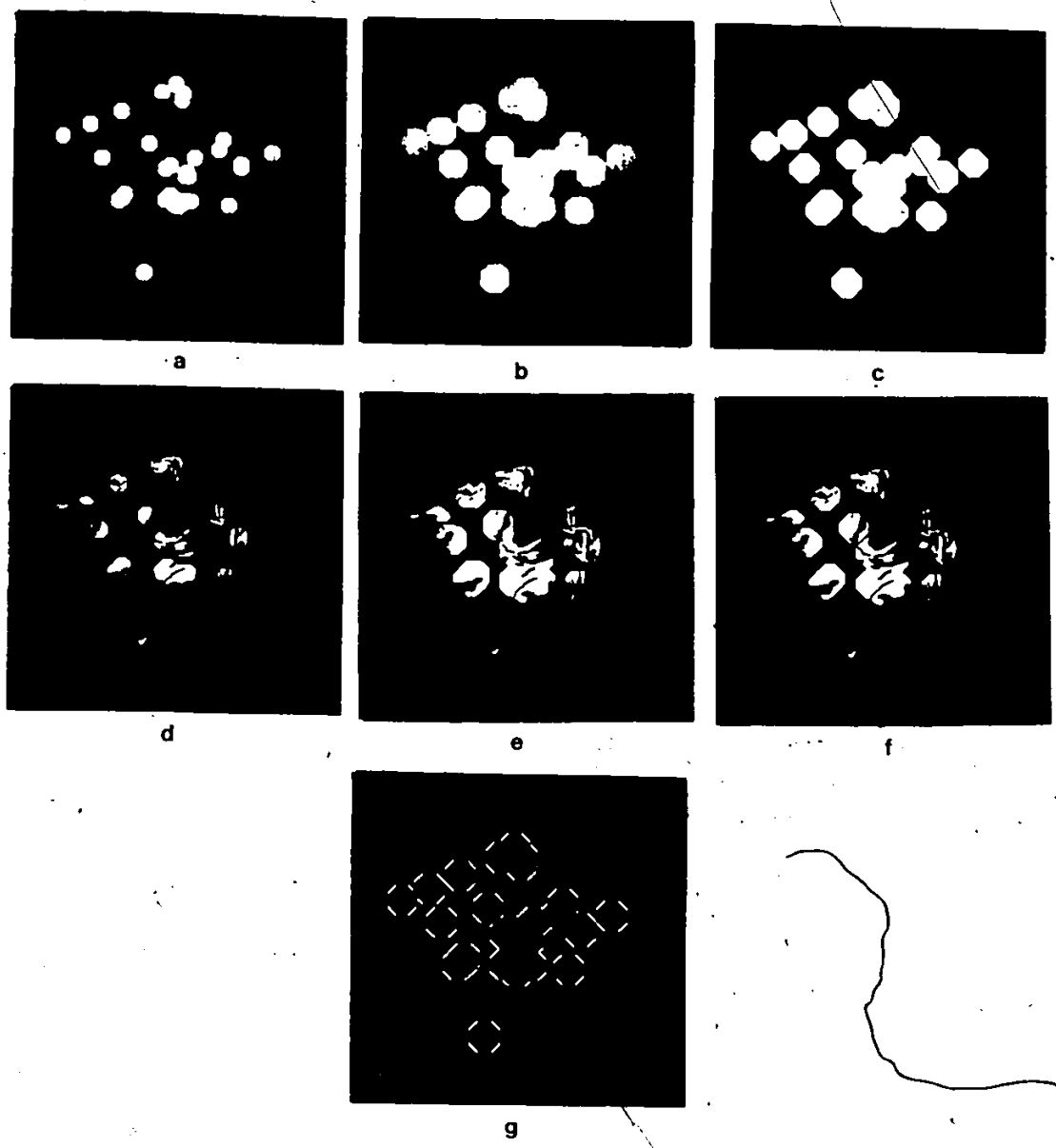

Figure 6.5: Concluded

diameter of the hexagon is equal to ((2n + 1) x 256) m or 7424 m for n = 14. The binary patterns of Figures 6.6a and 6.6b can be intersected, and the resulting image sets $(A \cap (C \oplus 14B))$ and $((C \oplus 14B) \cap A^c)$ are displayed in Figures 6.6c and 6.6d, respectively. For the pattern in Figure 6.6c M_{d_1} amounts to 0.538; for the pattern in figure 6.6d, where A^c is intersected, M_{d_1} amounts to 0.462 (= 1 - 0.538).

Different shapes of structuring elements have been exemplified for the two different geometrical arrangements of pixels: the square and the hexagonal raster, respectively. For isotropic transformations the closest approximation to a circle is desirable at the given resolution. For anisotropic transformations a rectangular structuring element or an approximation to an ellipse can be used. For direction-dependent transformations linear structuring elements are used which point at given senses of direction. There are instances in which the choice of structuring element is problem dependent: for example for relating geological data from maps with mineral deposit locations a square is preferable because it corresponds directly to the way the data are collected or digitized (according to the U. T. M. Projection and coordinate system). Also a square raster representation of the pixels is used for remotely sensed data.

The transformations described have all been computed using the generalized approach of GIAPP. Similar transformations also can be produced on special-purpose hardware-built instruments, such as the Quantimet 720 (octagons) or the Leitz TAS (hexagons). However, the degree of sophistication of those instruments does not yet allow a completely general approach to the technique of transformations by all types of structuring elements.

6.2.7 Covariance measurements

Let us now consider briefly few more types of transformations which are used to characterize further our spatial patterns. For measurements in the plane at the crossings of a regular grid a two-dimensional autocorrelation function can be computed which has an origin or a central point. Agterberg (1974) provided the theoretical background to the two-dimensional autocorrelation function as a direct extension of the one-dimensional function as follows:

> "Suppose that the elements of the (m x n) data matrix X are written as X_{ij} (i=0,1,...,m-1; j=0,1,...n-1). The two-dimensional autocovariance function C(r,s) is defined as:
>
> $$C(r,s)=\frac{1}{(m-r)(n-s)}\sum_{i=0}^{m-r-1}\sum_{j=0}^{n-s-1}(X_{i,j}-\bar{X})(X_{i+r,j+s}-\bar{X})$$
>
> and
>
> $$C(-r,s)=\frac{1}{(m-r)(n-s)}\sum_{i=r}^{m-1}\sum_{j=0}^{n-s-1}(X_{i,j}-\bar{X})(X_{i-r,j+s}-\bar{X})$$
>
> where r=0,1,...M, and s=0,1,...,N" [$\bar{X}$ is the mean value] (Agterberg, 1974: pages 340 and 341).

Each covariance C(r,s) can be converted into an autocorrelation coefficient R(r,s) by dividing by the variance C(0,0).

A model for the statistical covariance function of two-dimensional patterns (e.g., rock units on a map) which

Figure 6.6: Cross-correlation between mineral deposits and the geological map pattern from a map which was hexagonally scanned on a flying spot scanner. (a) binary image G of the map pattern of Middle-Upper acidic volcanic rocks in Bathurst mining camp, New Brunswick. Image is 313 x 349 pixels (= 109237 pixels) and plotted hexagonally from hexagonal scanning. there are 22925 black pixels in this image. (b) result of 14 hexagonal dilatations D of the pattern of 40 volcanogenic massive sulphide deposits in the same area of G; there are 13500 black pixels in this image; (c) result of cross-correlating D and G: $D \cap G$; there are 7269 black pixels in this image; (d) result of cross-correlating D and G^c: $D \cap G^c$; there are 6231 black pixels in this image.

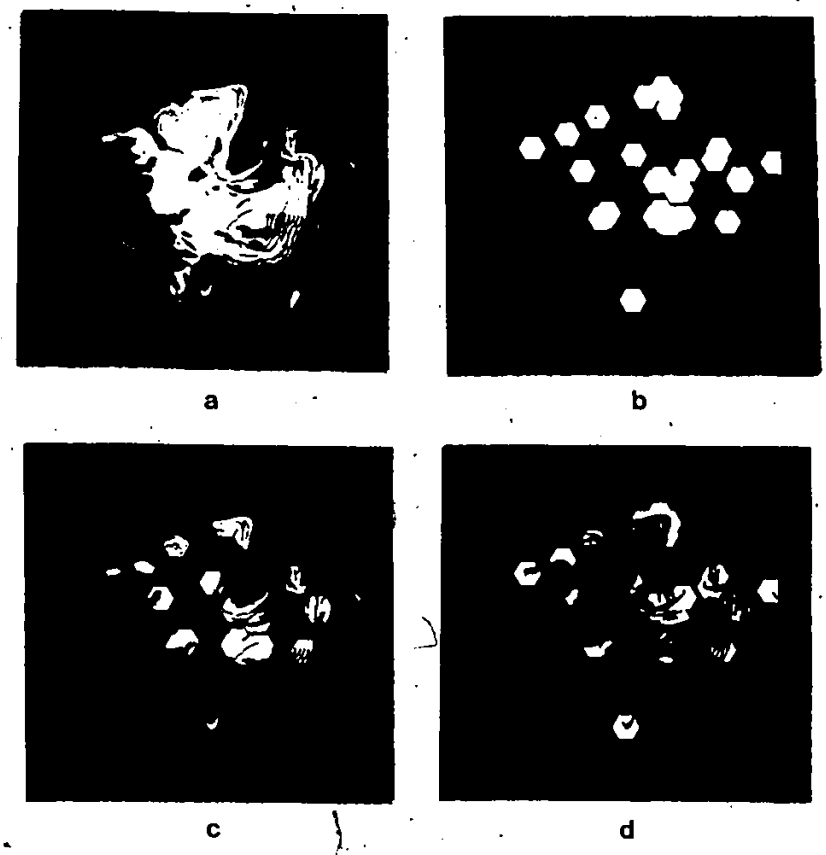

Figure 6.6: Concluded

has been proposed by Agterberg (1977) was applied to the original pattern of acidic volcanics shown in figure 6.1a. The geometrical covariance $K_\alpha(l)$ satisfies $K_\alpha(l) = mes(A \ominus \check{B})$, where A is the original pattern and B an operator set consisting of two points. One point is the origin of B and the other point occurs at a distance l in the direction α. The symbol $\check{}$ denotes reflection of a set with respect to its origin. $K_\alpha(l)$ is shown in Figure 6.7a for both the east-swest and the north-south directions. The measurements were obtained by the correlation algorithm described earlier in Chapter 5. Measurements are computed by translating a duplicate of the image being processed relatively to it from a position of perfect overlap to a given number of positions in all directions, and computing the intersections or matching values for each position. The number of black pixels overlapping for the different shifts provides the geometrical covariance function. In order to obtain the corresponding statistical covariance, the values of Figure 6.7a were first increased by the factor $mes\ T_0 / mes\ T_0 \ominus B$, where T_0 represents a square study area around A which measures 80 km on a side. The statistical covariances are obtained by subtracting m^2 from the corrected geometrical covariances where $m = mes\ A / mes\ T_0$ is the proportion of the study area underlain by acidic volcanics. The statistical covariances, the values of Figure 6.7b, were divided by

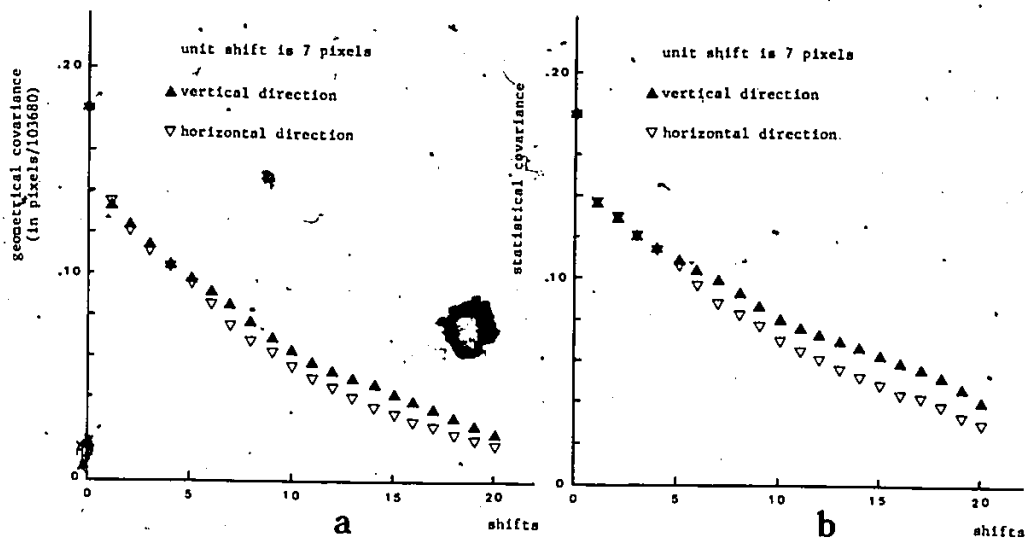

Figure 6.7: Geometrical, (a), and statistical, (b), covariances for the east-west and north-south directions for the image of acidic volcanics in Figure 6.1a. The autocorrelation coefficient computed from the first ten geometrical covariances for the north-south direction, (c), and the east-west direction,, (d), are also shown. The solid lines in (c) and (d) represent theoretical autocorrelation function of signal-plus-noise model.

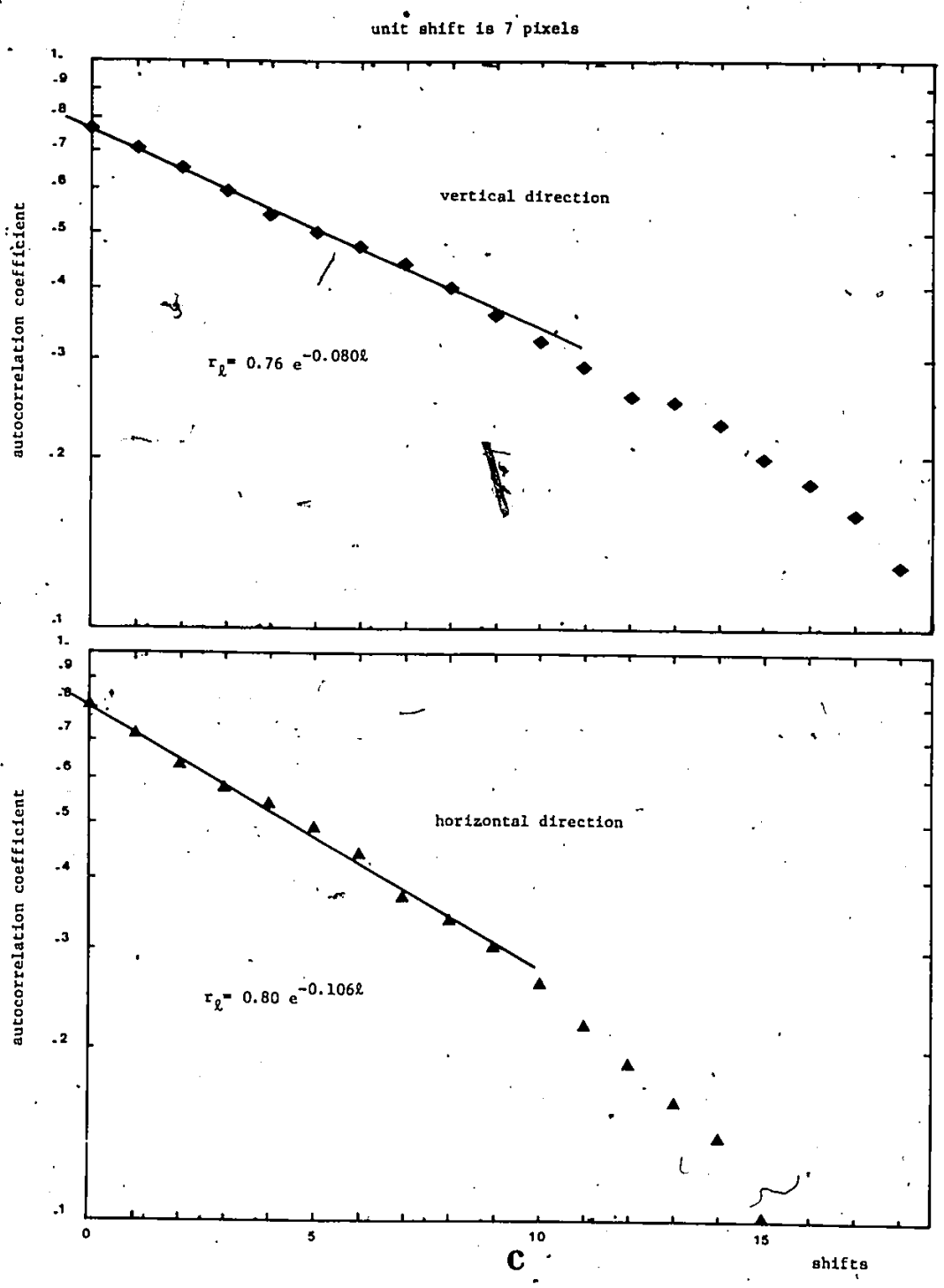

Figure 6.7: Concluded

the variance $C = m - m^2$ and this gave the auto-correlation coefficients r plotted along the vertical axis with the logarithmic scale in Figure 6.7c. The signal-plus-noise model with $r = c \exp(-p|l|)$ with c = 0.80 and p = 0.106 in the horizontal direction and c = 0.76 and p = 0.080 in the vertical direction, provide reasonably good fit. The two-dimensional covariance function shown in Figure 6.8 is isotropic by good approximation. The patterns corresponding to the values at east and south shifts (x 7 pixels) of (0,0), (5,0), (0,5) and (5,5) ,respectively, are shown in Figure 6.9a to 6.9d. The area of the light grey pattern / 10000, is the value in the corresponding position of Figure 6.8.

6.2.8 Hexagonal closings

A dilatation followed by an erosion is called "closing". This transformation if produced by a isotropic set B, a structuring element like the hexagon, can be used to describe distance relationships between the objects in a binary pattern. A hexagon B of the horizontal diameter of 5 pixels was used to produce first the set $(C \oplus B)$, dilatation of the pattern of 40 deposit pixels. This is shown in Figure 6.10a. The 40 deposit pixels in the original pattern form 39 objects. This is so because two pixels occur side

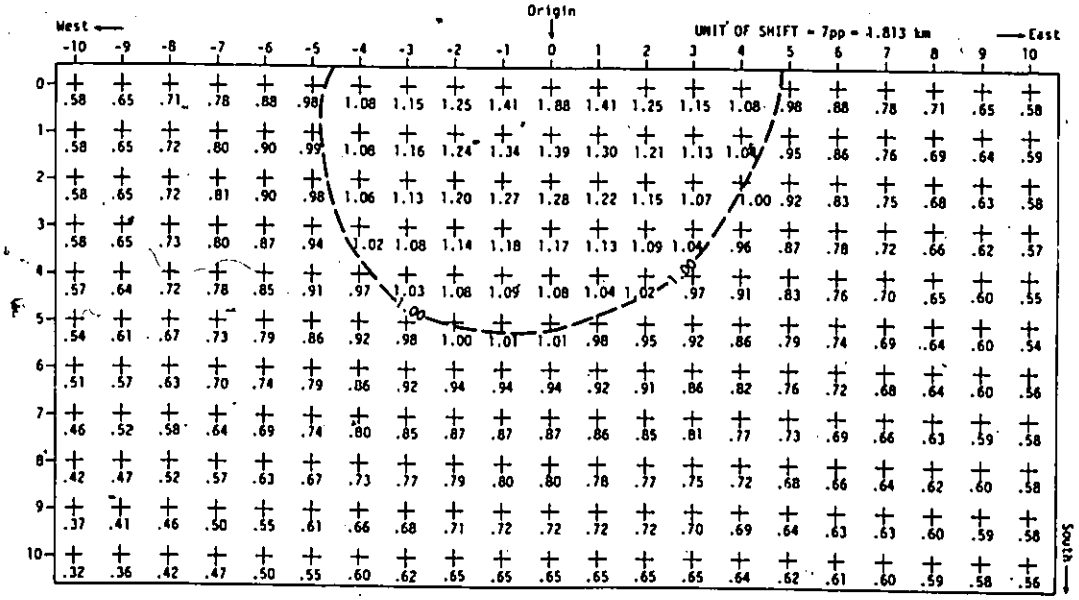

Figure 6.8: Two-dimensional geometrical covariance function obtained frombinary images of Figure 6.1a (only lower half is shown). Values are in pixels / 10000. Contour of 10000 pixels illustrate approximate isotropy.

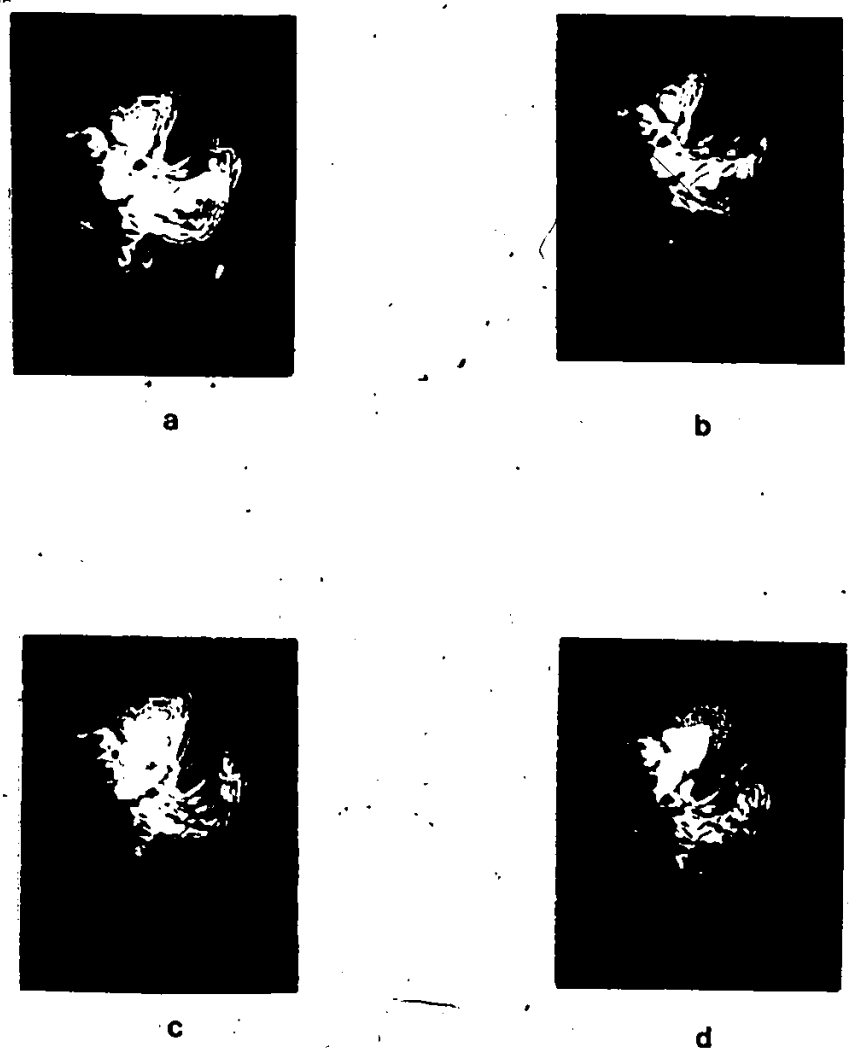

Figure 6.9: Shifting of a binary image during the computation of four of the geometrical covariance values shown in Figure 6.8. (a) (0,0) values for east and south shifts (x 7 pixels); (b) (5,0); (c) (0,5); and (d) (5,5). The area which is measured is the one of the light grey pattern.

Figure 6.10: hexagonal closings of a dilatated image of the 40 deposit pixels in the Bathurst area, New Brunswick, for describing the distance relationships between the hexagonal areas. (a) the 40 deposit pixels after a dilatation by a hexagon of horizontal diameter of 5 pixels; (b) to (g) one to six closings; (h) one erosion before obtaining the closing in (g). Additional information is in text.

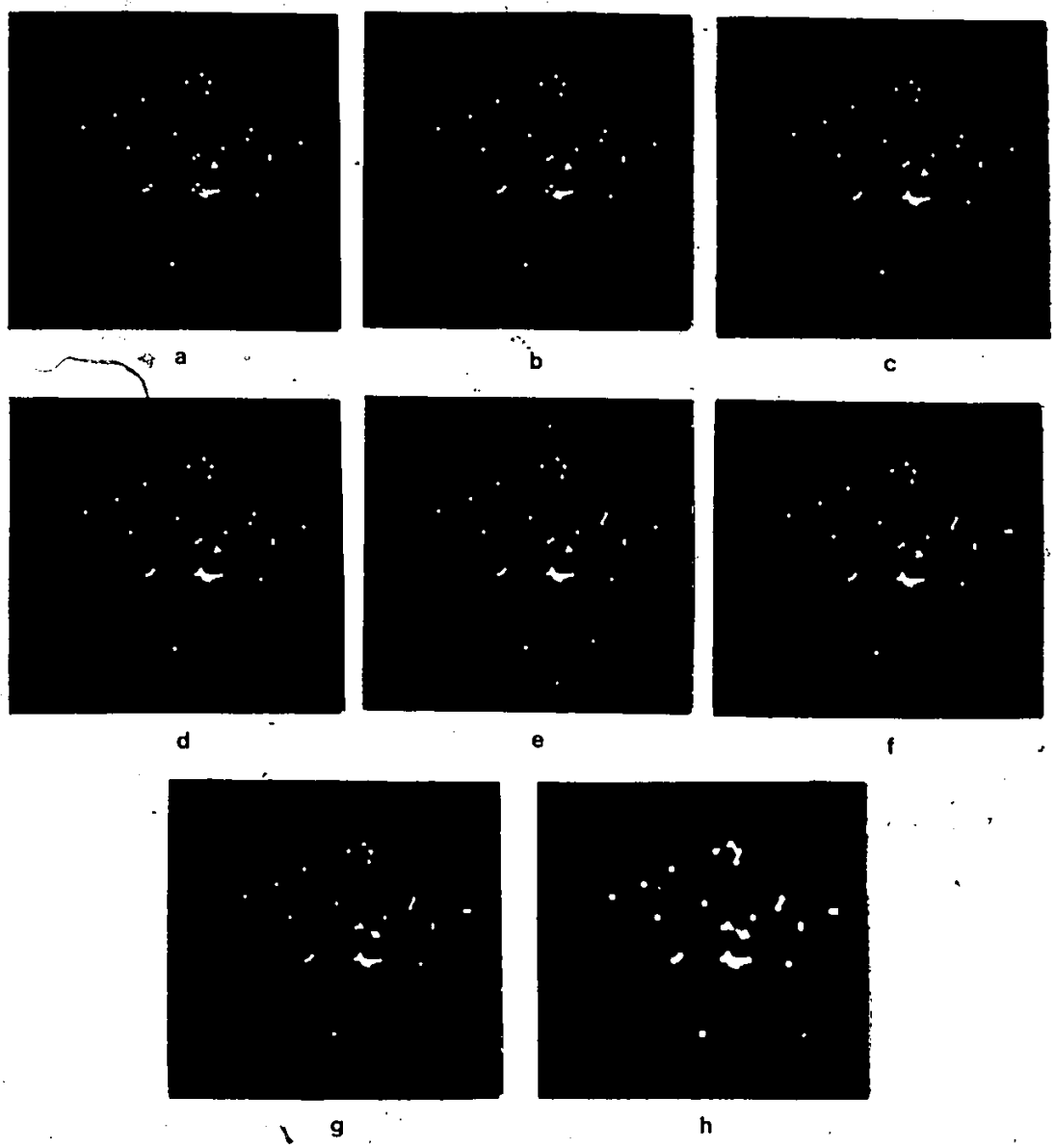

Figure 6.10: Concluded

by side and therefore are considered as connected to form a single object. The two pixels occur at a distance of 259 m. In Figure 6.10a there occur 24 objects after the hexagonal dilatation: this indicates that 39 - 25 = 15 deposit pixels are less than (4n + 1) x 256 m apart, which for n = 1 is 1280 m. The pattern of Figure 6.10a was subjected to 6 closings (Figures 6.10b to 6.10g) consisting of 1 to 6 dilatations followed by the same number of erosions. This process of transformations creates "bridges" between objects whenever their edges are located at distances from other object edges which are les than or equal to (2n + 1) x 256 m (n is the number of closings). This happens if during the n'th dilatation shapes are produced by merging object patterns which have their minimum diameter, in at least one of the three directions of the hexagonal raster, greater than the diameter of the n-dilatated hexagon used for the subsequent erosion. Object count after each closing iteration, provides the distribution of the interobject or interparticle distances. In Figures 6.10a to 6.10g, the object numbers are 24, 22, 20, 20, 17, 17, and 17, respectively. The pattern of Figure 6.10h was produced by performing 6 dilatations followed by only 5 erosions of the pattern in Figure 6.10a (one more erosion produced the pattern in Figure 6.10g). This pattern shows the growing trend between clusters or groups of linked objects.

The problem of histogramming interparticle distances occurs in textural studies for ore minerals. In this application of essentially illustrative character, object counting is performed readily by eye. However object counting in an hexagonal binary image can be performed automatically by the method previously described in Figure 5.6, which provides the connectivity number defined as the number of objects minus the number of holes. This number can be used for histogramming interparticle distances, as demonstrated by Serra and Verchery (1973).

6.3 Analysis of a portion of a thin section of a metamorphic rock

6.3.1 Digitization and preprocessing

In this application the boundaries of crystal grain profiles were digitized with a graphic tablet. The original drawing, not shown here, of a thin section of a granulite from Otter Lake, Quebec, was taken from Kretz (1978). The crystal phases in the section are: calcic pyroxene, plagioclase, hornblende and sphene. The processing of the grain boundary image consisted of several steps, which included minor editing of the binary image produced from the vectors computed from the graphic tablet output, expansion of binary

compressed data, line thinning, labeling of areas enclosed by contour lines, phase relabeling and extraction of binary compressed images from the phase-labeled image. The purpose of the preprocessing was to obtain the patterns of the four different phases in the section as binary images in registration with one another.

The unit spacing between the pixels in the binary image is 0.0278 mm; image dimension is 180 x 252 pixels. The total number of individual crystals of which the boundary was digitized is 398. The binary patterns obtained are shown in Figure 6.11 as follows: (a) thinned boundary image with rectangular frame added after thinning, (b) frame at the edges of the image, (c) image of thinned boundary without frame, (d) image of all the grains together obtained by computing the complement of the pattern in (a), (e) to (h), binary images of sphene, calcic pyroxene, hornblende and plagioclase, respectively, extracted from the pattern in (a).

6.3.2 Erosions, dilatations, openings, and closings

Let us consider some transformations which are representative of the measures which are commonly required about this type of rock material and which, at the same time,

Figure 6.11: Binary images of a thin section of granulite from Otter Lake, Quebec. (a) thinned boundary image with rectangular frame added after thinning. Image dimension is 180 x 252 pixels; (b) the rectangular frame; (c) the boundary image without the frame; (d) the complement of the image in (c); (e) to (h): binary images of sphene, calcic pyroxene, hornblende and plagioclase profiles.

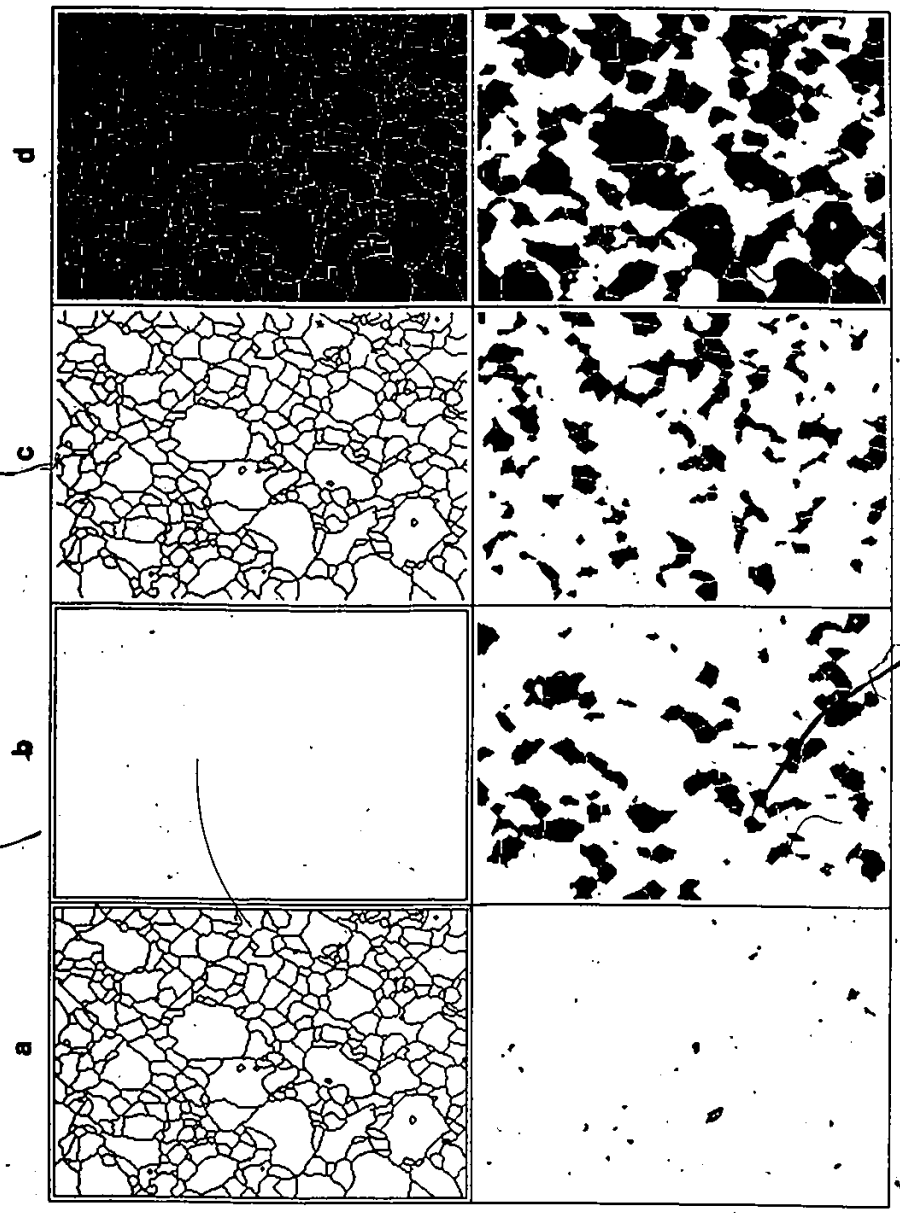

Figure 6.11: Concluded

illustrate the versatility of GIAPP.

During the interactive phase relabeling process, the patterns of all crystals adjacent to the frame was identified and extracted. Such pattern was then used as a mask, in order to eliminate, if so desired, the patterns of those crystals, from each phase in which they occurred. Figure 6.12a shows the binary pattern of all plagioclase crystals which were uncut by the edges of the picture or in this case the frame. Several transformations of the binary pattern in Figure 6.12a were computed using the pseudo-octagonal structuring element of minimum diameter equal to 5 pixels, also shown in Figure 6.4a. The resulting patterns are shown in Figures 6.12b to 6.12h. Figure 6.12b and Figure 6.12d show $(A \ominus B)$ and $(A \oplus B)$, single erosion and single dilatation, respectively, of the original set A in Figure 6.12a by the set B, the octagon. An erosion provides a measure of the probability that an octagon with the shortest diameter of 5 pixels which is moved at random everywhere in the image space is fully contained within the plagioclase crystals. A dilatation provides a measure of the probability that the octagon hits, i.e. falls partly or wholly on top of the plagioclase. These probabilities can be used, for example, for estimating the average circumpherence of the profiles of the plagioclase grains.

Figure 6.12: Minkowski type operations with pseudo-octagonal structuring element on square raster image of plagioclase profiles from thin section of granulite. (a) original image of 180 x 252 pixels after elimination of all crystal profiles which were cut by the edge of the image; there are 17344 black pixels in this image A. (b) octagonal erosion of A; there are 8996 black pixels in this image B. (c) octagonal opening of A; there are 15935 black pixels in this image C. (d) octagonal dilatation of A; there are 25939 black pixels in this image D. (e) octagonal closing of A; there are 18355 black pixels in this image E. (f) result of logical operation $A \cap B^{\circ}$; there are 8348 black pixels in this image F. (g) result of logical operation $A \cap C^{\circ}$; there are 1409 black pixels in this image G. (h) result of logical operation $E \cap A^{\circ}$; there are 1011 black pixels in this image H.

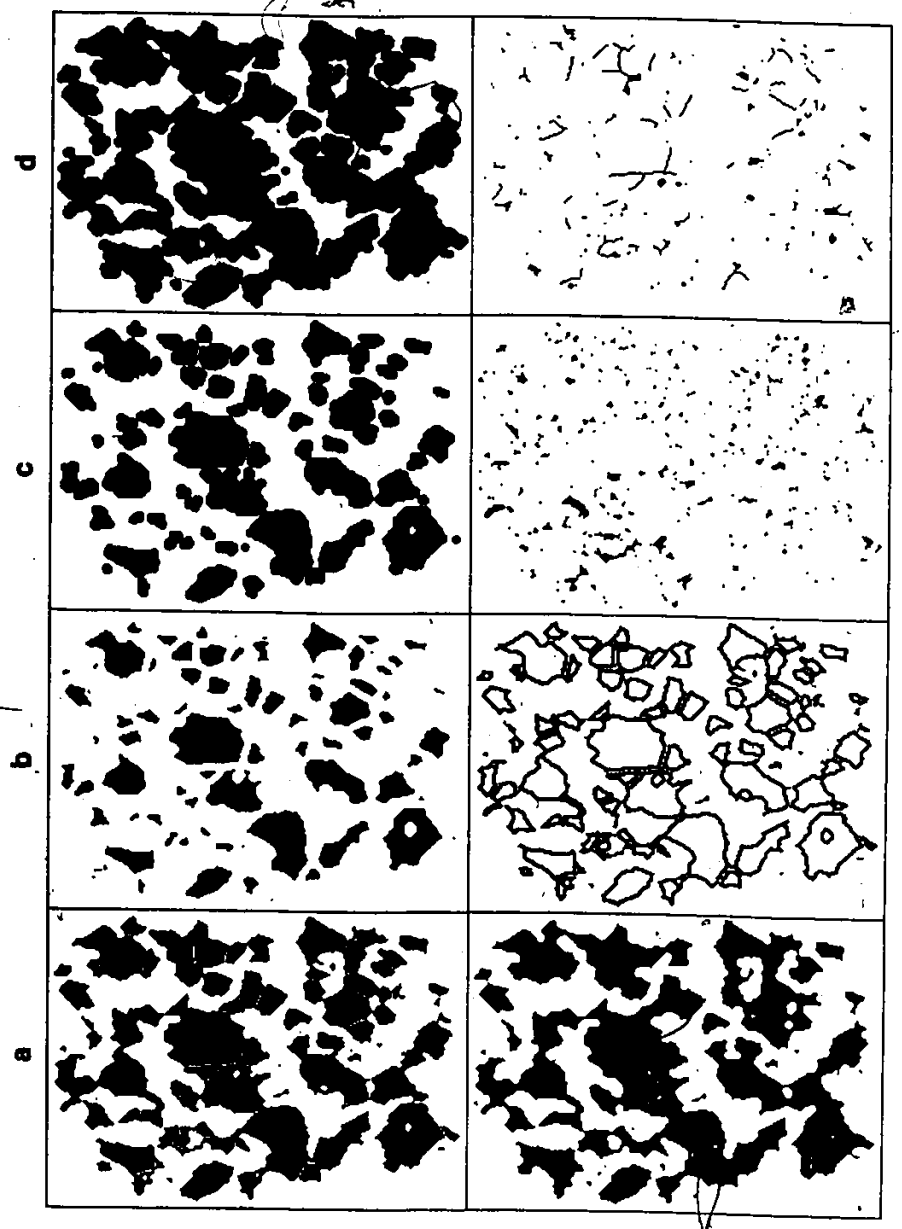

Figure 6.12: Concluded

An opening, an erosion followed by a dilatation, and a closing, a dilatation followed by an erosion, are displayed in Figure 6.12c and in Figure 6.12e. Opening can be used to estimate the grain size distribution of the grains; closing can provide information on interparticle distances. These measures should however take into account the irregularities of the boundaries of the grains which have curvatures greater than can be approximated by the octagonal structuring element. Such aspects of the transformed images can be better displayed by means of logical operations between the original and the transformed images. Figure 6.12f to 6.12h show the results of the following operations:

$A \cap (A \ominus 0)^c$, $A \cap ((A \ominus 0) \oplus 0)^c$ and $((A \ominus 0) \oplus 0) \cap A^c$,

where the symbol $\cap$ indicates intersection of the two sets, ^{c} stays for complement, A is the original set, and 0 is the octagonal structuring element set. Figure 6.12f shows the black pixels which have become white in the octagonal erosion. In Figure 6.12g the black pixels are shown which have turned from black to white during the octagonal opening of the image A in Figure 6.12a. The pixels added in the octagonal closing are displayed in Figure 6.12h instead.

6.3.3 Interparticle distances and particle counting

As previously mentioned, closing transformations can be used in order to characterize interparticle distances. We have seen an application of closing for a point pattern in Figure 6.10, for a hexagonal image. For patterns in a square raster, several structuring elements can be used, such as the octagons of Figure 6.4 or the square. The larger is the structuring element the broader are going to be the distance intervals used as unit. For example, horizontal and vertical distances of 7 and 5 pixels and multiples of these can be measured using the octagons in Figure 6.4d and Figure 6.4c, respectively. For narrower intervals in a square raster we can use the square as the smallest isotropic shape approximation to a circle. Square the shortest diameter or distance interval is 3 pixels.

The image of plagioclase crystals in Figure 6.11h was used to illustrate closing patterns and interparticle distance determinations, by a square structuring element of increasing sizes (3 and higher). Opening, i.e. a dilatation followed by an erosion, involves growing of a black pattern. The growth transformation, however, cannot exceed the dimension of the original 180 x 252 pixels image. An erosion, on the contrary is not affected by the image dimension, because it is a shrinking transformation. In order to avoid edge effects, the black pattern of plagioc-

lases was mapped within a larger image of dimensions 200 x 272 pixels so that a width of ten pixels surrounds the edges of the original image. In the new larger image the dilatated plagioclase crystals would reach the new image edge only at the tenth square dilatation. The patterns resulting from 0 to 5 closing transformations are shown in Figures 6.13a to 6.13f, respectively. The initial number of crystals in the pattern of Figure 6.10a was 137. The number of connected objects in the five closed patterns is 22, 11, 5, 3, and 1, respectively. This is the information needed for histogramming the interparticle distances versus the number of crystals whose edges are at less than a given minimum distance from the closest crystal edge. In the patterns of Figure 6.13 it can be seen how the bridges which develop connecting objects in a square raster image are elongated in either horizontal or vertical directions. Differently from the square raster, in the hexagonal raster the bridges develop along the three main directions of the raster as can be seen in Figure 6.10.

A set of transformations similar to the ones used for hexagonal images (see Figure 5.6) can be designed for square raster binary images, to compute the connectivity number for histogramming interparticle distances. The connectvity

Figure 6.13: Characterization of interparticle distances, for the image of plagioclase profiles from the granulite, by successive closing operations. (a) the original image mapped into a larger image space of 200 x 272 pixels; there are 137 profiles (objects) in this image. (b) to (h) results of one to five closing operations leaving 22, 11, 5, 3, and 1 "connected objects", respectively. (g) and (h) are the images of the black pixels which turned to white during the erosions of the image in (a) by the structuring elements

$$B_1 = \begin{matrix} \bullet 0 \bullet \\ 0\underline{1}\bullet \\ \bullet\bullet\bullet \end{matrix} \quad \text{and} \quad B_2 = \begin{matrix} \bullet\bullet\bullet \\ 0\underline{1}\bullet \\ 1 1 \bullet \end{matrix},$$

respectively, for the computation of the "connectivity number".

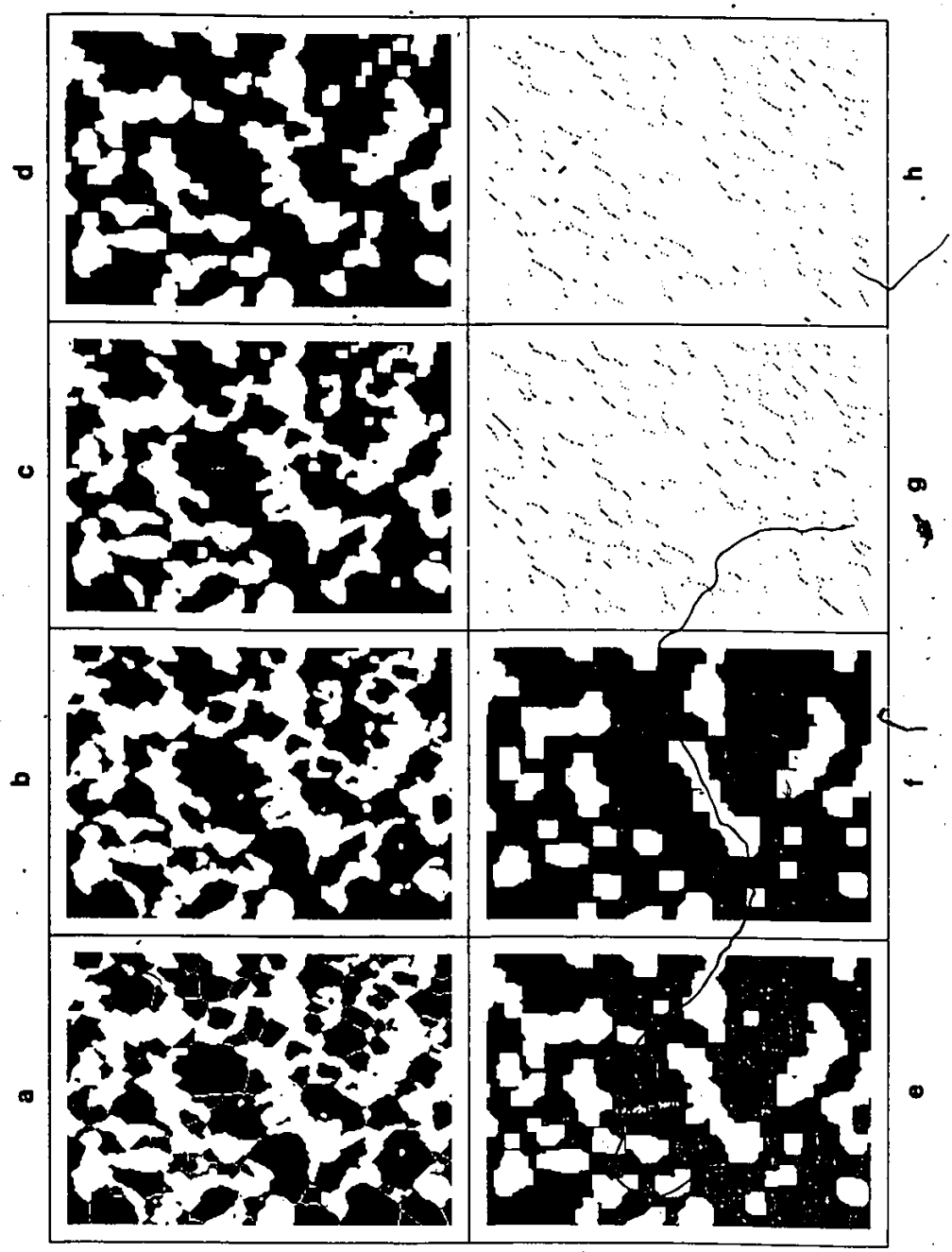

Figure 6.13: Concluded

number (number of objects - number of holes) can be computed by erosions with the following two structuring elements

$$B_1 = \begin{matrix} \bullet 0 \bullet \\ 0\underline{1}\bullet \\ \bullet\bullet\bullet \end{matrix} \quad \text{and} \quad B_2 = \begin{matrix} \bullet\bullet\bullet \\ 0\underline{1}\bullet \\ 11\bullet \end{matrix}$$

where 1 indicates a black pixel, 0 a white pixel, and • a pixel not considered in the transformation.

The procedure to follow to compute the connectivity number is: (1) erode the original binary pattern A by B_1, and compute how many black pixels have become white; (2) erode A by the structuring element B_2, and compute how many black pixels have become white; and (3) compute the absolute difference between the counts in (1) and (2) above. The expression for this computation the connectivity number cn can be written as follows:

$$|\text{mes } A - (\text{mes } A \ominus B_1) - (\text{mes } A \ominus B_2)| = cn$$

Figures 6.13g and 6.13h are the patterns of the black pixels which have become white after the erosions by the two elements mentioned above. They correspond to the following expressions: $(A \cap (A \ominus B_1)^c)$, and $(A \cap (A \ominus B_2)^c)$. The set A, the original image, is shown in figure 6.13a.

6.3.4 Transformations by linear elements

Figure 6.14: Minkowski type operations with horizontal linear asymmetric structuring elements of different lengths on binary image of calcic pyroxene from same granulite of Figure 6.11, after elimination of the crystal profiles cut by the image edges. (a) original image of calcic pyroxene crystal profiles; there are 6748 black pixels in this image. (b) image of pixels which turned from black to white during the erosion of image A in (a) by the structuring element

000000000
000011111
000000000

There are 3516 black pixels in this image. (c) image of pixels which turned from black to white during erosion of binary image A in (a) by the structuring element

000
011
000

There are 1030 black pixels in this image. (d) image of the pixels which turned from black to white during erosion of image A in (a) by structuring element

000
010
010

There are 860 black pixels in this image. (e) to (h): computation of the linear horizontal geometrical covariance for right shifts of 5, 10, 15, and 20 pixels, respectively. The vertical black bands of widths of 5, 10, 15, and 20 pixels in (e) to (h) represents the loss in significance for the covariance values after shifting the entire images in the horizontal direction. The pattern in (e) to (h) simply represents the intersection between the image A in (a) and a shifted duplicate of the same image.

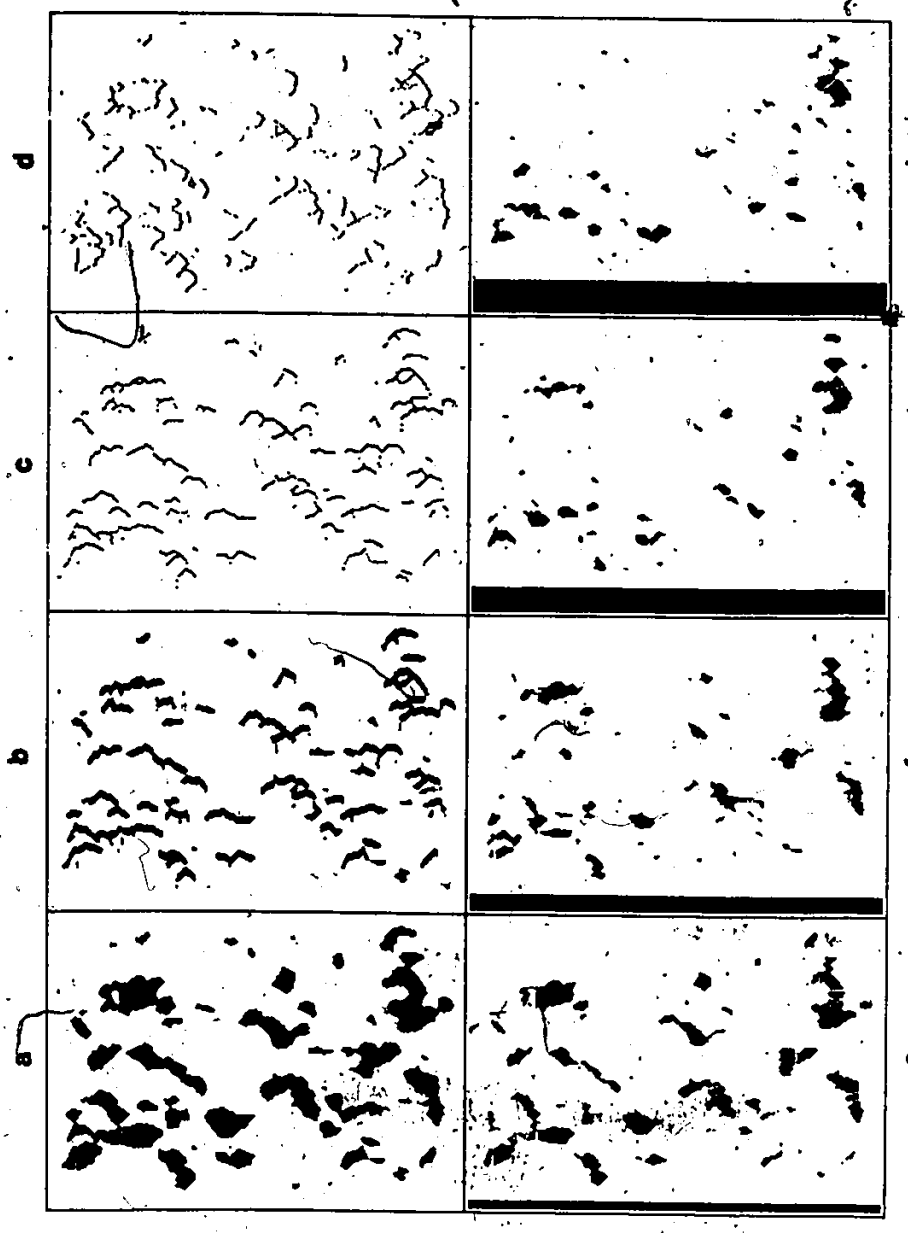

Figure 6.14: Concluded

Linear structuring elements can be used to study the shape anisotropy of the grains in binary images. Figure 6.14a shows the binary image of calcic pyroxene for the same granulite. Figure 6.14b displays the black pixels which turned to white in the erosion by a horizontal linear element of length 4 pixels extending to the right of the centre pixel. Figure 6.14c and Figure 6.14d show the elements eliminated by the erosion of a linear right and downward elements of length 1. In stereology, such patterns are termed horizontal and vertical intercepts, respectively. These images and the measurements that they provide, describe quantitatively the average elongation of the grains of pyroxene in the two vertical and horizontal directions. They can be considered as the probabilities that horizontal and vertical trajectories placed at random throughout all the grains in the image space, will intersect the right and the lower edges of the grains.

We also can represent the geometrical covariance as a transformation by a linear structuring element consisting of a set of two pixels, one black and one white, at a given distance from each other, and placed along a line oriented in a direction α. The origin of the set pair is at the 0 pixel. For $\alpha = 0$, we can consider the pair of pixels located in the horizontal direction. We can use this

structuring element for producing a shifted pattern by erosion. If the origin 0 is at the pixel to the left, the pattern will be shifted leftward; if the origin is to the right, the pattern will be shifted towards the right. During the shifting operation a strip of our image pattern elongated perpendicularly to the shift direction and of width equal to the shift length will be lost over the edge of the image in the direction of the shift. A white band pattern will be added in its place at the opposite edge of the image. The intersection between the shifted image and the original untranslated pattern is a new pattern from which we can compute the probability that a black pixel occurs at a distance equal to the shift in the direction of the shift. The pattern of Figures 6.14e to 6.14h, correspond to shifts of length 5, 10, 15, and 20 pixels respectively. A black vertical band of width equal to the shift length has been added to identify the narrowing of the shifted images. The number of black pixels in each pattern has to be compared with the pixel count at the origin, i.e. for shift of 0 pixels, or the proportion of black pixels in the original pattern over the entire universal image set T_0 (of 180 x 252 pixels). After each shift, however, new universal sets are produced, which are narrower than the set T_0, such as the sets T_5, T_{10}, T_{15} and T_{20}. Our probabil-

Figure 6.15: Computation of boundary length and transition matrix from the binary images of boundaries of profiles. (a) binary image of hornblende profile boundaries; (b) binary image of sphene/hornblende boundaries; (c) binary image of pyroxene/hornblende boundaries; (d) binary image of plagioclase/hornblende boundaries; (e) binary image of hornblende/hornblende boundaries; (f) to (i) binary images of the black pixels which turned from black to white during the erosions of the image in (d) by the following structuring elements:

$$\begin{matrix}000\\011\\000\end{matrix}\ ,\quad \begin{matrix}000\\010\\010\end{matrix}\ ,\quad \begin{matrix}000\\010\\001\end{matrix}\ \text{and}\ \begin{matrix}000\\010\\100\end{matrix}\ ,$$

respectively, for detecting the kind of black pixel adjacency in the four directions.

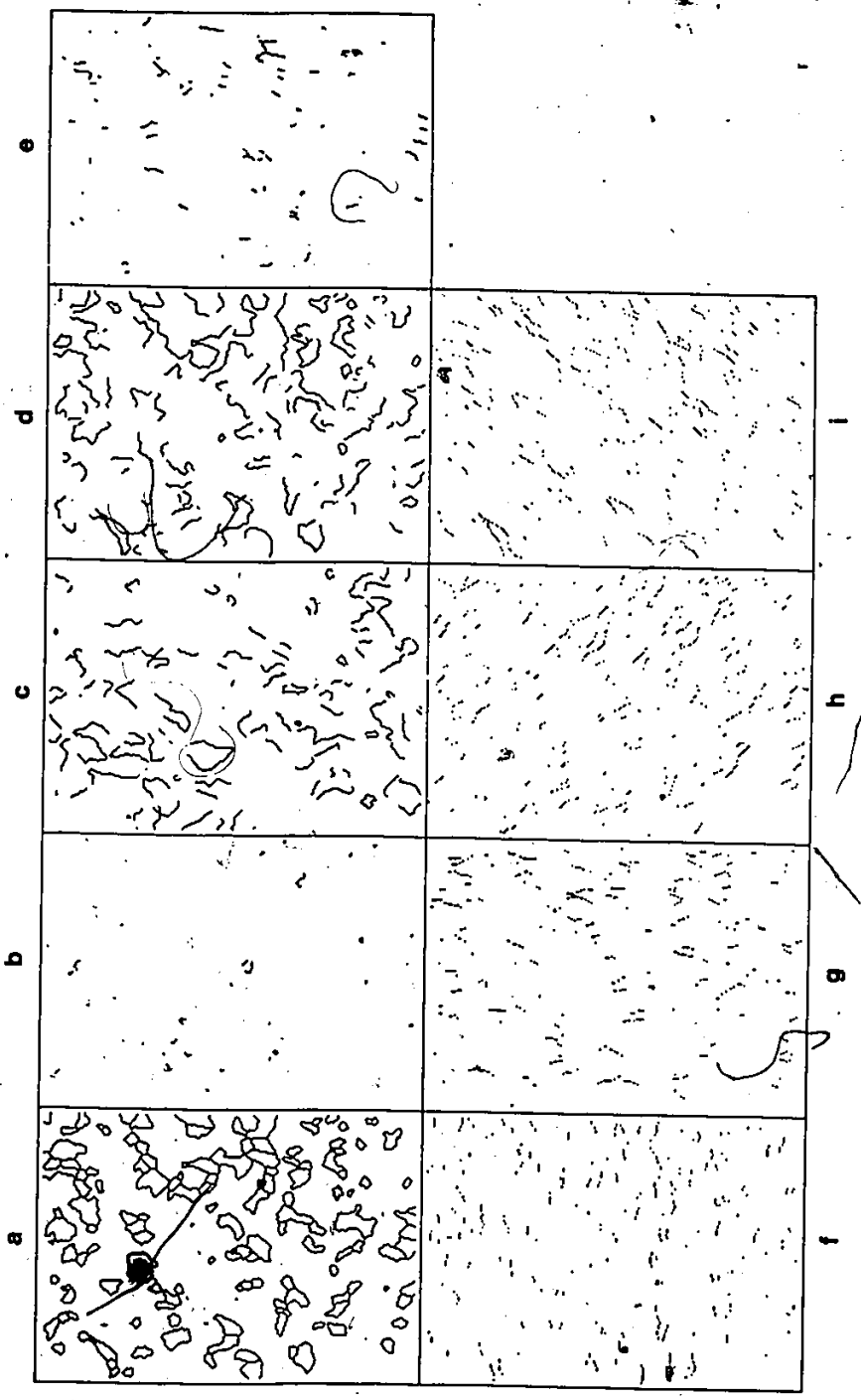

Figure 6.15: Concluded

ities will have to be scaled proportionally to those universal sets, smaller than T_0, for the areas marked by vertical black bands in Figure 6.14.

6.3.5 Boundary length and transition matrix computation

Let us now consider an application on the patterns of Figure 6.11, in order to produce and display separate images of boundaries between different crystals and also of boundaries betwee crystals of the same type. As is sometimes done in textural studies in petrology, crystal to crystal transitions are coded for grain sequences along equally spaced traverses in order to compute transition matrices which can be compared to Markov chains for texture characterization, as in Kretz (1969) or Whitten et al (1975).

The approach followed in this application consists of measuring directly the contact length for all contacts of the four minerals of the patterns in Figure 6.11 (e to h), and to compute the 4 x 4 transition matrix from these lengths. The images of Figures 6.11e to 6.11h were dilatated once by means of a square structuring element (3 x 3 pixels) and the resulting images were intersected with the image of boundaries of Figure 6.11c. This produced a

separate boundary pattern for each crystal type. Figure 6.15a shows the boundary of hornblende. Each boundary image then was intersected with any other one and this produced six partial boundary images, one for each possible pair of crystals. Figures 6.15b to 6.15d show the boundaries hornblende-sphene, hornblende-calcic pyroxene, and hornblende-plagioclase respectively. The three partial boundaries so obtained for each crystal pair were cumulated, logical union operations, with each other for every crystal type, and the resulting image was complemented and intersected with the boundary image of each crystal type. The results were images for the boundary patterns between crystals of the same type. Figure 6.15e shows all hornblende-hornblende boundaries.

From the different binary images of boundaries so produced, the boundary lengths were computed as multiples of 1 for pairs of black pixels on the same row or column of the binary image, and as multiples of $\sqrt{2}$ for pairs of diagonal points. The 4 x 4 transition matrix so computed is shown in Table 6.1, together with the contact length matrix, the percentage of contact length and area for each mineral and the number of grains for each mineral in the image. This type of transition matrix describes the texture in the two dimensions by expressing the probability for each crystal to be in contact with any other type of crystal and with

crystals of the same type. The values in the table show a distinct tendency for unequal contacts over equal contacts. This pattern may provide evidence on genetic relationships between the minerals and on metamorphic recrystallization events of the rock such as interfacial energy and nucleation.

It is of interest to consider briefly the problem of measuring the line lengths for the patterns of Figures 6.15a to 6.15e. Pairs of adjacent pixels with different orientations have been used as structuring elements for eroding the patterns in Figure 6.15d, the boundary between hornblende and plagioclase grains. The transformed patterns represent the proportions of boundary pixels adjacent to a boundary pixel to the right (Figure 6.15f), below (Figure 6.15g), to the lower right (Figure 6.15h) and to the lower left (Figure 6.15i). These four patterns, therefore, single out all point pairs at distances 1 from those at distances $\sqrt{2}$. Furthermore, the patterns in Figures 6.15h to 6.15i correspond to the values of the geometrical covariance of the pattern in Figure 6.15d, for the shifts in the horizontal and vertical direction (-1, 0) and (0, 1). The auto-covariance arrays of values are listed in Table 6.2, for both the hornblende/plagioclase (Figure 6.15d) and the hornblende/hornblende patterns (Figure 6.15e). These arrays of auto-correlation values, however, underestimate the boun-

dary lengths since no weight is given to the single points (which are eliminated by the erosions or by the unit shifts), and to the end points of line segments. This happens because the line patterns were measured out of their context. A better approximation of boundary lengths can be obtained by cross-correlating the patterns of Figures 6.15d and 6.15e with the pattern of Figure 6.15a, the total grain boundary pattern for hornblende. The cross-correlation values are also listed in Table 6.2.

In these arrays, each valuecorresponds to distance units of 1/2 for horizontal and verical directions, and of $\sqrt{2}/2$ for oblique directions. Boundary lengths can be computed by multiplying the the cross-correlation values by those factors and computing the sums of the eight values in the arrays. Such computation gives a length of 2786 units for the pattern in Figure 6.15d, and of 442 units for that of Figure 6.15e. This approximation was used for the values of Table 6.1.

TABLE 6.1

Contact length matrix computed for boundaries of sphene, calcic pyroxene, Contact length matrix computed for boundaries hornblende and plagioclase digitized from a thin section of granulite. Percentage of contact length and area, and number of crystals are also in the table for each crystal type. A transition matrix P has been computed from the contact length matrix.

	sphene	pyro-xene	horn-blende	plagi-oclase	% con-tact length	% area	No. of crystals
sphene	0.0000	.0122	.0109	.0208	4.39	.42	25
pyro-xene		.0340	.1496	.2578	45.36	20.41	97
horn-blende			.0474	.3572	56.41	20.44	139
plagi-oclase				.1101	74.59	58.72	137

$$P = \begin{bmatrix} .0000 & .2779 & .2843 & .4738 \\ .0269 & .0750 & .3298 & .5683 \\ .0193 & .2647 & .0839 & .6321 \\ .0279 & .3456 & .4789 & .1476 \end{bmatrix}$$

6.3.6 Skeletonization by line thinning

Skeletonization is a transformation which detects all the pixels within objects which lie or are closest to points at equal distance from opposite boundaries. Several algorithms have been proposed for such transformations, for either allowing object reconstruction or for facilitating object description and recognition. Algorithms exist for square raster images and for hexagonal raster images. The transformations are not necessarily limited to binary images, of course, but are sometimes computed for grey level images. Rosenfeld and Kak (1976) describe a few line thinning algorithms. One type of skeletonization process of binary images is the one produced by applying a line thinning algorithm to patterns not necessarily made up of lines. Figure 6.16b is the set S, the "skeleton" pattern of calcic pyroxene, the set A, after a closing transformation which joined all grains which were adjacent. The image was derived from the pattern in Figure 6.11f. In Figure 6.16c the pattern $(A \cap S^{\circ})$ shows how closely the central pixels of the pyroxene crystal profiles are detected in the transformation. This type of transformation is, however, not computed in one single scan through the image, but it is iterative: processing continues and the image is trans-

TABLE 6.2

Auto- and cross-correlation values for the computation of boundary lengths of binary images of thinned boundaries

AUTO-CORRELATION plag/horn boundary			
	-1	0	+1
+1	547	528	522
0	526	2195	526
-1	522	528	547

AUTO-CORRELATION horn/horn boundary			
	-1	0	+1
+1	41	163	67
0	16	353	16
-1	67	163	41

CROSS-CORRELATION horn bXplag/horn b			
	-1	0	+1
+1	608	575	587
0	551	2195	544
-1	565	565	599

CROSS-CORRELATION horn bXhorn/horn b			
	-1	0	+1
+1	64	176	96
0	21	353	25
-1	102	195	68

DISTANCE FACTORS FOR CORRELATION VALUES			
	-1	0	+1
+1	$\sqrt{2}/2$	1/2	$\sqrt{2}/2$
0	1/2	*	1/2
-1	$\sqrt{2}/2$	1/2	$\sqrt{2}/2$

L E N G T H S
plag/horn = 2786
horn/horn = 442

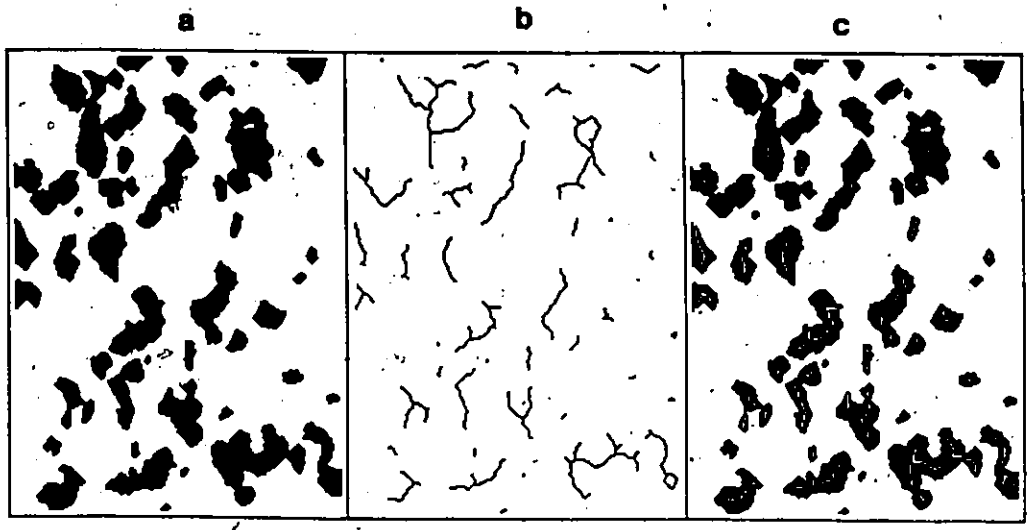

Figure 6.16: "Skeletonization" of a binary image by "line thinning". (a) image A of calcic pyroxene crystal profiles after a closing transformation by a 3 x 3 structuring element; (b) the image S of the skeletons of the pyroxene profiles (clusters) after line thinning; (c) result of the logical operation A S which shows the performance of the line thinning algorithm in the context of the original binary image.

formed little by little, in cycles, until the process stops automatically because no further change is possible (the analogy can be made with the peeling of an onion). In the case of Figure 6.16a, the binary image was first expanded (one word per pixel) and then it was processed by a line thinning algorithm adapted after Tamura (1975). The grains of the black pattern were thinned so that a 8-connectivity between black pixels was maintained. The algorithm assigns labels of increasing negative values to the pixels belonging to consecutive shells (from the boundaries inward) to be later transformed into white pixels.

The completely thinned pattern was then compressed as shown in Figure 6.16b, where the apparent tendency of the grain cluster skeletons to be preferentially oriented in the vertical direction is clearly visible.

6.4 Concluding remarks

We have reviewed a number of transformations for two examples of small images. This was done, primarily, for providing a broad visual impression of the applications of binary transformations. However, as a general procedure, it is not so meaningful to apply many transformations to the material analyzed (evidently the choice of transformations can be as wide as one's imagination), but rather to select

or design those transformations that, depending on the problem at hands, are more likely to quantitatively describe the desired critical properties of the material analyzed.

Serra (1978) classified the transformations used in texture analysis according to the number of steps required: one, two, three, ... infinity. (i.e., iterative transformations). Such approach can be logically extended from binary to grey level images, as demonstrated by Goetcherian (1980). In addition, the neighborhood or structuring element approach to transformations can be further generalized by modelling any given function within a neighborhood and assigning a given value to the pixel in a given position in it in relation to that function. It is of interest to observe that the transformation approach, developed in this way, has now made a complete circle and so the old method of template matching has been rediscovered. Indeed a full exploitation of template matching techniques can be done best by a specialized parallel or pipeline processor. While it may be remarked that there is nothing new under the sun so far in image processing, worthwhile new applications are being discovered every day, that make it useful at present, to use the methodologies developed in the past.

7. Quantitative characterization of geological and ancillary map patterns and their relationships to the distribution of mineral occurrences in the Wiskey Jack Lake-Kasmere Lake area, Northwestern Manitoba

7.1 Previous approaches to the systematic analysis of geological map patterns

Conventionally, geological maps are constructed so that they contain all the information that the geologist, responsible for mapping or compilation, judges to be essential to a qualitative description and interpretation, at the level of detail required by the scale of mapping. Recently, the need became apparent to produce specialized maps which portray more quantitative information for special purposes: e.g. mineral potential estimation, soil evaluation, geotechnical assessement or environmental terrain classification. For those maps, different kinds of data have to be quantified, either manually, digitally or electronically, and stored on computer processable files for subsequent statistical analysis and visual display.

Several resources related geomathematical projects were developed since 1968 at the Geological Survey of Canada. To

produce estimates of the mineral potential for metal commodities in large areas of Canada, methods of statistical analysis of regional geological data, extracted from maps and retrieved from computer files on mineral deposits, were extensively applied by Agterberg et al (1972). These applications required the systematic compilation of special-purpose geological maps designed to reveal metallogenic features. The quantification and coding of regional geological information for resources estimates in the Appalachian region was described by Fabbri, Divi and Wong (1975). For those projects usage was made of square grid patterns (equal area cells) produced according to the Universal Transverse Mercator geographic projection (U.T.M.). Transparencies of the grids were placed over the maps to be coded, and counts were made to express the areal amounts of all rock units occurring in each square cell of the grid.

As exemplified by Fabbri (1975), systematically quantified regional geological data could be useful to a variety of statistical applications. The data, however, which were manually coded and computerized for several thousands of 10 km x 10 km cells, represented only part of the information contained in the maps. Only one cell size could be chosen each time for manual compilation, therefore, the data units were either single cells or larger cells consisting of mosaics of individual unit cells. Such data have been used

for correlating statistically the geological composition of the cells with the occurrence of mineral deposits (Leech, 1975). A main drawback of such procedure was represented by the great time and labour required in the manual collection and computer editing of the data. Additionally, in those manually collected files, no direct information was coded on the two-dimensional shapes of the geological units or the lengths of their contacts. Equally, the spatial distribution of the different map units or the orientation of the lithologic contacts were not directly quantified. This information can be of importance in deriving estimates of the probability of occurrence of mineralizations, and in characterizing the spatial distribution of the mineral deposits.

A statistical approach to the analysis of geological variables from maps was put forward by Switzer (1976) who wrote:

> "Complex spatial geological patterns may be regarded as realizations of random processes. The estimate parameters of such processes serve as convenient summary characterization of the observed geological patterns, and provide a basis for their classification and composition. The statistical properties of the estimates of process parameters, e.g. prevalence and patchiness, are related to the rate and methods of sampling, as well as to the model of the process itself." (p. 124).

As he proposed, the scale of the phenomena to which investigations of these relationships apply, range from the texture of rocks in thin sections to satellite surface imagery. Switzer paid particular attention to the study of models of spatial variation representable by simple two-color or multicolor patterns. Important applications where the data are characteristically obtained at discrete locations are offered by soil samples, grab rock samples, points on a thin section, weather stations, digitized photographs and other imagery, and scoop samples from the ocean bottom. Discretely spaced sample data are used to estimate areal proportions (as in thin section modal analysis), pattern complexity, to make pattern reconstructions, and to obtain estimates of parameters of the pattern-generating process. Switzer proposed a method for estimating algebraically the spatial dependence of map patterns.

Some recent techniques of digitization of geological maps have been described by Bouillé (1975) who used a graph theory approach, and by Anuta et al (1976) who used a polygon technique to digitize geological maps for exploration purposes involving remote sensing and geophysical data.

7.2 Digitization, preprocessing and processing of large regional geological maps

Whenever the need arises to convert picture information into computer-readable form, several alternative methods may be used. The nature of the data normally dictates the most appropriate method. Thus, in case of colored pictures, normally the data is raster scanned using red, green and blue filters. At each raster point the red, green and blue color intensities are recorded as numbers. In this case the digitized data consist of three quite large matrices of numbers. In case of grey tone pictures only one matrix is necessary since only the grey level intensity is recorded. In case of images containing lines only, like the present contour maps, an alternative to systematic raster scanning consists of some form of line tracing or line following. Given adequate equipment, automatic line tracing is feasible, but frequently the lines are traced manually by using a specialized stylus and a so called graphic tablet. The tablet and stylus system is connected to a computer, which receives and stores the x-y coordinates of the stylus while the operator traces the lines on the map.

In raster scanning the data is a matrix of numbers while the data received from the tablet is a sequence of x-y coordinates or "vectors" approximating the line being traced by the operator. The data structures stored in the computer are radically different. Whether the raster or the vectori-

al form of data is to be preferred is to a degree a matter of taste and available computer programs, but the solution to some problems is easiest in the raster form while other are easiest to solve if the data is in vectorial form. However, computer programs which are written for vectorial type of data cannot use raster data and vice versa. In principle, all data structures are equivalent, and if no loss of information occurs, they are convertible from one to the other, but the conversion may not be very simple.

In the present case the contour map data is traced interactively and received by the computer in vector form. However, since the rest of the programs all use raster formatted data, the vector data is converted to raster format for subsequent processing. In many situations the raster format is desirable, but it may be wasteful in the required digital storage space. The necessary computing time is so problem and equipment dependent that generalized statements tend to be meaningless.

Of necessity, the computer programs at N.R.C. had to be taylored to the available Modcomp II minicomputer environment at the Computer Graphics Laboratory. Efforts have been made to minimize the amount of computer equipment and human resources needed while emphasizing an interactive environment with adequate automation and quickest turnaround time.

The problem considered here is to convert large regional

geological maps to computerized form and to process the data as images. The conversion process is usually called digitization. The maps to be digitized are much larger than the present equipment (34 cm x 34 cm tablet) allows. Many different large maps which cover the same area are to be digitized and processed. It is desirable that the maps are in registration with one another in order to facilitate cross-correlations or matchings which imply point to point correspondence.

It is important to follow a systematic procedure in map preparation for digitizing. On the map, rectangular subareas with no gaps and preferably no overlap between them, are selected and clearly marked. These rectangles are to fit within the active area of the graphic tablet. The final composite binary image will be rectangular.

To obtain suitable resolution (i.e. best digital accuracy) a large map should be divided into adequate size rectangular subareas. Each subarea or submap is digitized independently, and the maximal resolution obtainable from the tablet is preserved. A balance is needed between the number of submaps and the overall digital accuracy of the final product.

An overall view of the procedure, without the details and reasons, consists of the following steps:

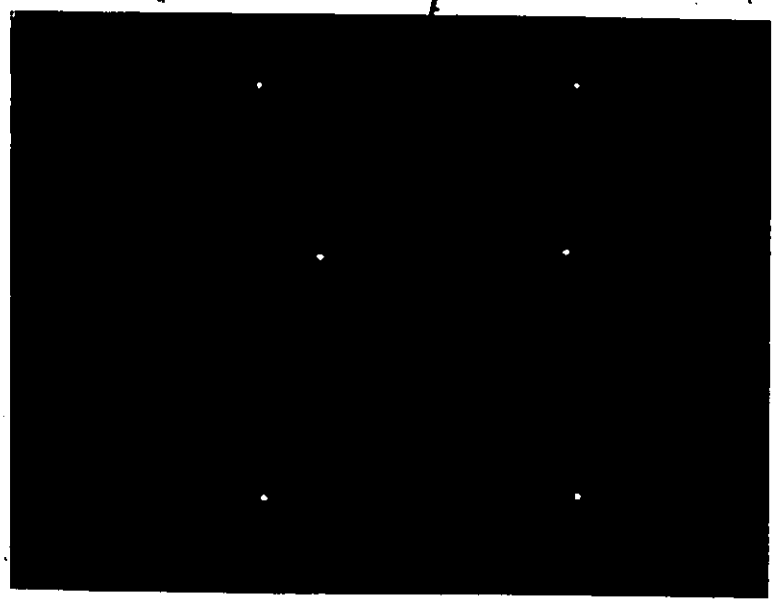

a

```
17
TABLT6      1     7     1     1     1
ENTER T#P LEFT C#RNER #F PICTURE
ENTER T#P RIGHT C#RNER #F PICTURE
ENTER B#TT#M RIGHT C#RNER #F PICTURE
ENTER B#TT#M LEFT C#RNER #F PICTURE
ENTER P#INT #1 #N MAP SCALING INTERV
ENTER P#INT #2 #N MAP SCALING INTERV
TYPE SCALING INTERVAL IN MAP UNITS:F
GIVE SINT:F10.0
50000.
    50000.
ISIT#K? 1=YES, 2=N#, 3=AB#RT:I1
1
RECTANGULARITY TEST ERR#RS=  0.10142E+01 -0.99072E+00
RECTANGLE SL#PE ANGLE (DEGREES)=   359.1558
IG#05:I2
```

b

Figure 7.1: (a) Plot on Tektronix 611 video display of the four corners of the rectangle to be digitized and the scaling interval; (b) the conversation on the teletype related to this plot.

(a) A submap is mounted onto the graphic tablet with the sides preferably parallel to the coordinate system of the tablet in order to minimize rotation of the data. The tablet is provided with adequate grids to facilitate map mounting.

(b) A relationship is then established between the rectangular submap and the tablet coordinates by pointing with the tablet stylus at the four corners of the submap and at the two ends of the scaling interval (see Figure 7.1). This process can be repeated several times in order to get averages and minimize pointing errors.

(c) The digitization is performed on-line, i.e. an operator traces the map contours which the computer approximates by appropriate short line segments (vectors). During this tracing process, which is done on a graphic tablet by means of a pen-like cursor, or stylus, both the trace of the pen and the endpoints of the vectors computed are displayed on a Tektronix 611 storage display, as shown in Figure 7.2.

(d) The raw digitized contour points, the corners of the rectangular subarea, the scaling interval in the map units and the map identification code are stored on digital magnetic tape for further usage.

a

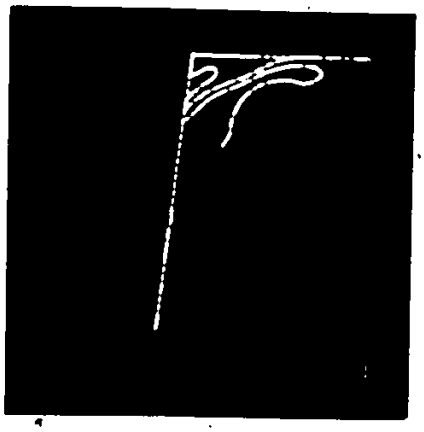

b

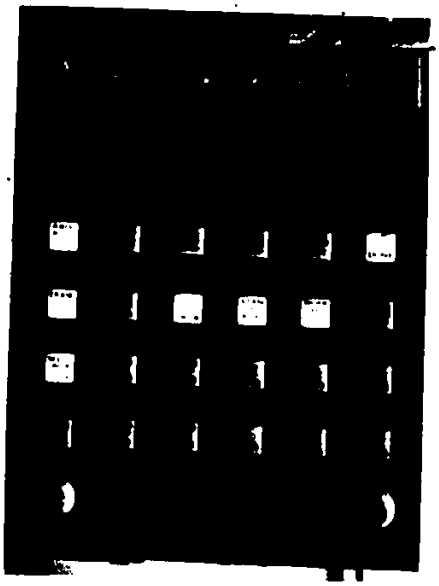

c

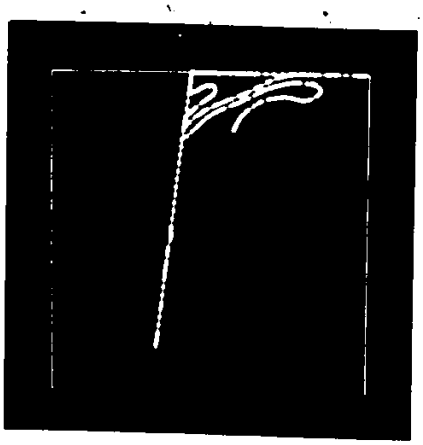

d

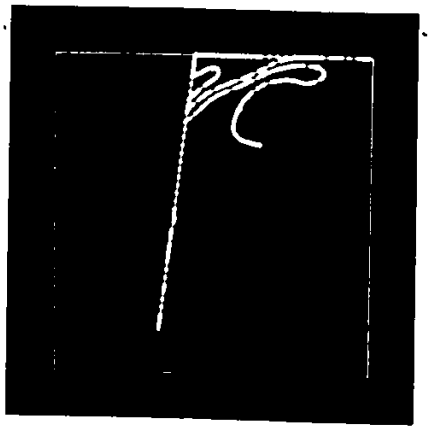

Figure 7.2: Tektronix 611 vector displays during interaction for digitizing.
(a) the digitized portion of a boundary: an error was made while digitizing. It was detected by looking at the display. Vector ends are marked by small circles, the position and lenth of each endpoint is marked by a brighter dot.
(b) The push-button box or command console. Editing on line can be done by erasing via push-button action the last stored vector.
(c) Tektronix 611 display after erasing the recent erroneous vector and replotting the remaining stored vectors. The last seven vectors have been eliminated.
(d) Display of the corrected boundary after removal of the wrong vectors and substitution by the corrected vectors.

```
18
TABLT7    300     1
NPIXEL,FPIXEL,DPIXEL =    300    167.2241      2.6757
AVERAGE DIMENSI#NS:IDIMA,JDIMA =    380   502
C#RNERS =  -511   668   505  -672
  -511.05408   668.97949   505.07739  -672.03271
T,C#,SI =    0.359663E+03   0.999983E+00  -0.587649E-02
IG#05:I2
```

Figure 7.3: Interactive conversation which provides the constants for scaling values to be used in the processing.

(e) A program divides the given scale interval into a desired number of resolution units (picture elements or pixels), gives the ground distance (resolution) per pixel and the overall size of the subpicture in picture element units. The resultant constants or scaling values are used in the subsequent step of processing (see Figure 7.3).

(f) When all the rectangular submaps have been digitized, and the raw data preserved, these maps are converted to binary two-dimensional form and stored as matrices or binary pictures. The procedure is equivalent to laying a transparent squared paper onto each map segment and by marking each square as one (1) if a contour line crosses the square, and as a zero (0), if no contour is in the square. The resultant marked overlay is a binary picture of the map contours. Obviously the resolution of the binary map depends on the size of the squares chosen. Each square is also called a picture element or pixel. The present maximum size of the binary submap is 512 x 512 pixels.

(g) Select the most complicated subpicture and determine an adequate resolution for the binary image. The above two processing steps may have to be repeated on

Figure 7.4: Binary images of a square portion of a geological map, obtained at different resolutions from the same vectors: (a) one pixel = 1000 m, (b) one pixel = 500 m, (c) one pixel = 375 m, and (d) one pixel = 250 m, the resolution selected. These plots have been obtained on a Versatec dot matrix printer. The frames are not part of the picture data.

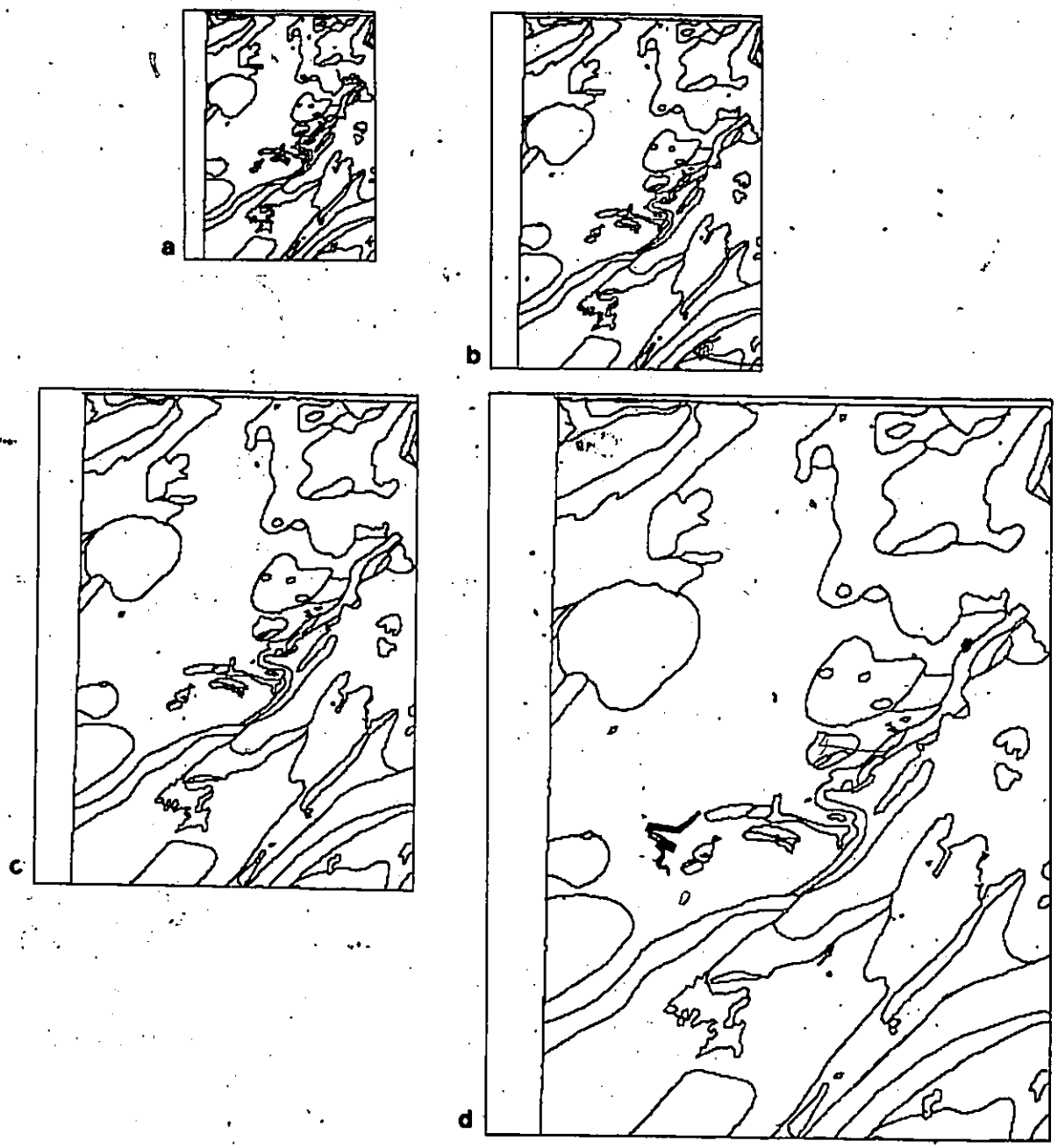

Figure 7.4: Concluded.

the chosen subpicture for a few times to select an adequate resolution. Once an adequate resolution is selected, this is then used for all subsequent related rectangles and for all maps of a set (see Figure 7.4).

(h) Since each binary submap corresponds to one of the map segments, a composite binary map is created by inserting each binary submap into its corresponding position in a large binary map. Due to its size the large binary map (mosaic) cannot be stored in the memory of the computer. The present maximum size of the binary mosaic (large map) is 1024 x 1024 picture elements. The accuracy with which one submap can be aligned with another is in the order of one picture element (see Figure 7.5).

(i) Alternatives to the above procedures, which are also available are:

(1) The binary submap for insertion into the mosaic is created directly from the raw digitized data without storage of the intermediate results (binary submaps).

(2) A binary submap can be obtained by scanning a 35 mm transparency of the map section.

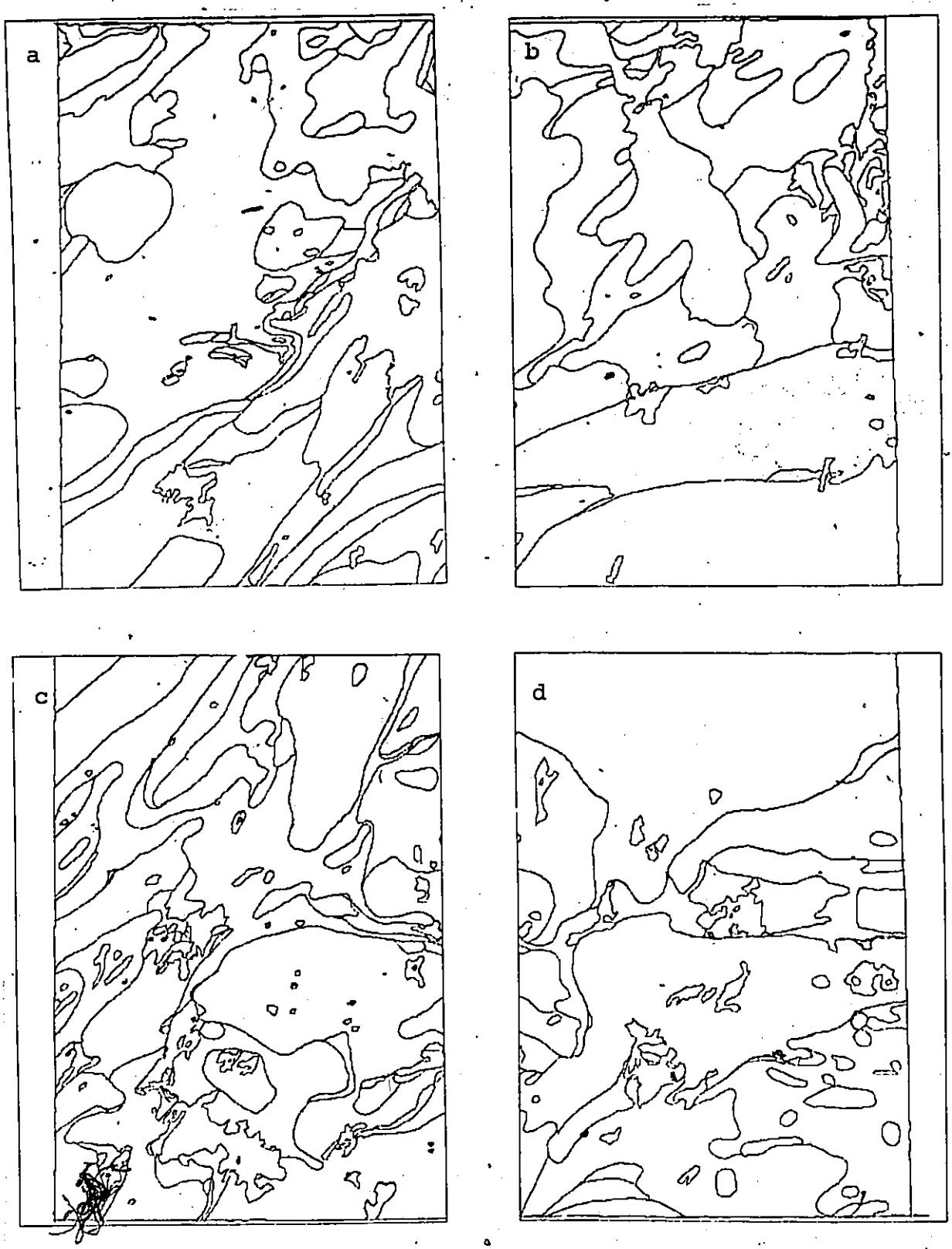

Figure 7.5: A mosaic of four independently digitized rectangular areas from a geological map. These plots have been obtained on a Versatec dot matrix printer. The four images have dimensions of 380 pixels x 502 pixels each. The mosaic displayed is 760 pixels x 1004 pixels. Plots (a) to (d) are the four independent subimages; (e) the resulting mosaic.

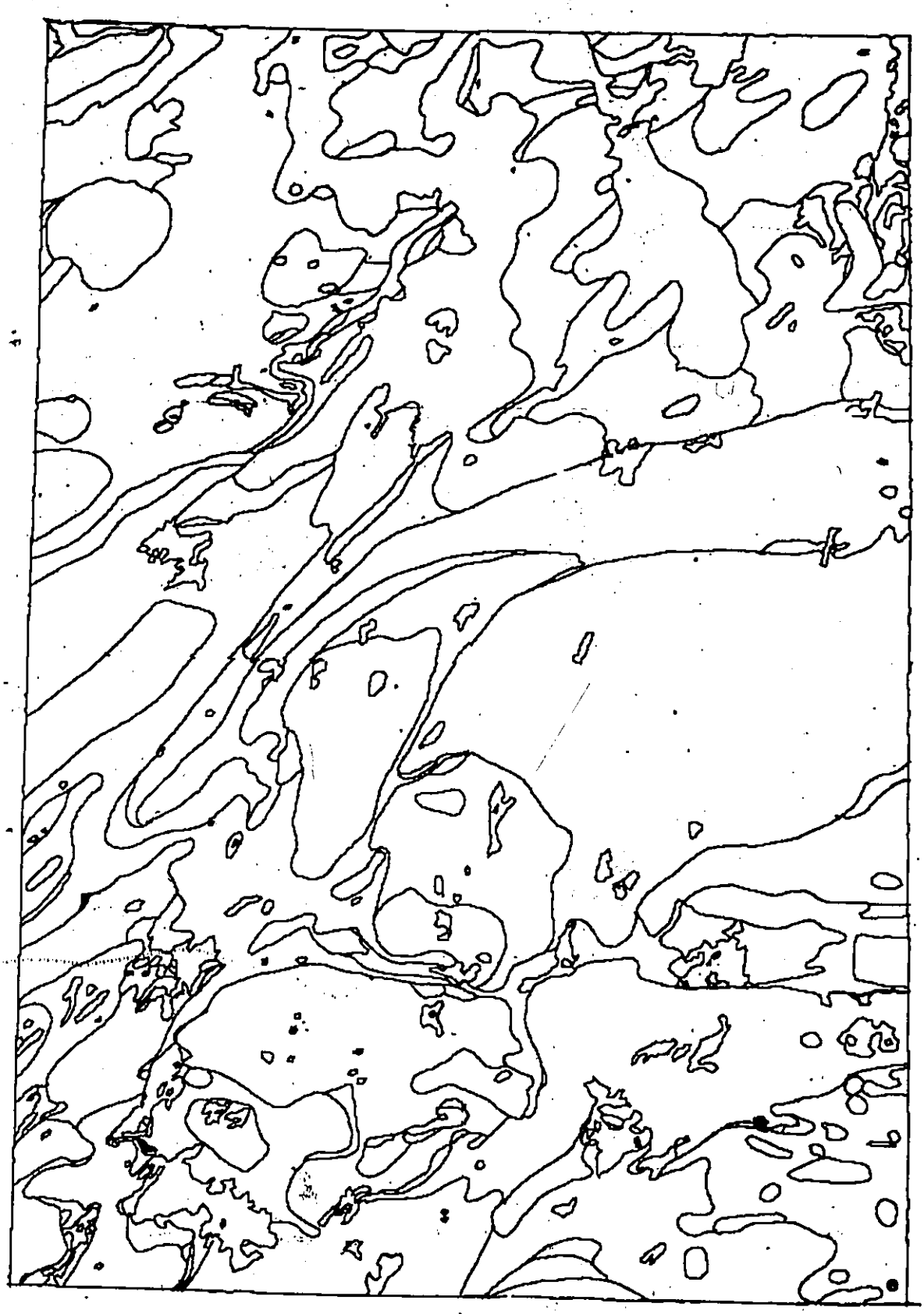

Figure 7.5: Concluded.

(j) Due to the resolution of the binary maps, certain very small areas may become closed, some adjacent contours may touch and some breaks or other defects may occur. To ascertain that the pattern of the binary (large) map corresponds as well as possible to that of the original, the binary map is printed and checked. Whenever feasible, the defects are removed by adding or deleting contour pixels via displays and manual online interaction via a special command console and online displays of enlarged portions of picture details (see Figures 7.6, 7.7, and 7.8). A hard copy of the area being edited can also be printed on the line printer (Versatec).

(k) The thickness of the contours, represented by the contour pixels in the binary picture, is now reduced to a minimum while preserving the connectivity of lines. The process is called line thinning which is a topology preserving operation. After this stage of processing, for which the image needs to be in binary expanded form, the maps are represented by binary pictures containing thin (single pixel) contours. The thinned form is more suitable for subsequent processing, since certain operations are simplified (see Figure 7.8).

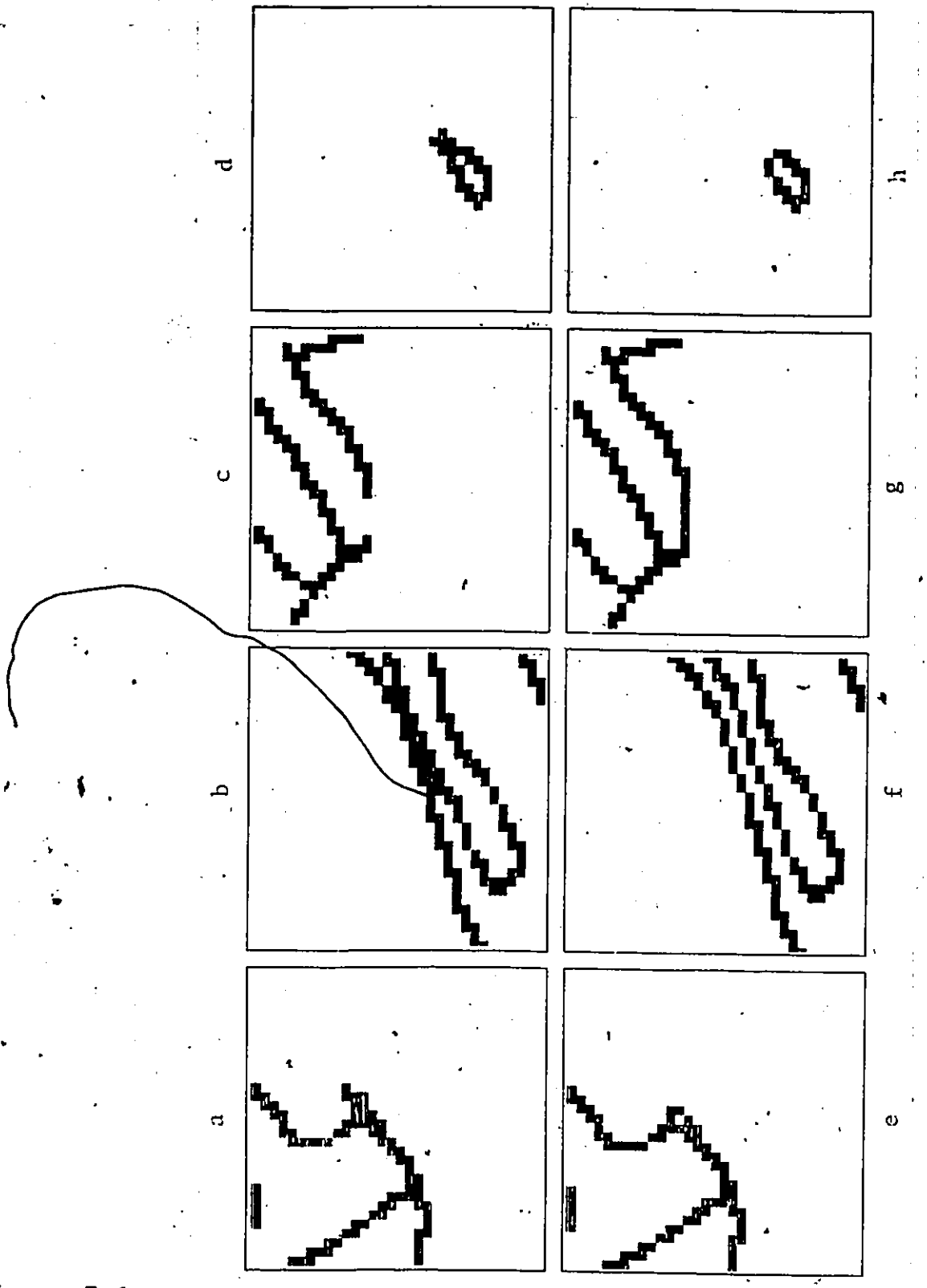

Figure 7.6: Occurrence and removal of digitizing defects from the binary images produced by transforming the vectors from the graphic tablet. Some examples of defects are as follows: (a) a small area which is closed, (b) two adjacent contours which touch, (c) a contour which is broken, and (d) overshooting an enclosed contour. These defects have been removed from figures (a) to (d), as can be seen in figures (e) to (h). In these enlarged subpictures each pixel is reproduced as an array of 6 dots x 6 dots.

Figure 7.7: Interactive editing (addition or removal of black dots or pixels) of binary images via a special command console and online displays of enlarged portions of picture details. The command console in (a) is used in order to select the options tabulated on the Tektronix 611 screen in (b). A selected window is plotted in (c) and points deleted by means of a pointer under the control of two wheels in the command console (d) now used in the updating mode. The complement of the image window can also be displayed in order to "add" black pixels (i.e., delete from the complement) as can be seen in (e). A hard copy of the area being edited is printed on a line printer (f). During these interactions the progressively edited versions of the binary picture are presently stored on two disks, while the subarea being edited is in computer memory.

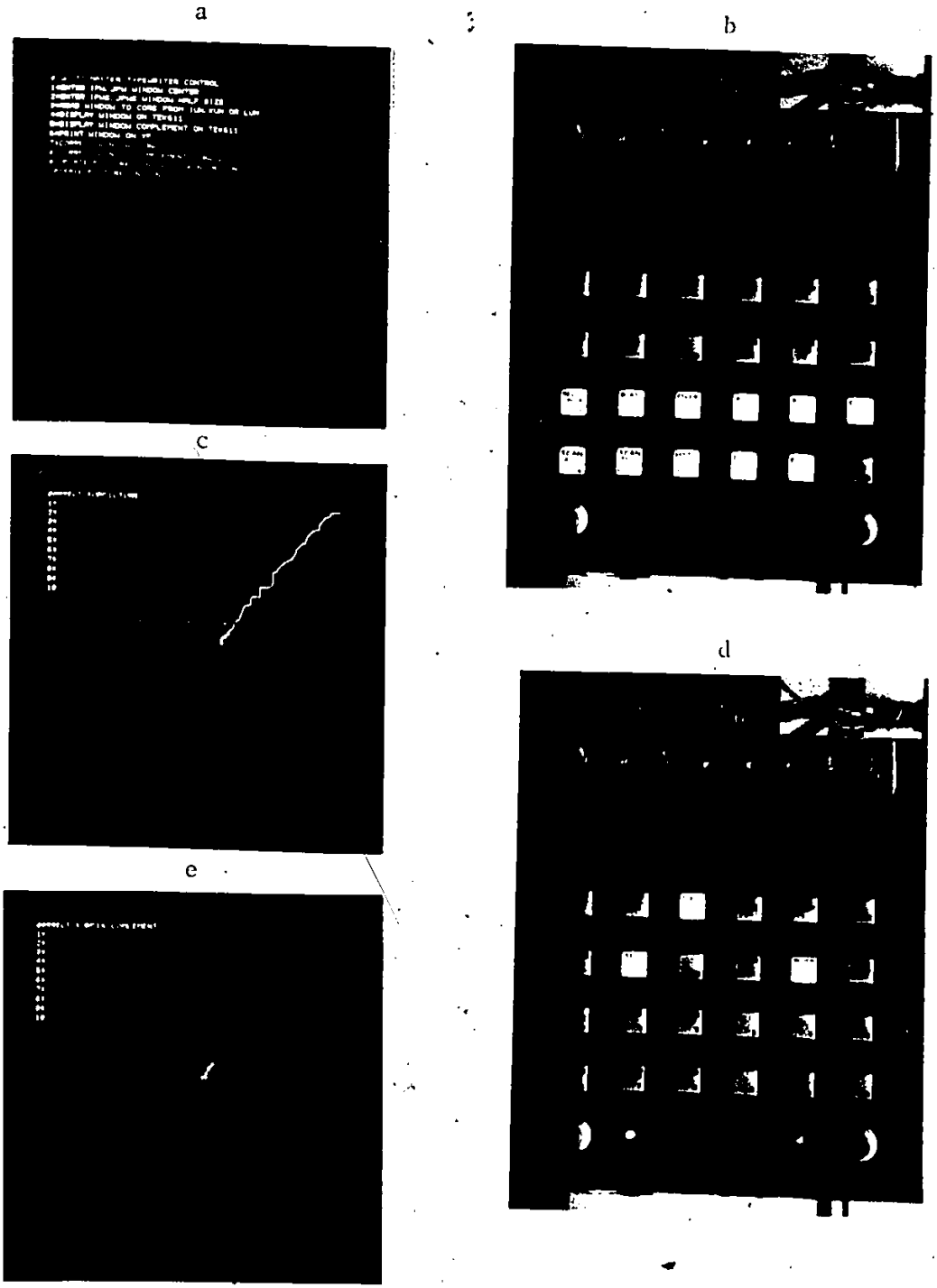

Figure 7.7: Continued.

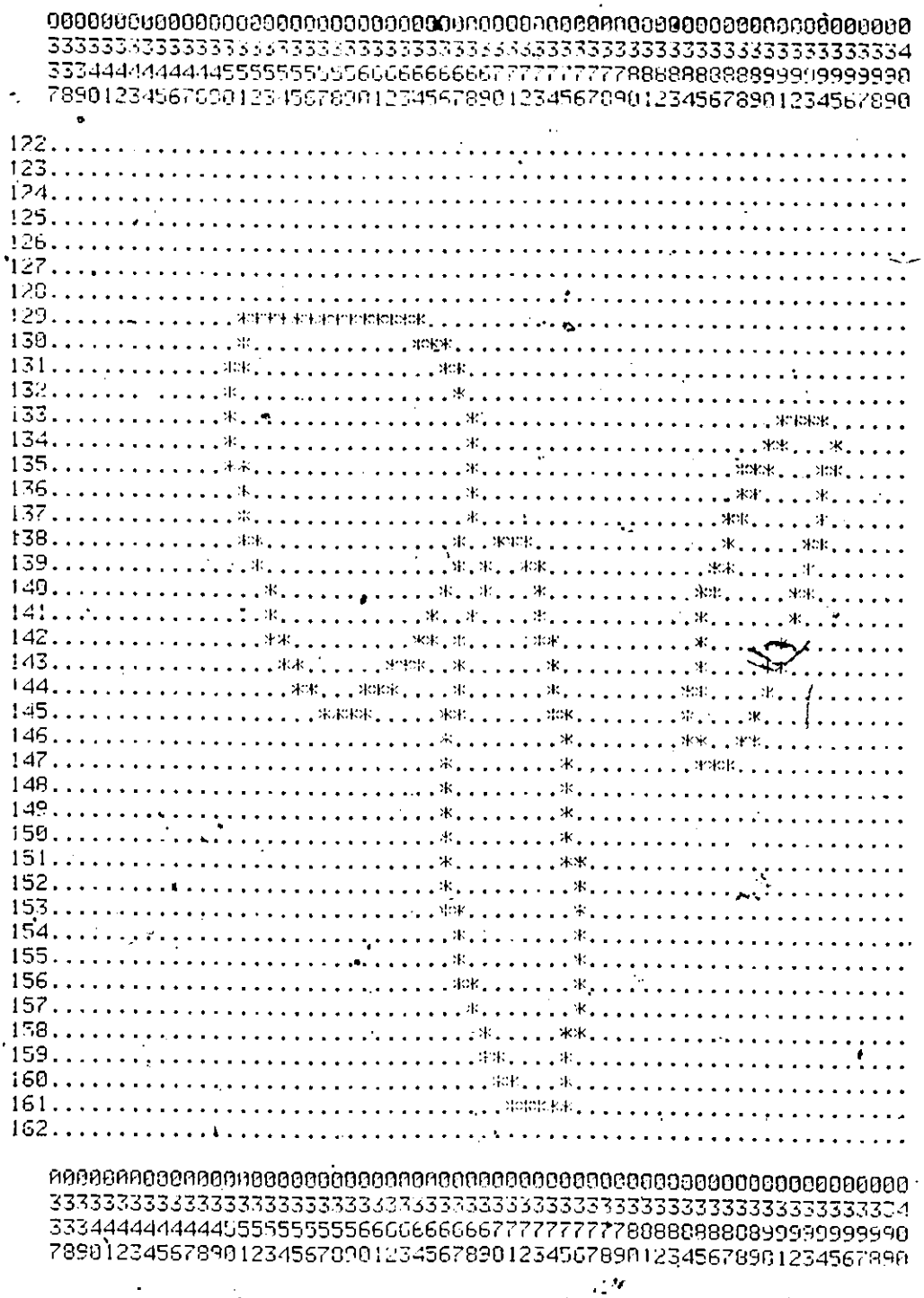

Figure 7.7: Concluded.

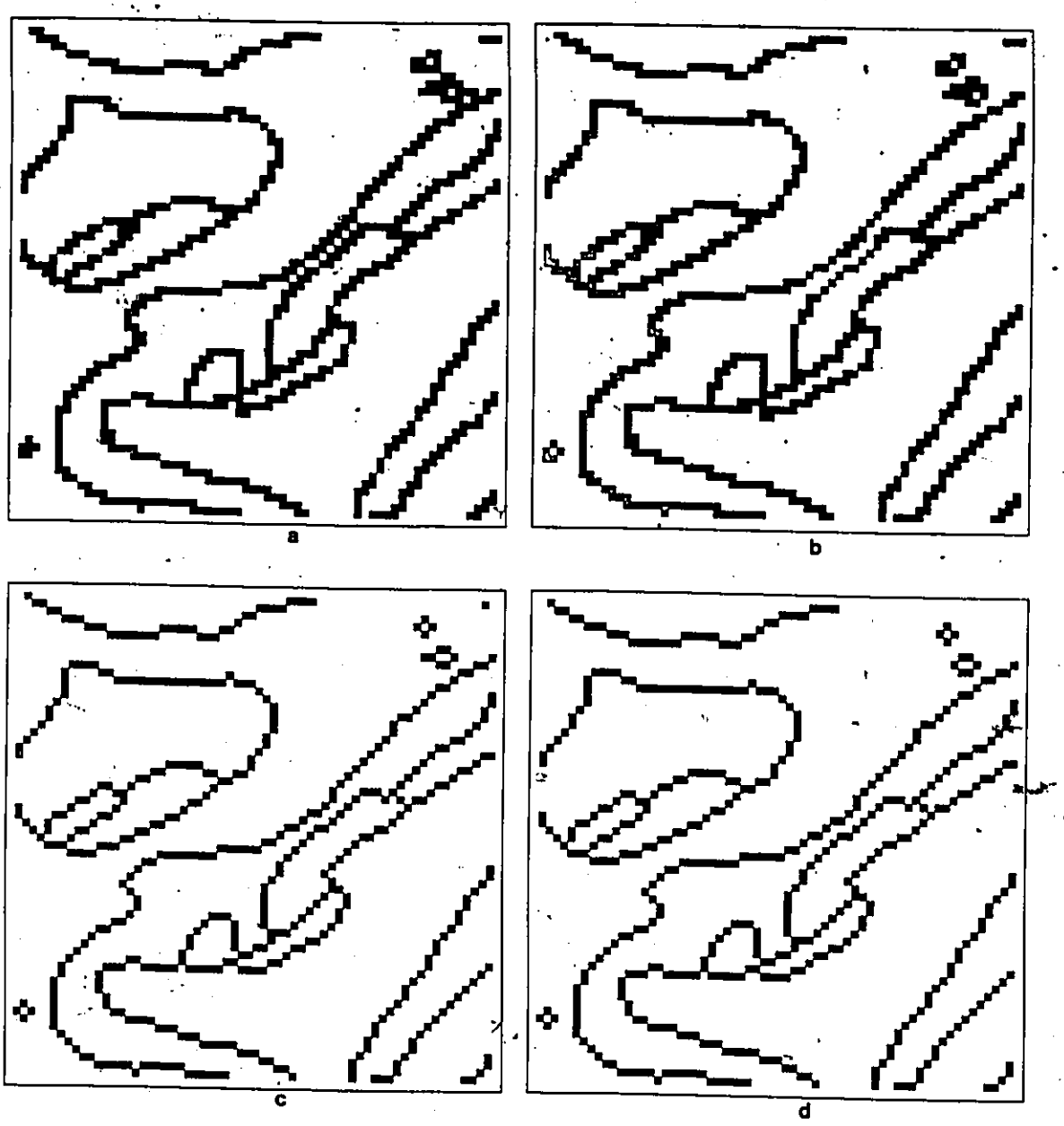

Figure 7.8: Editing and line thinning of the binary image of geological contours. A magnified portion is displayed before editing in (a), after a first editing but before thinning, in (b), after thinning in (c), and after additional minor editing in (d). A binary mosaic is displayed in (e) after a first editing but before thinning, in (f) after thinning, and in (g) after additional minor editing.

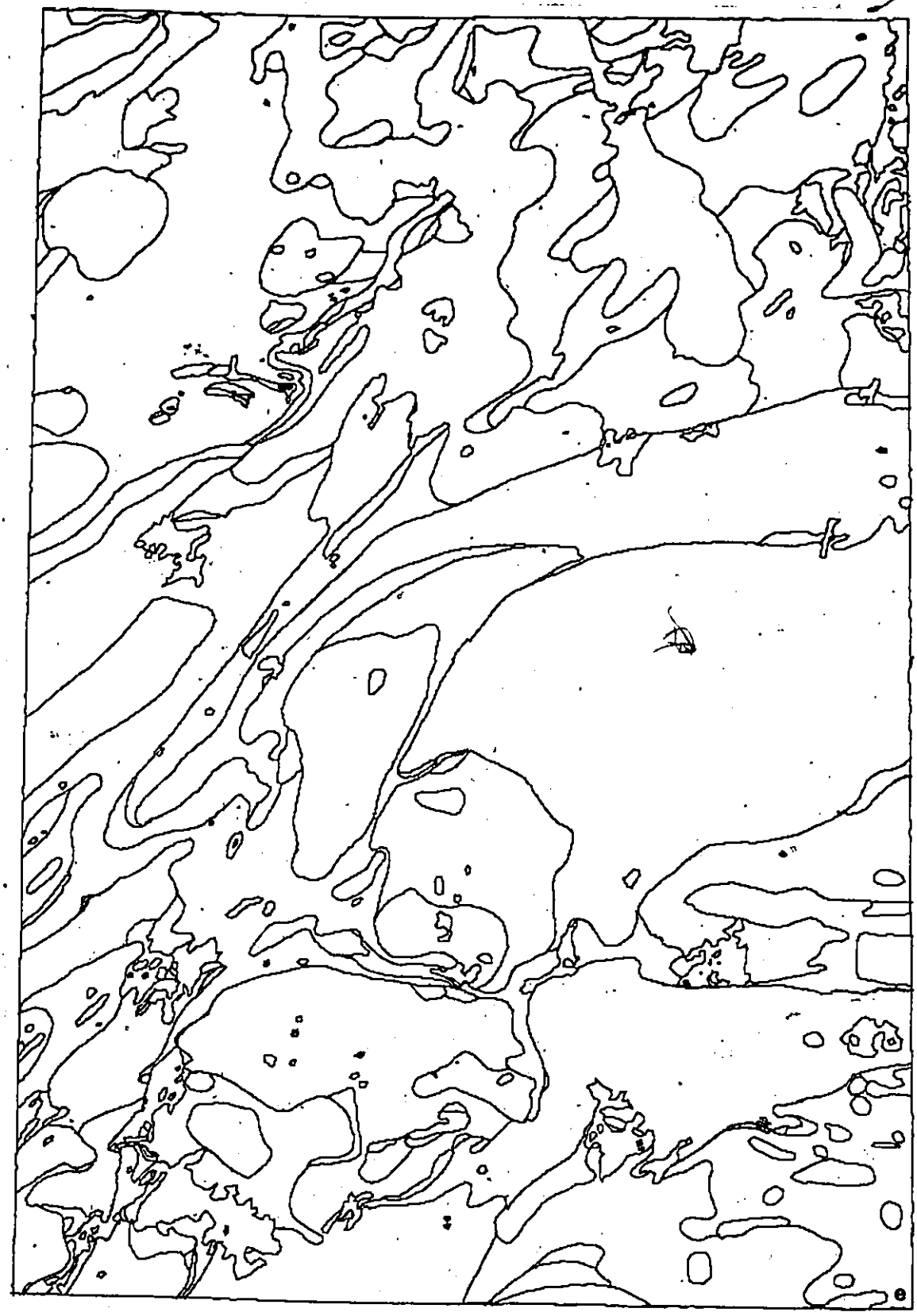

Figure 7.8: Continued.

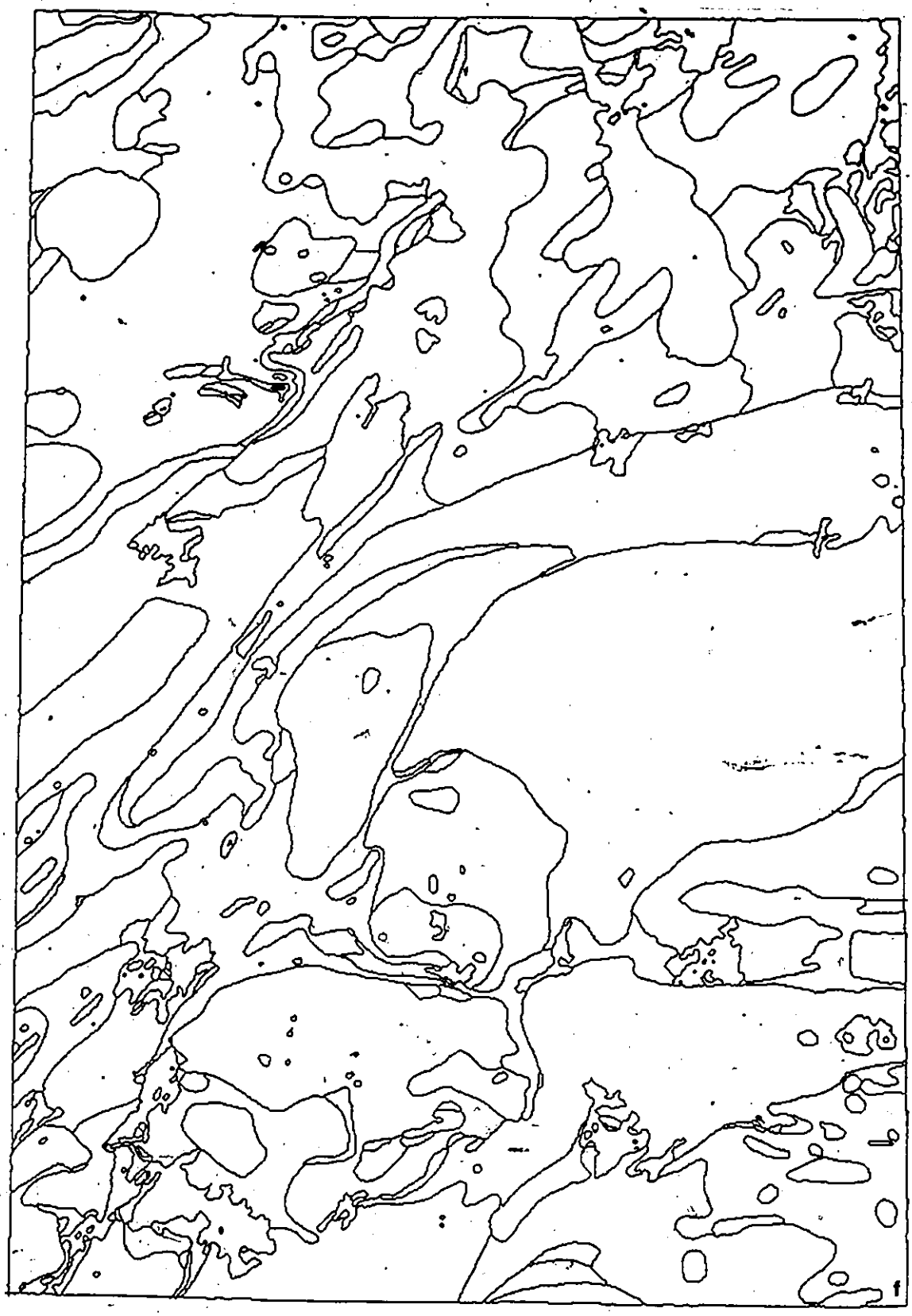

Figure 7.8: Continued.

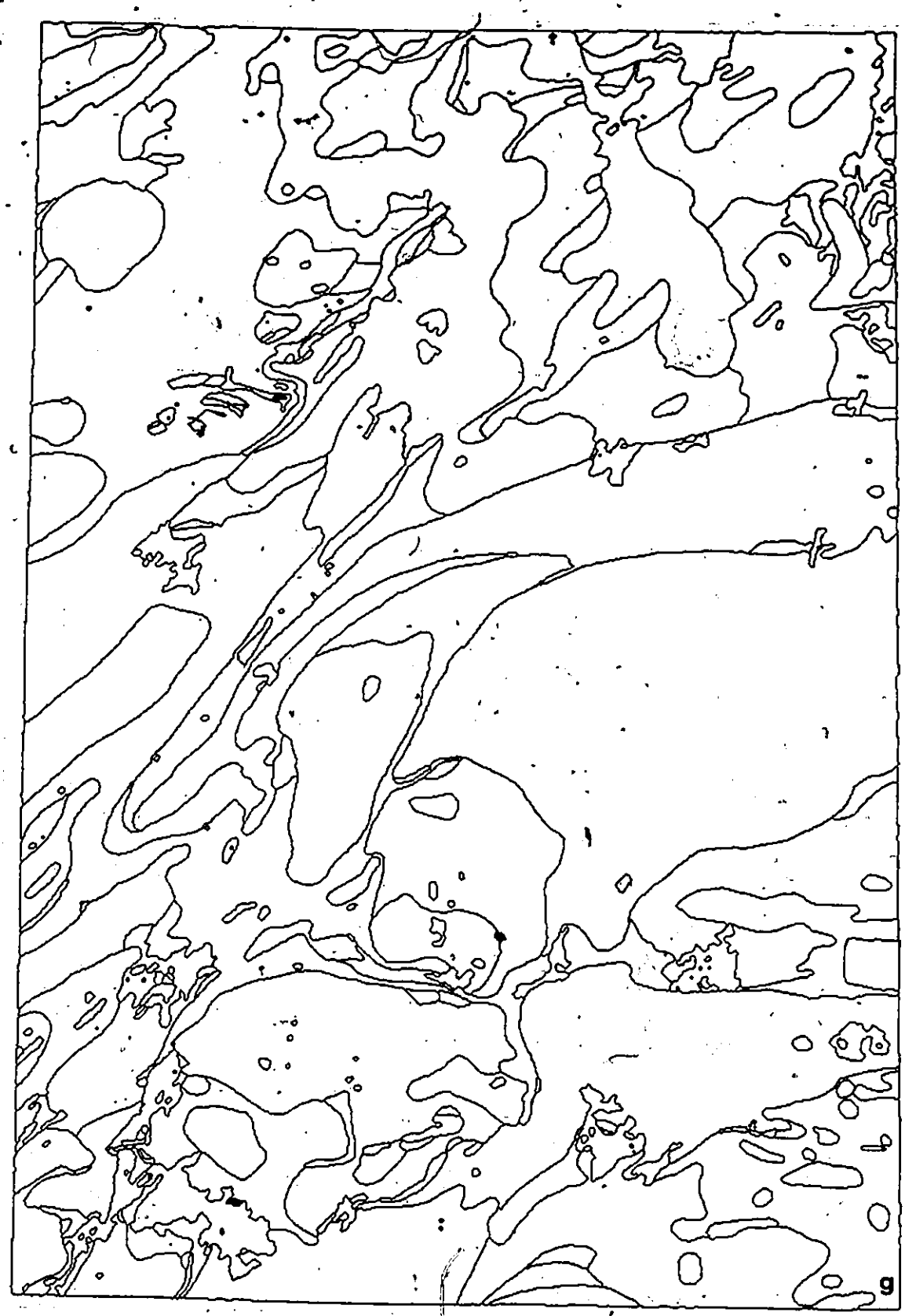

Figure 7.8: Concluded.

(l) In order to identify each enclosed area in the picture, a unique label or serial number is now automatically assigned to each area. The edges of the pictures are also considered as "contours", implying that all areas in the picture are "enclosed". The picture, however, is now no longer binary (see Figures 7.9 and 7.10).

(m) The enclosed area labeling has assigned a unique number to each area. However, the map only contains a certain number of map units (phases). The online operator now assigns a unique serial number to each phase, i.e. each enclosed area is identified as belonging to a given phase. The process is semi-automatic, carried out via interactive displays and pushbuttons. The computer associates the phase labels with the area labels. During this process, missing phase labels and duplicate labels are detected. These errors are corrected (see Figure 7.11) by displaying the appropriate areas and deleting or adding the appropriate data online. Returning to earlier stages is needed only if a topological error has been discovered, for example a missing contour line. Additional software is desirable to facilitate detection of inconsistencies and operator errors at the earliest stages of processing.

Figure 7.9: A binary expanded 21 pixels x 45 pixels portion of the image of thinned geological contours. 1's represent boundary pixels, 0's represent the areas contoured.

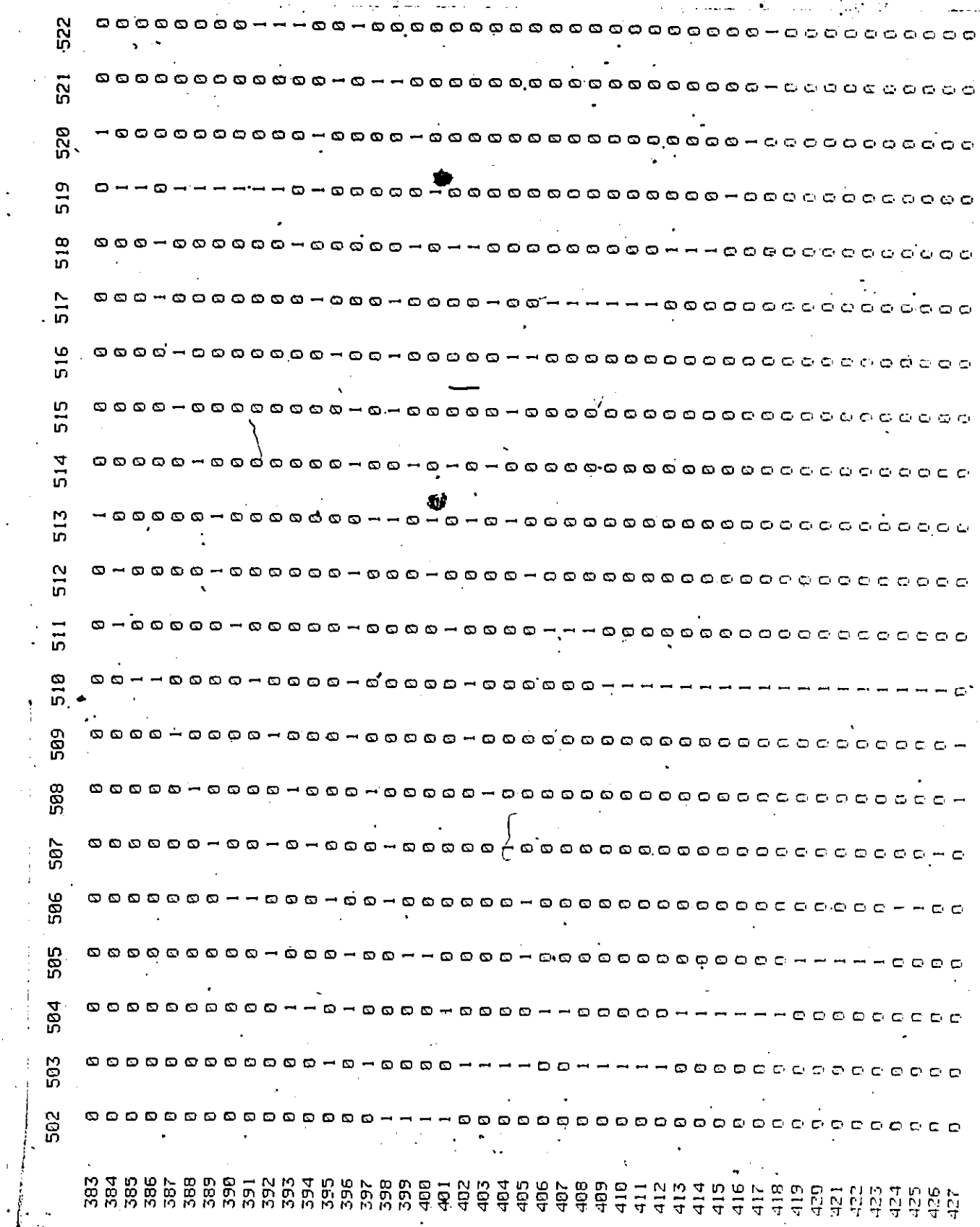

Figure 7.9: Concluded

Figure 7.10: A 21 pixels x 45 pixels portion of the image of geological contours in component-labeled form. 1's represent boundary pixels, values 2 and larger represent the sequential labels uniquely assigned to each area enclosed by the 1's.

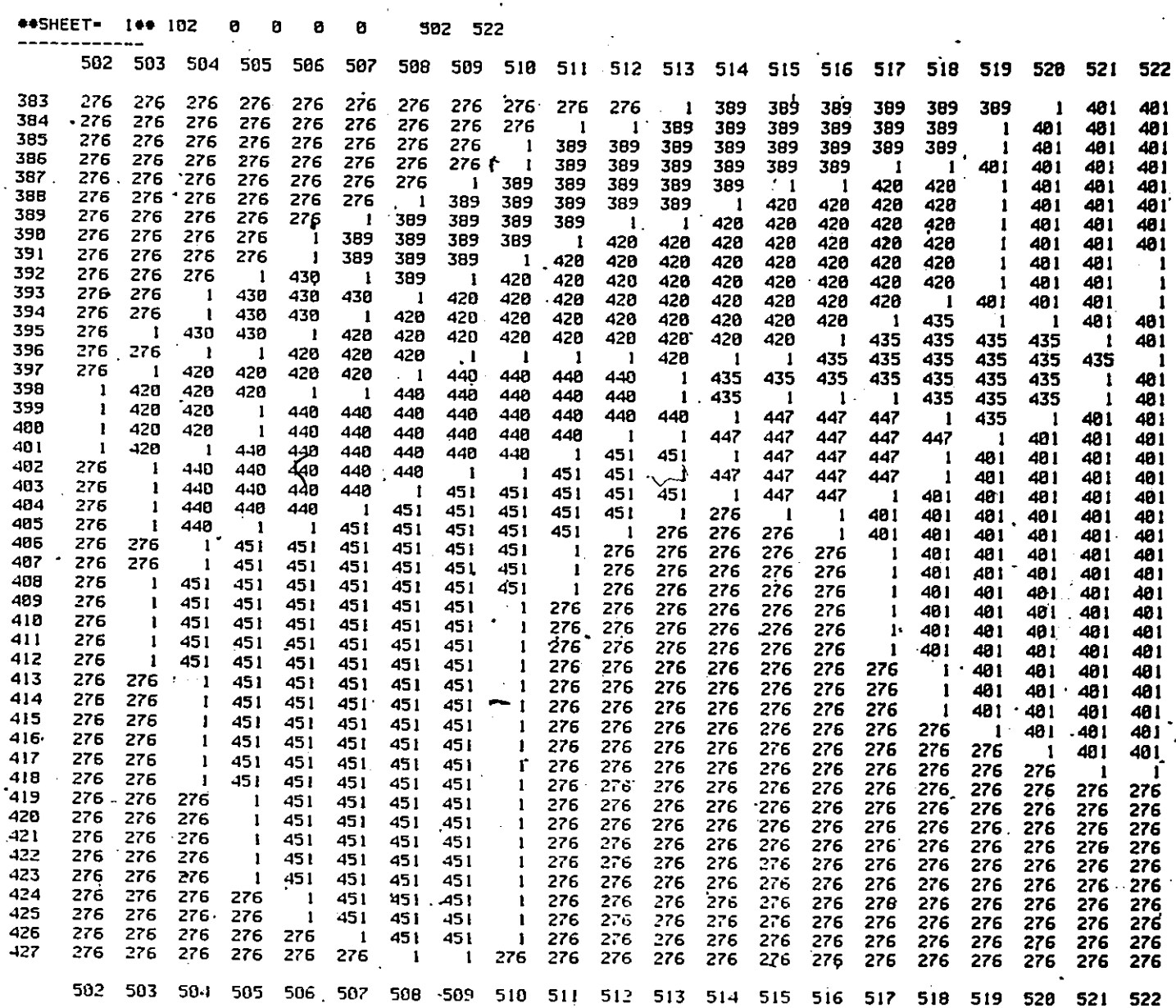

```
**SHEET- I** 102   0   0   0   0     502 522
------------
      502  503  504  505  506  507  508  509  510  511  512  513  514  515  516  517  518  519  520  521  522

383   276  276  276  276  276  276  276  276  276  276  276    1  389  389  389  389  389  389    1  401  401
384   276  276  276  276  276  276  276  276  276    1    1  389  389  389  389  389  389  389    1  401  401  401
385   276  276  276  276  276  276  276  276    1  389  389  389  389  389  389  389  389  389    1  401  401  401
386   276  276  276  276  276  276  276  276    1  389  389  389  389  389  389  389    1    1  401  401  401  401
387   276  276  276  276  276  276  276    1  389  389  389  389  389  389    1    1  420  420    1  401  401  401
388   276  276  276  276  276  276    1  389  389  389  389  389    1  420  420  420  420    1  401  401  401
389   276  276  276  276  276    1  389  389  389  389    1    1  420  420  420  420  420    1  401  401  401
390   276  276  276  276    1  389  389  389  389    1  420  420  420  420  420  420  420    1  401  401  401
391   276  276  276  276    1  389  389  389    1  420  420  420  420  420  420  420  420  420    1  401  401
392   276  276  276    1  430    1  389    1  420  420  420  420  420  420  420  420  420  420    1  401  401    1
393   276  276    1  430  430  430    1  420  420  420  420  420  420  420  420  420  420    1  401  401  401    1
394   276  276    1  430  430    1  420  420  420  420  420  420  420  420  420  420    1  435    1    1  401  401
395   276    1  430  430    1  420  420  420  420  420  420  420  420  420  420    1  435  435  435  435    1  401
396   276  276    1    1  420  420  420    1    1    1    1  420    1    1  435  435  435  435  435  435  435    1
397   276    1  420  420  420  420  420    1  440  440  440  440    1  435  435  435  435  435  435  435    1  401
398     1  420  420  420    1    1  440  440  440  440  440  440    1  435    1    1  435  435  435    1  401
399     1  420  420    1  440  440  440  440  440  440  440  440    1  447  447  447    1  435    1  401  401
400     1  420  420    1  440  440  440  440  440  440    1    1  447  447  447  447  447    1  401  401  401
401     1  420    1  440  440  440  440  440  440    1  451  451    1  447  447  447    1  401  401  401  401
402   276    1  440  440  440  440  440    1    1  451  451  451  447  447  447  447    1  401  401  401  401
403   276    1  440  440  440  440    1  451  451  451  451  451    1  447  447    1  401  401  401  401  401
404   276    1  440  440  440    1  451  451  451  451  451  451    1  276    1    1  401  401  401  401  401  401
405   276    1  440    1    1  451  451  451  451  451    1  276  276  276    1  401  401  401  401  401  401
406   276  276    1  451  451  451  451  451  451    1  276  276  276  276  276    1  401  401  401  401  401
407   276  276    1  451  451  451  451  451  451    1  276  276  276  276  276    1  401  401  401  401  401
408   276    1  451  451  451  451  451  451  451    1  276  276  276  276  276    1  401  401  401  401  401
409   276    1  451  451  451  451  451  451    1  276  276  276  276  276  276    1  401  401  401  401  401
410   276    1  451  451  451  451  451  451    1  276  276  276  276  276  276    1  401  401  401  401  401
411   276    1  451  451  451  451  451  451    1  276  276  276  276  276  276    1  401  401  401  401  401
412   276    1  451  451  451  451  451  451    1  276  276  276  276  276  276  276    1  401  401  401  401
413   276  276    1  451  451  451  451  451    1  276  276  276  276  276  276  276    1  401  401  401  401
414   276  276    1  451  451  451  451  451    1  276  276  276  276  276  276  276    1  401  401  401  401
415   276  276    1  451  451  451  451  451    1  276  276  276  276  276  276  276  276    1  401  401  401
416   276  276    1  451  451  451  451  451    1  276  276  276  276  276  276  276  276  276    1  401  401
417   276  276    1  451  451  451  451  451    1  276  276  276  276  276  276  276  276  276  276    1    1
418   276  276    1  451  451  451  451  451    1  276  276  276  276  276  276  276  276  276  276  276  276
419   276  276  276    1  451  451  451  451    1  276  276  276  276  276  276  276  276  276  276  276  276
420   276  276  276    1  451  451  451  451    1  276  276  276  276  276  276  276  276  276  276  276  276
421   276  276  276    1  451  451  451  451    1  276  276  276  276  276  276  276  276  276  276  276  276
422   276  276  276    1  451  451  451  451    1  276  276  276  276  276  276  276  276  276  276  276  276
423   276  276  276    1  451  451  451  451    1  276  276  276  276  276  276  276  276  276  276  276  276
424   276  276  276  276    1  451  451  451    1  276  276  276  276  276  276  276  276  276  276  276  276
425   276  276  276  276    1  451  451  451    1  276  276  276  276  276  276  276  276  276  276  276  276
426   276  276  276  276  276    1  451  451    1  276  276  276  276  276  276  276  276  276  276  276  276
427   276  276  276  276  276  276    1    1  276  276  276  276  276  276  276  276  276  276  276  276  276

      502  503  504  505  506  507  508  509  510  511  512  513  514  515  516  517  518  519  520  521  522
```

Figure 7.10 Concluded.

Figure 7.11: Interactive phase labeling of labeled areas from binary thinned contours. (a) the special command console, (b) the menu of options, (c) labeling areas, (d) the command console during the labeling mode and (e) eliminating a duplicate label.

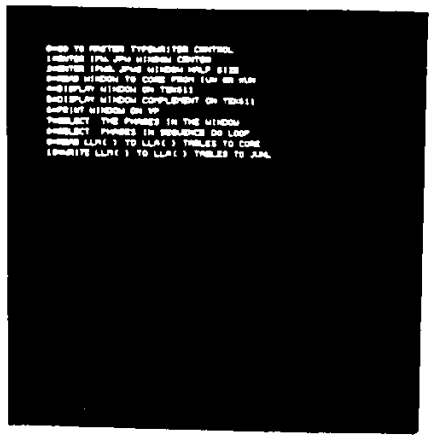

b

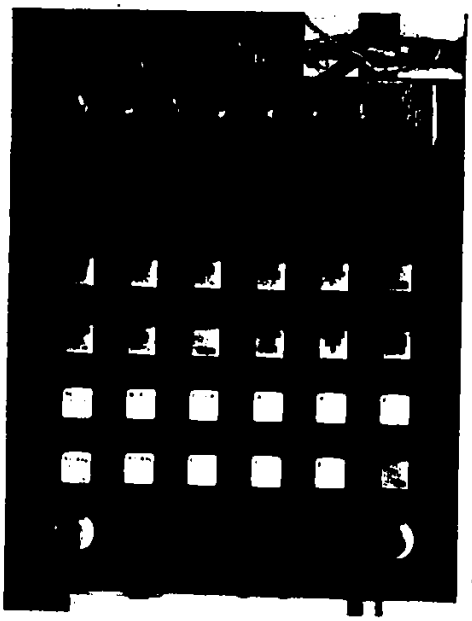

a

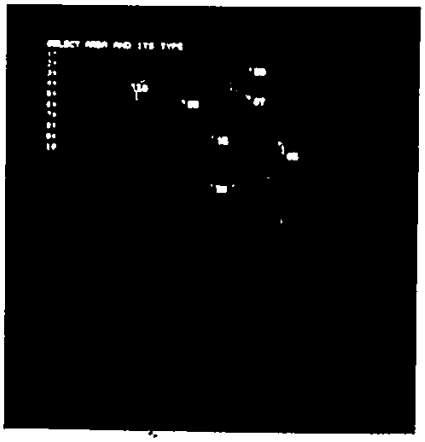

c

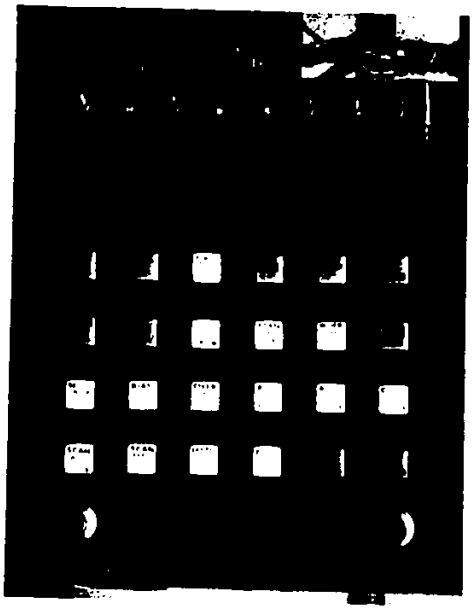

d

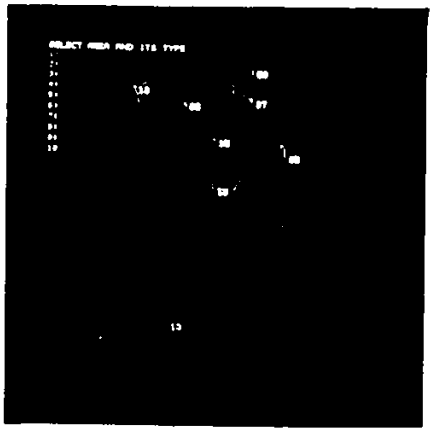

e

Figure 7.11: Concluded.

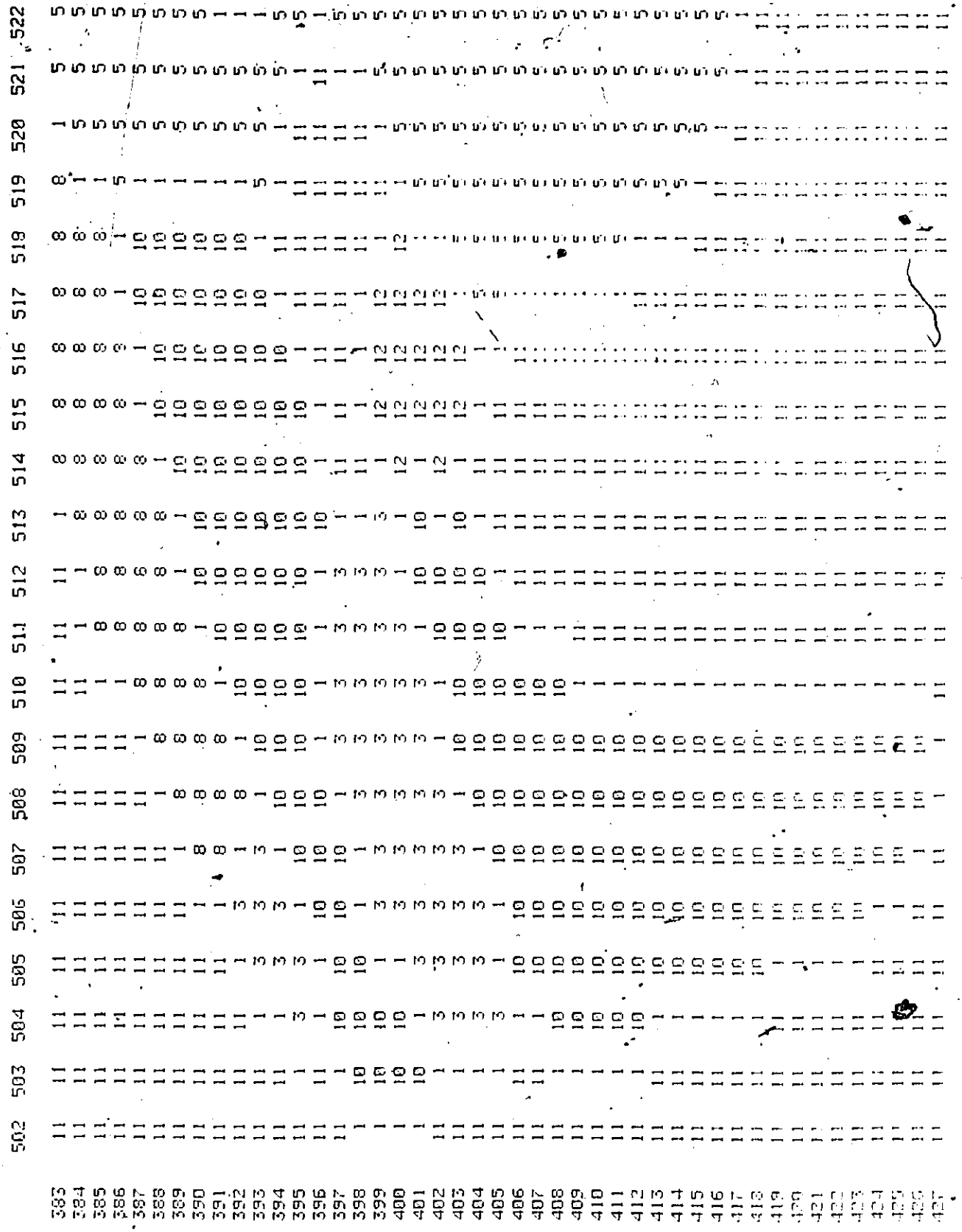

Figure 7.12: A phase-labeled 21 pixels x 45 pixels portion of the same image as in Figure 7.10. The 1's in this printout correspond to boundary pixels. The numbers 2 and higher are the new phase labels assigned interactively.

(n) The phase-labeled image may now be used in variety of ways, for example, to create a binary image for each phase, to study relationships between phases, etc. This data is also stored on magnetic tape and may be transferred to other computers for further analysis. The data is in raster format (see Figure 7.12).

In order to define alternative approaches to the above described procedures for map processing, these procedures may be summarized as follows:

(i) Online digitization of the contour data, resulting in tables of vectors [1].

(ii) Conversion of the vector data from the tablet to raster formatted images or submaps.

(iii) Patching of the submaps into into mosaics of binary raster formatted contour maps.

(iv) Interactive editing of the raster formatted binary images.

(v) Contour line thinning.

(vi) Closed area labeling.

---

[1] Submap creation and the subsequent patching to create mosaics was dictated by equipment limitations, i.e. too small a tablet, even though to have the option of creating mosaics is an advantage, irrespective of tablet size.

(vii) Interactive phase labeling.

(viii) Creation of phase labeled raster formatted images.

(ix) Subsequent processing of the phase labeled images.

The alternative approaches are as follows:

(1) If the digitizing is done on a larger tablet, submap generation can be avoided. The processing steps from (iv) onwards remain unchanged. It would, however, be highly advisable to carry out the phase labeling also as a part of the procedures, thereby eliminating most of the work in step (vii), interactive labeling. Step (vii) will, however, still be required for possible online correcting or editing.

(2) The contour maps may also be raster scanned to create or obtain a binary raster formatted mosaic directly. The maps, however, should be adequately registered on the scanner to avoid subsequent resampling. Processing steps (iv) and onwards will remain unchanged.

(3) The interactive editing stages in steps (iv) and (vii) are somewhat dependent on the peculiarities of the hardware and programming philosophy of the Modcomp II system at N.R.C. Some modifications to these programs will be needed before they can run successfully elsewhere.

7.3 The geological data base

The map information digitized covers the Kasmere Lake - Whiskey Jack Lake (North Half) Area, in Northwestern Manitoba, which is located between longitudes 100°00' W and 102°00' W, and between latitudes 58°30' N and 60°00' N (NTS 64N and 64K north half). Except for the gravity map at scale 1:500000, all maps for the quantification were available at the U.T.M. projection, scale 1:250000, and cover an area of approximately 20000 km².

A main source of information about the geology of the study area is a report by Weber et al (1975) which, beside containing several geological and ancillary maps, provides much detail about the stratigraphy and the economic geology of the region. Other relevant sources are a gravity map series by Gibb and McConnell (1969) covering the area with a sparse set of measuring stations at 1:500000 (Map 76: Wollaston Lake) and a set of three 1:250000 contour maps of airborne gamma ray spectrometric integer counts of equivalent uranium, thorium (eU and eTh) and the ratio eU / eTh, made available by the Geological Survey of Canada as open files (1976, numbers 317 and 318).

A table of geological formations which represent the stratigraphic reconstruction after Weber et al (1975, p. 17) is shown in Table 7.1.

TABLE 7.1

Table of formations in NBGA, modified after Weber et al. (1975)

Pleistocene and Recent			Sand-gravel, boulder fields, clay (glacial till, eskers, fluvioglacial boulder deposits, lake bottom sediments)		
GREAT UNCONFORMITY					
		Hudsonian igneous and metamorphic rocks	22 Fluorite-bearing quartz monzonite 21 Quartz-feldspar porphyry 20 Porphyritic quartz monzonite 19 Pink leucogranite to quartz monzonite, biotite-quartz monzonite 18 Migmatite: (a) Metatexite; (b) Diatexite 17 White granite to quartz monzonite, pegmatite, locally garnet-bearing		
INTRUSIVE CONTACT					
PROTEROZOIC AMPHIBOLITE	PROTEROZOIC PELITE	Metasedimentary rocks	13 Amphibolite, hornblendite 12 Meta-arkose 11 Conglomerate 10 Psammitic biotite gneiss, minor calc-silicate rocks	16 Dolomite - Hurwitz Group 15 Argillite " 14 Meta-greywacke, meta-siltstone "	
DISCONFORMITY					
	PROTEROZOIC AMPHIBOLITE		9 Albite-pyroxene rock 8a Calc-silicate rock 8b Marble 7 Pelitic biotite gneiss ± cordierite, garnet, sillimanite; minor calc-silicate rock and impure quartzite (a) Porphyroblastic biotite gneiss (b) Augen gneiss (c) Quartzite (d) Hypersthene paragneiss		
?UNCONFORMITY?					
			6 Cataclastic biotite gneiss 5 Grey quartz dioritic to granodioritic gneiss (a) Amphibolite		
UNCONFORMITY					
ARCHEAN		Igneous rocks	4 Foliated quartz monzonite (a) Aplitic quartz monzonite 3 Foliated alaskite 2a Hyperstene-quartz diorite 2b Hyperstene trondhjemite 2c Hyperstene-quartz monzonite		
INTRUSIVE CONTACT					
ARCHEAN			1 Hyperstene gneisses		

TABLE 7.2

Maps and map units of ancillary data digitized

MAP NUMBER	MAP NAME	MAP DESCRIPTION	UNITS DIGITIZED
76	Wollaston Lake	1:500000 Bouguer gravity anomaly contour map: contours at intervals of 5 milligals between -80 and -50	< -75,-70/-75 -65/-70,-60/-65 -55/-60,-50/-55
74-2-26	Kasmere Lake-Wiskey Jack Lake (North Half)	1:250000 aeromagnetic anomaly contour map: contour values above 58800 gammas ranging from 1900 to 3500	<1900,1900/2100 2100/2500, 2500/2900, 2900/3400,>3400
74-2-27	same as above	1:250000 surficial geology map: patterns of eskers deposits and of associated sand deposits	areas covered by either deposits
64N & 64K (North Half)	same as above	Topographic relief in 100 feet contour intervals between 900 and 1660	<1000,1000/1100 1100/1200, 1200/1300, 1300/1400, 1400/1500,>1500
eU p.p.m.	same as above	Equivalent uranium in p.p.m.: contour intervals in 0.2 p.p.m., between 0.0 and 6.0	0.0/1.0,1.0/2.0 2.0/3.0,3.0/4.0 >4.0
eTh p.p.m.	same as above	Equivalent thorium in p.p.m.: contour intervals in 1.0 p.p.m., between 0.0 and 41.0	<10.0,10.0/15.0 15.0/20.0, 20.0/25.0,>25.0
eU / eTh	same as above	Ratio of equivalent uranium to equivalent thorium contour intervals in 0.01 units between 0.0 and 0.55	<0.20,0.20/0.25 0.25/0.30, 0.30/0.35, 0.35/0.50,>0.50
74-2-30	same as above	Economic geology: location of the first 32 mineral occurrences in table 7.3, for the commodities pyrite, pyrrothite, sulphide, copper, molybdenum, cobalt, nickel, zinc, lead, uranium, and gossan	32 pairs of X-Y coordinates corresponding to the location of the nearest 167 m x 167 m pixel
64N & 67K (North Half)	CANMINDEX computer plot	1:250000 Calcomp plot: location of 12 uranium occurrences 6 of which coincide with location on map 74-2-30 and the last 6 of Table 7.3	6 pairs of X-Y coordinate as above

TABLE 7.3

Summary data on mineral occurrences in the study area

NUMBER	OCCURRENCE TYPE [1]	COMMODITIES PRESENT [2]	PICTURE COORDINATES OF CLOSEST PIXEL X	Y
1	1 4	U ,Mo,Cu,Ni	150	111
2	3 2	Pb,Cu,Ni	441	160
3	2	Cu,Pb,Zn,Ni	292	235
4	2	Cu,Pb,Ni	260	250
5	5 2	G	257	254
6	3 2	Pb,Cu,Ni,Co?	241	286
7	1	U	299	315
8	3 2	Co,Ni,Cu,Pb,Zn	264	383
9	3 2	Co,Ni,Cu,Pb,Zn	210	384
10	2	Cu,Zn,Pb,Ni,Co	168	398
11	1 2 3	U ,Ni,Cu,Co,Pb,Zn,Th	125	418
12	3 2	Co,Ni,Cu,Pb,Zn	257	436
13	1	U	261	438
14	6	Po,Py	108	439
15	6	Py	220	449
16	6 2	Py	134	460
17	2	Zn,Cu	137	547
18	6	Py	94	561
19	2	Zn,Cu	62	592
20	2	Zn,Cu	58	595
21	2	Zn,Cu	53	599
22	2	Zn,Cu	56	600
23	2	Zn,Cu	51	604
24	4 2	Mo,Cu,Ni	248	636
25	1	U	147	244
26	2 1	Cu	101	860
27	2	Cu	91	940
28	2	Cu	100	937
29	4 2	Cu,Mo	486	863
30	2	Zn,Cu,Pb	637	754
31	5 2	G	642	699
32	6 2	S	703	666
33	1	U ,Th,Mo	246	386
34	1	U ,Th	160	381
35	1	U ,Th	178	370
36	1	U	516	139
37	1	U	314	340
38	1	Th,U	365	295

[1] TYPES: 1=U, 2=Cu,Cu-Zn, 3=Co-Ni, 4=Mo, 5=G, 6=Py,Po,S

[2] COMMODITIES: Cu=copper, Zn=zinc, Co=cobalt, Ni=nickel, U=uranium, Mo=molybdenum, G=gossan, Py=pyrite, Po=pyrrothite, S=sulphur

The binary images in Figure 7.13 represent a multi-layered data base of map data in registration (pixel to pixel correspondence) which consists of: (a) bedrock geology map, (b) aeromagnetic contour map in gammas, (c) free air Bouguer anomaly contour map in milligals, (d) airborne gamma ray spectrometric contour map of the integral counts of uranium equivalent concentrations (eU) in parts per million (ppm), (e) of thorium equivalent (eTh), (f) contour map of the ratio eU/eTh, (g) topographic elevation contour map, in feet, (h) the binary pattern of eskers and sand deposits, and (i) the pattern of 38 mineral occurrences in the area, located at the nearest pixel, but displayed as arrays of 5 pixels x 5 pixels centered around the occurrences.

In Table 7.2 information is given on the contours digitized from the images of Figure 7.13. A summary of the data on mineral occurrences in the study area is provided in Table 7.3 for the 38 occurrences located in Figure 7.13i. Occurrence types correspond to the groupings made by Weber et al (1975). Figures 7.14 to 7.16 provide examples of binary patterns extracted from the labeled images derived from the boundaries images in Figure 7.13. The summary of the geology of the area which follows (see Weber et al, 1975) relates to the experiments described here. The geological unit numbers used are those in Table 7.1.

Archean foliated granitoid rocks (units 2 to 4) ranging

Figure 7.13: The multilayered data base in the Kasmere Lake-Whiskey Jack Lake area, Northwestern Manitoba. (a) bedrock geology boundaries; (b) aeromagnetic anomaly contours (gammas); (c) free air Bouguer gravity anomaly contours (milligals); (d) airborne gamma ray spectrometric contours of the integral count of uranium equivalent concentration, eU, (p.p.m.); (e) thorium equivalent, eTh (p.p.m.); (f) eU/eTh ratio; (g) topographic elevation contours (in 100 feet intervals); (h) the distribution of eskers and sand deposits; and (i) 38 mineral occurrences located at the nearest pixel (167 m).

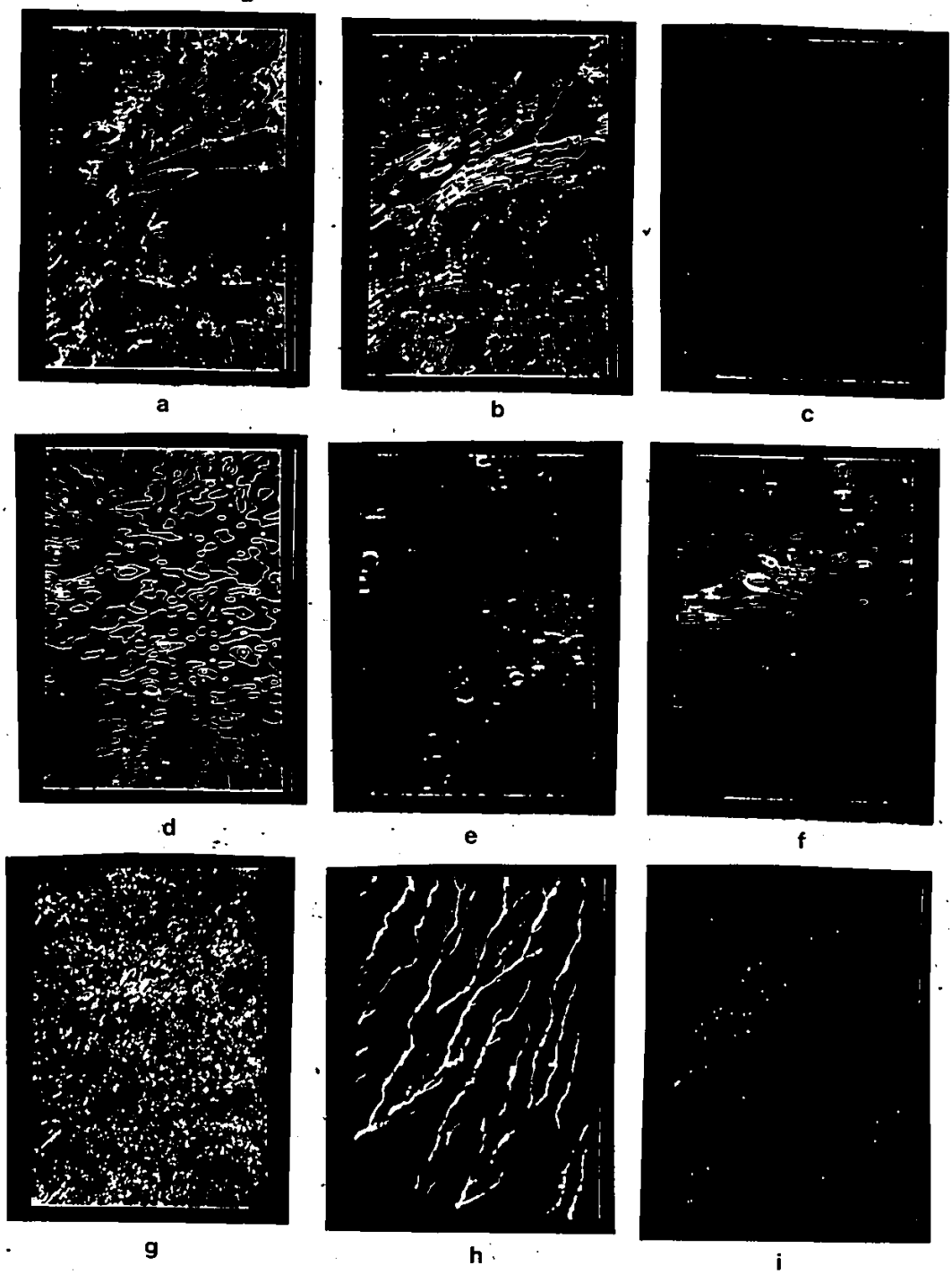

Figure 7.13: Concluded.

from quartz diorite to alaskite granite occupy the south half of the area, as shown in Figure 7.14a. Some of these rocks contain hyperstene and are associated to hyperstene gneisses (unit 1), probably the country rock. The Aphebian rocks which occur in the northern part of the area (units 14 to 16, see Figure 7.14e) display a continuity with Hurwitz Group sedimentary units, while the remainder of the Aphebian sediments (units 7 to 13) at the center and in the southern part of the area lie in the extension of the Wollaston fold belt. Units 7, 8a and 8b, and units 9 to 12 are shown in Figures 7.14b, c, and d, respectively. As can be seen by comparing Figures 7.14b to d with the pattern in Figure 7.15a, a central part of magnetic lows corresponds to the predominantly pelitic metasediments, surrounded by aeromagnetic highs (Figures 7.15 b and c) where Archean and Aphebian granitic and arkosic rocks occur, as shown in Figures 7.14 d and f to h. Units 7 to 13, Aphebian metasedimentary rocks, consist of pelitic (Fig. 7.14 b) conglomeratic and psammitic (Figure 7.14 d) and calcareous strata (Figure 7.14 c) which have been interpreted as geosynclinal, platformal and continental sediments. Younger, igneous and metamorphic rocks generated during Hudsonian orogeny consist of migmatites, plugs and stocks of anatexite and syn- and late-orogenic batholiths, most of which are massive and may truncate Hudsonian trends (units 17 and 19,

Figures 7.14 f and 7.14 g, and units 20 and 22, Figure 7.14 h). Pleistocene and recent sediments (drift) and water covered areas where geological mapping was not available, are shown in Figure 7.14 i.

In apparent coincidence with the Wollaston fold belt, there is a weak linear belt of low gravity values, containing a chain of isolated "lows" which occur within an area of gradually increasing gravity values, as shown in Figure 7.15 d to f. According to Weber et al (1975) the "low" over the pelitic sediments within the Wollaston fold belt can be due to widespread partial melting which formed large bodies which, beside being exposed at the surface are much larger at depth. As suggested for the Hurwitz Group, such pattern would indicate a cratonic basin.

The rocks in the area underwent regional metamorphism of upper greenshists to lower amphibolite facies in the northwest part, to upper amphibolite-hornblende granulite facies in the southwest. Schledewith (1978) described the pattern of regional metamorphism in the region. Such data, however, have not been considered in this study. Lithostratigraphic units such as Aphebian pelitic biotite gneisses (unit 7 shown in Figure 7.14 b) and psammitic gneisses, conglomerates and meta-arkoses (units 10 to 12, shown in Figure 7.14 d) define large scale folds. The two main trends in the area are indicated by major and minor folds and their

Figure 7.14: Some geological binary images obtained by processing the bedrock geology boundary image. (a) Archean igneous rocks; (b) Proterozoic or Aphebian pelitic metasediments (biotite gneiss); (c) Aphebian calc-silicate rocks; (d) Aphebian psammitic and conglomeratic metasediments (biotite gneiss, conglomerate and metaarkose); (e) Aphebian units of the Hurwitz Group (dolomite, argillite, metagreywake and metasiltstones); (f) white granite to quartz monzonite and pegmatites; (g) pink leucogranite to quartz monzonite; (h) porphyritic and fluorite bearing quartz monzonite; and (i) Pleistocene, Recent and unmapped areas.

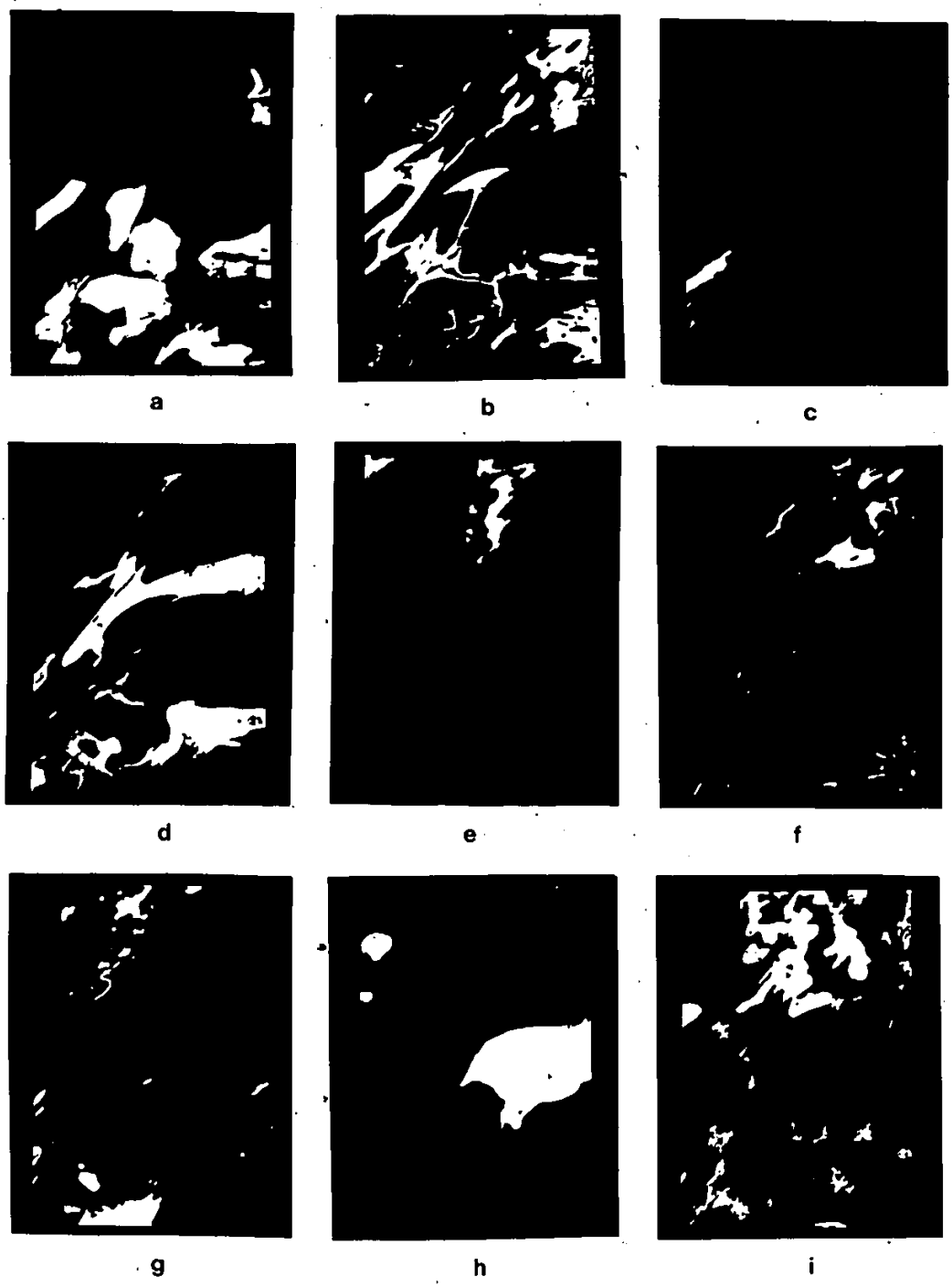

Figure 7.14: Concluded.

related planar and linear structures. The major tectonic trend is in the northeast direction: it occurred during Aphebian sedimentation and is represented typically by the Wollaston fold belt. A Pre-Aphebian, less pronounced, slightly curvilinear major fold trend occurs in a roughly east direction. A third minor folding phase has also occurred in the area. Structural maps, and tectonic maps which also accompany the report by Weber et al (1975) have not been digitized.

Three quarters of the area are covered by glacial drift while the rest is mostly covered by lakes and rivers, leaving less than 2 percent to rock exposures. Till, sand, and gravel associated with the eskers system, make up the drift cover. The till is composed of sand, gravel and large rounded boulders up to 2 m in diameter. These may form extensive boulder fields in low-lying areas. Some of the more resistant granitic boulders can be traced from local bedrock outcrop. In most cases the boulders are not transported far from their sources. Many eskers, which form southwesterly extending long sinuous ridges, occupy topographic depressions typical of meltwater channels. The ridges run subparallel and are spaced approximately 15 km apart. They meander in a southerly to southwesterly direction and form steep-sided ridges which rise up to 150' (50 m) above the surrounding drift. Their pattern can be seen

Figure 7.15: Some geophysical interval and topographic elevation binary images obtained by processing geophysical anomaly contour interval images. (a) aeromagnetic anomaly lows < 2100 gammas; (b) aeromagnetic anomaly interval between 2100 and 2500 gammas; (c) aeromagnetic anomaly interval between 2500 and 2900 gammas; (d) gravity lows < -75 milligals; (e) gravity lows between -75 and -70 milligals; (f) gravity interval between -65 and -70 milligals; (g) topographic elevation below 1100 feet; (h) topographic elevation between 1100 and 1300 feet; (i) topographic elevation above 1300 feet.

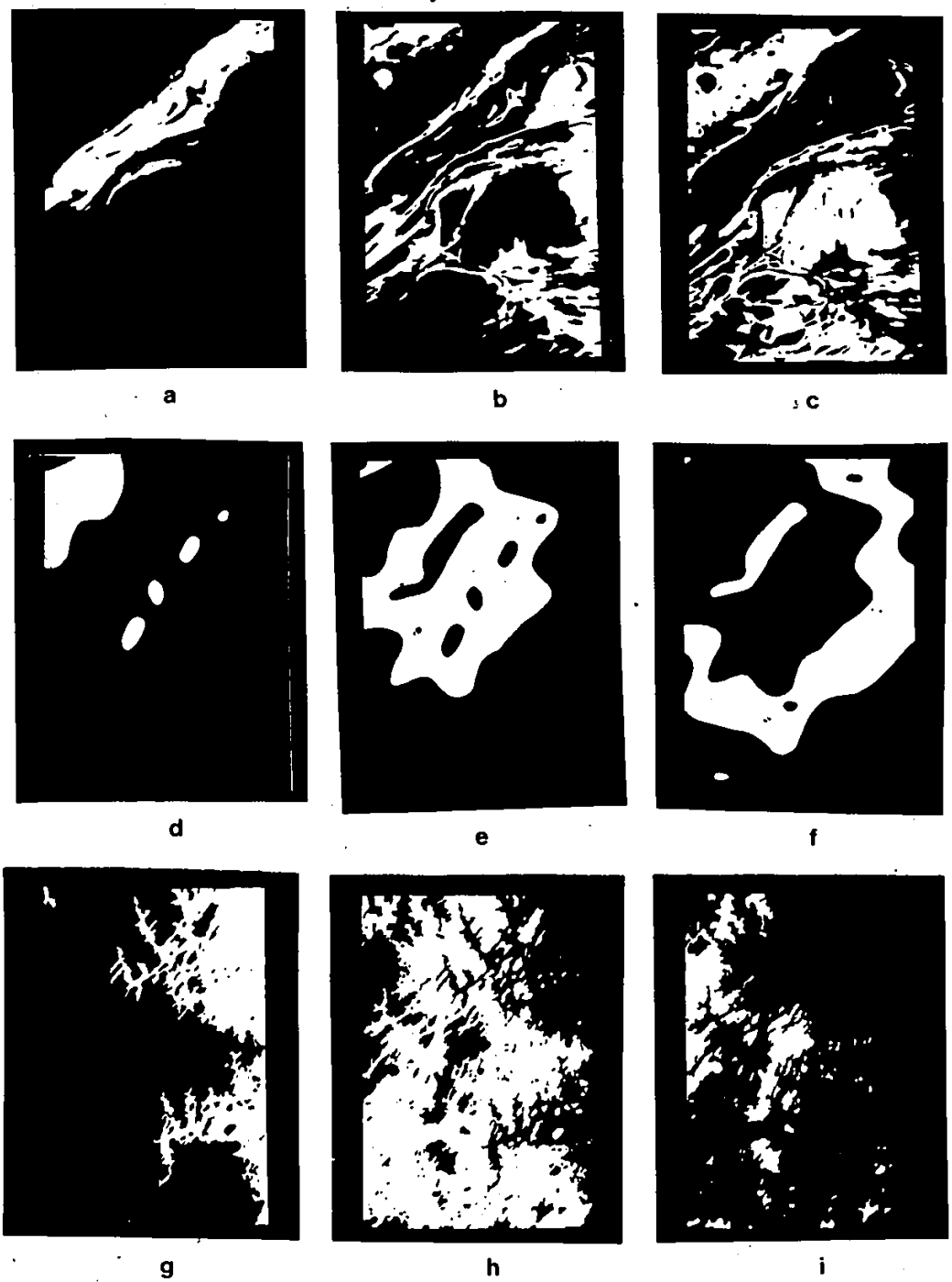

Figure 7.15: Concluded.

Elevations in the area are between 900' and 1800' (300 and 600 m) above sea level. The percentage of bedrock exposure is lowest in a central belt in the area (see Figure 7.15 g) where the poor bedrock exposure corresponds to more easily eroded pelitic metasedimentary rocks. The digitized map pattern, however, does not show this relationship. In the southwestern and northwestern parts of the area more resistent granitic and arkosic rocks tend to form hills of up to 300' (100 m) relief (see Figures 7.15 h and i).

Some of the patterns extracted from the airborne gamma-ray spectrometric contour maps of Figures 7.13 d to f, are shown in Figure 7.16. The contour values for the radioelement concentrations are "average surface concentrations" over the area sampled by the airborne spectrometer, which include some outcrop, overburden and water in small ponds, streams ans swamps, therefore, providing contour values considerably lower than the concentrations in the bedrock, but which still reflect the regional distribution of the elements in it. Because of compilation and contouring procedures, the contours in some cases may be distorted in the east-west direction.

Several companies begun in 1967 combined airborne magnetic, electromagnetic and radiometric surveys along the main metasedimentary part of the Wollaston fold belt. A first discovery of uranium mineralization at Rabbit Lake, near

Wollaston Lake, caused an increase in uranium and base metal exploration activity all along the metasedimentary belt in the Kasmere Lake area, which by 1969 was covered by exploration reservations. Airborne surveys were followed by electromagnetic, geological and geochemical mapping. In spite of this, only few radioactive and electromagnetic anomalies were drilled because of the very small outcrop areas. No major discovery was found and by 1975 all exploratory reservations and claim blocks elapsed. Regional geochemical surveys, carried out in Northwestern Manitoba during 1975, have been described by Coker (1976). As mentioned by Soonavala et al (1977), new exploration activity started during 1976 and brought to the staking of all the areas characterized by anomalously high uranium. More recent exploration activities in the area consisted of additional mapping, and more detailed airborne spectrometric surveys as part of a Federal/Provincial Uranium Reconnaissance Program.

Almost all mineral occurrences were discovered by means of airborne geophysical methods. In general the radioactive anomalies in the area (see Figure 7.16 a to c) are caused by boulder fields of slightly radioactive granitic rocks, containing disperse uranium bearing minerals or their weathering products. The intensities of the anomalies are exaggerated because of the proportionally greater surface

area exposed in the boulder fields.

Weber et al (1975) described disseminated uranium mineralization in: (I) white granite and pegmatite (unit 17) and similar granitic rocks occurring as sills in pelitic biotite gneisses (unit 7); (II) red and pink pegmatite (part of unit 19); (III) calc silicate gneiss (unit 8a) and marble (unit 8b); (IV) foliated quartz-monzonite (unit 4); and (V) granitic and arkosic granite gneiss or meta-arkose (units 19 and 12). They concluded that uranium mineralization is restricted to units 17, 19, 8a, 12 and 4 in order of importance.

Base metal mineralizations are grouped into occurrences of: (I) cobalt-nickel in metasedimentary rocks of the Wollaston fold belt, for example within calc-silicate rocks (unit 8a) and marble (unit 8b) near the contact with meta-arkose (unit 12); (II) zinc-copper (and copper-lead-zinc) in: (a) zones of massive and disseminated sulphides in calc-silicate rocks (units 8a and 8b) near the contact with hyperstene-quartz monzonite (unit 2c), (b) disseminated sulphides in pelitic gneisses (unit 7), and (c) as Cu-Pb-Zn in pelitic gneiss; and (III) copper (± molybdenum) as sparsely disseminated mineralization in the southern part of the area in pelitic gneisses (units 7 and 7d) in calc-silicate interlayers (units 8a and 8b) and in pegmatitic calc-silicate rocks.

Figure 7.16: Some binary images obtained by processing the radiometric contour binary maps. (a) eU < 2 p.p.m.; (b) eU between 2 and 3 p.p.m.; (c) eU > 3 p.p.m.; (d) eTh < 2 p.p.m.; (e) eTh between 2 and 3 p.p.m.; (f) eTh > 3 p.p.m.; (g) eU / eTh < .20; (h) eU / eTh between .20 and .30; and (i) eU / eTh > .30.

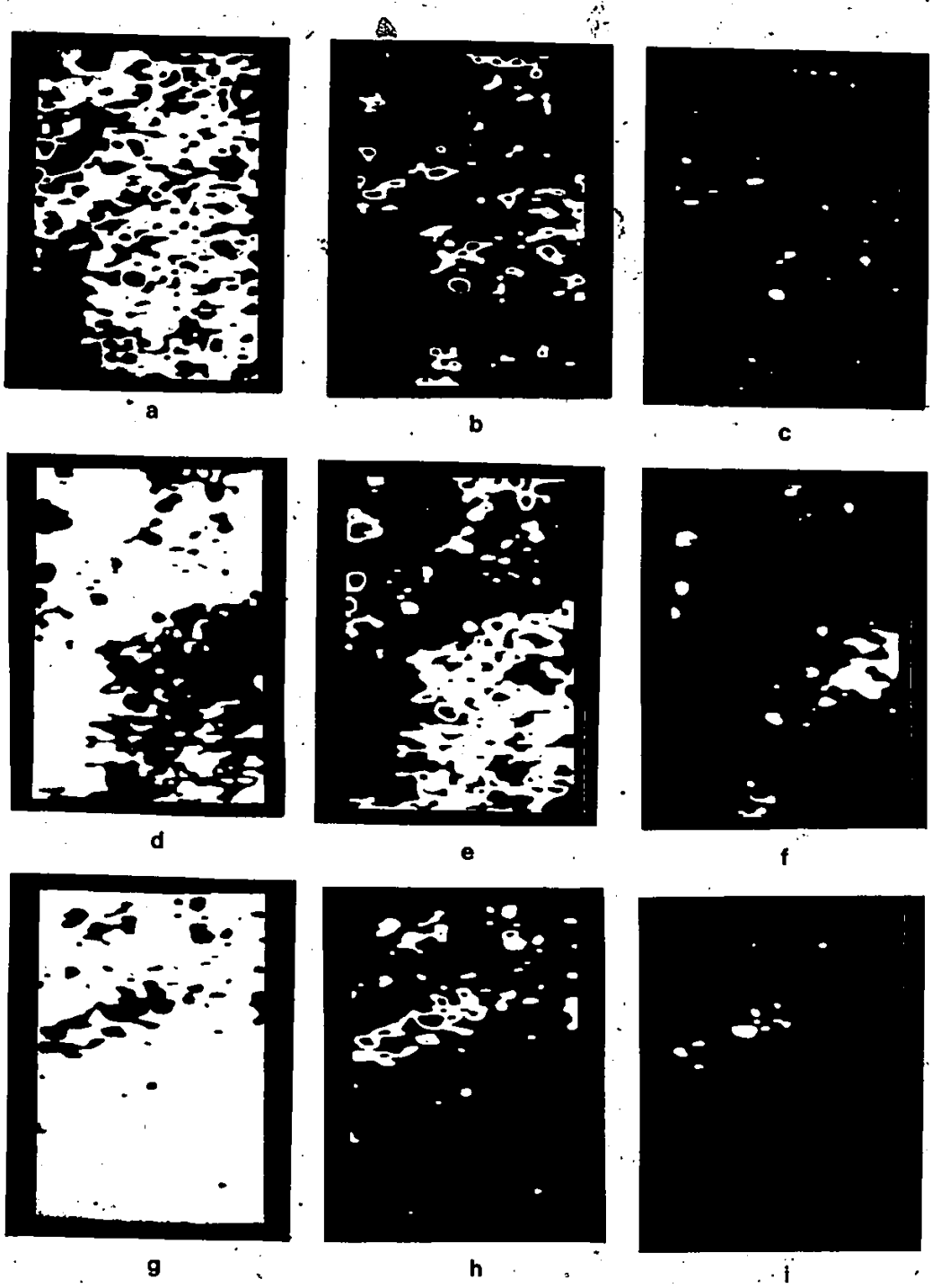

Figure 7.16: Concluded.

The geological and ancillary information described above, is in part used to model experiments for relating 12 uranium occurrences and 24 base metal occurrence (group II above) to geological and ancillary map patterns in their vicinities. The applications presented here, use transformations of binary compressed images in the lines of Mathematical Morphology concepts developed by Matheron (1975) and Serra (1966) in France. The binary images are transformed and combined by logical operations to obtain derived patterns as coincidences of desirable characteristics. The proportions of pixels in these patterns over the total number of pixels in the study area can be considered as the probability that a random pixel swept throughout the image "HITS" the pattern. Patterns of probabilities can be built, displayed and quantitatively characterized in the study of regional mineral resources-evaluations. Thus the present technique can be considered as a new geological tool.

7.4 Applications to uranium and base metal occurrences

7.4.1 Derivation of binary patterns related to uranium mineralization

Using the mineralization concepts of the previous sec-

tion, a number of separate models were tested for all litho-stratigraphic units considered to be important hosts for uranium.

The applications performed use tranformations of binary compressed images. Logical operations or boolean algebra and binary neighborhood transformations are computed on the Modcomp II minicomputer. Figure 7.17 shows examples of such operations and transformations. In Figure 7.17a, D is the pattern of 61 x 61 pixel neighborhoods (corresponding to 10 km x 10 km squares) of 12 uranium occurrences; it can be generated by 30 successive dilatations of the original image by a 3 x 3 pixels black template. On that image the 12 occurrences are identified by 12 black pixels in point-to-point correspondence with the occurrence locations. Each black pixel grows into an array of 61 x 61 black pixels. A measure of D is its area, mes D = 38973 pixels each corresponding to a square area of 167 m x 167 m . We can also say that .057 or 5.7% is the area proportion of the pattern, i.e., the probability that a 10 km x 10 km square array of pixels "HITS" or contains an occurrence of uranium. Incidentally, 2^{-5} or .002% is the probability that a single pixel translated at random throughout the study area of 684076 pixels[1], "HITS" a uranium occurrence pixel.

---

[1] The total image area which is 760 x 1004 (= 763040) pixels, is 78964 pixels greater than the study area within the geological boundary image.

The area of the pattern G, Aphebian pelitic metasediments in Figure 7.17b, is 119212 pixels; i.e., .174 or 17.4% is the probability that a random pixel "HITS" G. The intersection or overlap or better the coincidence between the two patterns, $D \cap G$ in Figure 7.17c, has an area of 9075 pixels; i.e., .013 or 1.13% is the probability that the random pixel "HITS" both patterns in coincident positions. Figure 7.17d shows the pattern obtained by the union of the two non-overlapping subsets of D and G; it represents another way of visually displaying their relationship. Figure 7.17e shows $G \ominus B$; i.e., G eroded by B, a 5 x 5 pixels black template. The pattern of eroded pixels is shown in Figure 7.17f. Figure 7.17g shows the pattern of the complement of G. Figure 7.17h shows the pattern of $G \oplus B$; i.e., of G dilatated by B. The pattern of the black pixels "added" to G during the dilatation is shown in Figure 7.17i.

In similar ways, binary images are transformed and combined to obtain derived patterns as coincidences of desirable characteristics. Let us consider an example of application of such a tool. All the zones within 420 m of the gradational contact between Aphebian pelitic metasediments (units 7 and 7c in Table 1) and the more porous conglomeratic and psammitic Aphebian metasediments (units 9, 10, 11, and 12) which are considered as potential traps to uranium mineralization due to the increased porosity, have

Figure 7.17: Transformations of binary images. The numbers of black pixels in the images (here displayed in white on a Tektronix 611 storage display unit) are shown below the right corners of the plots. Below the left corners the expressions for the transformations are shown. (a) image D of 61 pixels x 61 pixels neighborhoods (10 km x 10 km squares) of 12 uranium occurrences; (b) the image G of Aphebian pelitic metasediments; (c) the intersection (overlap or coincidence) between D and G; (d) the image produced by the .EXOR. or exclusive .OR.'ing logical operation (the union of two non-overlapping subsets) between D and G, which shows one image in the context of the other; (e) image G eroded by a 5 pixels x 5 pixels black template; (f) image of the pixels eroded from G; (g) the image of the complement or negation of G; (h) image G dilatated by a 5 pixels x 5 pixels black template; and (i) image of the black pixels "added" to the image G during the dilatation.

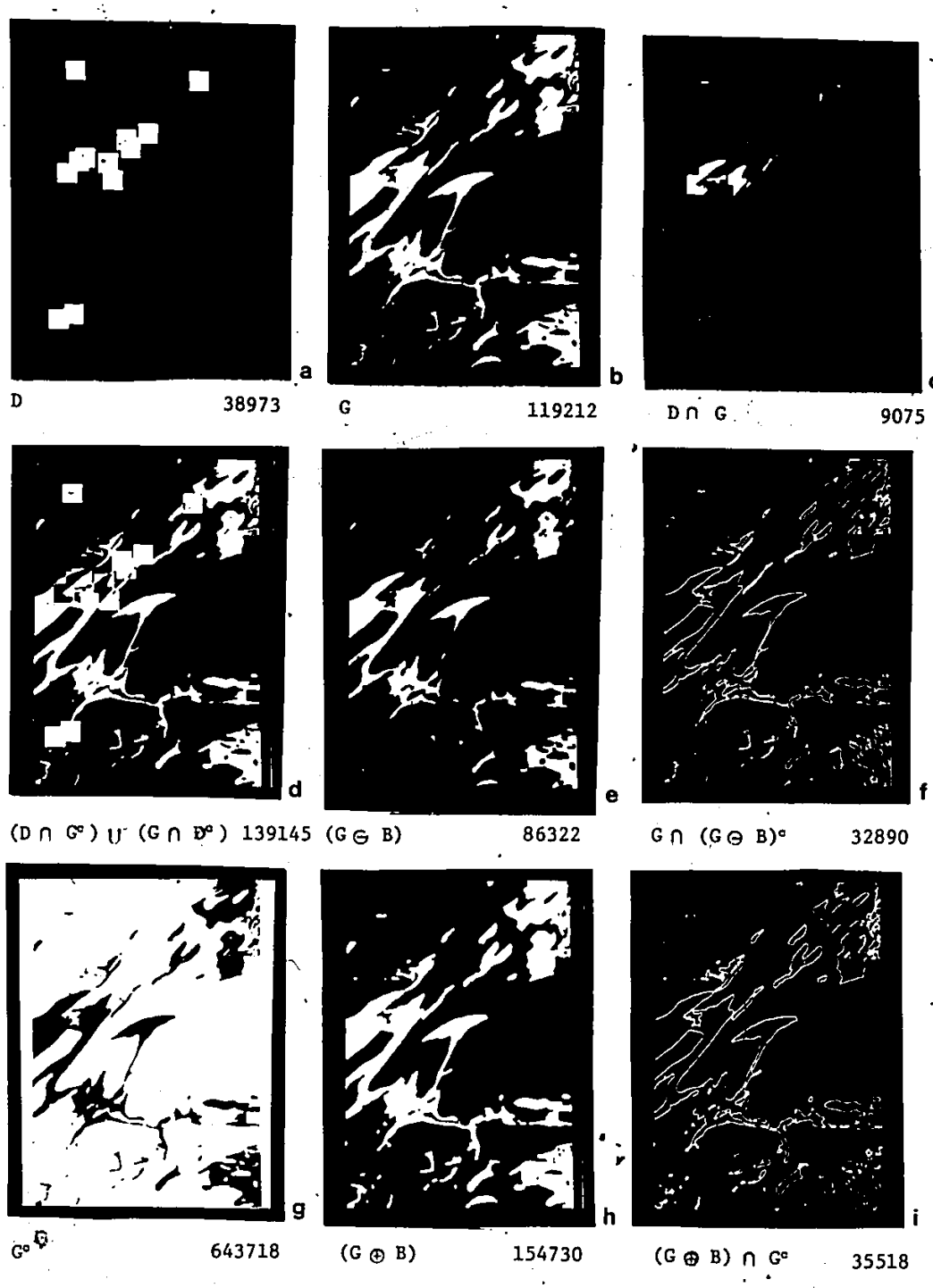

Figure 7.17: Concluded.

been extracted as follows. First the union between the patterns (7) ∪ (7c) and the patterns (9) ∪ (10) ∪ (11) ∪ (12) were computed. The resulting binary images were then dilatated by a square structuring element of 5 x 5 black pixels and the intersection between the two dilatated patterns was computed. This represents the 840 m wide zone which in Figure 7.18a is displayed together with the pattern of 10 km x 10 km cells centered around the 12 uranium occurrences. What is represented in Figure 7.18a, is the result of the logical operation of exclusive .OR., .EXOR., the union of non-overlapping subsets. This artifice is used here in order to display within one single binary image the relationship between two binary patterns characterized by strongly different shapes. Here a linear pattern and a pattern of squares are clearly visible, and the interruption of the line pattern, as the holes in the square pattern, represents the overlap or coincidence between them. We can see in Figure 7.18a, the gradational contact between Aphebian metasediments of different porosity: it coincides with part of the neighborhoods around the uranium occurrences. The same artifice, which allows us to see one pattern in the context of another, will be used in the remainder of the binary images shown in Figure 7.18.

Figure 7.18: Partitioning of the binary image of a transitional contact into "environments" favourable to uranium mineralization. (a) binary image of the 850 m wide contact zone between Aphebian pelitic metasediments and the coarser psammitic and conglomeratic metasediments of Aphebian age. The contact image is compared (exclusive .OR.'ing) with the square areas surrounding the 12 uranium occurrences; (b) the contact is compared with the image of aeromagnetic lows < 1900 gammas; (c) the contact is compared with the image of gravity lows < -70 milligals; (d) the contact is compared with the images of uranium highs > 2 p.p.m.; (e) the contact image is compared with the image of eU / eTh ratio highs > .20; (f) the image of aeromagnetic anomaly lows < 2100 gammas is compared with the image of the square areas surrounding the 12 uranium occurrences; (g) promising parts of the image of the contact which coincide with areas in which gravity lows (< -70 milligals) and aeromagnetic lows (< 2100 gammas) coincide, i.e., the line pattern cutting across the larger shapes; (h) promising parts of the image of the contact which coincide with areas in which aeromagnetic lows (< 2100 gammas) and eU / eTh ratio highs (> .20) coincide, i.e., the line pattern cutting across the larger shapes; and (i) the union of the intersections between the contact, aeromagnetic and gravity lows, and the contact, aeromagnetic lows and eU / eTh highs, i.e., the extracted pattern.

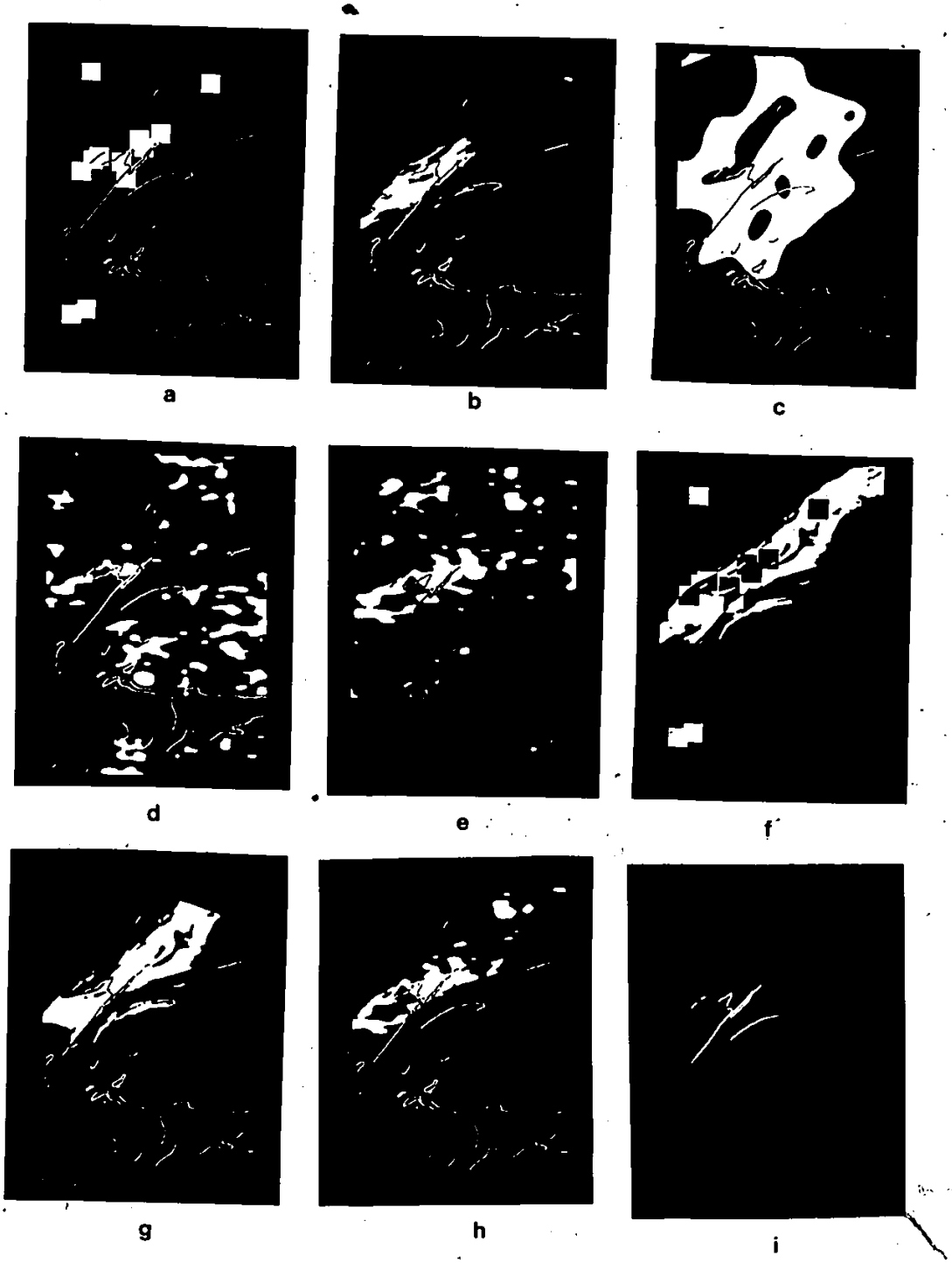

Figure 7.18: Concluded.

As exemplified in Figure 7.18a, the feature extraction experiment which follows considers coincidences of the pattern of gradational contacts with other binary patterns, such as: the pattern of aeromagnetic anomaly lows < 1900 gammas (Figure 7.18b), the pattern of gravity lows <-70 milligals (Figure 7.18c) the pattern of eU highs > 2 p.p.m. (Figure 7.18d), and the pattern of eU / eTh highs > .2 (Figure 7.18e). In Figure 7.18f, a comparison is made between the pattern of aeromagnetic lows < 2100 gammas (which corresponds to the Wollaston fold belt metasediments) and the pattern of 10 km x 10 km neighborhoods around the 12 uranium occurrences. Figure 7.18g shows the relationships between the Aphebian gradational contact, the aeromagnetic lows < 2100 gammas, and the gravity lows <-70 milligals. Here the coincidence or area proportion is .005 or .5%, which can be compared to .019 or 1.9% of the entire gradational contact in the study area. In Figure 7.18h, the coincidence is shown between the gradational contact, the pattern of pixels corresponding to the aeromagnetic lows < 2100 gammas, and eU / eTh highs > .2. This coincidence corresponds to .002 or .2% of area proportion, and is almost entirely a subset of the pattern in Figure 7.18g. This can also be seen by computing the union of the two patterns which is displayed in Figure 7.18i. This pattern represents a probability of .5% that a random pixel "HITS" a pixel

belonging to our Aphebian gradational contact where it either coincides with aeromagnetic lows and gravity lows or it coincides with aeromagnetic lows and eU / eTh highs. This pattern which represents one aspect of the uranium depositional environment in the area, can be considered as a probability, furthermore, it can be characterized in several different ways either by itself, or in the context of other patterns.

Figure 7.19: Other aspects of uranium related environments. (a) comparison between eU / eTh ratio highs (> .20) and the square areas around the 12 uranium occurrences; (b) comparison between the image of Aphebian pelitic metasediments with the square areas around the uranium occurrences; (c) binary image of the areas in which Aphebian pelitic metasediments, aeromagnetic anomaly lows (< 2100 gammas) and eU / eTh highs (> .20) coincide; (d) comparison between the image of white and pink granites and pegmatites and that of the square areas around the 12 uranium occurrences; (e) binary image of the areas in which white and pink granites and pegmatites coincide with aeromagnetic anomaly lows (> 2100 gammas) and eU / eTh highs (> .20); (f) comparison between the image of Aphebian calc-silicate rocks and that of the square areas around the 12 uranium occurrences; (g) binary image of the areas in which Aphebian calc-silicate rocks coincide with aeromagnetic lows (< 2100 gammas) and with eU / eTh ratio highs (> .20); (h) comparison between the image of Archean igneous rocks and that of the square areas around the uranium occurrences; and (i) binary image of the areas in which Archean igneous rocks coincide with gravity highs (> -55 milligals) and aeromagnetic highs (> 2500 gammas).

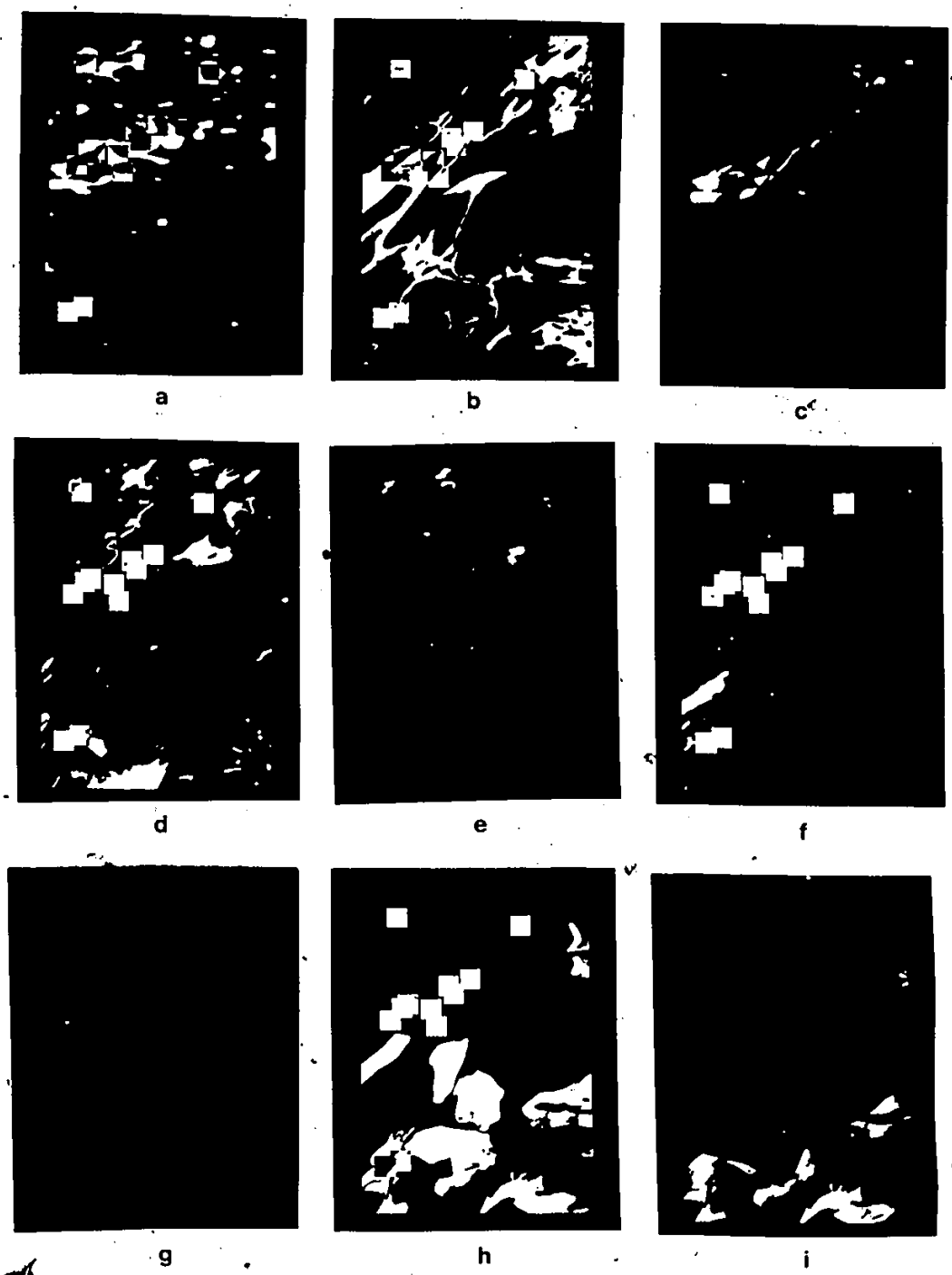

Figure 7.19: Concluded.

The results of these experiments point to the portions of the Aphebian metasedimentary gradational contact within the Wollaston fold belt where uranium occurrences have not yet been discovered. Additional information, such as more recent geological mapping, geochemistry, or a more detailed gamma ray spectrometric survey which have not been considered here, might restrict these searching areas even further down to operational areas for direct exploration.

Aspects of uranium related map patterns within other lithologies can be extracted for a model of areas characterized by aeromagnetic lows (< 2100 gammas) and of eU / eTh highs (> .2) as follows. Figure 7.19a, shows the coincidence between the pattern of eU / eTh highs and that of the uranium occurrence 10 km x 10 km neighborhoods. Figure 7.19b shows the coincidence between the latter and the Aphebian pelitic metasediments (unit 7), and Figure 7.19c shows the pattern of Aphebian metasediments where the following conditions hold: eU / eTh > .2, gravity anomaly < -65 milligals, and aeromagnetic anomaly < 2100 gammas. The same three conditions are modelled for the patterns in Figures 7.19e and f. Figure 7.19d shows the coincidence between map units (17) and (19), white and pink granites and pegmatites, respectively, and the uranium occurrences neighborhoods. This coincidence is poor, as can be expected, for heavily underrepresented map units such as the pegmatites

most of which cannot be properly displayed on either 1:250000 or 1:50000 maps. This is so because such rocks occur as outcrops which are too small to be drawn at those two scales. Nevertheless, as it is shown in Figure 7.19 e, from the binary images of those map units, it is possible to extract the portions of those terrains which are characterized by the three coincident conditions previously selected for Figure 7.19c. Similar considerations can be made for the calc-silicate rock units (8a) and (8b), and their coincidence with the uranium occurrence neighborhoods in Figure 7.19f. Here only one outcrop can be extracted from the image of these terrains, as can be seen in Figure 7.19j, for those same conditions.

The last lithologic environment considered for uranium occurrences is in Archean ineous rocks (map units 1, 2a, 2b, 2c, 3, 4a and 4). In Figure 7.19h this is shown in coincidence with the pattern of the uranium occurrence neighborhoods. For the two occurrences to the south west of the image, two broad characteristics seem to concide with these Archean igneous rock map units: aeromagnetic anomaly values ranging between 2100 and 2900 gammas, and gravity anomaly values ranging between -55 and -60 milligals. This pattern of coincidences which is shown in Figure 7.19i, is quite arbitrary, and probably not interpretable without additional information, here not available. However, pat-

terns like this last one, are not easily imaginable and cannot be practically extracted by hand from sets of maps. They can induce the geologist to postulate models which hopefully are more realistic in terms of what the image data base contains. This may be particularly important in cases, like this one, in which a significant lack of control exists for the regional mineralization environment.

To conclude this section, it must be duly noted that, the derived patterns here described as subsets of pixels or regional environments, can also be generated by other techniques of automatic classification which, for example, are applied either in remote sensing (pixel classification) or in several multivariate statistical analysis applications. In many cases, however, a geologist may still prefere to look at patterns of overlays like the ones shown here, and observe his or her metallogenic models developed as combinations of binary patterns at first, before considering automatically produced probability contours. Two such contours are shown in Figure 7.20 a and b, in which they have been produced by multiple regression and by characteristic analysis, respectively.

The data analyzed have been extracted from the phase-labelled images used in this section for producing the various binary patterns described. The seven phase-labeled images produced from the binary contour images shown in

Figures 7.13 a to g, the binary image of eskers and sand deposits in Figure 7.13 h, and the information on location in picture coordinates, on occurrence classification for the 38 occurrences shown in Figure 7.13i, have been transferred from the Modcomp II computer of N.R.C. to the Cyber 74 computer at the Department of Energy, Mines and Resources in Ottawa. The data have been entered into SIMSAG, an interactive system with graphical input/output for multivariate statistical analysis, which has been developed at the Geological Survey of Canada by Chung (1979).

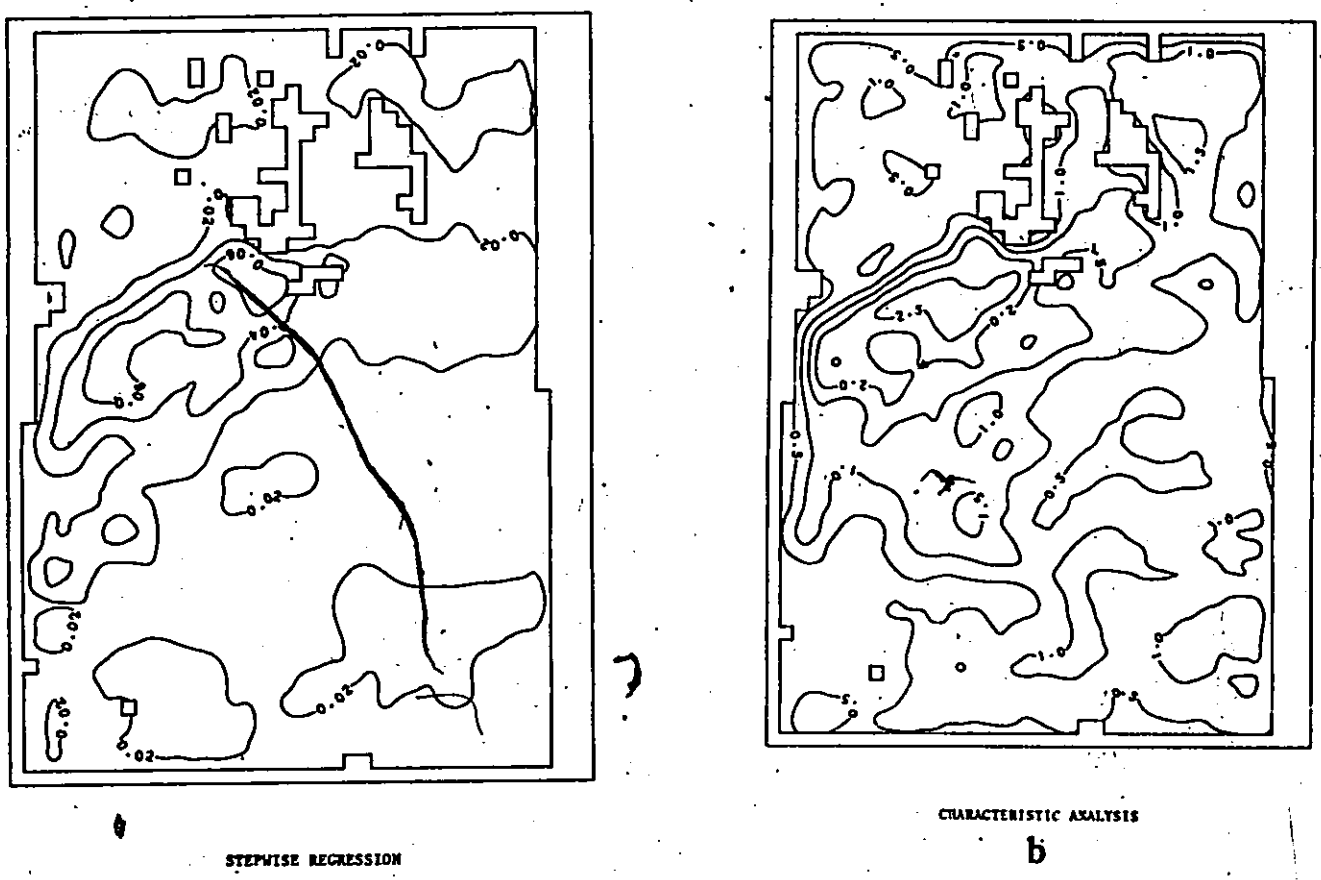

Figure 7.20: Probability contours obtained by analyzing the image data in the Kasmere Lake - Whiskey Jack Lake area by SIMSAG, an interactive package for statistical analysis programmed by Chung (1980). (a) the contour pattern obtained by stepwise regression; (b) the contour pattern obtained by characteristic analysis. The high contours indicate the areas which are more favourable to uranium mineralization.

The contour maps in Figure 7.20, have been generated as a preliminary attempt to detect favourable uranium mineralization using the same overall models of the experiments for Figure 7.18 and 7.19. The results shown in the two contour patterns, are very close to those in the binary patterns derived here. As expected, the aeromagnetic anomaly lows (< 2100 gammas) which characterize the Wollaston belt, show up as the most important variable in the analysis. In the contour maps the high values represent environments similar to those surrounding the known occurrences of uranium. The contour values have been computed for square cells measuring approximately 9.5 km x 9.5 km (= 90 km^2). The data have been transformed into binary (0-1) variables indicating the absence or presence of geophysical anomaly, interval values or geological map unit labels or mineral occurrences for each type of occurrence in each square cell.

Further experiments of this type are being considered as extensions of the approach. For example, the images of eskers and sand deposits distribution and the contour interval of the topographic relief in Figure 7.13g and h, are to be used in order to correlate those binary patterns with the patterns for gamma ray radiometric contours and those for some of the geological map units. At present, however, it is the opinion of the writer, that additional experiments of this type are beyond the scope of this

section. Clearly, a complete study of the regional patterns related to uranium mineralization in the study area is likely to represent a major undertaking in its own right. What has been introduced here, is a methodology which is being proposed and developed, and which is being applied to point out the kind of problems and of results to be expected in studies in which these methods are employed. A second application on different commodities, Cu-Pb-Zn mineralization, is being described in the next section.

7.4.2 Derivation of binary patterns related to base metal mineralization.

Zinc-copper mineralization, type II of Weber et al (1975), is described in this section in terms of binary patterns extracted from the phase labelled images of: bedrock geology, aeromagnetic anomaly and gravity anomaly contour maps shown in figures 7.13 a, b, and c, respectively. Zones of massive and disseminated sulphides in calc-silicate rocks (units 8a and 8b in Figure 7.21b), near the contact with hyperstene-quartz monzonite (unit 2c in Figure 7.21a), disseminated sulphides in pelitic gneisses (unit 7 in Figure 7.21c) and Cu-Pb-Zn in pelitic gneisses (unit 7) are correlated with the patterns of 10 km x 10 km neighbor-

hoods around 24 base metal occurrences known in the area. The intersection between the latter pattern of occurrences and the union of the binary patterns of the map units (2c), (8a), (8b), and (7) represents the .392 or approximately 39% of the area of the base metal occurrence binary pattern. In the following derived patterns, such area of overlap is subdivided into portions which coincide with combinations of patterns for different ranges of aeromagnetic and gravity anomaly values. Of the many binary patterns so obtained, six have been selected which coincide best with the binary pattern of the 10 km x 10 km neighborhoods of the Cu-Pb-Zn occurrences (i.e. occupy the central part and also much of the area of the neighborhoods), and which therefore represent environments similar to those in the neighborhoods.

Figure 7.21: Extraction of binary images representing environments related to base metal mineralization in the Kasmere Lake - Whiskey Jack Lake area in Northwestern Manitoba. (a) comparison (exclusive .OR.'ing) between the image of Aphebian hyperstene-quartz monzonite and the 10 km x 10 km square areas around the 24 base metal occurrences; (b) the image of base metal occurrences is compared with the image of Aphebian calc-silicate rocks; (c) the image of base metal occurrences is compared with that of Aphebian pelitic metasediments; (d) comparison of the image of base metal occurrences with that of the areas in which aeromagnetic anomaly values are < 2100 gammas and the gravity values range between -65 and -70 milligals; (e) comparison of the image of base metal occurrences with that of the areas in which aeromagnetic anomaly values are < 2100 gammas and the gravity anomaly values range between -60 and -65 milligals; (f) comparison of the image of base metal occurrences with that of the areas in which the aeromagnetic anomaly values range between 2100 and 2500 gammas, and the gravity anomaly values are < -65 milligals; (g) comparison of the image of base metal occurrences with that of the areas in which the aeromagnetic anomaly values range between 2100 and 2500 gammas and the gravity anomaly values range between -60 and -70 milligals; (h) comparison of the image of base metal occurrences with that in which the aeromagnetic anomaly values range between 2100 and 3400 gammas, and the gravity anomaly values are < -70 milligals; and (i) comparison of the image of base metal occurrences with that in which the aeromagnetic anomaly values range between 2500 and 3400 gammas, and the gravity anomaly values range between -65 and -70 milligals.

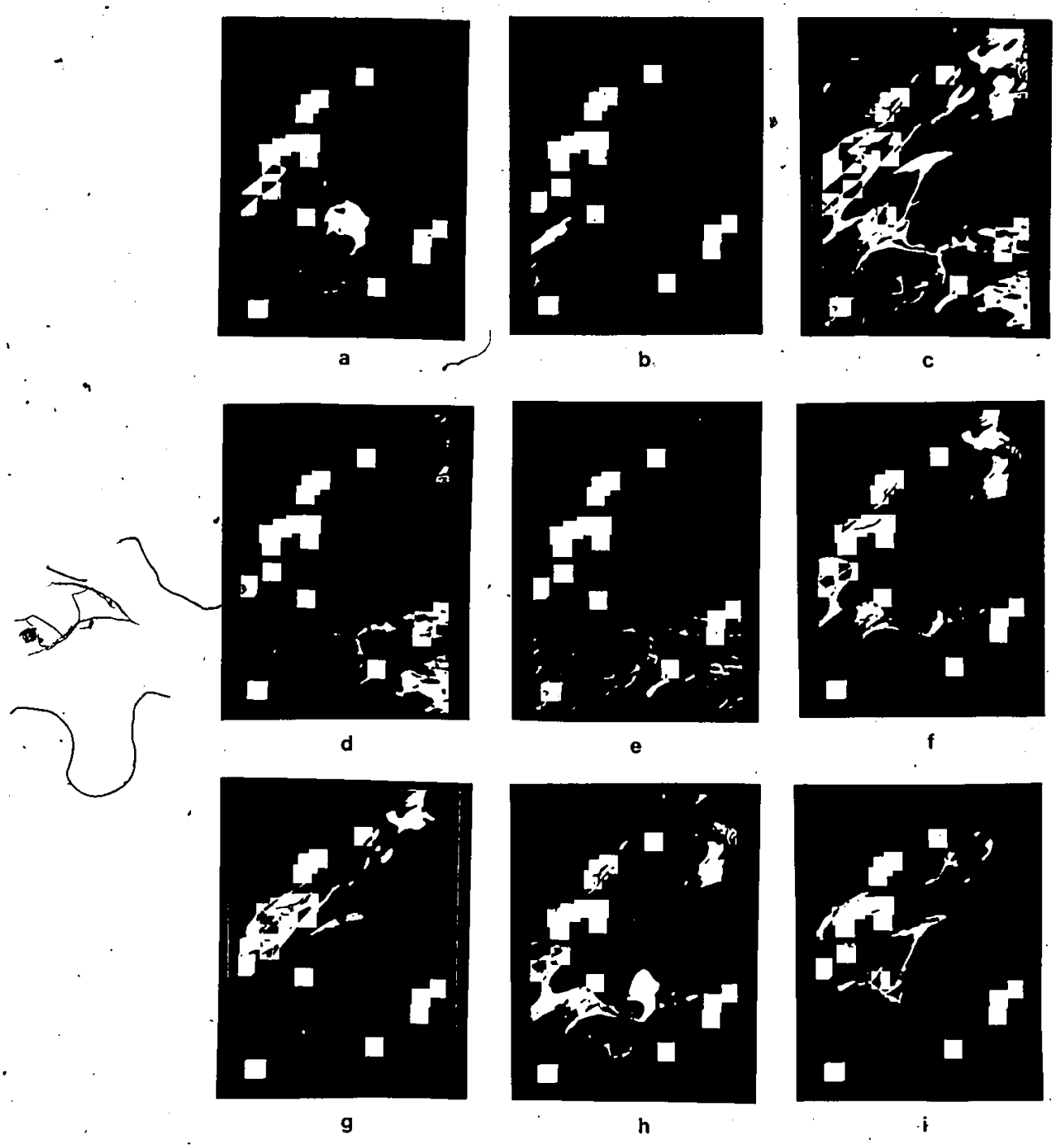

Figure 7.21: Concluded.

In Figure 7.21d, the terrains are shown for which aeromagnetic anomaly values are < 2100 and gravity values range between -65 and -70: three occurrences are in this environment.

In Figure 7.21e, terrains are shown for which aeromagnetic anomaly values are < 2100 gammas, and the gravity anomaly values range between -60 and -65 milligals: three occurrences are in this environment.

In Figure 7.21f, terrains are shown for which the aeromagnetic anomaly values range between 2100 and 2500 gammas, and the gravity anomaly values are < -65 milligals: six occurrences are in this environment.

In Figure 7.21g, terrains are shown for which the aeromagnetic anomaly values range between 2100 and 2500 gammas, and the gravity anomaly values range between -60 and -70 milligals: four occurrences are in this environment.

In Figure 7.21h terrains are shown for which the aeromagnetic anomaly values range between 2100 and 3400 gammas, and the gravity anomaly values are < -70 milligals: seven occurrences are in this environment.

In Figure 7.21i terrains are shown for which the aeromagnetic anomaly values range between 2500 and 3400 gammas, and the gravity anomaly values range between -65 and -70 milligals: one occurrence is in this environment.

The results of this application, as shown in Figure 7.21,

suggest the existence of several environments and that different types of base metal mineralization are represented in the data analyzed. The derived patterns provide the opportunity for discussing some of the critical variables which must be used in modelling map patterns. The size, shape and orientation of the occurrence neighborhoods to be used for establishing the initial coincidence with geological unit map patterns is of importance. We may want to experiment with circular, square or rectangular or elliptical neighborhoods, neighborhoods with grain size smaller than the geological grain size of the outcrops, subparallel to geological trends or of arbitrary geometry and orientation, which will provide different kinds of controlling relationships in better correspondence with the geological units hosting the mineralization.

In selecting the contour intervals to be digitized from the geophysical maps, several intervals have been lumped together. This may cause that the extracted binary patterns represent ranges of values which are too broad. The transformation of continuous variables, like the contour values, into discrete variables, like the binary patterns extracted here, may result in a loss of information. It is only the prior knowledge of the geologist and of the geophysicist, which can guide in decisions of this nature.

Additionally, the knowledge of mineralization characteri-

stics of the occurrences used in constructing the controlling neighborhoods, and the availability of additional information, are essential tools to the model building experiments.

The patterns derived in Figure 7.21, represent an initial stage of an application which brings out what kind of geological decisions often have to be made, even during an interactive session.

7.5 Concluding remarks

The target of the analysis of binary images like the ones considered in this chapter, is to recognize patterns of areas to which a greater probability of discovering mineral deposits is associated. In the effort to hit the target, we must always keep in mind that in building the necessary geological models for recognition, it is important to decide what to measure from our images, given the various uncertainties associated with the data:

(a) uncertainties in the geological boundaries represented on the geological maps and in the contours of the geophysical maps;

(b) uncertainties in the resolution of the original data mapped or contoured (of course not all available information

can be mapped);

(c) uncertainties in the digital resolution of the images, in their registration and in the selection of the information digitized.

These uncertainties will have to be built into the uncertainty, the greatest perhaps, associated with our classification model to be built relying mostly on prior knowledge.

The transformations of the contour intervals in geophysical (or geochemical) maps into binary images and, most of all, the selection of the intervals, has to be done by expert knowledge of what the geophysical anomalies represent in terms of the phenomena under study. The contouring itself is, to some extent, an artistic endeavour. According to the different applications, geophysicists produce special purpose contour maps for their work: for this reason a published geophysical (or geochemical) anomaly contour map is not necessarily the most appropriate data base for a given study. Additionally it may be remarked that the binary transformation of continuous data represents a gross simplification, and it could be desirable to treat contour maps like grey level images, which in essence they are. It naturally follows that the applications described here can only be of a general nature: only few fundamental aspects are considered in order to suggest a broader family of promising techniques still unfamiliar to geologists.

The results of the experiments that have been described in this chapter have shown that it is possible for a geologist to perform by himself, fast processing of mineral resources map data on a general purpose minicomputer with GIAPP 's software, even at a digital resolution of 1024 pixels x 1024 pixels.

It also has been demonstrated that it is useful to have methods which make probability concepts visible and therefore more understandable by geologists, such as map overlays like the ones shown here.

Additionally it is important that geological and ancillary map data are transformed and processed like remote sensing type of data. This represents one more step towards the integration of geoscience data.

8. Digitization and computer processing of microscopic images of rock thin sections

8.1 Introduction

This chapter analyzes the philosophy of capturing image data and the techniques which were developed for the digitization of microscopic images of rocks. Under the microscope, rocks in thin sections or polished sections, appear as mosaics of tightly interlocked grain profiles. The sections correspond to projections of the crystalline boundaries onto a plane: the geometrical characteristics of these profiles, including their apparent shapes, orientations and distributions, belong to what is generally called "texture". In the Dictionary of Geological Terms (A.G.I., 1957), under the term texture we read: "geometrical aspects of the component particles of a rock, including size, shape and arrangement".

A more precise definition of texture and a formal approach to its study do not exist. For example, the characterization of textures still represents a complex and unresolved problem; a great variety of different textural aspects and methods for measuring textural properties are being applied in very diverse fields of study. Haralick

(1979) in a recent review of approaches to textures in image processing, emphasizes that in order to characterize textures, both the tonal primitives, e. g. a particular range of gray levels or a single phase, and the spatial interrelations between them must be characterized. He considered the following eight groups of statistical approaches: (a) autocorrelation function, (b) optical transforms, (c) digital transforms, (d) textural edgeness, (e) structural element, (f) gray tone co-occurrence, (g) run lengths, and (h) autoregressive models. As Haralick observed, each of the methods, existing to date, tends to emphasize either the analysis of tonal primitives or their spatial interrelations, and not to treat each aspect equally. In describing the approach (e) above, which was proposed by Matheron (1967, 1975) and by Serra (1978), he writes (p. 787): "The power of the structural element approach is that it emphasizes the shape aspect of the tonal primitives. Its weakness is that it can only do so for binary images".

In the opinion of the author of this thesis, however, this approach can in fact be well extended to non-binary images as exemplified by Serra (1976), Goetcherian (1980) and also by Sternberg (1978) and Gillies (1978) for the Cytocomputer, a pipeline processor of recent design (Preston et al, 1979). The same approach is also used in this chapter, and the technique is described for transferring

microscopic images into digital images from which, by image processing, features are extracted for texture analysis of binary images.

A microscopic image can also be considered as a raw gray level picture. From it we can extract a sample (or better a discrete array of gray level values) at regular intervals (digitized image). For obtaining a colored image we can scan the image with different color filters. A scanner is either a mechanical or an electronic instrument, which measures the gray level tones from our original image material and transforms them into digital values. These can also be stored for later use, for example, on a magnetic tape. In this case, for transferring the information provided by the different colors, many images will have to be combined. Some crystals, for example, appear colored under plane polarized light, whereas other crystals are colorless. The color of pleochroic crystals will, however, change with their orientation with respect to the plane of polarization. Under cross-polarized light, the colorless crystals will assume different colors, according to their orientation relatively to the polarization planes and also due to their individual lattice and optical properties. Under these general circumstances the recognition of grain identity and grain boundaries becomes a problem even in the relatively simple cases of clear and homogeneous crystalline

fabrics.

For example, whenever crystals of the same type (phase) are in contact, the grain boundary may or may not be visible unless the microscope setting is changed. Even in the special case of an already available colored draft being scanned, the scanner cannot easily resolve the colors as uniform gray tones because colors are often made up of colored dots, and there are defects even in very uniform looking colors. For these reasons it is not yet possible for automatic scanning devices to capture and process sufficient information for a satisfactory phase recognition and extraction.

There are several kinds of scanners which can be used for digitizing thin section material. They can be grouped as follows: (1) Flying Spot Scanner (FSS), (2) television scanner (TV camera), (3) drum scanner, (4) flat bed scanner, and (5) scanning microscope (microdensitometer).

The FSS is a custom made electronic device with normal resolution ranging from 1024 pixels x 1024 pixels to 4096 pixels x 4096 pixels. Its position accuracy is not very good bacause it uses a magnetically deflected electron beam. The scanning speed is equivalent to computer speed if the FSS is controlled by a computer.

Broacast commercial television cameras (scanners) are electronic devices with resolution of 525 lines in North

America, and 625 lines in Europe (for the PAL system). The aspect ratio is 4:3. Special TV cameras go up to 1200 or more lines. This scanner is the least expensive and also the fastest: it grabs the input in 1/30 of a second. There are problems of position accuracy with electronic television scanners, but not so for the solid state chips television cameras. We do not yet have, however, a 500 x 500 pixels "chip" available at reasonable cost in solid state chips TV cameras.

Mechanical drum and flat bed scanners are not limited in resolution, except for the physical limits of the particular equipment. They are quite position accurate, however, they are very expensive, particularly the flat bed scanners. They are slow devices: for example what could take half an hour on a drum scanner, might require hours on a flat bed scanner.

A scanning microscope has a television camera which looks at the image in the microscope, and also a single photocell (a photomultiplier for photometric accuracy): these complement one another. The television camera has a low resolution and position accuracy, and a fast speed. The photocell has a high resolution, good position accuracy, but it is very slow. Scanning microscopes are very expensive instruments.

The present solution of tracing the boundaries of crystal

present stage of image processing, or even the quickest solution in the light of the present equipment and knowledge.

The applications considered in this chapter make use of a flying spot scanner. The digitization of boundaries of grain profiles of a microscopic image could also be performed by projecting the microscopic image on the surface of a graphic tablet. This was not done both because it would have required some special equipment (a transparent tablet digitizer and projection devices) and also because the recognition and manual digitization of several thousands grain profiles is too time consuming to be performed interactively on a single user computer.

The digitization of grain profile ink drawings by a flying spot scanner is described in detail for the equipment presently available. Experimental applications to the analysis of the images of a granulite and an amphibolite exemplify the capabilities of the software which was programmed. They also provide the ground for further work on quantitative characterization of rock textures.

From the analysis of binary images of grain profiles, the study of properties in the third dimension is feasible, which is a typical stereological problem. Texture characterization as performed in the following sections, is only a small aspect of a broader field of texture analysis.

To complete the subject within the field of geological applications to the study of crystalline morphometry and texture, a review of some of the more interesting experiments made during the past two decades is made. This section is followed by several remarks on possible developments of the approach which was used and which is being proposed in this thesis.

Some new problems can be studied if the assumption is made of having at our disposal a computer image of our study material which can be identified as a data bank from which we can read or retrieve information on many quantitative aspects. Indeed in such a situation, in the absence of a comprehensive theory of texture formation and characterization, the limits to what can be asked our data bank are in our practical knowledge and ingenuity.

8.2 Digitization of grain profiles by scanning transparencies of line drawings

The procedures described in this section could be automated to some extent, by using a more expensive scanner, than the one which was used. This description faithfully represents the experiments and the processing actually performed for the practical applications.

In summary the steps for digitizing the microscopic images of grain profiles from the thin sections are as follows:

(1) tracing of the original microscopic image by projecting it onto a wall or by using a special projecting screen. A 35 mm negative drawing of such a tracing, taken after Kretz (1969) is shown in Figure 8.1a.

(2) the image is scanned first within a properly positioned box, and displayed on a Tektronix 611 storage display screen. A histogram of the gray level value readings is also produced, as shown in Figure 8.1b. A cross section of the gray levels between two selected points can also be obtained and plotted over the scanned image plot, for further assisting in deciding on a proper resolution, as shown in Figure 8.1c. A printout of 256 gray level readings along the cross section can be

a

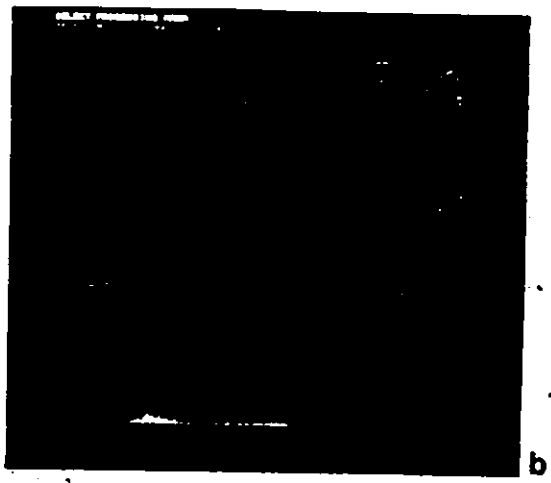

b

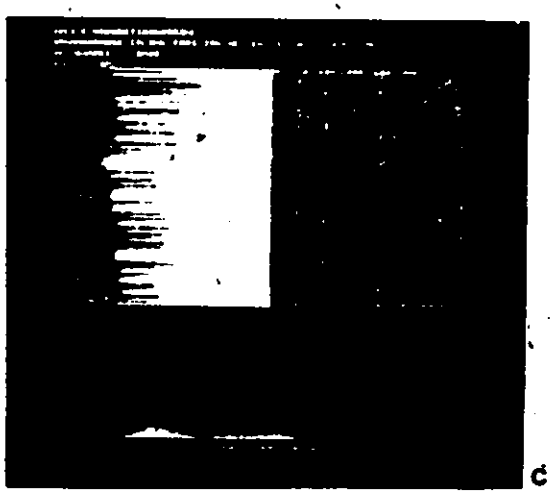

c

LINUR1: 300 -65 -88 -76 3072 -1256 908 -8.8769 -14.4749

1& 20	-2488	-2973	-2923	-2839	-1540	-1423	-1973	-2499	-2847	-2819	-2833	-2839	-2651	-1635	-1317	-1719	-2447	-2365	-1740	-1432
21& 40	-1317	-1258	-1211	-1224	-1346	-1555	-1839	-2178	-1783	-1507	-1667	-1960	-1415	-1354	-2203	-2675	-2642	-2771	-2797	-2801
41& 60	-2807	-2716	-1618	1450	-2283	-2653	-2748	-2720	-2749	-2739	-2387	-1598	-1652	-1262	-1390	-1644	-1303	-2081	-2529	-2627
61& 80	-2733	-2721	-2713	-2781	-2741	-2746	-2630	-2265	-1901	-1846	-1364	-2227	-2541	-2692	-2607	-2589	-2473	-2161	-1816	-1372
81&100	-1725	-1759	-2502	-2758	-2785	-2795	-2797	-2865	-2876	-2776	-2743	-2320	-1518	-1619	-1432	-2073	-2641	-2733	-2732	-1847
101&120	-1529	-2351	-2694	-2566	-2560	-2586	-2725	-2864	-2884	-2889	-2939	-2974	-3043	-2989	-2932	-3011	-2987	-3050	-3065	-3015
121&140	-3043	-2954	-2946	-2969	-2924	-2942	-2956	-2729	-1641	-1504	-2104	-2741	-2832	-2819	-2891	-2798	-2548	-1875	-1513	-2142
141&160	-1809	-1461	-2379	-2730	-2655	-2097	-1559	-1451	-2044	-2631	-2719	-2794	-2826	-2844	-2805	-2158	-2843	-2881	-2858	-2888
161&180	-2855	-2910	-2856	-2866	-2853	-2842	-2068	-1829	-1642	-2593	-2764	-2836	-2843	-2809	-2837	-2809	-2853	-2879	-2838	-2848
181&200	-2497	-1735	-1984	-1507	-2159	-2575	-2372	-1484	-1873	-1600	-2266	-2607	-2715	-2733	-2749	-2785	-2770	-2684	-2083	-1428
201&220	-1837	-1578	-2112	-2496	-2660	-2541	-2173	-1637	-1934	-1497	-2329	-2094	-2036	-1316	-2261	-2546	-2599	-2205	-1512	-1058
221&240	-1901	-1863	-1469	-2179	-1775	-1960	-1413	-2290	-2588	-2762	-2711	-2741	-2783	-2836	-2795	-2801	-2803	-2807	-2786	-2795
241&260	-2782	-2828	-2757	-2549	-1539	-2061	-1746	-1344	-1705	-2105	-1981	-1548	-2060	-2610	-2681	-2667	-2673	-2706	-2688	-2125
261&280	-1849	-1481	-2346	-2582	-2671	-1894	-2713	-2737	-2733	-2775	-2644	-2693	-2522	-2105	-1629	-2105	-1883	-1436	-2245	-2436
281&300	-2571	-2617	-2695	-2669	-2648	-2657	-2465	-1989	-2023	-1908	-1437	-2301	-2577	-2581	-1504	-1429	-2226	-2612	-2772	-2773

d

Figure 8.1: (a) negative print of the line drawing of 1300 grain profiles redrafted after Kretz (1969); (b) Tektronix 611 video display plot of the scanned image, and of the histogram of gray levels; (c) same plot of (b) with the cross section plot of the gray levels; (d) printout of the gray level readings displayed in the cross section in (c).

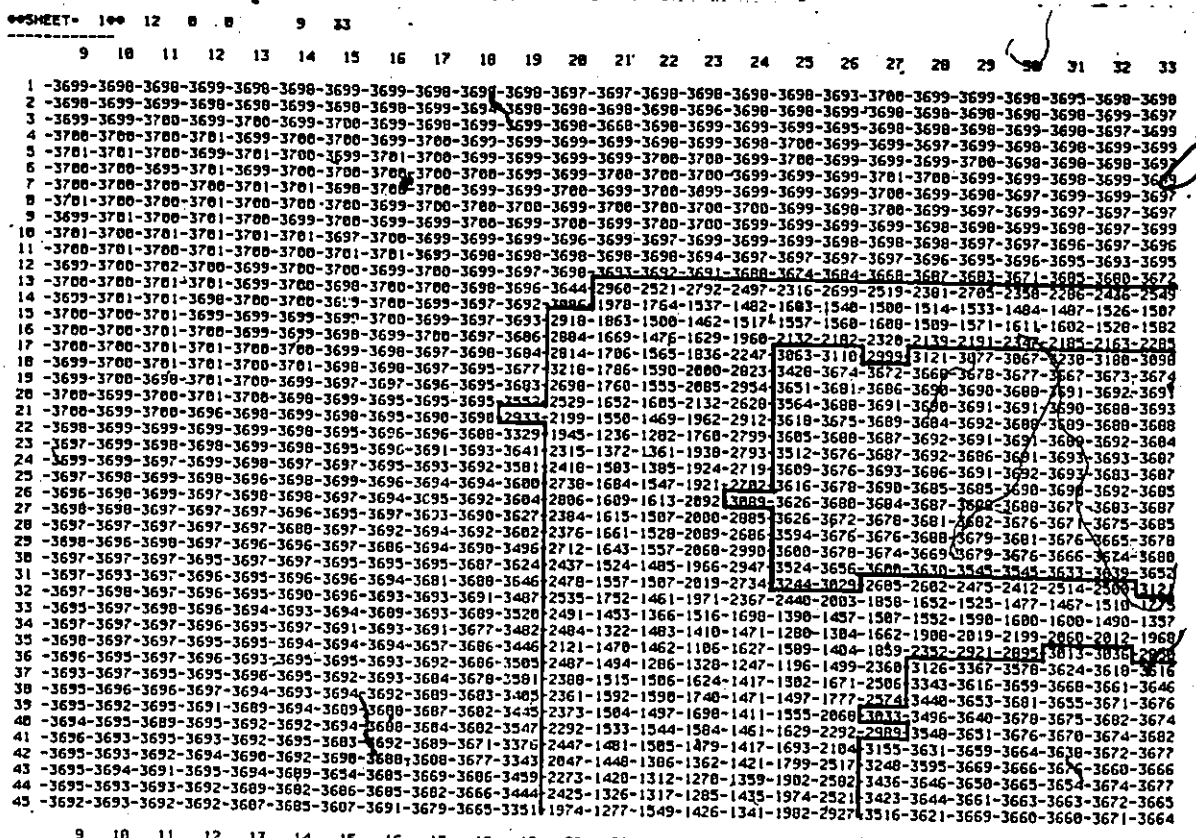

Figure 8.2: Portion of the square raster scanned image of 1300 grain boundary profiles of the same granulite shown in Figure 8.1a. The dimensions of the original image are 1000 pixels x 595 pixels: a 23 pixels x 45 pixels portion is displayed here as a printout of the gray level readings. Contours were added by hand to emphasize the location of the boundary pixels.

produced, like the one shown in Figure 8.1d. From these preliminary tests, a decision is taken on the desired resolution: for example, at least three pixels should represent line thickness and most small areas should be represented by at least one pixel.

(3) after deciding on the resolution, the FSS is programmed to scan the transparency and to provide the computer with the desired number of gray level readings for the desired number of scan lines. In the case shown in Figure 8.2, a 1000 pixels x 595 pixels square raster image was produced: the gray level values of few pixels are displayed between x-coordinates 9 and 33, and y-coordinates (rows) 1 and 45. A second hexagonally scanned image for the same resolution (same density of scanned points per unit distance in the horizontal direction) was also produced, with 1000 pixels x 687 pixels. Each pixel corresponds to 1/53 mm or .019 mm.

(4) the gray level image is analyzed by producing first a gray level histogram, both as plot and as listing, as shown in Figures 8.3a and 8.3b, respectively. This histogram is needed to decide on how best to select a thresholding level or thresholding rule, also called gray level slicing, for obtaining a corrected binary image. In such image all the pixels belonging to the

lines are black, gray level value of 1, and all the remaining pixels are white, gray level value of 0. After this, one or more cross sections are computed across the image (Figure 8.4a) and the gray level values along them are plotted to see if the desired detail is properly expressed (Figure 8.4b). In this case the cross section has a concave pattern, which means that the scanner sensitivity varies from the center to the edges of the scanning area.

(5) different thresholding levels can be set for producing binary images and studying the plots of relevant details in critical parts of the binary images obtained. This is shown in Figures 8.5a to 8.5f, for both the upper left and the upper right corners of the thresholded images. Square and pseudo-hexagonal plots of binary images thresholded between the same values can also be produced for comparison of the detail digitized by the two raster types with identical resolution (Figures 8.6a and 8.6b).

a

RAW HIST 17 1000 595 256 -813 -3702 596 -3702

0.088612

1 TO 10	-3702(	11.)	-3589	1719	1385	891	748	663	637	668	798	689	729	
11 TO 20	-3589(	11.)	-3476	755	657	567	537	613	555	529	630	567	601	
21 TO 30	-3476(	11.)	-3363	619	758	759	884	1026	1050	1125	1107	1268	1153	
31 TO 40	-3363(	11.)	-3250	1168	1348	1379	1404	1543	1750	1610	1701	2016	2087	
41 TO 50	-3250(	11.)	-3137	2236	2375	2665	2638	2538	2917	2780	2940	3079	3415	
51 TO 60	-3137(	11.)	-3024	3298	3396	4078	4207	4616	5298	6466	6359	7007	8096	
61 TO 70	-3024(	11.)	-2912	7633	7808	7986	8927	8317	8513	9332	8818	8844	9076	
71 TO 80	-2912(	11.)	-2799	10082	9387	9426	10180	9352	8867	8799	9187	7837	7208	
81 TO 90	-2799(	11.)	-2686	6998	6679	5056	4382	4374	3511	3181	3149	2621	2461	
91 TO 100	-2686(	11.)	-2573	2235	2298	1911	1048	1871	1599	1487	1473	1577	1395	
101 TO 110	-2573(	11.)	-2460	1347	1467	1238	1215	1198	1273	1195	1180	1190	1104	
111 TO 120	-2460(	11.)	-2347	1056	1118	1203	1084	1074	1093	1046	1051	1086	1113	
121 TO 130	-2347(	11.)	-2234	996	985	1038	986	975	970	1053	899	973	1050	
131 TO 140	-2234(	11.)	-2122	957	916	944	1037	935	928	1043	944	915	952	
141 TO 150	-2122(	11.)	-2009	1012	917	875	986	919	884	912	965	955	917	
151 TO 160	-2009(	11.)	-1896	992	982	888	893	954	953	927	1013	902	960	
161 TO 170	-1896(	11.)	-1783	1028	1106	1001	1064	1289	1204	1322	1405	1622	1651	
171 TO 180	-1783(	11.)	-1670	1654	1928	1943	1988	2140	2346	2312	2440	2641	2583	
181 TO 190	-1670(	11.)	-1557	2616	2570	2925	2735	2756	3100	2712	2709	2706	3016	
191 TO 200	-1557(	11.)	-1444	2731	2651	2989	2730	2662	2685	3001	2641	2654	2959	
201 TO 210	-1444(	11.)	-1332	2662	2676	2789	2939	2756	2672	2964	2801	2720	2804	
211 TO 220	-1332(	11.)	-1219	3159	2977	2934	3306	3061	3153	3100	3460	3231	3105	
221 TO 230	-1219(	11.)	-1106	3313	2965	2765	2653	2723	2262	1929	1861	1473	1248	
231 TO 240	-1106(	11.)	-993	1032	973	760	590	476	360	250	214	164	117	
241 TO 250	-993(	11.)	-880	67	46	29	27	14	9	8	4	5	2	
251 TO 256	-880(	11.)	-813	8	3	0	1	0	1					

b

Figure 8.3: (a) gray level histogram of the scanned image in Figure 8.2; and (b) list of the gray level values in the histogram in (a).

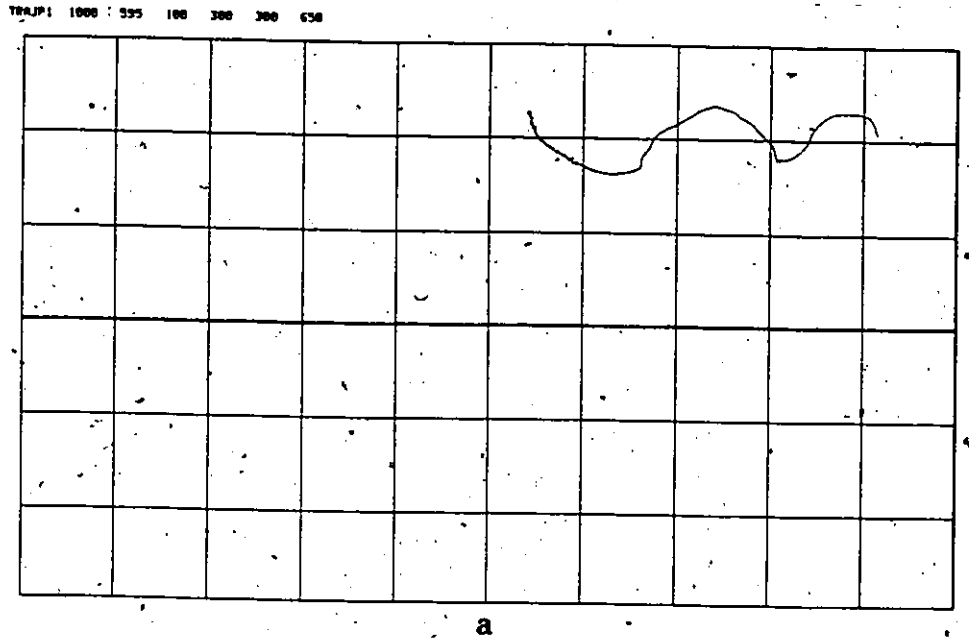

a

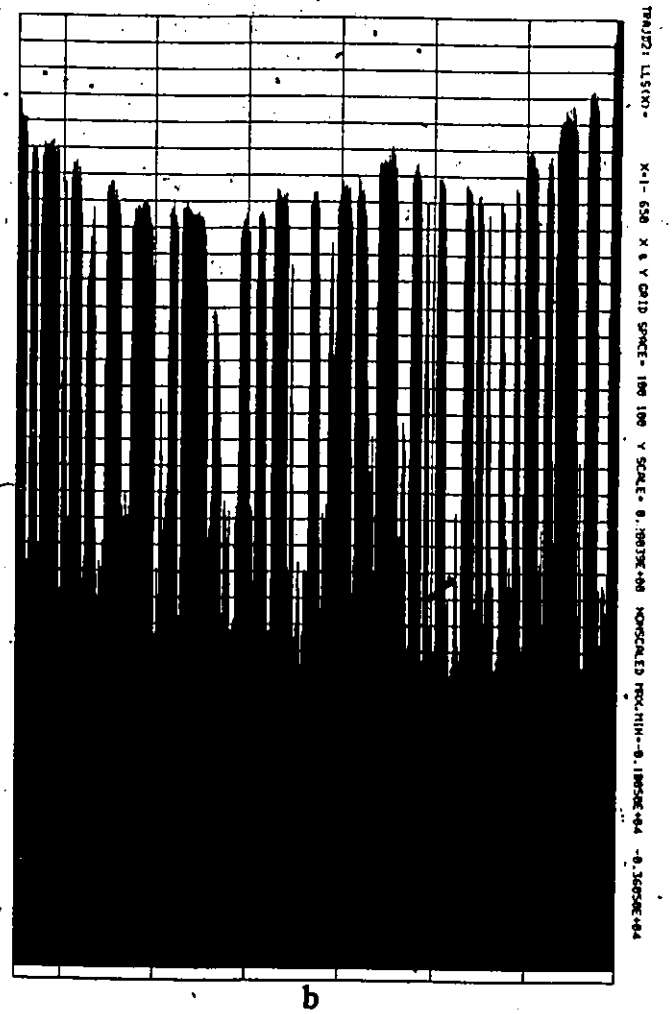

b

Figure 8.4: Cross section of gray level values horizontally across the scanned image in Figure 8.2. (a) plot of the 650 points on the cross section or trajectory; (b) plot of the gray level values in the cross section.

(6) in order to correct for the scanning defects observed in (4) and (5) above, the principles of high pass filtering are used. Andrews (1970) describes the usages of filters for image enhancement. In this instance the equivalent effect of high pass filtering is obtained by computing first the average values for 19 pixels x 19 pixels areas and then creating a picture in which the values of the pixels are the differences between the original values and the average values. Figure 8.7a shows a part of the original grey levels from the scanned image, and Figure 8.7b, the 19 pixels x 19 pixels average for the same area. The newly computed difference values are shown in Figure 8.7c. Further filtering is obtained by reaveraging the averaged values, for example averaging within 19 pixels x 19 pixels arrays again. This is shown in Figure 8.7d. A better filtered image is obtained by subtracting the latter averaged values from the original gray level values, as shown in Figure 8.8. This second filtering, eliminates entirely the concavity of gray level values distribution observed earlier in Figure 8.4b. The resulting cross sections are shown in Figures 8.9a to 8.9d.

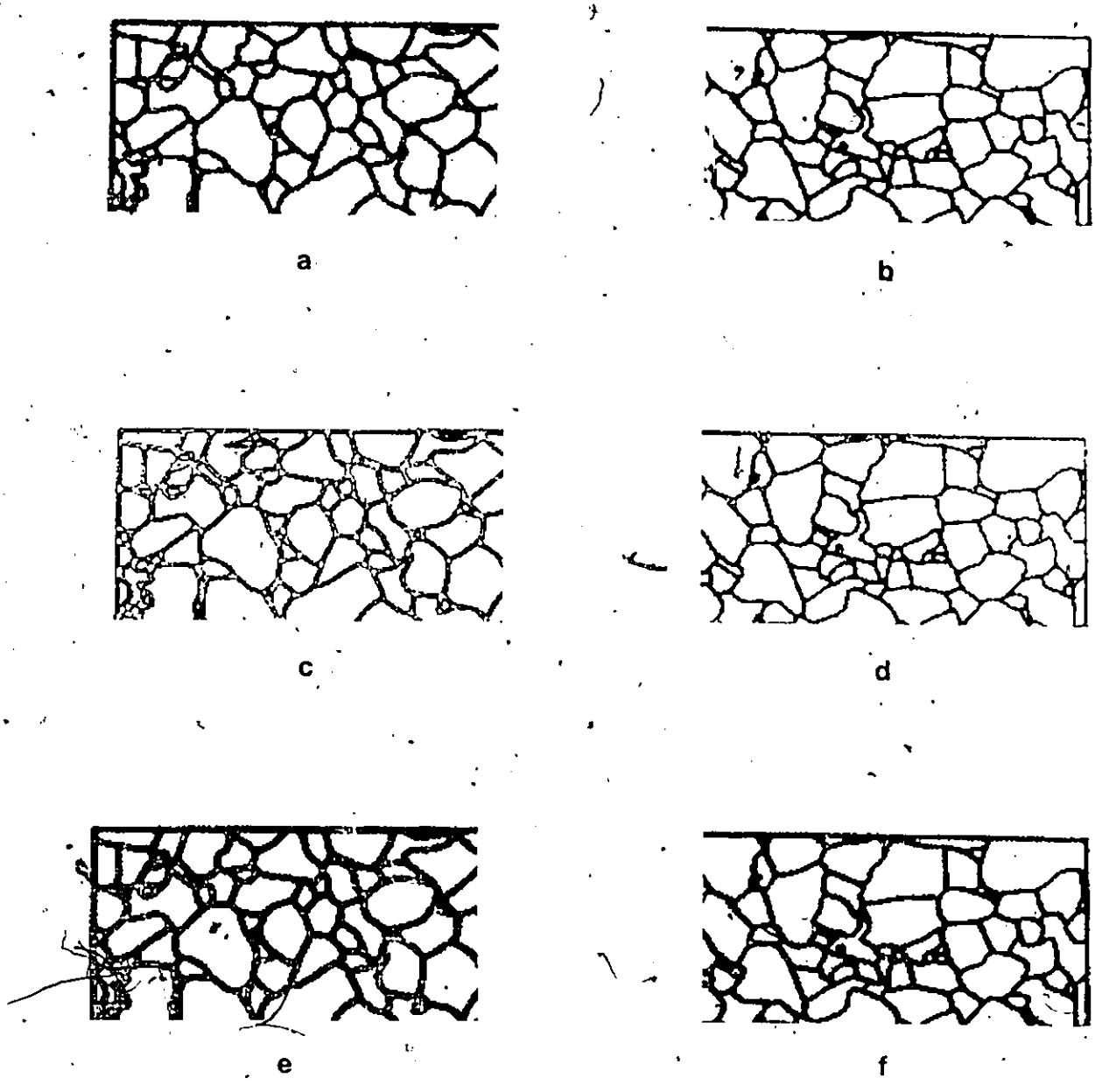

Figure 8.5: Three different thresholdings (gray level slices) of the square raster scanned image in Figure 8.2. Plots are for portions of 256 pixels x 128 pixels of the upper left corners, (a), (c), and (e), and of the upper right corners, (b), (d), and (f), of the images. (a) and (b): thresholding between the values -1800 and -3702; (c) and (d): thresholding between the values -1600 and -3702; and (e) and (f): thresholding between the values -2300 and -4500.

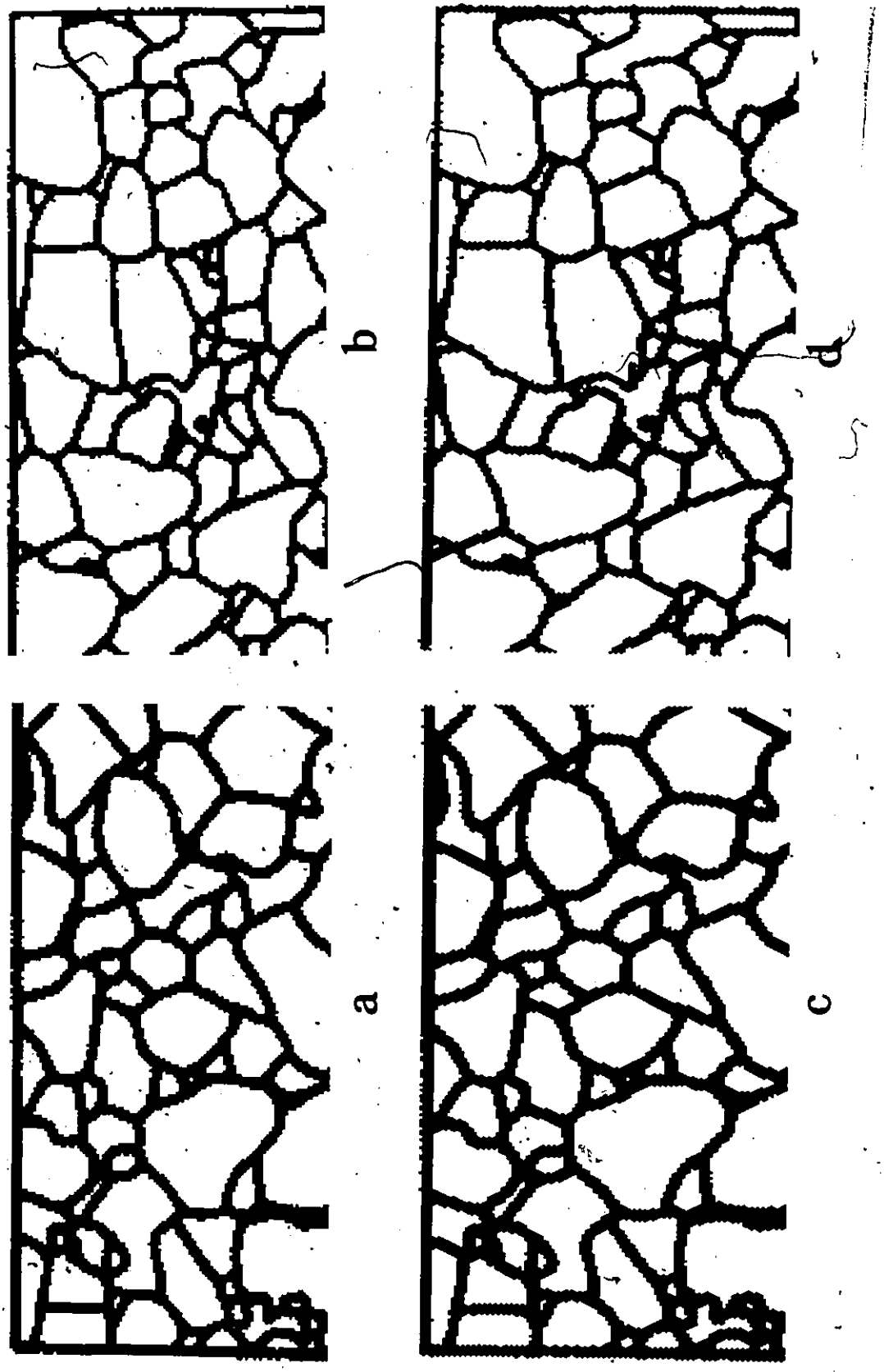

Figure 8.6: Thresholding of two images scanned with a square raster, (a) and (b), and hexagonal raster, (c) and (d). Thresholding is between the values -1900 and -9000 for both the images. In the plots arrays of 2 x 2 black dots correspond to the black pixels. The pseudohexagonal plots in (c) and (d) is obtained by shifting one dot to the right every even row of picture data.

(7) after high pass filtering, several thresholding values are tested again, and are displayed as plots of parts or whole of the binary images obtained, as shown in Figure 8.10. An optimal thresholding interval is then selected, as shown in Figure 8.11a and in Figure 8.11b.

(8) the binary image of grain boundary profiles is then edited interactively in places of poor resolution: for example, black pixels are "added" where boundaries are broken, white pixels are "added" for areas totally filled with black pixels. This interactive procedure, described in more detail elsewhere (Chapter 7), produces an edited binary image as shown in Figure 8.12a.

(9) the edited, thresholded, and filtered image is then thinned so that boundary lines become one pixel thick in width. The process produces images of the kind displayed in Figure 8.12b and Figure 8.12c.

(10) minor editing might still be required in places which have been omitted during the editing step (8) and where the thinning process leaves a few tails, as shown in Figure 8.12d. A final boundary image is then obtained, which is displayed in Figure 8.13.

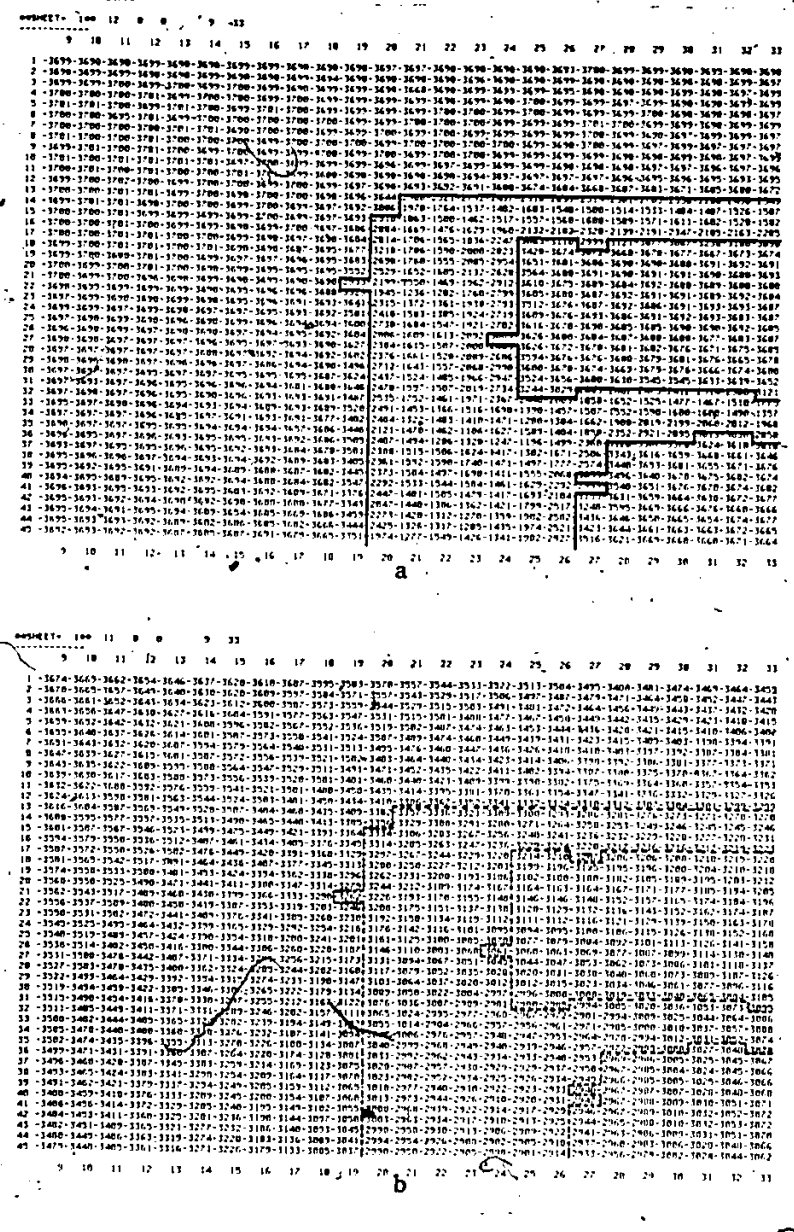

Figure 8.7: High pass filtering of the scanned gray level image of granulite; (a) original gray level values; (b) average values computed for square neighborhoods of 19 pixels x 19 pixels; (c) difference between the values in (a) and those in (b); and (d) average values computed for square neighborhoods of 19 pixels x 19 pixels from the averaged values of the image in (b). Contours were added by hand to emphasize the location of the boundary pixels; broken lines represent the contours in (a).

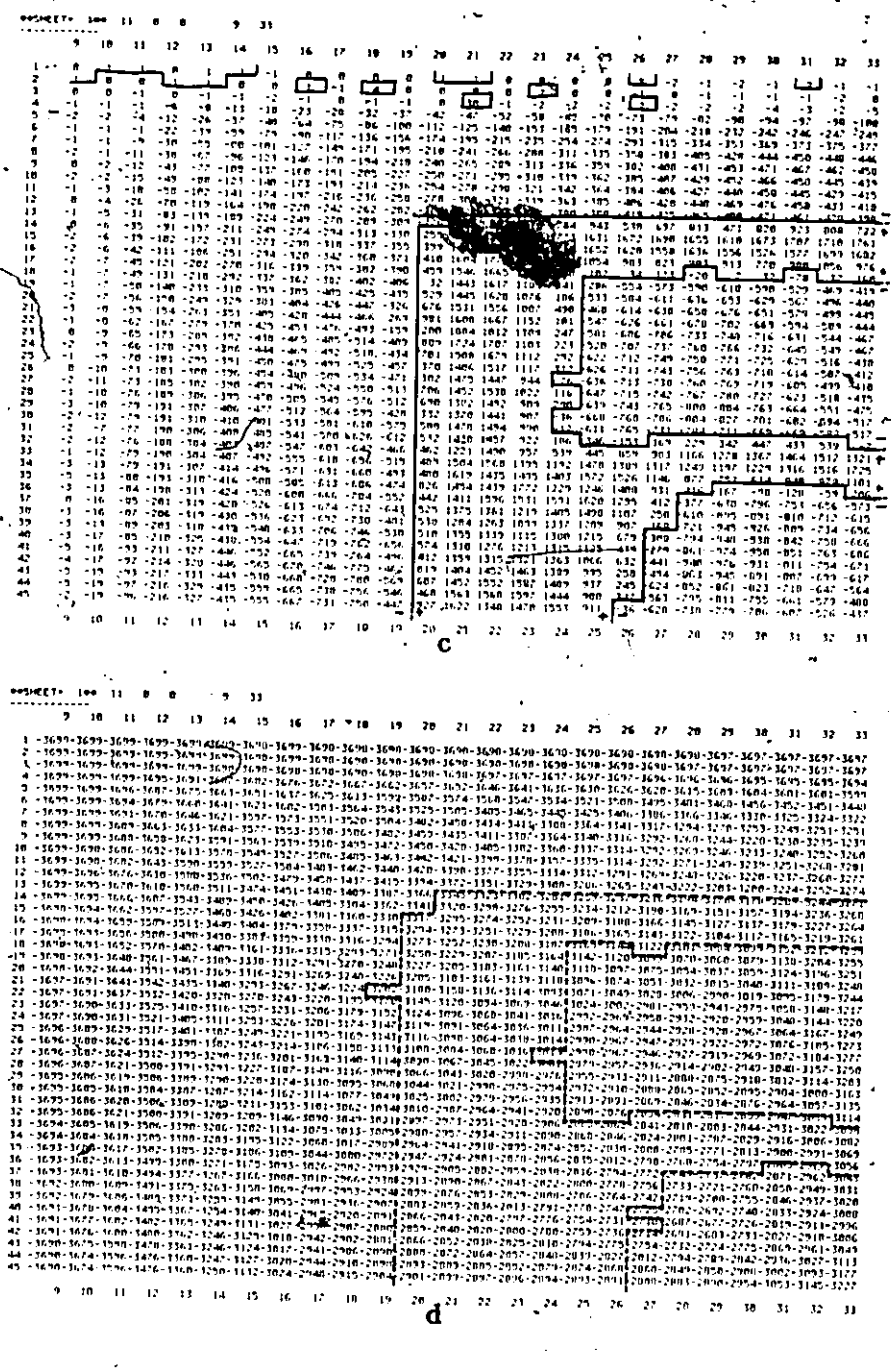

Figure 8.7: Concluded.

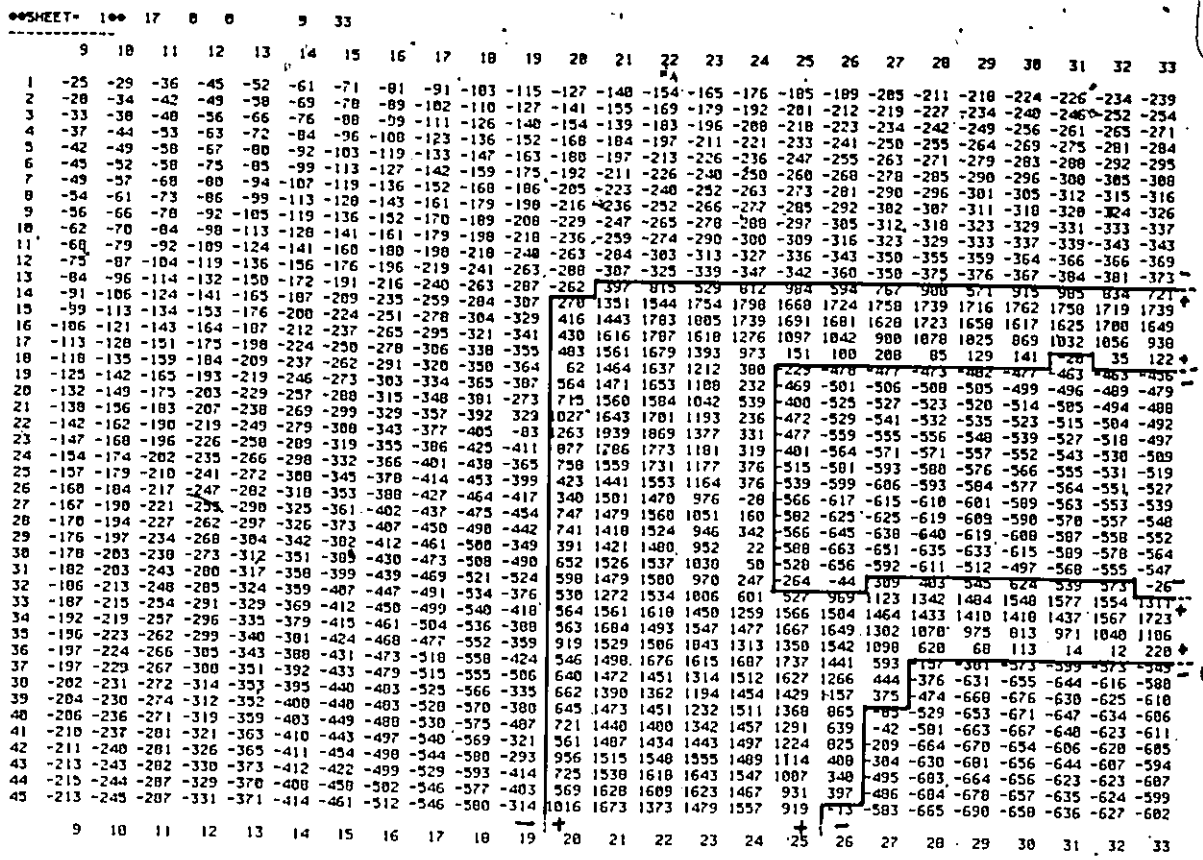

Figure 8.8: High pass filtered image. The values plotted are differences between the original gray level image in Figure 8.7a and the doubly averaged valued image in Figure 8.7d.. Hand contours enhance the desired feature.

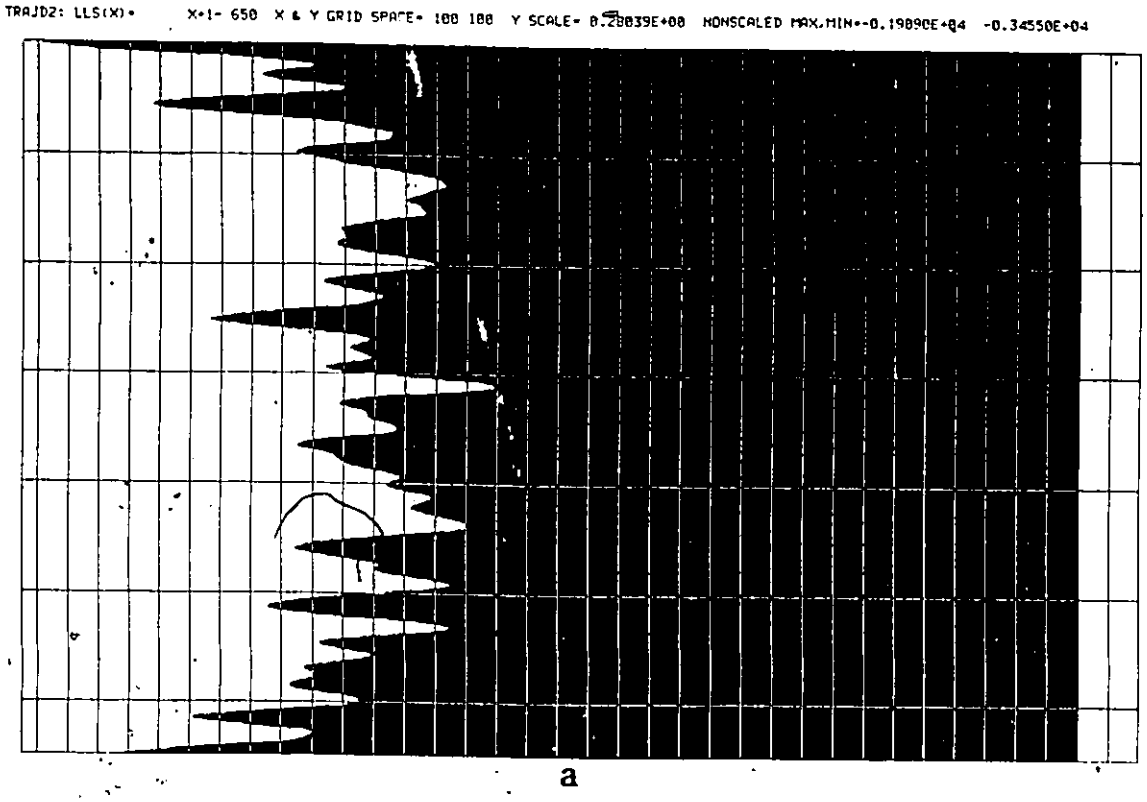

Figure 8.9: Cross sections of the gray level values for the same trajectory shown in Figure 8.4a, for the averaged and filtered images in Figures 8.7 and 8.8: . (a) plot for the image in Figure 8.7b, (b) plot for the image in Figure 8.7c, (c) plot for the image in Figure 8.7d, and (d) plot for the image in Figure 8.8.

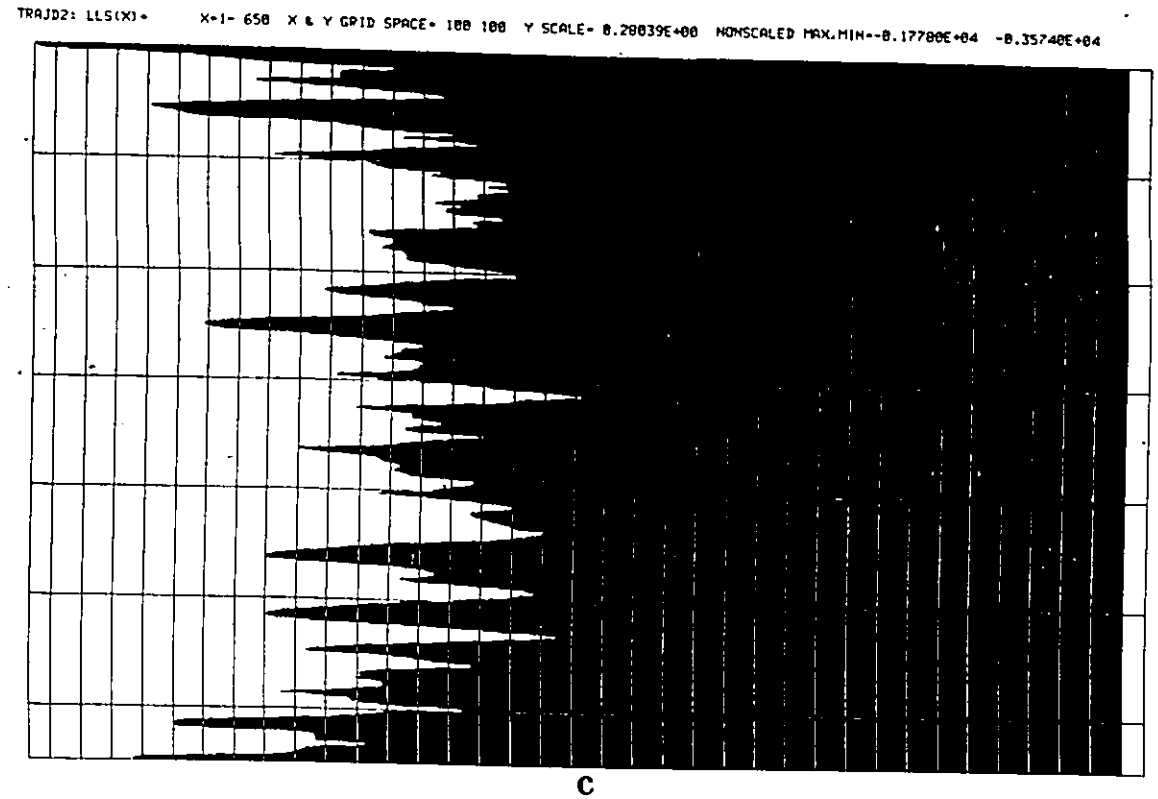

c

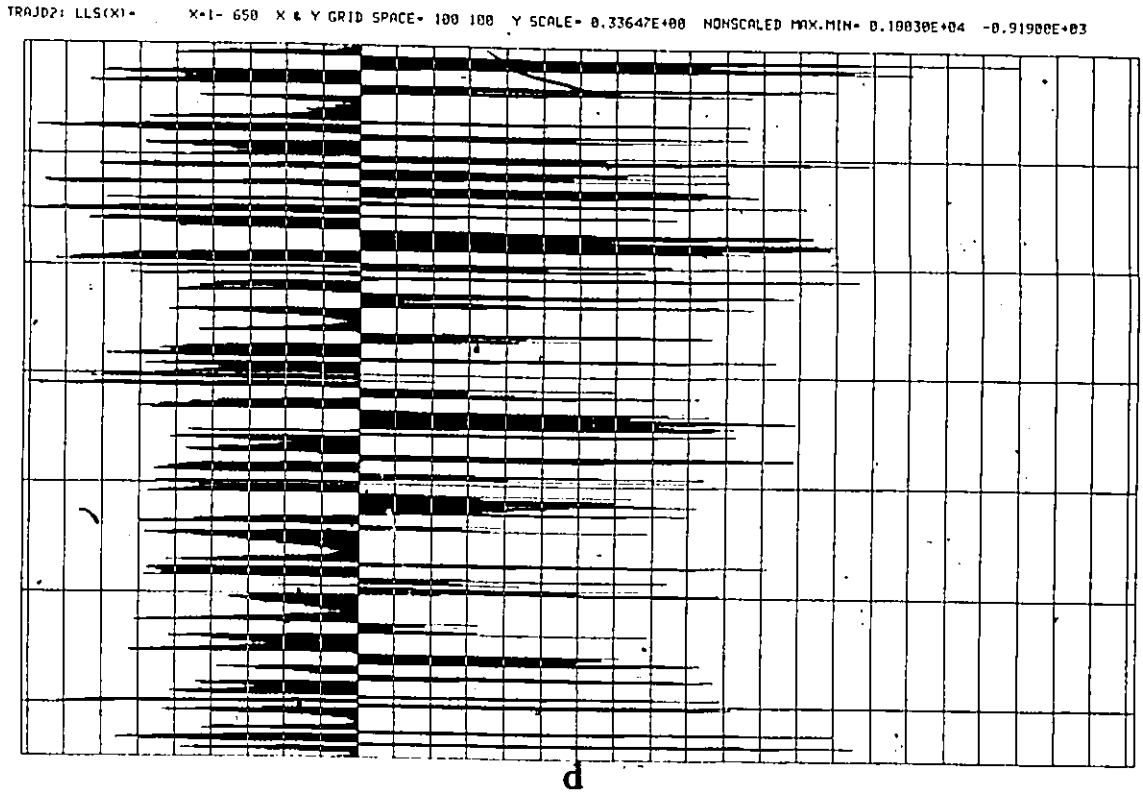

d

Figure 8.9: Concluded.

Figure 8.10: Different thresholdings of the high pass filtered image in Figure 8.8. (a) thresholding between the values 4000 and 100; plot represents the upper left corner of image; (b) same as in (a) for the upper right corner of the image; (c) thresholding between the values 4000 and 50, the plot represents the upper left corner of the image; (d) same as in (c) for the upper right corner of the image; (e) thresholding between the values 10000 and 100, plot represents the upper left corner of the image; (f) same as in (e) for the upper right corner of the image; (g) thresholding between the values 10000 and 100, plot represents the upper left corner of the image; (h) same as in (g) for the upper right corner of the image; (i) thresholding between the values 10000 and 50, plot represents the upper left corner of the image; (j) same as in (i) for the upper right corner of the image.

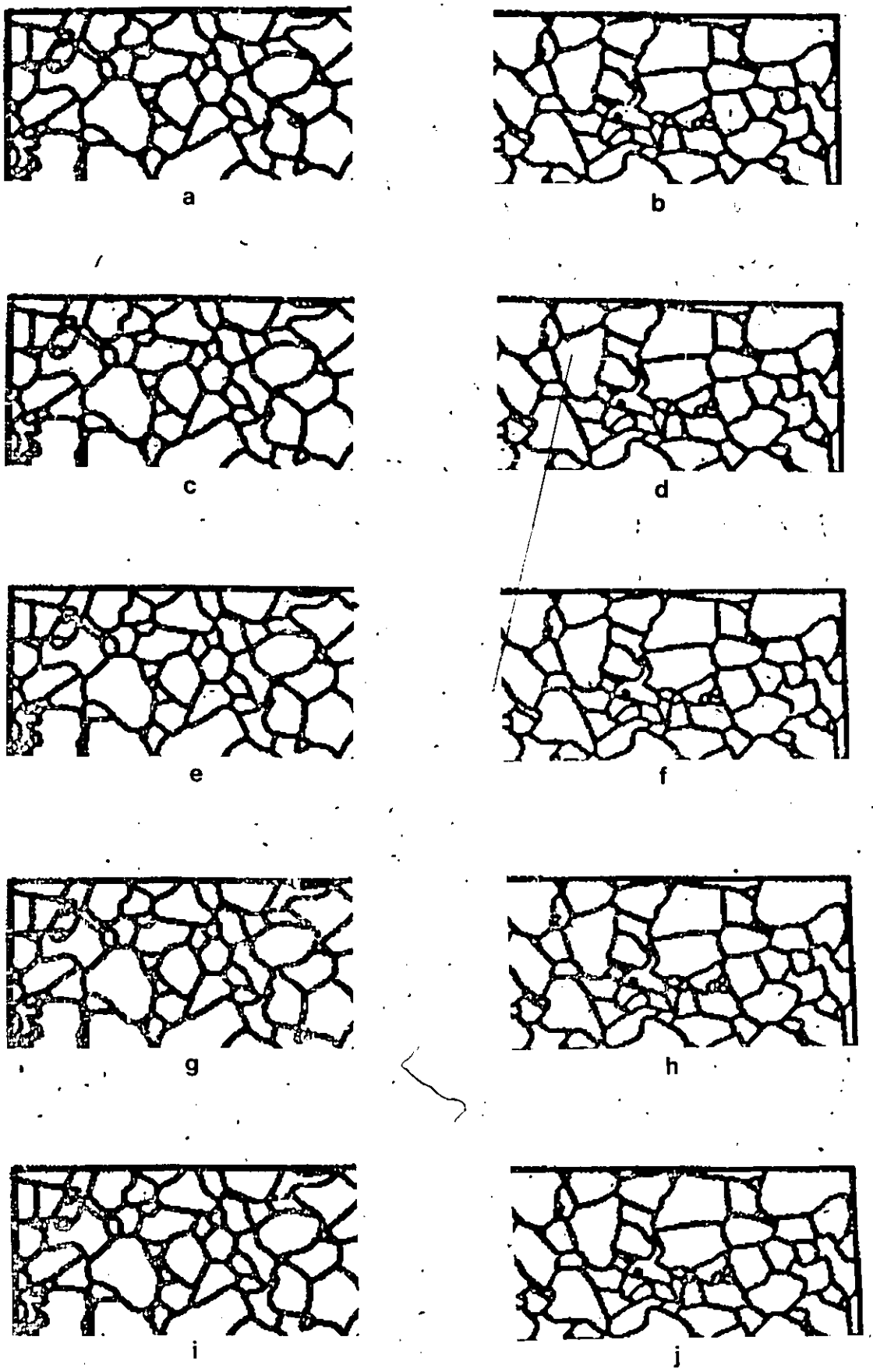

Figure 8.10: Concluded.

(11) for further processing, which requires to assign a unique sequential label to each 0 pixel entirely surrounded by 1 boundary pixels, the image is not any more binary, as shown in Figures 8.14a and 8.14b.

(12) an interactive procedure, identical to the one described earlier (in Chapter 7), assigns to all pixels belonging to each different area, grain, a new label, phase label or crystal type label. A portion of phase labeled image is shown in Figure 8.14c.

(13) a phase labeled image is therefore produced on magnetic tape, which can be transferred to another computer for further computations. In Figure 8.15, for example, an Applicon color plot is shown in which each label is associated to the color density values for the three basic colors: yellow, magenta and cyan.

(14) the phase-labeled image, here displayed as a color image, Figure 8.15 represents a data bank, from which many measurements can be made, and many features can be extracted. For example a binary image of each phase, crystal type, can be extracted, for further processing. Eight binary images have been extraqted from the image of Figure 8.15, as can be seen in Figures 8.16a to 8.16h. They corresponds to the eight phases labeled in the image.

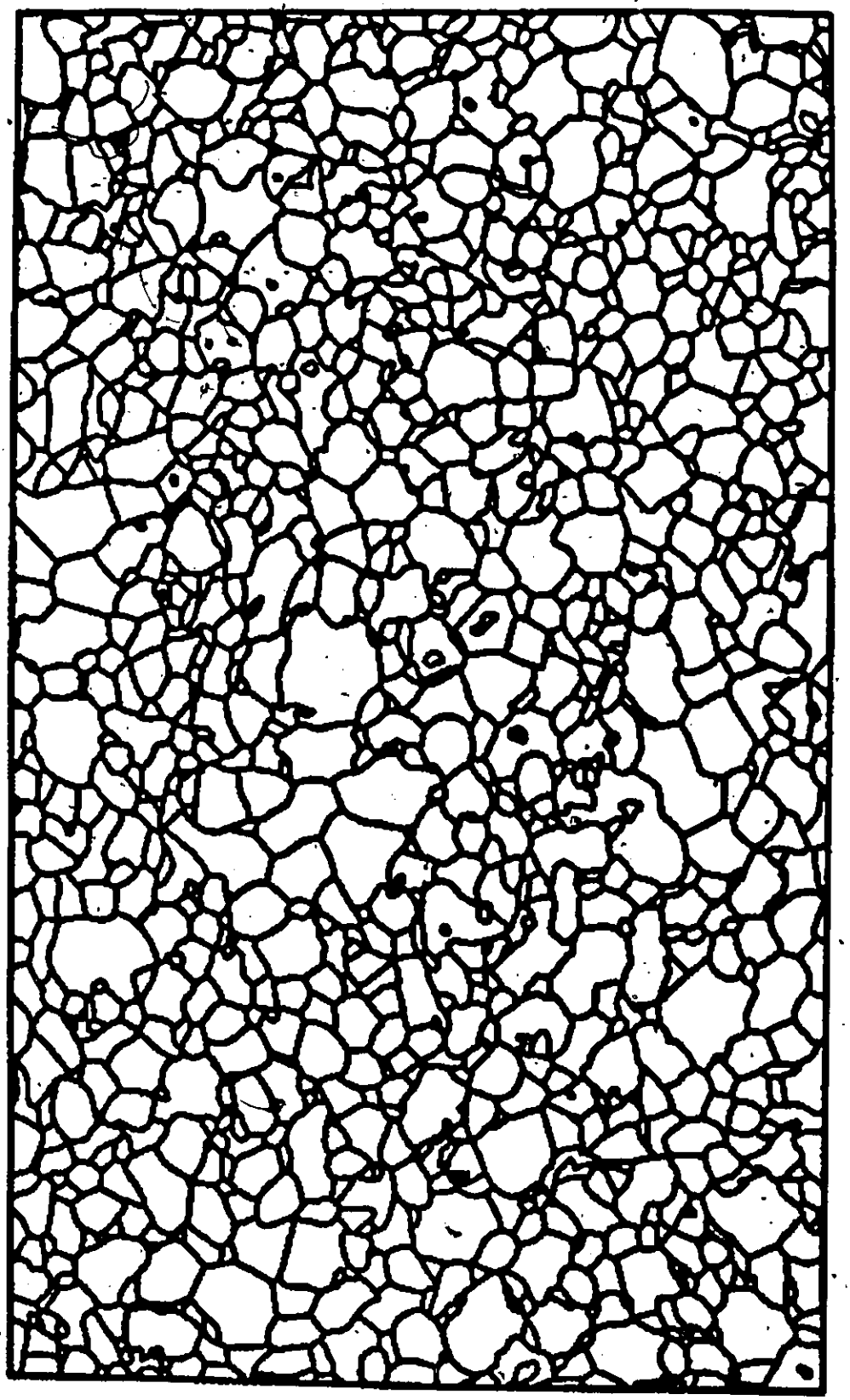

Figure 8.11: Final thresholding selected between the values 10000 and 65; the entire binary image is displayed.

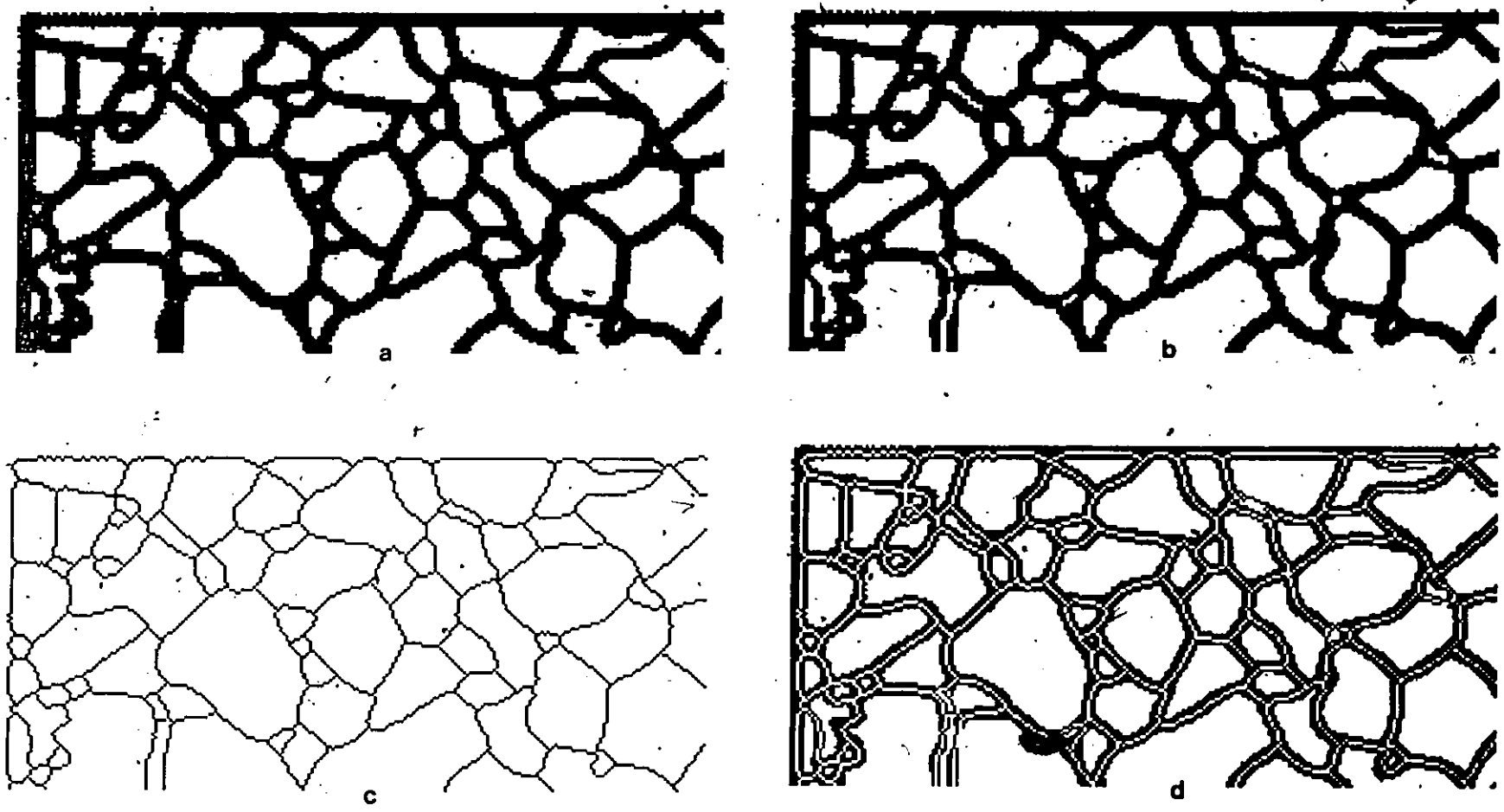

Figure 8.12: Editing of the binary image of scanned boundaries of grain profiles. (a) portion of the original binary boundary image; (b) portion of the binary image after a first editing stage; (c) line thinning of edited binary image of boundaries; and (d) the black pixels which have been changed to white pixels during line thinning.

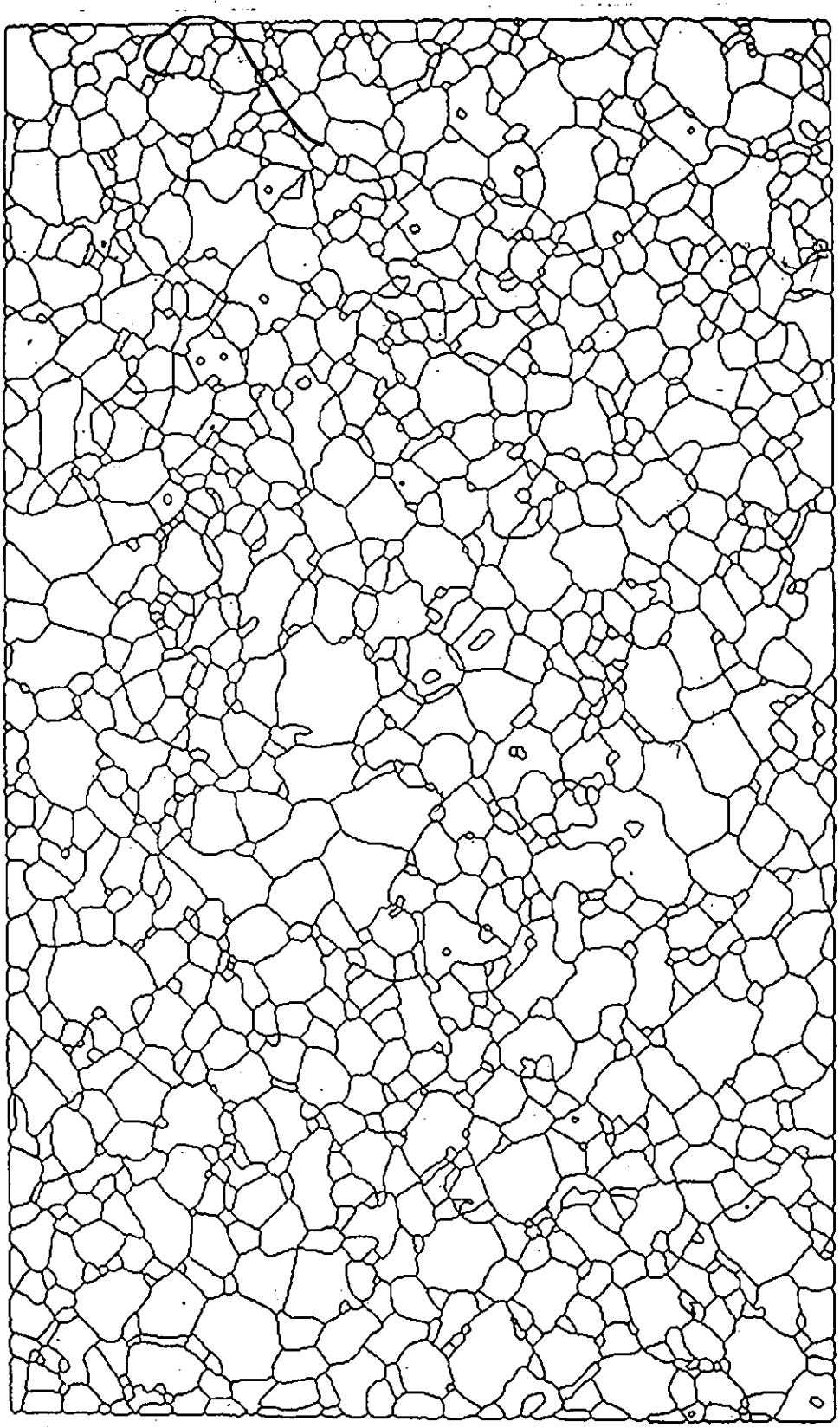

Figure 8.13: Final edited and thinned binary image of boundaries of grain profiles of the granulite.

With the completion of step (14) above, we have terminated the task of digitization and preprocessing, which is a prerequisite to the analysis of binary images to be described in the two sections following this. Clearly steps (3) to (10) could be automated to a great extent by using a more expensive flying spot scanner. In that case then, the steps would only be required for very minor improvements.

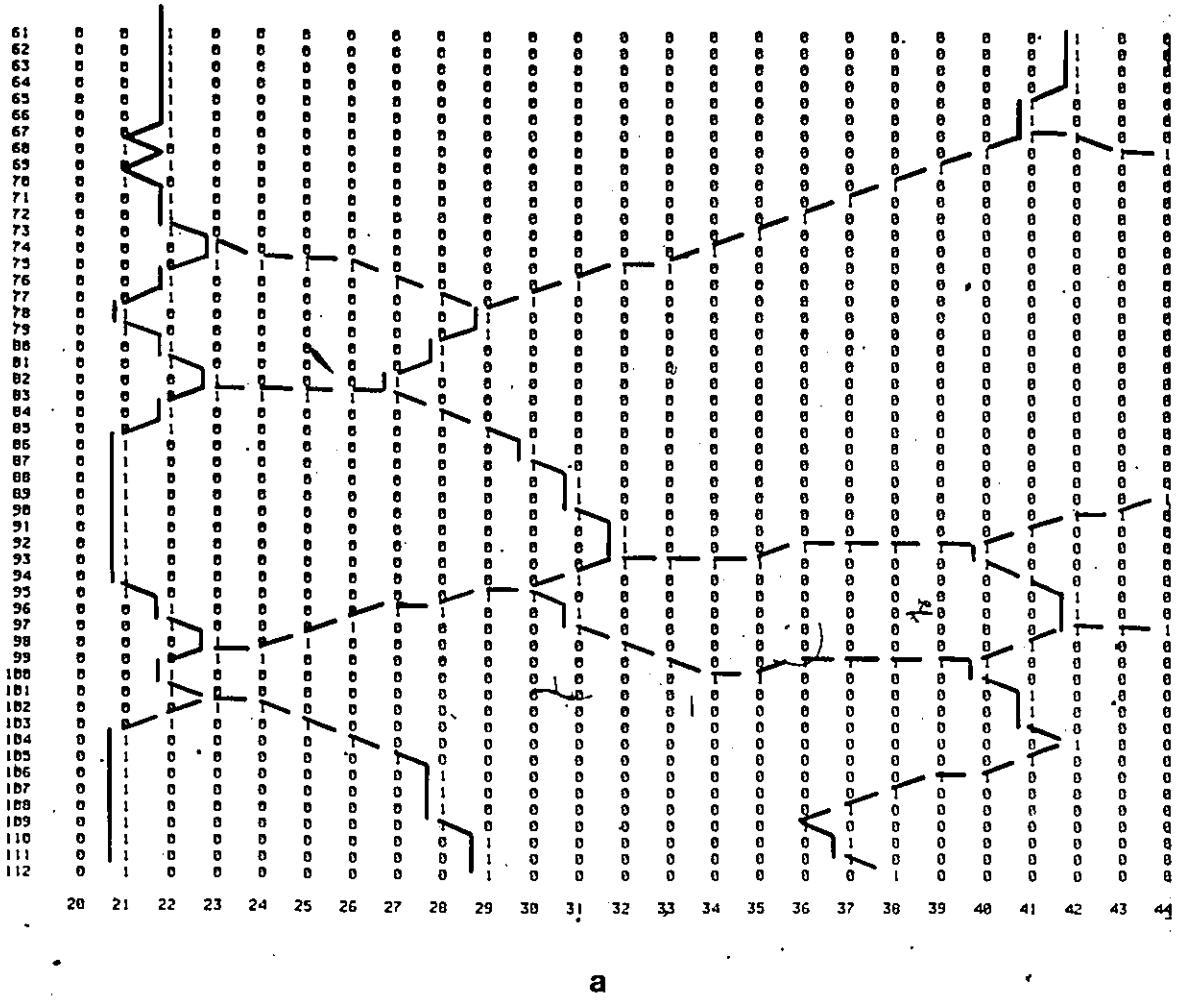

a

Figure 8.14: Further preprocessing of the binary image of boundaries in Figure 8.13. (a) portion of expanded binary image of boundaries; (b) component-labeled image: each pixel belonging to a separate grain profile (component) is assigned a unique serial number (label), this process is called component labeling; (c) phase-labeled image: each pixel belonging to the same grain type (phase) is assigned the same phase label.

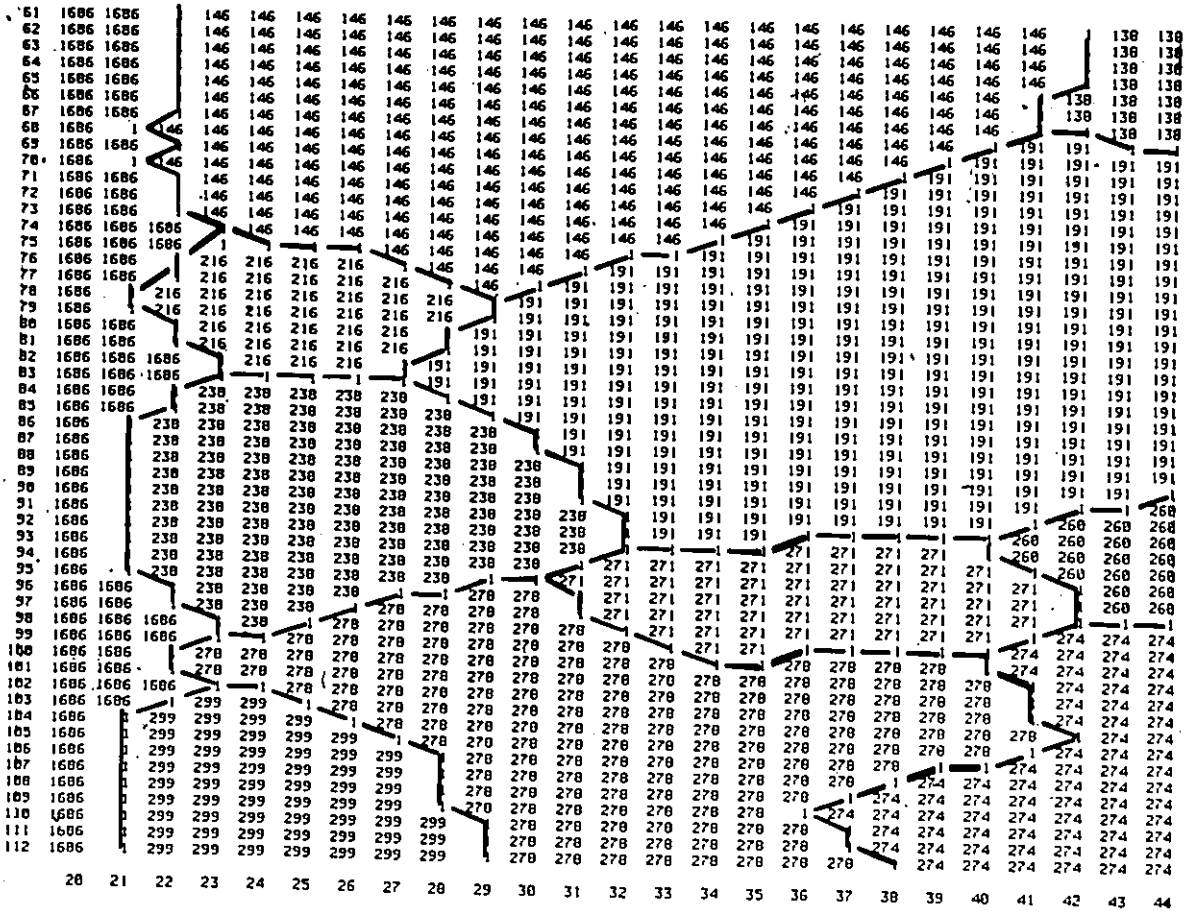

b

Figure 8.14: Continued.

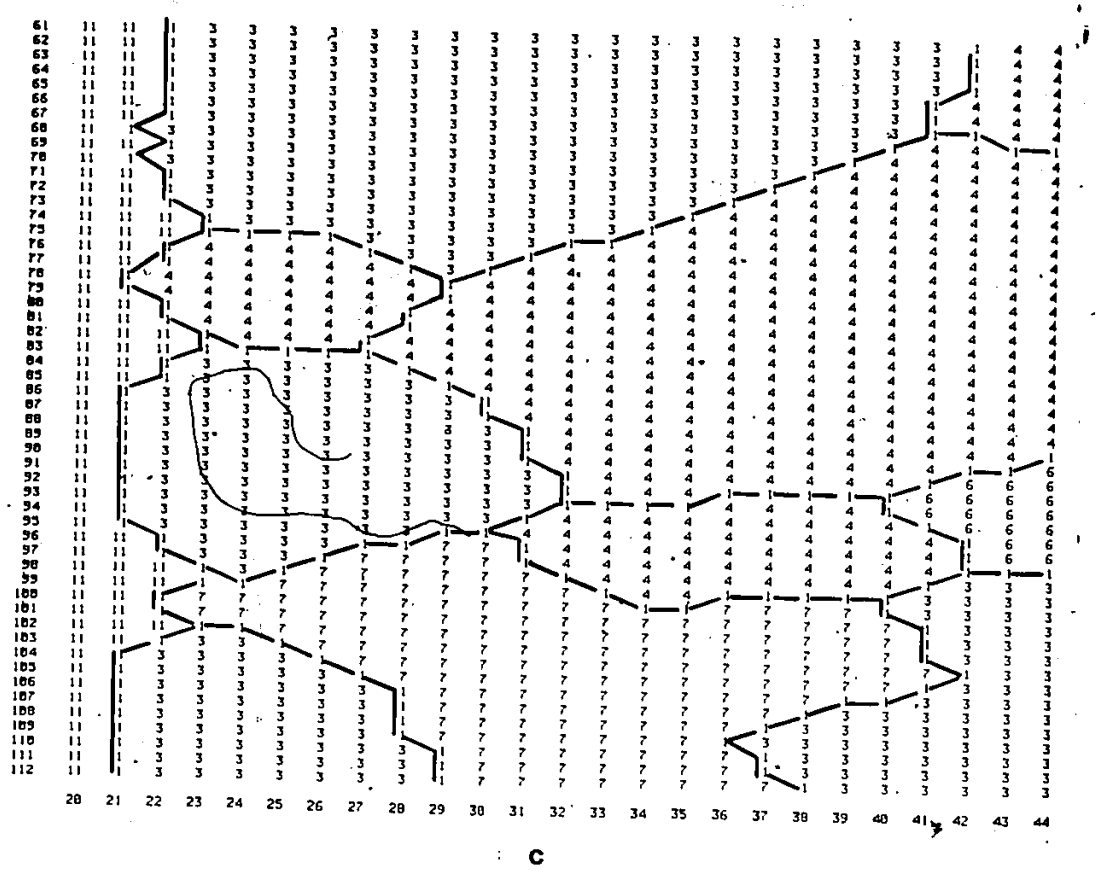

Figure 8.14: Concluded.

COLOURED PICTURES

Figure 8.15: Applicon color plot of the phase-labeled image of granulite digitized and preprocessed: each pixel is represented by a 2 x 2 array of colored dots. Red is scapolite, purple is pyroxene, green is apatite, blue is hornblende, dark blue is sphene, white is zircon, black are the grain boundary profiles, and light blue is the part of the image between the edges of the line drawing and the edges of the image (frame).

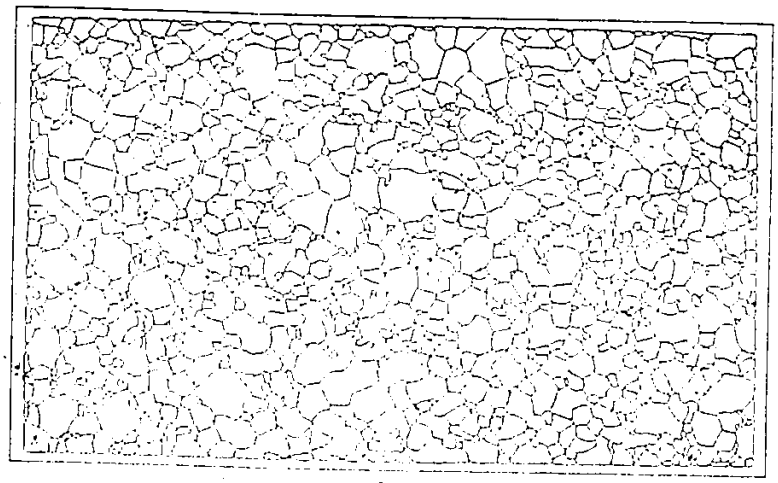

a

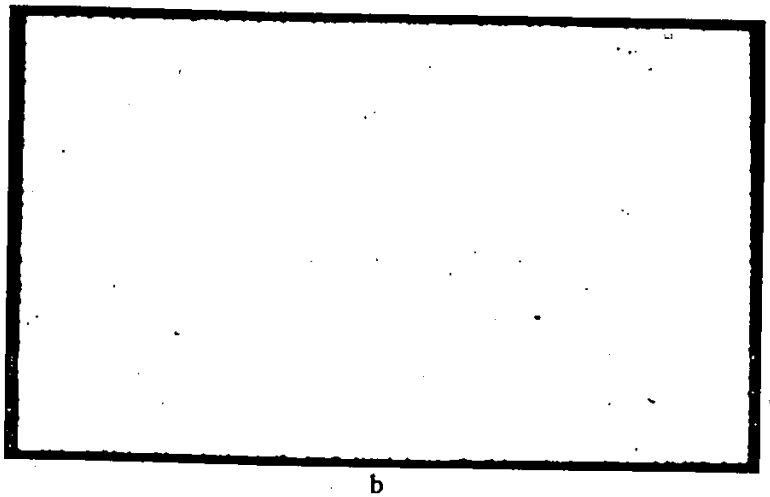

b

Figure 8.16: Extraction of binary images from the phase-labeled image of grain boundary profiles of granulite. The image dimension is 1000 pixels x 595 pixels (= 595000). (a) image of edited thinned boundaries: there are 38225 black pixels in this image; (b) image of the frame: there are 87100 black pixels in this image; (c) image of the pyroxene profiles: there are 278010 black pixels in this image; (d) image of the scapolite profiles: there are 204741 black pixels in this image; (e) image of the sphene profiles: there are 10909 black pixels in this image; (f) image of the hornblende profiles: there are 12360 black pixels in this image; (g) image of the apatite profiles: there are 1835 black pixels in this image; and (h) image of the zircon profiles: there are 45 black pixels in this image.

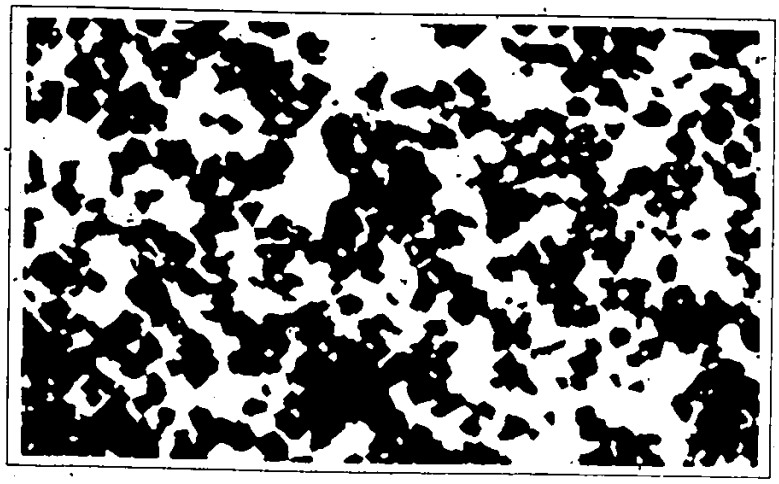

c

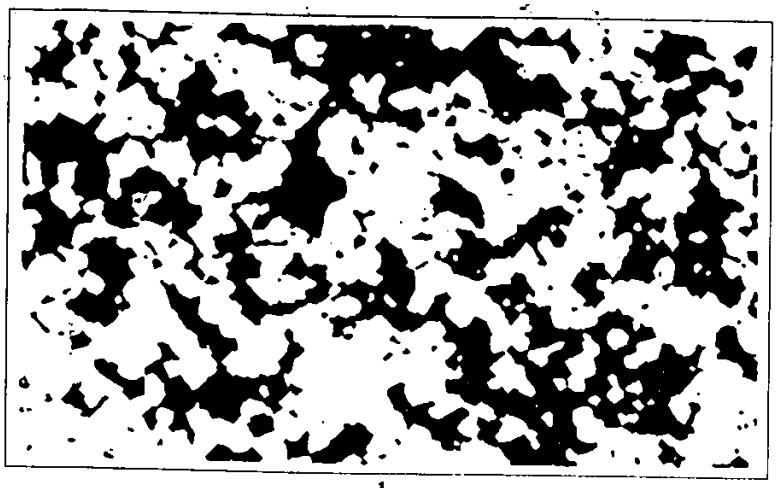

d

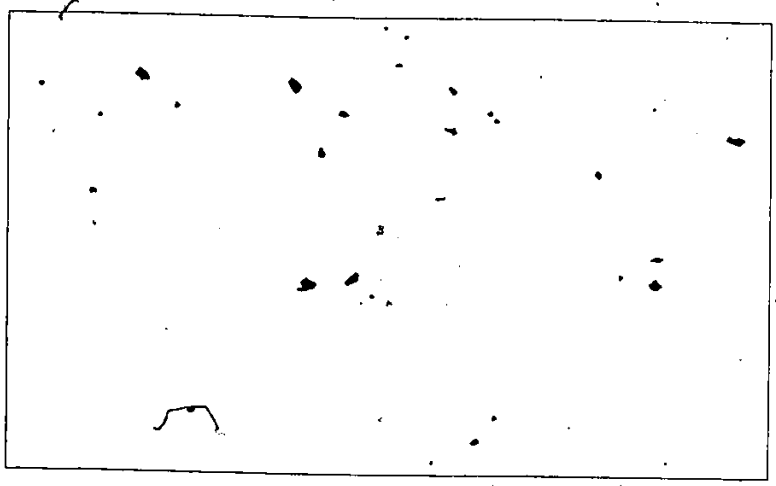

e

Figure 8.16: Continued.

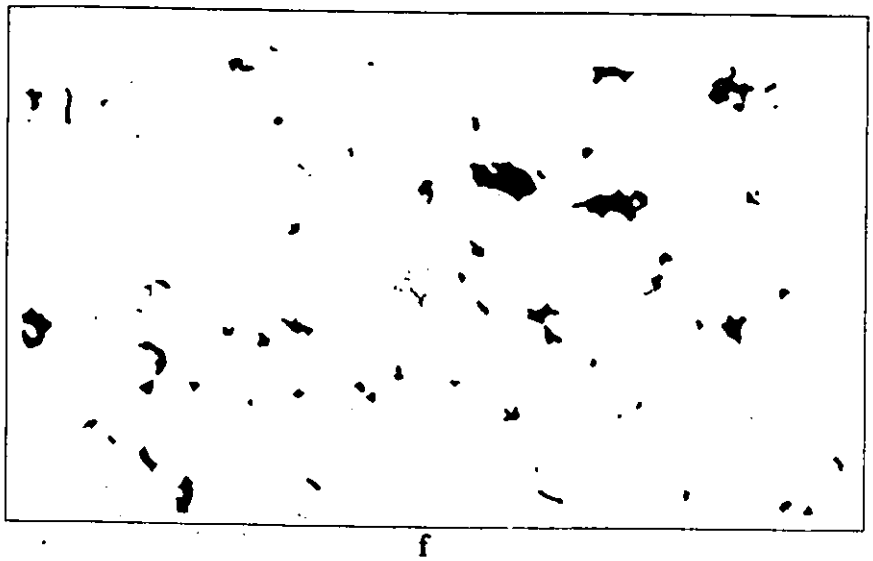

f

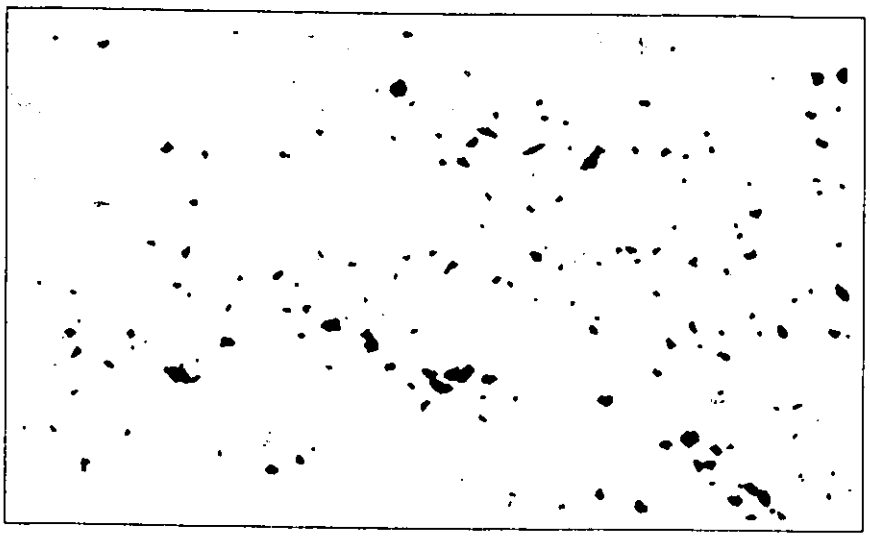

g

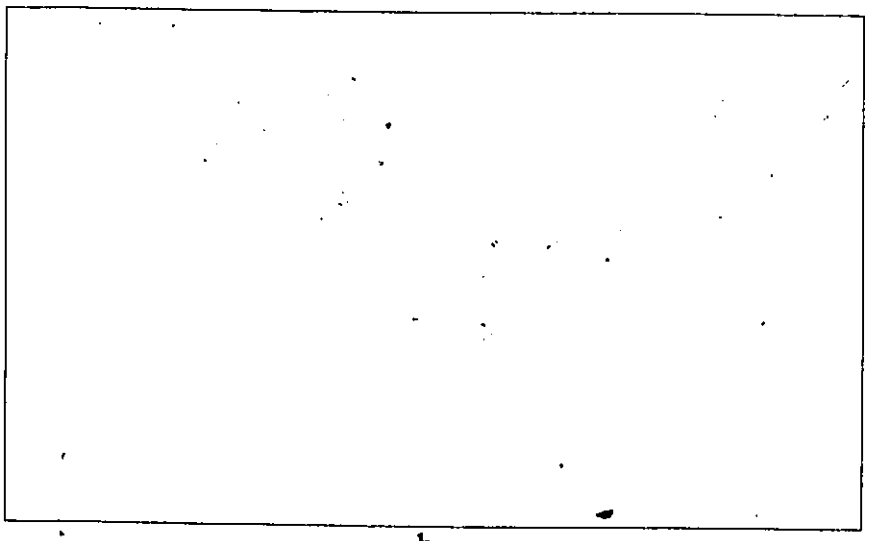

h

Figure 8.16: Concluded.

8.3 Some aspects of quantitative characterization of a thin section of a granulite

8.3.1 Introduction

As previously mentioned, the tracing of the profiles of approximately 1300 grains of crystals in a thin section of a granulite was obtained from Kretz (1969). He was the first to give particular attention to the statistical analysis of grain profiles for quantitatively relating their geometrical attributes to nucleation and crystallization processes which could be modeled for this rock. Kretz used several manual methods for obtaining the measurements from a complete drawing of a thin section (Kretz, 1969, fig. 1). The same measurements, and also many more measurements, can be made from the drawing, once this is in digital form, i.e. computer processable as in the case of the explicit image form shown in Figure 8.15.

Only some experiments are described here, particularly those which would be too cumbersome to perform manually. The experiments are for exemplifying the kind of studies which are possible with relative ease by programming and processing images on a small computer.

The applications described in this section deal with the following topics: (1) computation of the area and of the circumference (perimeter) of the grain profiles; (2) measurement of grain profile contacts and of their distribution; (3) determination of the orientation of grain and grain cluster profiles; and (4) computation of the geometrical covariance function of the fabric.

While these applications serve the purpose of explaining how to study a rock fabric in a systematic manner, they also provide some new unconventional geological tools for detecting the presence of and for describing the type of crystal shape or of crystal cluster anisotropy which causes gneissossity or foliation in a crystalline fabric.

8.3.2 Computation of the area and the circumference of grain profiles

In general, basic data which are needed about the geometrical characteristics of grain profiles from a thin section are the area and the perimeter length or circumference of all the grains belonging to each phase. A summary of data for the Grenville granulite is given in Table 8.1. There, because of the particular partitioning of the image data, separate areas are given for the frame (see

image in Figure 8.15a) and the boundary (see image in Figure 8.15b) and also of the boundary pixels in contact with the frame. Because the boundary itself is distinguished as a separate phase, one method of calculating the area proportion in percent of the crystalline phases, is to divide the number of pixels belonging to each phase by the sum of all the pixels belonging to a crystalline phase, which is 507900 pixels. The six percentages so computed in column 2 of Table 8.1, can be compared with the percentages , in column 3, obtained by Kretz (1969) for a portion of the draft used here for digitizing the image of the granulite. The numbers of crystals, crystal proportions, and average area per crystal for each phase are also given in the table, in columns 4 and 1, respectively. The latter data show that the pyroxene profiles have the largest grain size and are followed by scapolite, amphibole, apatite, sphene and zircon in decreasing order of mean grain size.

Figure 8.17: Partitioning of the grain profile boundary image of the granulite into images of perimeters of the individual phases. (a) image of phase boundaries with frame/boundary contact; (b) image of phase boundaries without frame/boundary contact; (c) to (h) images of the individual boundaries: (c) pyroxene, (d) scapolite, (e) sphene, (f) amphibole (hornblende), (g) apatite, and (h) zircon. The numbers of boundary pixels in these images and the boundary lengths are listed in Table 8.1.

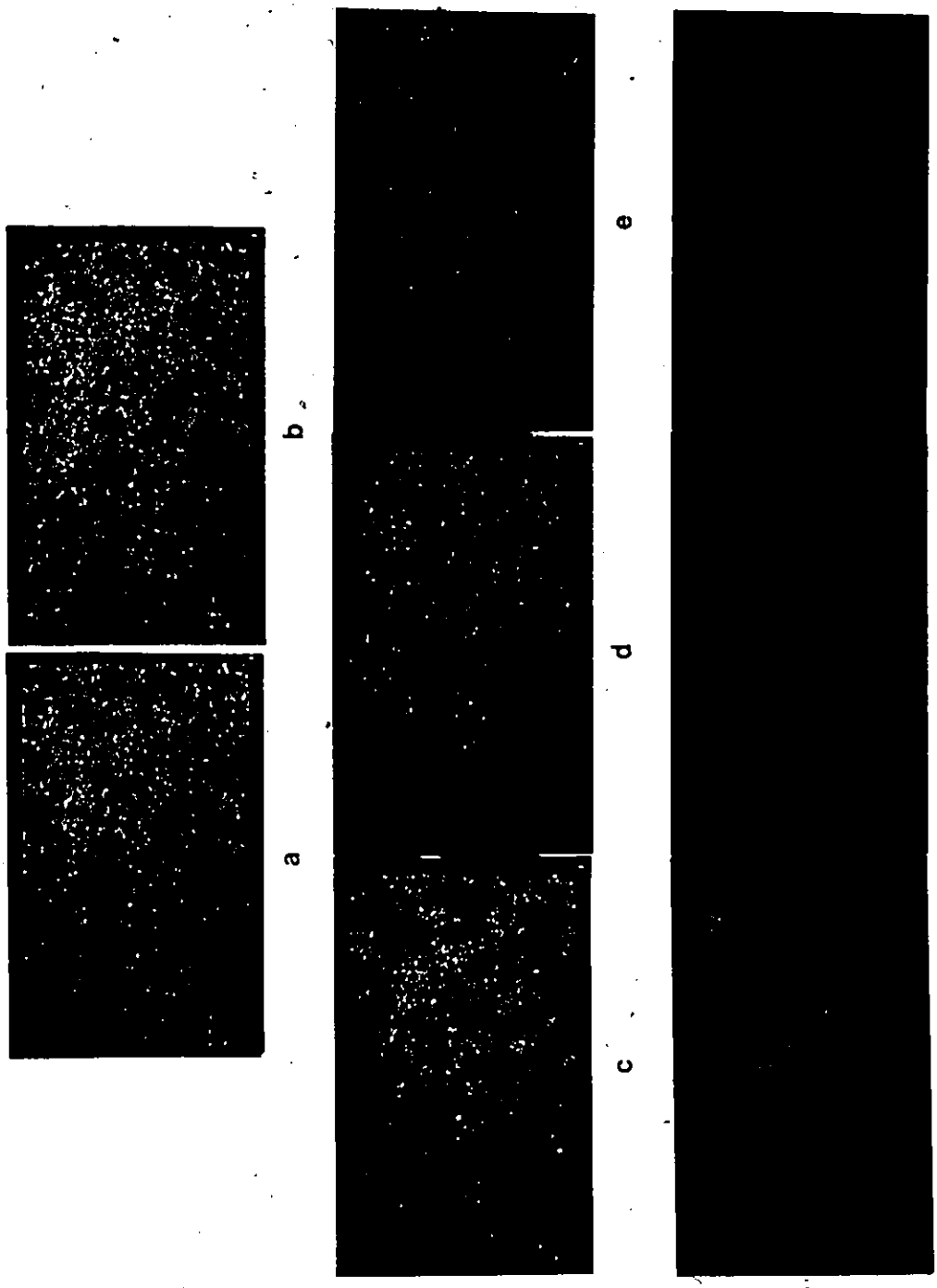

Figure 8.17: Concluded.

The total circumference of the grain profiles was computed as follows: (a) from the image of boundaries in Figure 8.17a, the pixels at the contact with the frame (shown in Figure 8.15a) have been "eliminated" by dilatating the frame image with a 3 x 3 black structuring element, and then computing the image in which the boundary pixels do not overlap with the dilatated frame image, as shown in Figure 8.17b; (b) the separate overlaps between the dilatated phases and the boundary image in Figure 8.17b, have produced the images of grain-profile boundaries shown in Figures 8.17c to 8.17h. The number of pixels belonging to each boundary is listed in column 5 of Table 8.1; (c) such boundary images, however, do not take into account the fact that the boundaries between grain profiles of the same phase have to be measured once for each of the adjacent grain profiles. The separate contacts between adjacent grain profiles of the same phase can be obtained, for example, by "closing" each phase (a dilatation followed by an erosion) and by computing the intersection or overlap between the closed image and the boundary image. Pyroxene-pyroxene boundary and scapolite-scapolite boundary are shown in Figures 8.18a and 8.18g, respectively. The number of pixels on the boundaries between the profiles of the same phase are also given, in brackets, in column 5 of Table 8.1; (d) the computations of the boundary lengths was accomplished by

cross-correlating each partial boundary image with the total boundary image in Figure 8.17b, for shifts in vertical and horizontal directions of one pixel in both senses. The values for shifts (-1,-1), (+1,-1), (+1,+1) and (-1,+1) were summed, divided by 2 and the result multiplied by the square root of 2. This value, the total length of the boundary in directions 45° and 135°, was added to the total length of boundary in directions 90° and 180°. This was computed as the sum of the values for shifts (0,-1), (+1,0), (0,+1) and (-1,0) divided by $\sqrt{2}$. This procedure was also used in Chapter 6. The sums of the lengths of boundary between grain profiles of all phases and those of of grains of the same phase, is the final length entered in Table 8.1 under the header circumference in column 6.

TABLE 8.1

Summary of quantitative characterization data of the grain profiles in the granulite

	1	2	3	4	5	6	7(1)	
Phases	No. of pixels (average no. per crystal)	Area % over 507900 pixels	Area % from Kretz (1969) *	No. of crystals (proportion)	No. of pixels on boundaries (between crystals of same phase)	Circumference	Complexity index, C.I. a (b)	c (d)
Frame	45828							
Frame/boundary contact	3047							
Boundary	38225							
Pyroxene	278010 (592)	54.74	50.31	470 (.363)	28579 (8136)	47495	.15 (.17)	.14 (.22)
Scapolite	204741 (357)	40.31	41.89	574 (.444)	26627 (7123)	44041	.18 (.17)	.17 (.19)
Sphene	10909 (67)	2.15	3.38	164 (.127)	4296 (99)	6012	.39 (.54)	.37 (.43)
Amphibole	12360 (203)	2.43	4.05	61 (.047)	3107 (114)	4202	.27 (.33)	.22 (.25)
Apatite	1835 (83)	0.36	0.34	22 (.017)	668 (---)	912	.36 (.50)	.33 (.39)
Zircon	45 (15)	0.01	0.03	3 (.002)	44 (--)	64	.72 (1.4)	.50 (.92)
Crystal phases only	507900	100.00	100.00	1294 (1.000)	63321 (15472)	102726		
Total image	595000							

a: C.I. with boundary pixels as part of crystals
b: C.I. without boundary pixels as part of crystals
c: C.I. for circle of same average area computed as in (a)
d: C.I. for circle of same average area computed as in (b)

(1) Note on C.I. computations. For example, for pyroxene the complexity index computations in column 7 are as follows: (a) 47495 / (28579 + 8136 + 278010) = .15; (b) 47495 / 278010 = .17; (c) for A (area of circle) = r^2, and C (perimeter of circle) = 2r, C / A = 2 / r = C.I.. For A of 278010 / 470 = 592, r = 13.73, C = 129.38, and C / A = 129.38 / 592 = .2185 or .22; (d) for A of (28579 + 8136 + 278010) / 470 = 670, r = 14.60, C = 91.76, and C / A = .1370 or .14.

* For a portion of the study area.

A geometrical measure which relates the circumferences and the areas of the grain profiles for each phase is the "complexity index" C.I. (Underwood, 1970, p. 228-229). It should reflect the jaggedness of the perimeter per area of the particles or grain profiles. This is simply computed as the ratio between the total circumference and the total area of the grain profiles for each phase (see column 7 in Table 8.1). Because of the particular structure of the data in this application, binary images in which the boundary is a separate phase, such index can be affected by the resolution so that the phases with the smaller grains tend to have a relatively larger circumference. This is the case for zircon in column 7 of Table 8.1. For this reason, two different computations for the complexity index have been entered in the table: one in which the boundary pixels have been summed to the areas of the grain profiles, and one in which only the areas of the grain profiles were used. In the table we can see that in general the larger grains have smaller C.I.'s. In column 7 the C.I.'s computed for circles of the same average areas (no. of pixels per crystal, listed in column 1) are also shown. According to Underwood (1970) the complexity index can be computed without assumption on grain size.

TABLE 8.2

(a) distribution of boundary pixels, n, and boundary lengths, l (in brackets), between all pairs of phases of the granulite. Letters P to Z indicate the phases pyroxene to zircon. (b) the distribution is recomputed for the compressed 3 x 3 arrays of boundary data (the less frequent boundaries have been grouped under O, other phases), n and l, with the observed values above, and the expected values below (in brackets). (c) the transition matrices are computed, P(n) and P(l), respectively, and compared with the transition matrix P(k) obtained by Kretz (1969). The fixed vectors (n), (l) and (k) represent the expected transition matrix based on the supposition that the crystals are randomly distributed. They represent the proportions of the sums for n and l in (b) above. The elements of those vectors are multiplied by the sums in (b) in order to compute the expected values in terms of boundary pixels and boundary lengths distributions. Additional explanation is in text.

TABLE 8.2

Concluded

a

	P	S	T	H	A	Z	
P	8136 n (10571) 1						
S	17231 (22525)	7123 (9387)					
T	2281 (3174)	2099 (2944)	99 (136)				
H	2072 (2694)	986 (1351)	125 (185)	114 (156)			
A	300 (423)	365 (510)	34 (49)	20 (28)	- (-)		
Z	25 (38)	20 (34)	-- (--)	-- (--)	6 (9)	- (-)	
Total	30045 (34425)	27813 (36751)	9627 (9488)	3317 (4414)	725 (1019)	51 (91)	41025 (54214)

b

n	P	S	O	Sum		1	P	S	O	Sum
P	8136 (13610)	17231 (12589)	4678 (3846)	30045		P	10571 (17781)	22525 (16401)	6329 (5248)	39425
S	17231 (12599)	7123 (11654)	3559 (3560)	27813		S	22525 (16575)	9387 (15288)	4839 (4888)	36751
O	4678 (3866)	3459 (3576)	398 (1092)	8535		O	6329 (5291)	4839 (4880)	563 (1560)	11731
Sum	30045	27813	8535	66393		Sum	39925	36751	11731	88407

c

P(n) =	(.271 .573 .156) (.620 .256 .124) (.548 .405 .047)	P(1) =	(.268 .571 .161) (.613 .255 .132) (.540 .412 .048)
P(k) =	(.389 .466 .145) (.536 .384 .080) (.613 .290 .097)		
π(n) =	(.453 .419 .128)	π(1) =	(.451 .416 .133)
π(k) =	(.474 .412 .113)		

8.3.3 Measurement of grain- profile contacts and their distribution

Binary images of the separate grain-profile contacts can be obtained for each phase, by computing the intersections between all possible pairs of the boundary images shown in Figure 8.17c to 8.17h. The extraction of the contacts between grain profiles belonging to the same phase has been discussed in the previous section. Nine of the most revealing partitioned boundary images are shown in Figure 8.18. Intraphase boundaries, Figures 8.18a and 8.18g, are characterized by the presence of junctions between segments of boundary. These occur wherever three profiles of grains of the same phase are in contact. The other types of boundary images are typically of "meander" like appearence, with different degrees of dispersion or clustering in relation to those of the grain profiles. Of particular interest is the boundary between the two main phases pyroxene-scapolite, shown in Figure 8.18b, which strongly characterizes the entire fabric.

As previously mentioned, the length of each extracted boundary image can be computed, and a table of boundary length distribution is constructed, as shown in Table 8.2. In the table, in (a), both the number n of pixels on the

boundary, and the boundary length l are enterd for comparison. From both kinds of data, a boundary length distribution for a compressed array of boundaries (contacts) pyroxene, P, scapolite, S, and other phases, O, are easily constructed and compared with the expected values for boundary distributions for the supposition that the crystals are randomly distributed, which are shown in brackets in (b). From these arrays, two different transition matrices are computed, P(n) and P(l), respectively, in which the sums of each row equal unity. The transition matrices represent the probability that a grain belonging to a phase is in contact with a grain of the same or of any other different phase. As explained by Kretz (1969, eq. 4) we can obtain the transition matrix based on the supposition of random distribution of crystals by the following equation which is valid if events pyroxene, P, and scapolite, S, are independent:

$$p(P/S) = p(P) \quad \text{and} \quad p(P/P) = p(P) \qquad (8.0),$$

where p(P/S) is the probability of event pyroxene, given scapolite, and p(P) is the probability of event pyroxene alone. The two matrices, P(n) and P(l) in Table 8.2, are almost identical, which suggests that the computation of boundary length is not required to compute the transition matrices. In the table these matrices can be compared with

the transition matrix, P(k), obtained by Kretz (1969), using Equation 8.0, from a portion of the draft for the same rock. Given the similarity between the three matrices, the same statistical tests and the same conclusions drawn by Kretz, i. e., that: "fewer P-P and S-S transitions and more P-S were found than expected, owing possibly to departure from randomness in the direction of a more regular distribution for pyroxene and scapolite." (1969, p.61). A chi square test to determine if the differences between expected and observed values are significant makes the model of randomness in the distribution of the two crystals just acceptable at the 95 percent level of significance.

Figure 8.18: Nine binary images of separate grain-profile contacts in the granulite. (a) pyroxene-pyroxene, (b) pyroxene-scapolite, (c) pyroxene-sphene, (d) pyroxene-amphibole, (e) pyroxene-apatite, (f) pyroxene-zircon, (g) scapolite-scapolite, (h) scapolite-sphene, and (i) scapolite-amphibole.

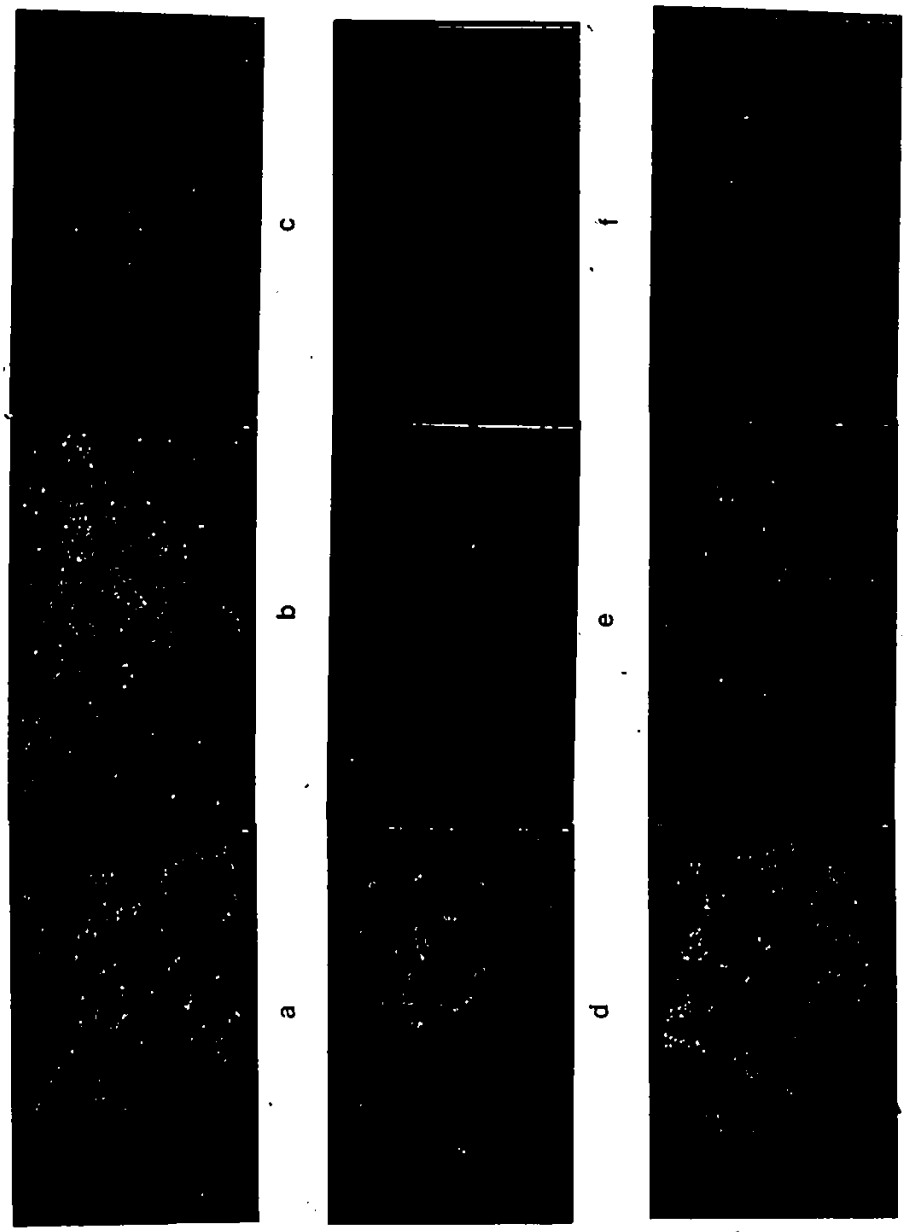

Figure 8.18: Concluded.

8.3.4 Determination of the orientation of grain and of grain-cluster profiles

A granulite is a high grade metamorphic rock consisting of even sized interlocking grains with a very weak preferred orientation. The orientation of the fabric can be expressed either as an anisotropic distribution of grains of both major and minor constituents or as a shape anisotropy of the grains and therefore of the grain profiles. In crystalline fabrics all possible interrelationships of these two types of anisoptropies can be observed in nature for the same texture. The latter characteristic is measured in this section.

A method of measuring shape anisotropy consists in computing the rose diagram of the boundaries of grain profiles for each phase. A simple but laborious way to study the rose diagram of the boundaries is to approximate them by successive straight line segments that are sufficiently short, and to plot the histogram of the combined length of all line segments pointing in directions bounded by class limits a few degrees apart. An alternative method to determine the preferred orientation consists of first obtaining measurements for narrower class intervals, one or two degrees, and to construct a moving average for wider

classes in order to reduce the random fluctuations that generally arise when the classes are too narrow.

Recently, a computer program called RODIA (for ROse DIAgram) has been developed by Agterberg (1979), also used by Agterberg and Fabbri (1978b) and by Agterberg et al (1980), which constructs a smoothed histogram for the contact between the two phases ("black" and "white) in a binary image. The input for RODIA is the so-called geometrical covariance of a binary image, which can be computed by GIAPP.

A number of experiments have been performed in order to produce the rose diagram of the following images: (a) the boundaries of the individual grains of pyroxene and of scapolite profiles, (b) the boundaries of the clusters of grains of the two phases, (c) the boundaries of all the individual grains in the granulite, and (d) the "skeletons" of the pyroxene grain profiles.

Some preprocessing was required to produce the binary images input for the computation of the geometrical covariance in two dimensions. For studying the individual grains, the image of octagonally eroded pyroxene grains and scapolite grains, and of all the grains in the granulite (of sizes greater than that of the octagon used for the erosion) were computed. They are shown in Figures 8.19a, 8.19b, and 8.19c, respectively. The 3 x 3 square dilatation of the

scapolite and pyroxene images was also computed for studying the grain-profile clusters. The image of the dilatated pyroxenes is shown in Figure 8.19d. A rectangular binary mask was produced, of dimension 521 x 901 black pixels, at least 5 pixels away from the edges of the frame of the image. The mask is contained in a 1000 pixels x 595 pixels binary image which is shown in Figure 8.19e. The intersection of this "mask image" and the images to be analyzed, was computed for the covariance measurements. In Figure 8.19f, the image is shown of the intersection between such mask and the image of the octagonally eroded grains in the granulite (i.e., between the images in Figure 8.19c and in Figure 8.19e). The geometrical covariance was computed by shifting the masked images (like the one in Figure 8.19f) for 5 pixels, one pixel at a time, to the right, to the left and downward, and then computing the intersections between the shifted image and the unshifted image (like the one in Figure 8.19c). The resulting array of intersections from the image in Figure 8.19f, is shown in Figure 8.19g. It consists of 66 values, 61 of which are used for the computations. Similar arrays were obtained for the other experiments previously mentioned.

Figure 8.19: Processing of binary images for computing the orientation (slope histogram) of the boundaries of grain profiles of the individual phases. (a) image of octagonally eroded pyroxene grains; (b) image of octagonally eroded scapolite grains; (c) image of all grains in the granulite after one octagonal erosion; (d) image of pyroxene grains after one square dilatation; (e) 1000 pixels x 595 pixels image containing a 901 x 521 white pixels mask; (f) image of the intersection between the image in (e) and the image in (c). This image has been shifted and intersected with the image in (c) in order to obtain the geometrical covariance array in (g) used for computing the slope histogram shown in Figure 8.20e.

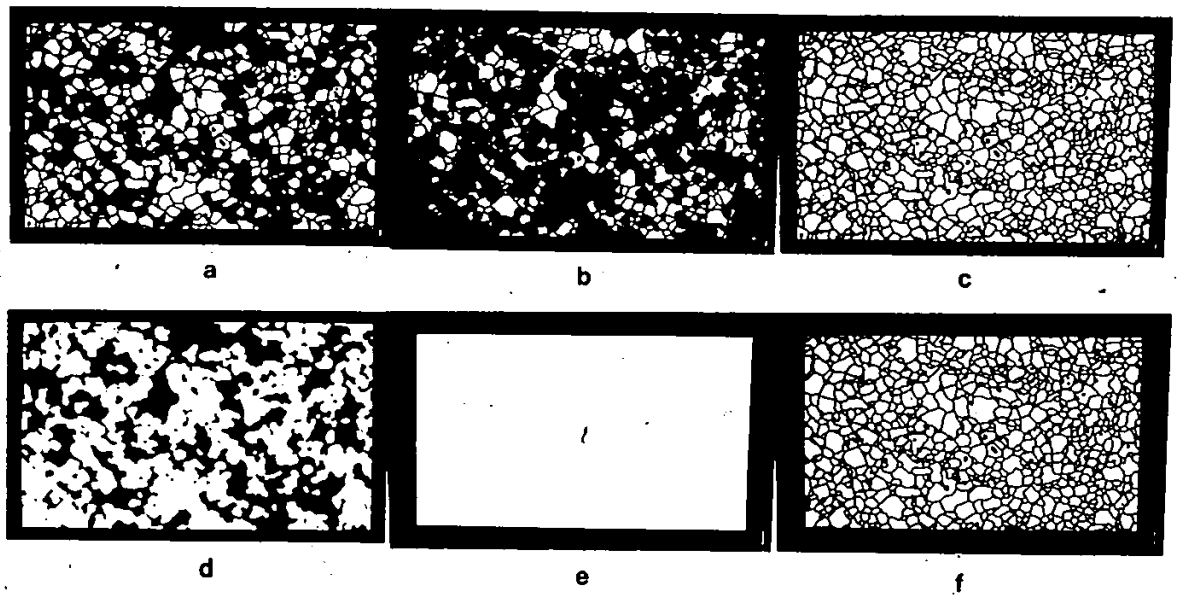

	-5	-4	-3	-2	-1	0	1	2	3	4	5
0	128538.	138318.	148613.	159428.	170756.	182670.	170754.	159424.	148625.	138337.	128582.
-1	127587.	136838.	146501.	156222.	165241.	169456.	165498.	156323.	146552.	136828.	127419.
-2	124359.	132775.	141163.	148998.	154420.	156956.	154829.	149403.	141437.	132943.	124394.
-3	119611.	126957.	133911.	139449.	143417.	145167.	143844.	140064.	134448.	127245.	119736.
-4	113773.	120002.	125362.	129737.	132771.	134066.	133153.	130422.	126075.	120528.	114061.
-5	107239.	112297.	116697.	120172.	122609.	123597.	122968.	120894.	117497.	112984.	107720.
	-5	-4	-3	-2	-1	0	1	2	3	4	5

g

Figure 8.19: Concluded

The rose diagrams for the experiments performed are shown in Figure 8.20, in the form of histograms of directions. Each histogram should be interpreted as follows. The frequency is plotted vertically. The corresponding direction is plotted for clockwise rotation in the horizontal direction starting from 0 for the horizontal left-right direction. Consequently 90 is for the top-to-bottom vertical direction, and 180 is for the horizontal right-left direction. All the orientation patterns in Figure 8.20 (a to g) show two maxima for directions 45° and 130°. The patterns for square dilatated pyroxenes, PYSD1 is in Figure 8.20a; that for octagonally eroded pyroxenes, PYOE1 is in Figure 8.20b. They both show two maxima which are stronger than the corresponding patterns for the scapolite grains shown in Figures 8.20c and 8.20d. The strongest orientation pattern was obtained for the octagonally eroded grains of the entire granulite, AXOE1 in Figure 8.20e for one erosion, and AXOE2 in Figure 8.20f for two erosions. The orientation pattern of the binary image of a circle is shown in Figure 8.20h after appropriate scaling, for comparison. In this diagram the variation of the frequencies are restricted to a narrow interval, very small in comparison to the estimated perimeter of the circle itself. The rose diagram computations in the program RODIA are based on the estimation of the total particle perimeter from the measurement of the

"intercepts" of the particles in all directions. The intercept is a measure of particle profile elongation in a particular direction, and it can be easily computed from the geometrical covariance values for small shifts (e.g. 4 to 10 pixels in length in the program). Except for Figure 8.20h, the rosé diagram for the circle, all diagrams in Figure 8.20 have been similarly scaled between the values of 0 and 1000. Within this range fall all the estimated perimeters in the various experiments.

Figure 8.20e Slope histograms or rose diagrams computed for the pyroxene and scapolite grain-profile images. On vertical axes frequencies (0 to 1000) are plotted versus angles (0° to 180°) on horizontal axes: 0° is for horizontal left to right direction, 90° is for vertical top to bottom direction, and 180° is for horizontal right to left direction. (a) rose diagram for pyroxene after one square dilatation; (b) for pyroxene after one octagonal erosion; (c) for scapolite after one square dilatation; (d) for scapolite after one octagonal erosion; (e) for all crystal profiles after one octagonal erosion and (f) after two octagonal erosions; (g) for the pyroxene "skeletons" complemented after two octagonal dilatations; and (h) for a circular shaped profile (frequencies between 0 and 10).

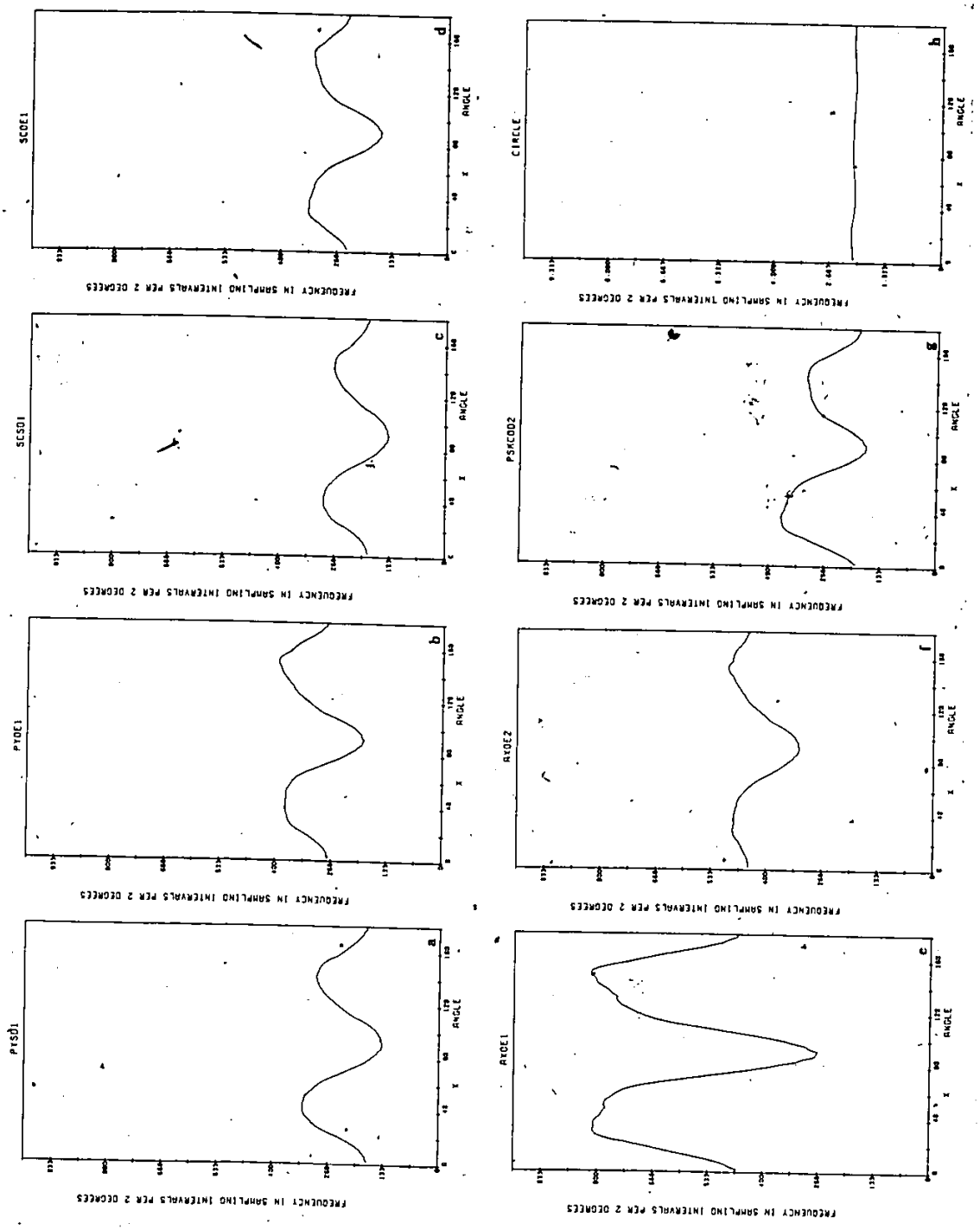

Figure 8.20: Concluded.

The orientation diagram for the "skeletons" of pyroxene grain profiles, which also shows two peaks of different magnitudes in the same directions, was obtained from images which were preprocessed as follws. The operation of square "closing", a dilatation followed by an erosion by a 3 x 3 black pixels structuring element, was computed for the image of pyroxene grain profiles, shown in Figure 8.21a. After expansion of the "closed" binary image, a line thinning algorithm, the same one used for the image of the digitized boundaries of the grains described in Section 8.2, was applied to the image. The line thinning process is an iterative procedure, which computes the "backbones" of the grain clusters. Figure 8.21b shows a partly thinned binary image after 10 thinning iterations. The pyroxene profile pixels eliminated (changed from black to white) during the first 10 iterations are shown in Figure 8.21c, as white on black. The binary image after 20 iterations is shown in Figure 8.21d, and the completely thinned image ("skeletonized" image) after 41 iterations is shown in Figure 8.21e. From this image the tendency can be seen for the profile skeletons to produce strings with a preferential orientation at 45°, but also at 135°. In Figure 8.21f, the skeletons are compared (union) with the image of pyroxene boundaries, where it can be seen that the skeletons represent the pixels at the maximum distances from the profile

boundaries. Figure 8.21g, shows the image of the skeletons of the pyroxene clusters, after two consecutive octagonal dilatations. Figure 8.21h shows the complement of the latter. Figure 8.21i is the intersection between the complemented doubly dilatated cluster skeletons and the binary mask in Figure 8.19e. The last two images have been used to construct the geometrical covariance array input to RODIA for the rose diagram shown in Figure 8.20g, PSKCOD2, the orientation of the boundary of the skeleton image.

All the rose diagrams in Figure 8.20 reflect the anisotropy of the granulite texture as orientation of the grain profile boundaries. This orientation pattern can be explained as follows. The pyroxene grains form chains of profiles in the 45° direction, where the contacts between adjacent pyroxene profiles are mostly oriented perpendicularly to that direction (i.e. in the 135° direction). Very likely the 45° direction corresponds to a lithologic layering and to a faint gneissossity. Such anisotropy is also measured for the scapolite grains, however it is less visible. While our eyes cannot detect the anisotropy for the entire granulite fabric, the overall pattern of grain boundary anisotropy is the strongest.

Figure 8.21: Experiments for computing the binary images of the "skeletons" of pyroxene profiles by line thinning, and for deriving the skeletons orientation pattern. (a) binary image of the pyroxene profiles after one square closing transformation (a dilatation followed by an erosion); (b) the image in (a) after 10 thinning iterations; (c) image of the pixels which changed value after the 10th thinning iteration which produced the image in (b); (d) the image in (a) after 20 thinning iterations; (e) the completely thinned "skeletonized" image in (a) after 41 thinning iterations; (f) the union of the skeleton image in (e) with the image of pyroxene boundaries; (g) the image of pyroxene skeletons after two octagonal dilatations; (h) the complement of the image of dilatated skeletons in (g); (i) image of the intersection between the image in (h) and the mask shown in Figure 8.19e, for computing the slope histogram shown in Figure 8.20g.

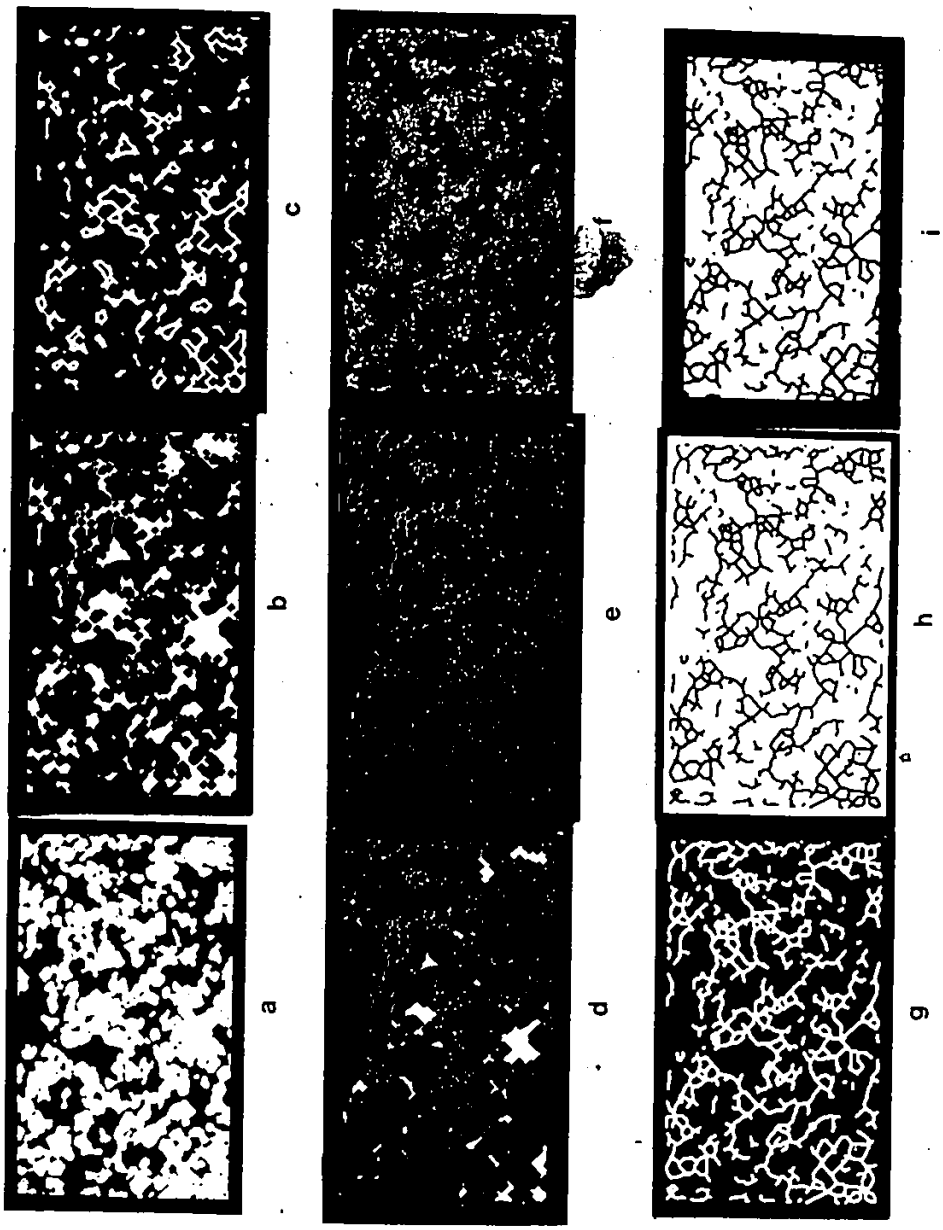

Figure 8.21: Concluded.

A possible reason why the "Markovity" property in this fabric was observed by Whitten et al (1975), and also why various randomness tests gave negative results in the study by Kretz (1969), is the anisotropic pattern of the grain profile boundaries. The possibility should also be considered that such property of the grain-profile boundaries occurs in "ideal granites" (Vistelius and co-workers, 1966 to 1972). This consideration would justify a rather interesting study project in its own right, on the previously studied thin sections of such ideal granites.

8.3.5 Computation of the geometrical covariance of grain profiles of the granulite fabric in different directions

This section deals with the following question: is there in the images of the two major components of the granulite, pyroxene and scapolite profiles, a preferential distribution of the areas of the profiles in the different directions ?. This question can be answered by computing the geometrical covariance for distances of pixels corresponding to several hundreds of individual shifts.

Figure 8.22: Preprocessing for computing the geometrical covariance of grain profiles in the granulite. (a) image of pyroxene profiles; (b) image of scapolite profiles; (c) upper half mask (1000 pixels x 295 pixels); (d) left half mask (500 pixels x 595 pixels); (e) intersection between the image of pyroxene profiles in (a) and the image in (c); (f) intersection between the image in (a) and the image in (d); (g) intersection between the image in (a) and the non-overlapping part of the images in (c) and (d); (h) intersection between the image in (a) and the overlapping part of the images in (c) and (d). Similar intersections were computed with the image of scapolite profiles in (b).

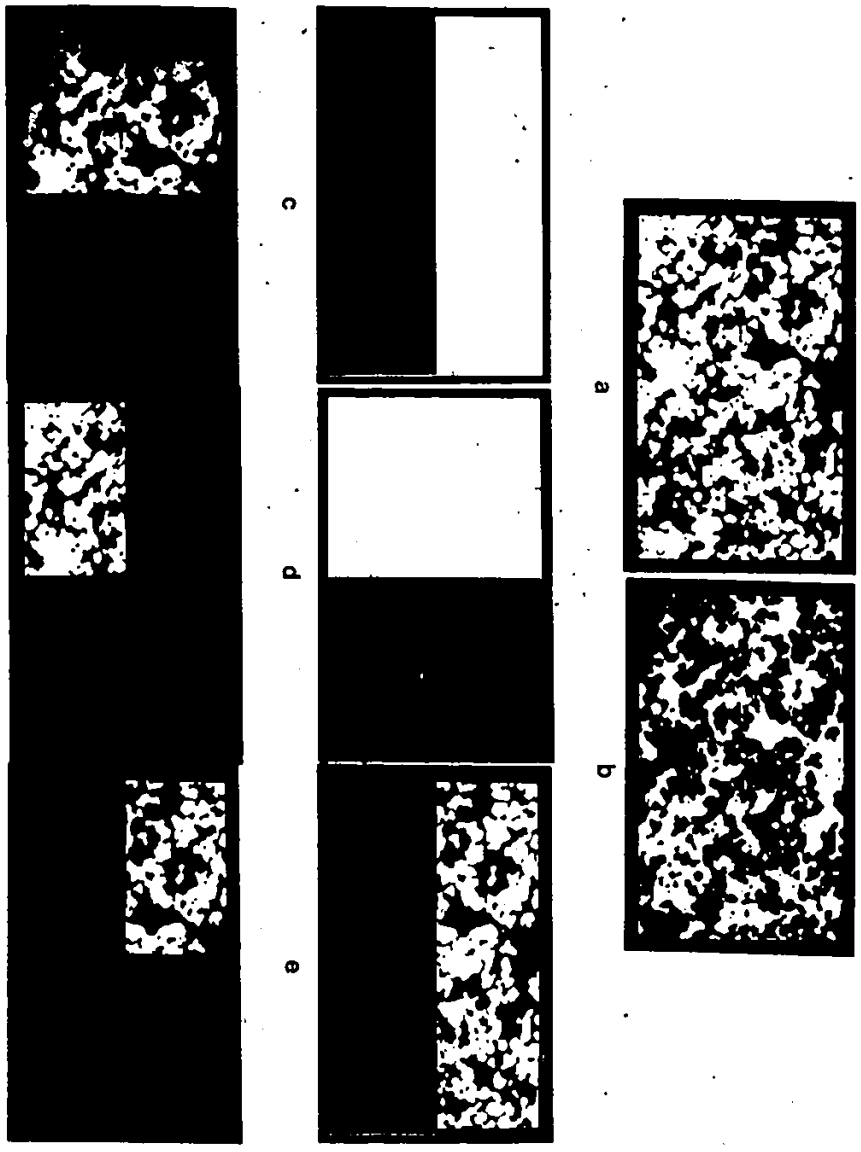

Figure 8.22: Concluded.

The preprocessing of the binary images of the two phases, shown in Figures 8.22a and 8.22b, before the computation of the covariance, is as follows. Masks for the upper (Figure 8.22c) and lower half of the images, and the left (Figure 8.22d) and right halves were computed, as well as for the upper left and lower left quarters. The intersections of the pyroxene image with some of these binary masks are shown in Figures 8.22e to 8.22h. Each masked image was intersected with the entire original image after being shifted in the directions in which it could travel without its edges reaching the edge of the latter. Linear geometrical autocovariances for 0°, 90°, and 180° were obtained for both pyroxene and scapolite. They are shown in Figures 8.23 and 8.24. For the pyroxene, also the covariances for 45° and for 135° were computed, as shown in Figure 8.23e and 8.23f. The diagrams of Figures 8.23 and 8.24, are plots of the areas of overlap (intersection) relatively to the initial area for shift equal to 0 in the two directions, which has the value of 1, and is plotted on the vertical axis. On the horizontal axis the shifts are plotted in pixels. It can be seen that the area decreases stabilize within shifts of sixty pixels. For this reason the two-dimensional geometrical covariance arrays shown in Figure 8.25 were obtained for unit shifts of five pixels between -60 and +60 pixels in all directions.

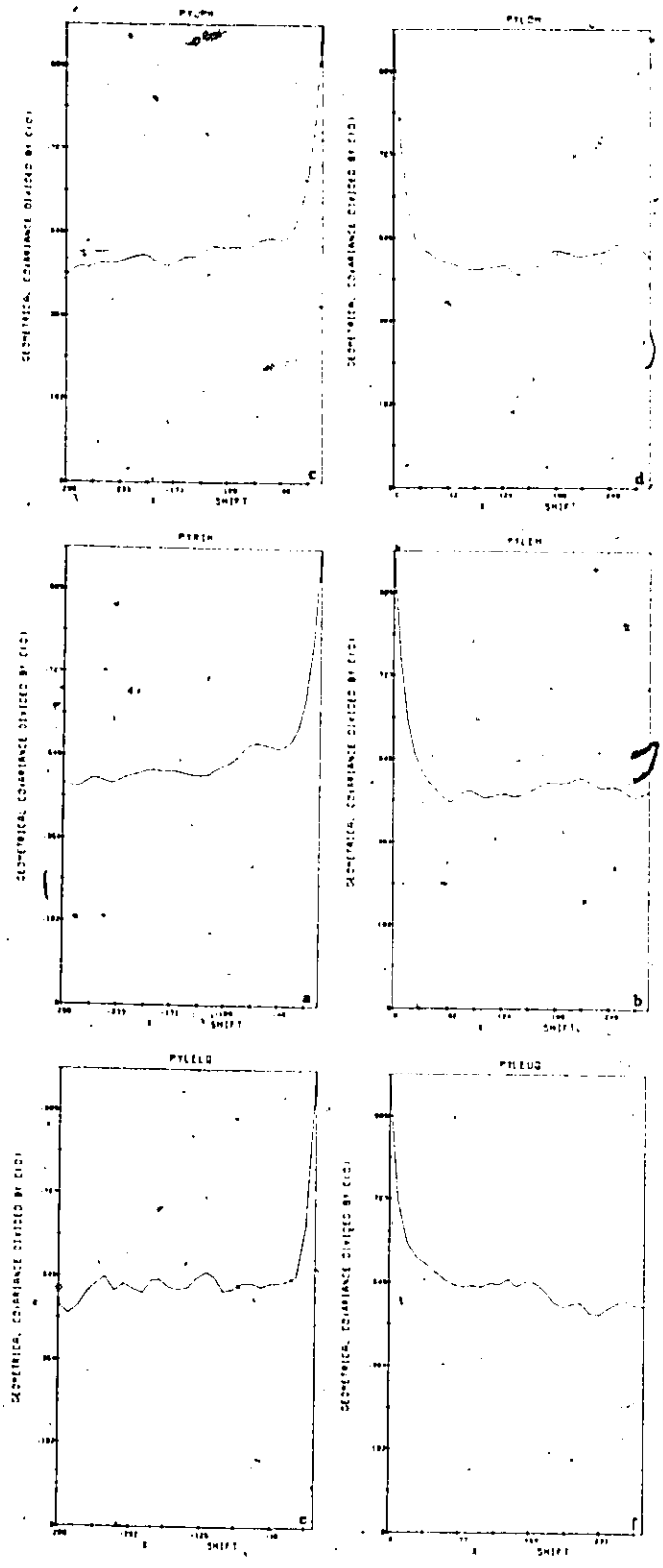

Figure 8.23: Linear geometrical covariances for the pyroxene profiles of the granulite computed in different directions. (a) horizontal direction, right to left; (b) horizontal direction left to right; (c) vertical direction top to bottom; (d) vertical direction bottom to top; (e) 135° direction bottom to top; (f) 45° direction top to bottom.

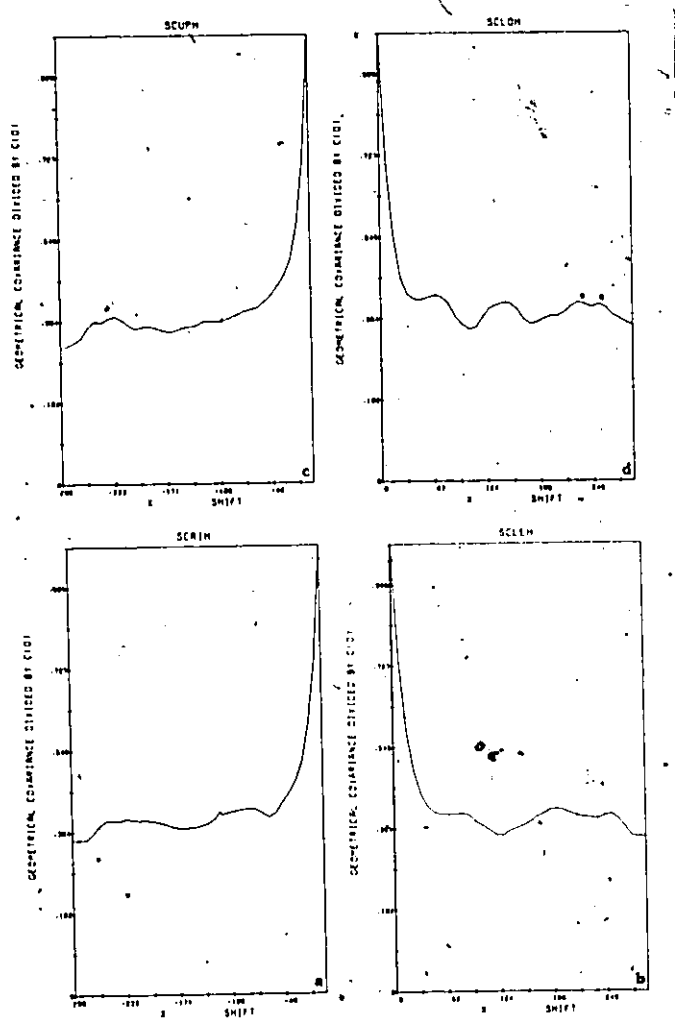

Figure 8.24: Linear geometrical covariances for the scapolite profiles of the granulite in different directions. (a) horizontal direction, right to left; (b) horizontal direction left to right; (c) vertical direction top to bottom; (d) vertical direction bottom to top.

The values in Figure 8.25a for pyroxene, and in Figure 8.25b for scapolite, are the raw intersection pixel counts. The mask used for the images to be traslated has the size of 801 x 381 black pixels and is not shown here. Contours are added by hand for intervals corresponding to 70%, 55%, 52%, and 40% of the area for shift (0,0). The contours show mildly anisotropic patterns, elongated in the 45° direction, which correspond to the direction of the gneissossity.

In Figure 8.25a, the anisotropy of the pyroxene profiles, is indicated by the contours for all values; in Figure 8.25b, the anisotropy of the scapolite profiles is indicated by only the 40% contour.

A clearer simplified expression of these anisotropies in profile areas distribution can be seen in the other two diagrams of Figures 8.25c and 8.25d. There the spacing between the covariance values are the same in the two directions. The same contour lines of Figures 8.25a and 8.25b have been redrafted in Figures 8.25c and 8.25d, for the covariance patterns of pyroxene and scapolite, respectively. Here not only the area distribution anisotropy can be observed, but also the fact that the slopes of the geometrical covariance function is steeper for scapolite, which is a more disperse phase, than for pyroxene, a more clustered phase.

Figure 8.25: Two-dimensional geometrical covariances for pyroxene (a) and for scapolite (b) profiles of the granulite for 12 shifts of 5 pixels in all directions. Hand contours for 70%, 55% and 52% (broken line) of the central value (no shift) in (a); contours for 70%, 55% and 40% (broken line) for the scapolite were drawn in (b). The patterns of contours are distorted because the spacings of the values in the two directions are different. Simplified drawings of the contours for 70%, 55% and 52% (broken line) of the geometrical covariance of pyroxene profiles (c) and of the contours for 70%, 55% and 40% (broken line) for the scapolite profiles (d).

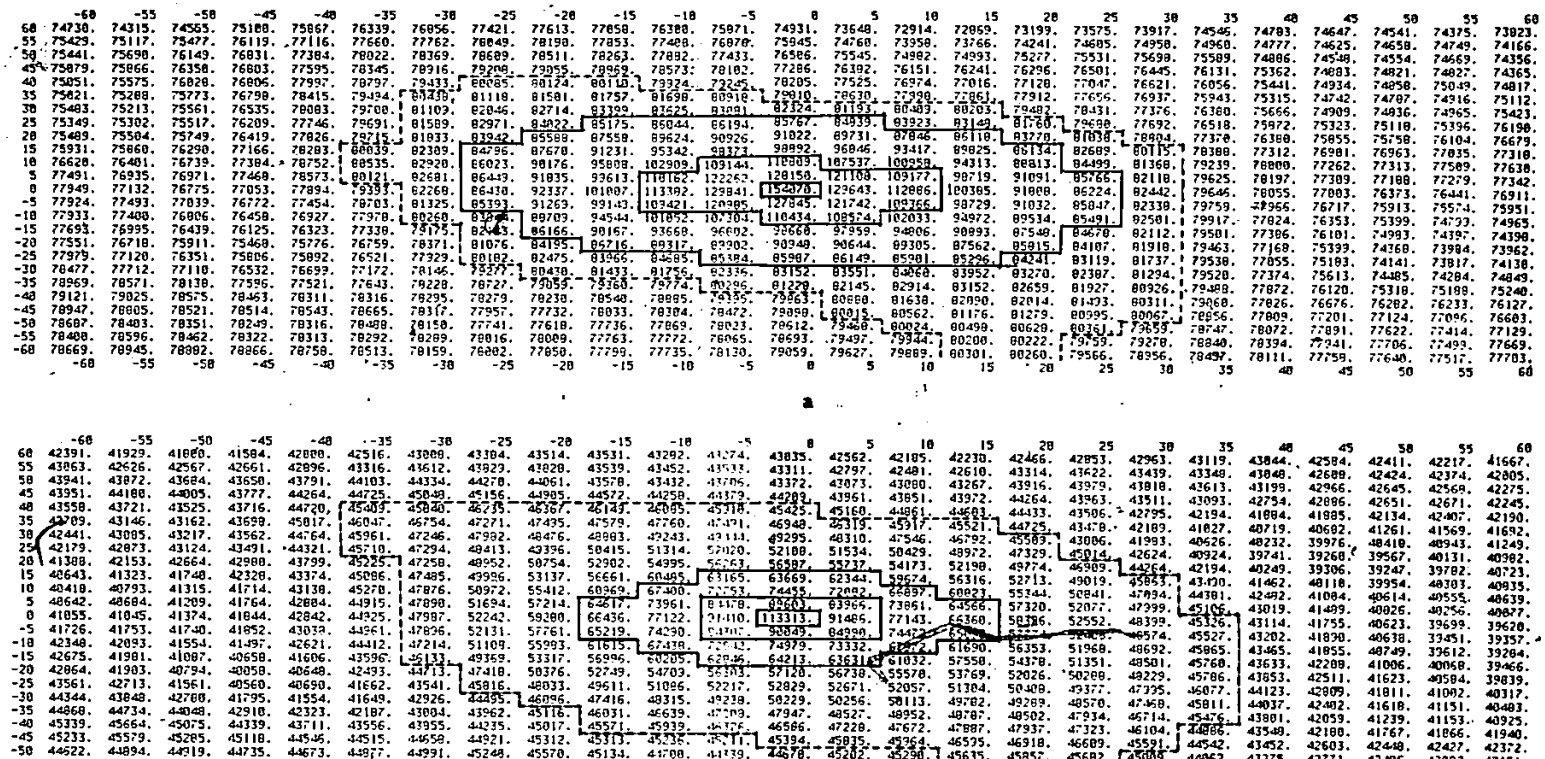

Figure 8.25: Continued.

pyroxene

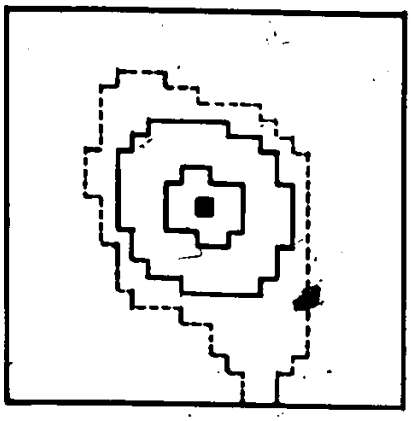

c

contours for 70%, 55%, and 52% (broken line)

scapolite

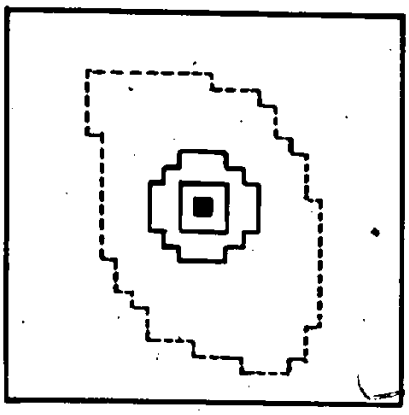

d

contours for 70%, 55%, and 40% (broken line)

Figure 8.25: Concluded.

These results, therefore, support the suggestion of a high degree of homogeneity in grain-profile area distribution in the texture for both the major component of the crystalline fabric. This suggestion would leave the shape anisotropy as the strongest property of the fabric.

8.3.6 Concluding remarks

The study of the granulite serves as an introduction to the kinds of problems which should be studied by image analysis and also to the kind of methods which are applicable. Some of these apects have not yet been formally considered previously by anybody. The present approach certainly brings them to our attention. The visual side of the approach is of further assistance in method development and data analysis.

Contrary to the preceding section, the following one deals with a more formal geometrical statistical approach which is part of stereology.

8.4 Experiments on the characterization of metamorphic textures from a micrograph of an amphibolite

8.4.1 Introduction

The content of this section represents a contribution, coauthored by J. Masounave, which was orally presented at the V International Congress for Stereology, held during September 3-8, 1979, in Salzburg, Austria. It also was submitted in manuscript form to the Journal of Microscopy (Fabbri and Masounave, 1980). The text of this section corresponds to that of the manuscript in press. The subsections on the material analyzed and on the preparation of the image material (Subsections 8.4.2 and 8.4.3) have been expanded in the thesis, and Figures 8.26, 8.27, and 8.28 were inserted. Tha author of this dissertation is the senior author of the contribution and has made the initial experiments on the Modcomp II computer and on the Quantimet 720 image analyzer. The junior author performed additional experiments on the latter instrument so that sufficient data could be gathered for comparing the performance of the two instruments and approaches used. The junior author also suggested additional experiments to be made on the Modcomp

II computer.

This section decribes some experiments on texture characterization from a thin section of a metamorphic rock and compares the results obtained by different interactive approaches. One approach uses a Quantimet 720 image analyzer, a specialized hardwired instrument working in real time, but which has limited processing capabilities. The other approach is computationally slower but has general programming capabilities. As described by Fabbri (1980), it uses a Modcomp II minicomputer (64 K's of 16 bit words of memory), a flying spot scanner, and image processing software written in Fortran with only few machine-dependent routines.

The Quantimet 720 image analyzer is faster, but it has a limited computational power; it is ideal for routine work. On the Modcomp II general purpose minicomputer it is possible to perform any type of computation, however, certain tasks can require much computing time. This could be costly in cases in which there is a charge for computing time. The two approaches are compared in order to determine which measures or transformations more efficiently describe the particular material analyzed.

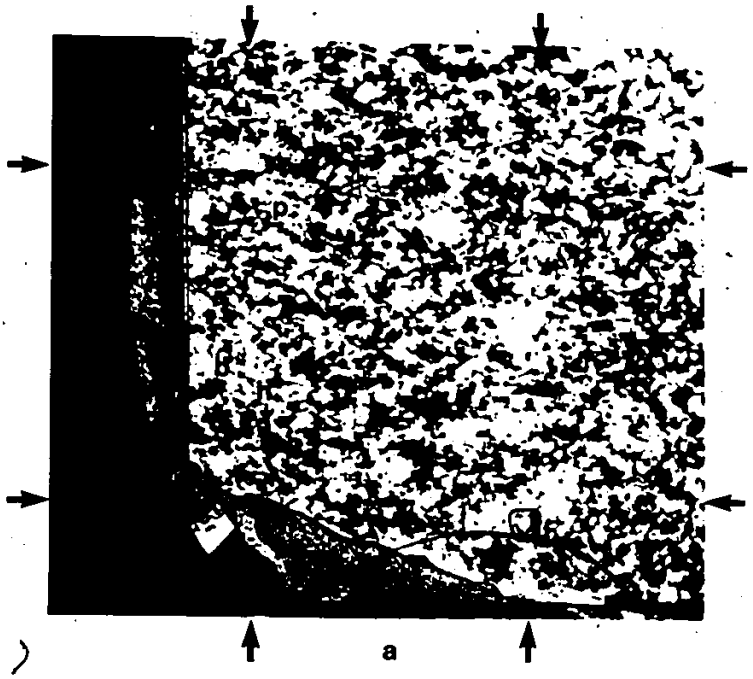

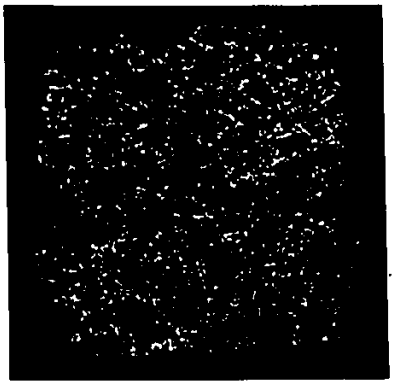

Figure 8.26: (a) portion of the thin section of amphibolite which was studied. The study area is indicated by arrows; the trace of the foliation plane is horizontal. The letters h, b, and p, indicate hornblende, biotite and plagioclase crystals, respectively; (b) the boundary tracing of all grains in the study area.

8.4.2 The material analyzed

The microscopic image of a thin section of a Precambrian amphibolite from Sparrow Lake (Muskoka area), Ontario, is analyzed in this paper. The photograph of a portion of the thin section is shown in Figure 8.26a. The sample was collected in Precambrian terrains of the Grenville Province of the Canadian Shield. The orientation of the macroscopically visible foliation and lineation was recorded in field, and the thin section was cut perpendicularly to both the foliation plane and the lineation direction. The six different crystalline phases in the section are: hornblende (50.19%), plagioclase (40.39%), biotite (5.48%), sphene (3.24%), apatite (0.68%) and zircon (0.02%). Frequently, the grains are not distinctly and uniformly colored; crystals of the same phase are in contact so that the boundaries between individual grains are not easily detected. For these reasons it is not yet possible to achieve a satisfactory phase recognition and extraction with automatic scanning devices.

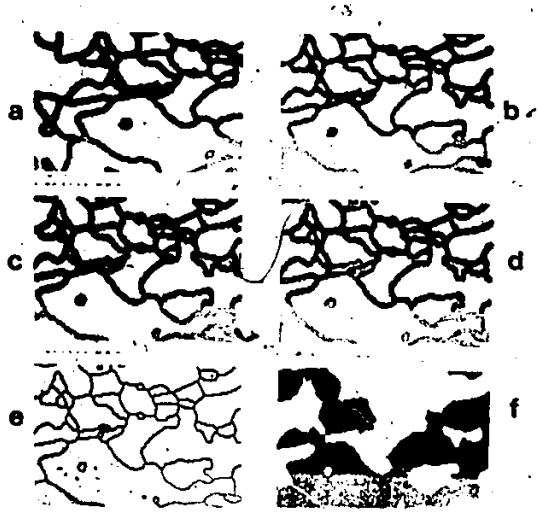

Figure 8.27: Digitization of boundary tracing and extraction of the binary image of amphiboles. (a) part of a binary boundary image obtained on the Modcomp II computer by thresholding an image after square raster scanning of the negative in Figure 8.26b, on a flying spot scanner; (b) thresholding after hexagonal scanning; (c) thresholding after hexagonal scanning at a gray level range different from (b); (d) edited version of the image in (c); (e) line thinning of the image in (d); (f) extraction of the binary image of hornblende crystal profiles from the image in (e), after component labeling and interactive phase labeling.

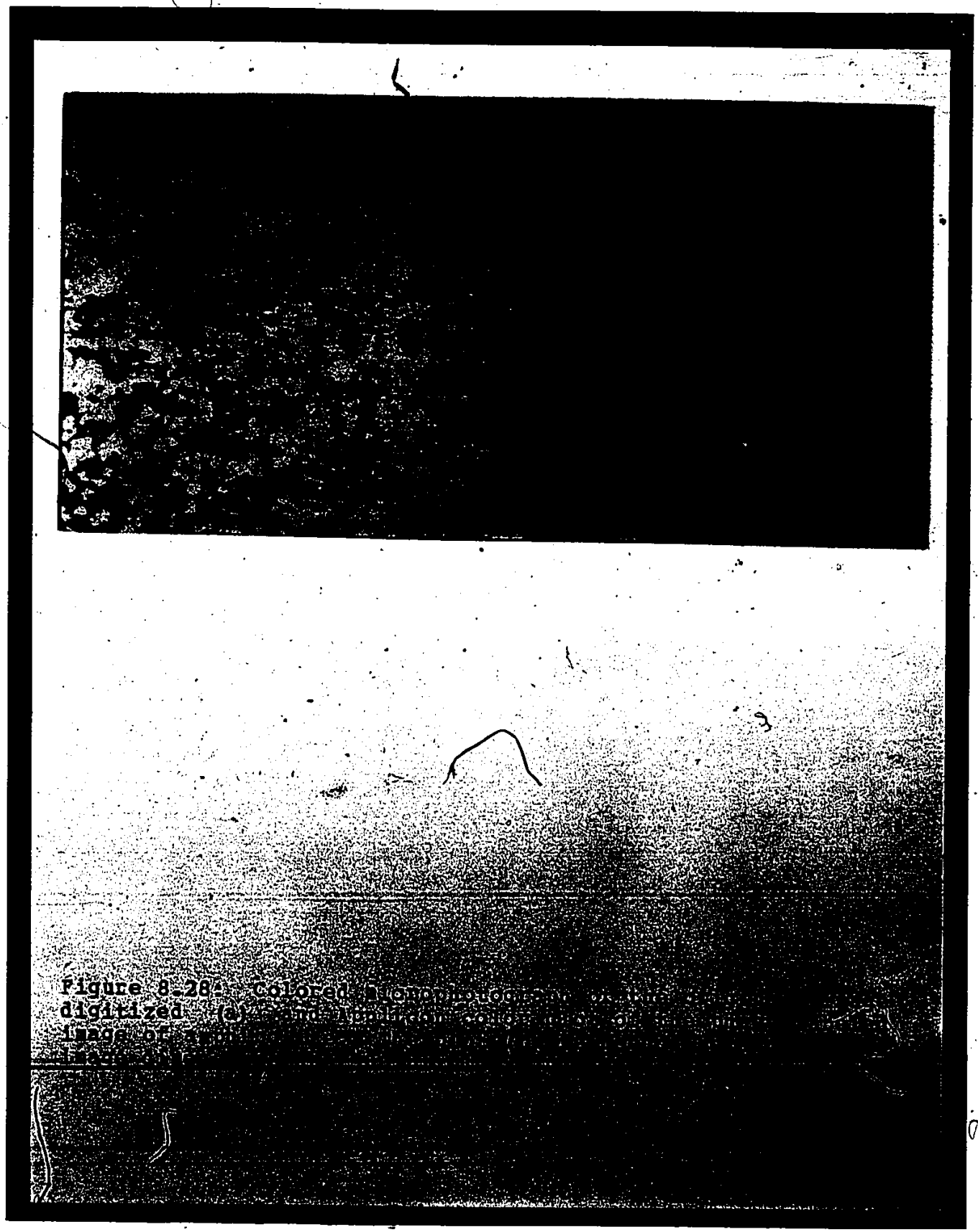

Figure 8.28: Colored [illegible] digitized [illegible] image of [illegible]

COLOURED PICTURES

8.4.3 Preparation of image material

An 8 mm x 8 mm square portion of the thin section was projected onto a tracing film, and the boundaries of over 2000 crystals, whose profiles were entirely contained within the square, were drafted at a magnification of 100X. The transparency (shown in Figure 8.26b) was photographed, using a 35 mm film, for scanning by a flying spot scanner. A grey level image was produced according to a hexagonal raster configuration of 900 pixels x 1016 pixels in size. The image was thresholded to produce a binary image of the line drawing of crystal boundaries to be studied. After minor amounts of interactive editing in places of poor resolution, and hexagonal line thinning of the boundaries, the extraction of the different phases as separate binary images was obtained by component labeling and phase labeling as exemplified by Fabbri and Kasvand (1980). Some of the processing steps for this image are shown in Figure 8.27. The original microscopic color image and a plot of the phase labeled image obtained, are shown in Figure 8.28.

Two crystalline phases were selected for textural measurements: biotite and hornblende. These phases display marked shape complexity and distinct orientation properties. The two black and white ink drawings of the phases which are

shown in Figures 8.29a and 8.29b, have been obtained from the original draft for the Quantimet 720 experiments. To allow the separation of adjacent grains, care was taken that the white gaps between them was wide enough to be detectable on that instrument. Displayed in Figure 8.30 are portions of: the thinned boundary image (a), the images of biotite (b) and hornblende (c) and the image of vertically eroded hornblende (d). The plots are pseudo-hexagonal; they were produced on a Versatec dot matrix printer from the Modcomp II computer system.

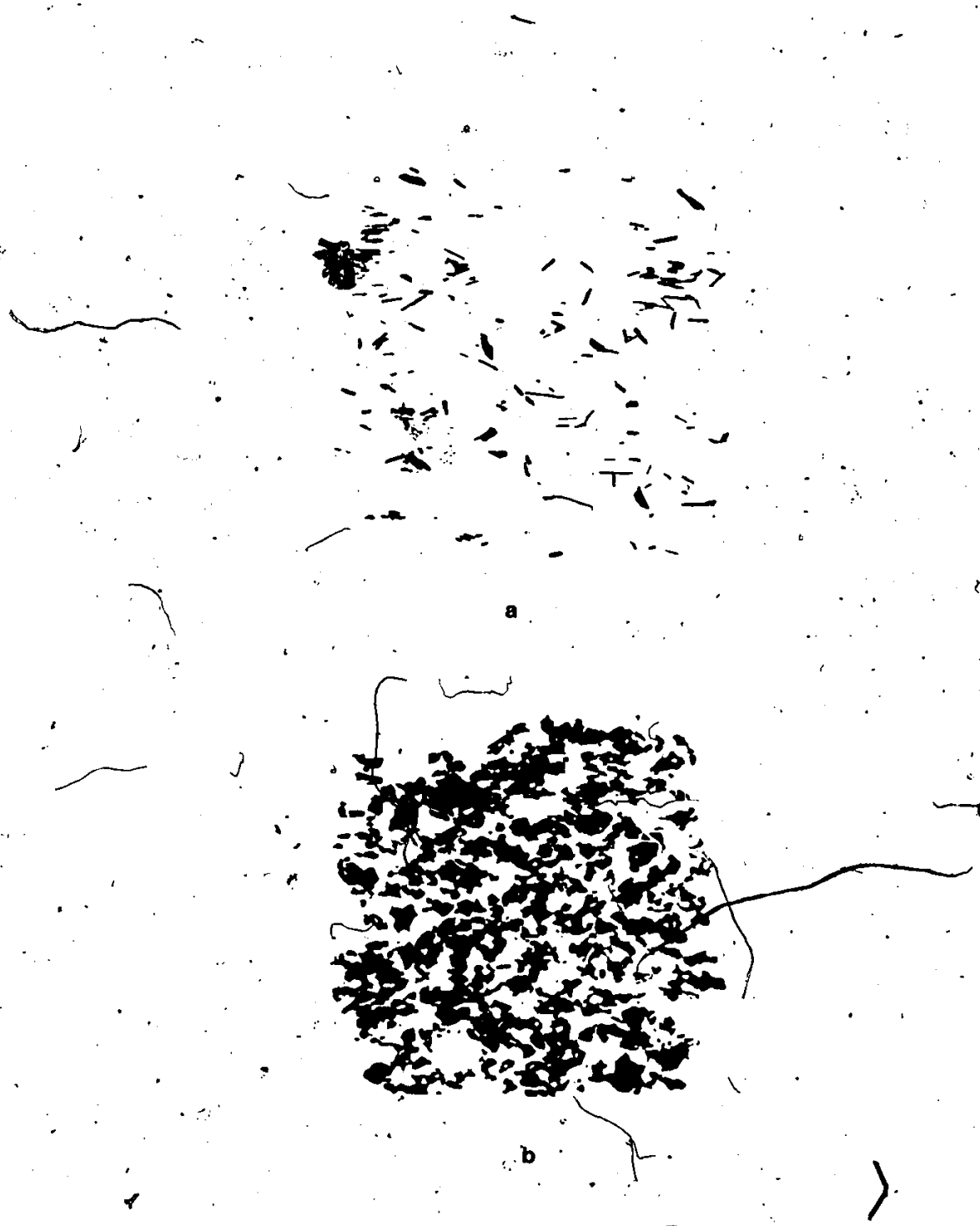

Figure 8.29: Ink drawings of biotite (a) and hornblende (b) crystals obtained from the boundary line tracing for the Quantimet 720 experiments. The foliation trace in these drawings is horizontal.

Figure 8.30: (a) part of the hexagonally digitized binary image of boundaries of crystal profiles from the thin section of amphibolite; (b) binary image of biotite grains, and (c) of hornblende grains; (d) vertical linear downward erosion of the hornblende image by a structuring element of 15 pixels in length.

8.4.4 Theoretical background

The experiments have been restricted to the following three selected characteristics: mean traverse, orientation and structure.

A commom method to measure the mean traverse of particles is based on the size distribution of their intercepts. The intercept function I(l) is used, which is a function of the total number of chords detected after an erosion of length l. This function is used to compute the mean traverse "in number": all the traverses across the particles in a given direction have the same weight.

The mean traverse in number in a given direction can be defined as:

$$m_1 = 1/I(0) \int_0^\infty l(\partial I/\partial l)\, dl \qquad (8.1)$$

where l is the length of the linear structuring element used for the erosion and I(0) is the total number of intercepts with non-eroded profiles. The subscript $_1$ indicates a one-dimensional measure.

The experimental problem with Equation (8.1) comes from the instability of the I(l) function on an image analyzer where the image is scanned continuously. The total number of intercepts, like the perimeter, is very sensitive to the

instrumental noise. It is possible to partly avoid this problem by using the P(l) function which is the probability that a segment or a structuring element of length l is included in the grains. It can be shown (Matheron, 1967) that the I(l) function is proportional to the first derivative of the P(l) function. In this case Equation (8.1) becomes:

$$m_1 = -1/P'(0) \int_0^\infty l(\partial^2 p/\partial l^2)\, dl \qquad (8.2)$$

which gives, by integration by parts:

$$m_1 = -P'(0)/P(0) = \beta_1 \qquad (8.3)$$

where P'(0) is the first derivative, for l = 0, of the P(l) function. The P(l) function, measured with the area function after an erosion is less sensitive to the instrumental noise than the I(l) function. We want to compare the results from Equations (8.1) and (8.3) to decide which of the two is to be preferred.

8.4.5 Experimental results

The mean traverse m_1 is obtained by computing all the intercepts for the eroded particles for all possible successive erosions of length l in a given direction α. β_1 can

be computed by producing a few successive erosions to obtain: P(1), P(2), ... In practice, two or three erosions are sufficient.

The P(l) function is measured by the Quantimet with the area function after an erosion of length l; on the Modcomp II it is measured by a routine performing hexagonal erosions and dilatations of binary "compressed" [1] images with structuring elements of any size and shape.

In order to take care of the frame bias during the erosion and the covariance measurements which will be described for the Quantimet and the Modcomp II computer, the computations were all obtained within a rectangular area smaller than and fully contained within the image analyzed, also after the transformations. Therefore, the P(l) function measured is not sensitive to the frame bias: the reduction of the frame during the erosions or during the translations.

The relationship between the two measures in microns, m_1 and β_1, is shown in the diagram of Figure 8.31a for hornblende and biotite for different angles of direction in degrees. The diagram suggests that β_1 is a more reliable measure of mean traverse on the Quantimet. Because of the

---

[1] "ON" bits for black pixels, "OFF" bits for white pixels. Compression is done for economizing in storage space, I/O time and to use fast bit manipulating routines usually available on most computers.

absence of noise, on the Modcomp II both measures have the same values in different directions.

The Modcomp II measurements confirm that m_1 and β_1 have values which are very close. This could not be done on the Quantimet. Clearly the mean traverse β_1 is a more desirable measure in both instruments, where it is quickly computed with only three succesive erosions. In the case of β_1 both approaches are satisfactorily fast.

In Figure 8.31a we can also observe an orientation effect: the mean traverse values vary with α. A phase can be considered oriented if it contains elongated particles and the orientation of each particle is appreciably related to that of its neighboring particles. For both biotite and hornblende most grains are elongated in the horizontal, α = 0. degrees direction. Because the areal proportion of biotite (5.48%) is far less than that of hornblende (50. 19%), from the diagram of Figure 8.31a we can say that biotite is much more strongly oriented: its mean traverse variation range is proportionally greater.

Figure 8.31: Mean traverse and orientation tests. (a) Relationship between m_1 and β_1, two measures of mean traverse in microns (μ) for biotite and hornblende profiles, and their variation with the angle of direction α. Open (m_1) and solid (β_1) circles indicate Modcomp II computer measurements; triangles and squares indicate Quantimet 720 measurements. (b) Definition of horizontal (h) and vertical (v) intercepts for a convex object at the origin (I(0)) and after a vertical erosion of length l (I(l)). P(l) is the area of the eroded object. (c) Variations of the ratios of horizontal over vertical intercepts with successive linear erosions of length l, for different values of the angle of direction, α. The data are from the Quantimet. (d) Variations of the maxima of the ratios of horizontal over vertical intercept for eroded biotite (triangles) and hornblende (squares) with the angle of direction α. Solid symbols are measurements from the Modcomp II computer; open symbols are from the Quantimet.

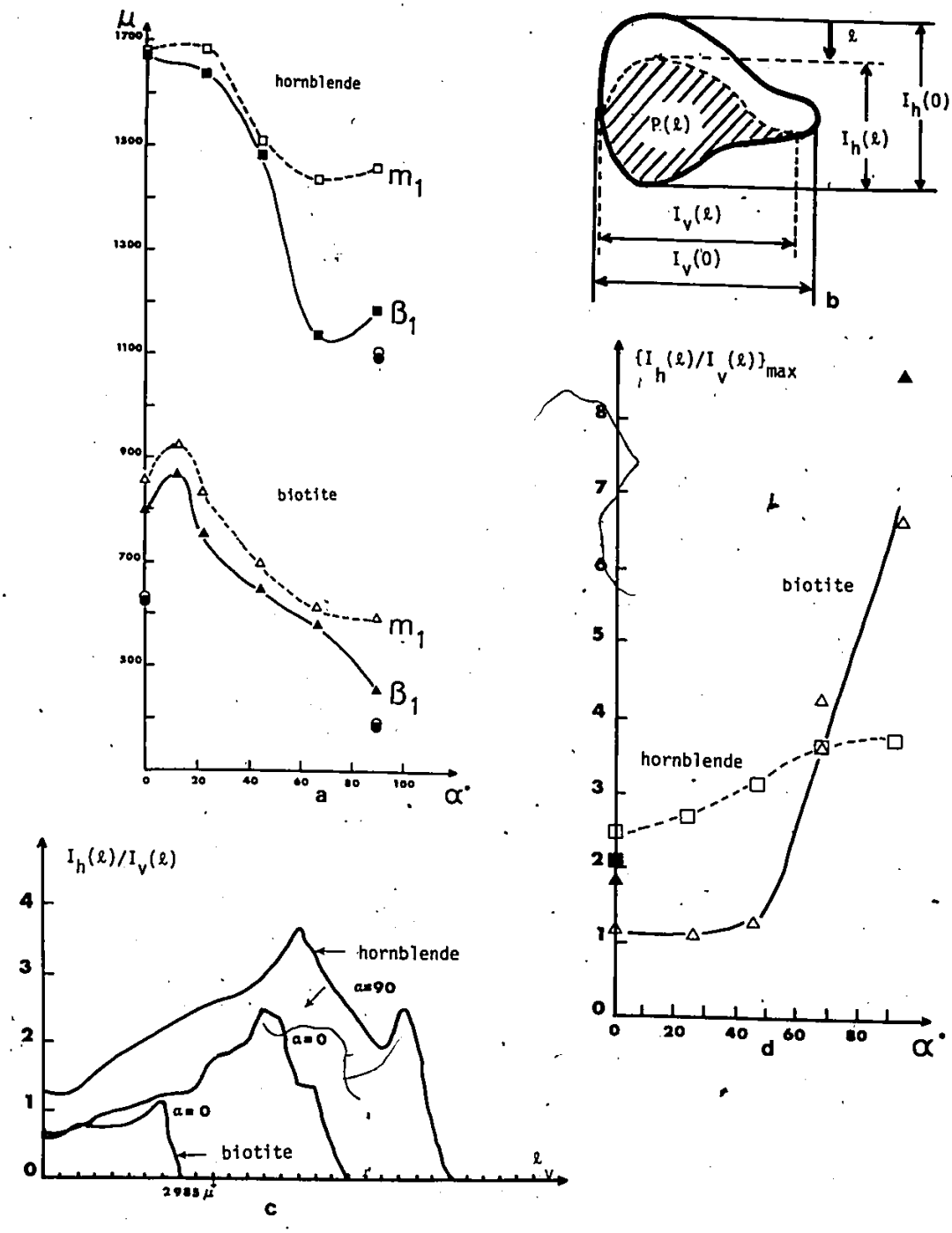

Figure 8.31: Concluded.

More information can be obtained from measuring the ratios of horizontal to vertical intercepts as functions of a linear erosion by a segment l, in different directions. Figure 8.31b shows the vertical and horizontal intercepts at the origin (i.e. for l =0), $I_v(0)$ and $I_h(0)$, and after a vertical linear erosion by l, $I_v(l)$ and $I_h(l)$. Figure 8.31c shows the ratio, computed on the Quantimet, of intercept functions versus the cumulative length of horizontal linear erosion. This ratio for different directions, in cases of convex grains with no holes (inclusions), describes an orientation effect in mixtures of large and small particles: large particles are more strongly oriented. The maxima of the curves, in Figure 8.31c, emphasizes maximum anisotropy of the particles which have their largest diameter in the direction of erosion. The variation of the maximum ratios for different directions is a good measure for characterizing the orientation pattern of biotite and hornblende, as shown in Figure 8.31d. The smooth pattern for hornblende is partly due to the pronounced concavity of the crystals, the presence of holes, the elongated shape of these holes and their positions within the host crystals. This can be seen in the erosion pattern of hornblende shown in Figure 8.30d.

The correspondence between Quantimet and Modcomp II measurements is quite good (see Figure 8.31d). The perfor-

mance of the Quantimet is, however, much faster (minutes versus hours) for sequences of tens of erosions in different directions like those shown in Figure 8.31c for the Quantimet only.

The structure effect occurs when the individual particles of a phase present some repetitive character in their distribution in some direction. This effect may also depend on the orientation. The effect is expressed in quantitative form by the covariance function which represents the probability that both extremities of a linear segment oriented in a given direction α, are included in the grains belonging to the same phase. This function is measured on the Quantimet by a linear correlator module which works in the horizontal direction only, and from left to right. Measurements in all directions can be made by rotating the image. On the Modcomp II computer this function is programmed in the two dimensions: two identical copies of a binary image are shifted along columns and rows and then compared (or correlated) after the translation. The result is a coefficient expressed in picture points of overlap, from which the geometrical covariance can be easily computed.

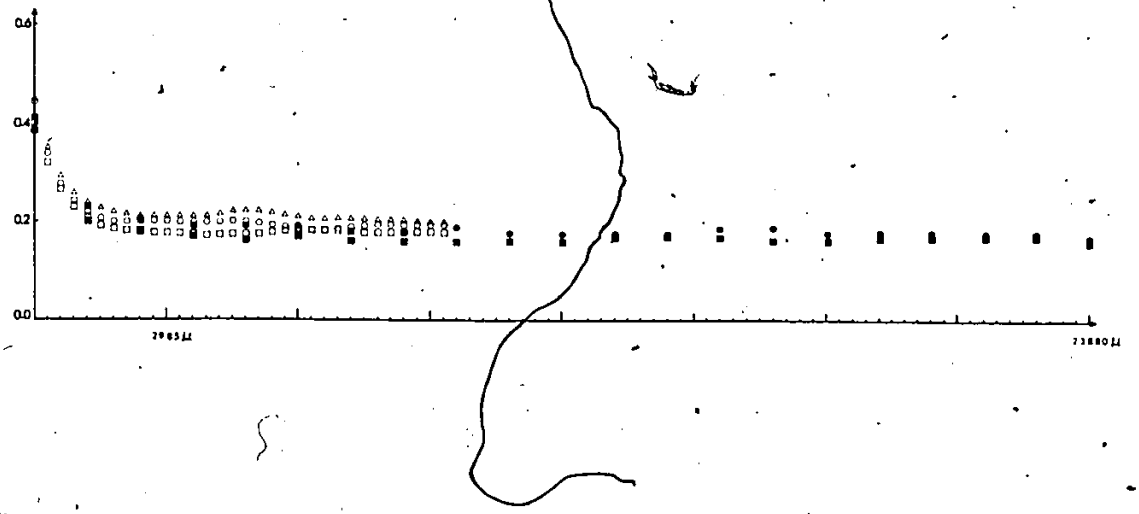

Figure 8.32: Covariogramme for the image of hornblende crystals for different angles of direction α. Open symbols are for Quantimet 720 measurements, solid symbols are for Modcomp II measurements. Different symbol shapes indicate the different directions of measurement: circles for α = 0 degrees, squares for α = 90 degrees, and triangles for α = 45 degrees.

The values of the geometrical covariance, expressed as proportions of picture points of overlap within the area analyzed, are plotted (vertical axis) against the shift lengths in microns (horizontal axis) in Figure 8.32. Individual subdivisions of shift length correspond to 5 picture points. For the two images analyzed no strong effect of structure can be seen. The texture can be interpreted as the result of a homogeneizing metamorphic process indicated by microfolding and shearing of foliation planes and recrystallization along the different planes. The metamorphic processes have obliterated any periodical pattern of grain distribution which may have existed before, within a distance of 9000 microns.

Linear covariance measurements can be computed within one or two minutes for each direction on the Quantimet. On the Modcomp II computer they are at least ten times slower. One advantage of the latter approach is the possibility of computing the covariance in any direction without changing the setting of the image.

8.4.6 Concluding remarks

Microscopic morphological features of amphibolites, usually, are not described quantitatively. The phases studied

have mean traverses, orientation and distribution patterns that can be characterized by the two approaches used in this paper. Therefore, it will be possible to develop quantitative models for nucleation and metamorphic crystallization processes also based on the morphological and textural properties of rock fabrics. This approach has not yet been properly investigated.

The extraction of image information from the material analyzed, which was not attempted before, is cumbersome and technically complex: It is also for this reason that little is known on the quantitative characterization of metamorphic textures from thin sections.

More work will be needed to further speed up the computing time required for the binary transformations programmed on the Modcomp II computer, especially so for lengthy sequences of transformations which are produced in real time by the Quantimet. The image processing approach is useful for testing measures which are affected by high noise on the Quantimet, and in paticular for extending the processing to more generalized structuring elements and also beyond the analysis of binary patterns.

It is clear that in a near future hard-wired image analyzers and medium to large size computers will merge or be interfaced, thus closing the gap between the two approaches. The results of the simple experiments performed

in this paper, suggest how software and hardware can be used in further developments of image analyzing systems.

Because of its working speed, an image analyzer is particularly well suited for routine work. However, it can compute a limited repertoire of transformations. The experiments described here are a first step in searching for efficient measurements or transformations by comparing two instruments. A software dependent system is not restricted in the choice of transformations so that new programs can continuously be designed for better characterizing image material before building a more efficient hardware for routine work.

8.5 Review of studies of rock textures for the analysis of microscopic sections

During the past two decades several attempts have been made to explain textural patterns in igneous and metamorphic rocks in terms of free energy at grain boundaries. The following is a review of contributions which are related to the study performed in this thesis in that they deal with the analysis of rocks in thin or polished sections. Most approaches in those contributions provide the background for more extensive applications, particularly if the assumption can be made of having at our disposal a digitized image of the section to be studied. While this review is not complete (the literature on textural patterns of rocks is not easily accessible and also is not particularly rich) the topics reviewed are thought to be a sufficiently representative sample of geological studies.

Rogers and Bogy (1958) in a study of grain contacts in granitic rocks assumed that if the distribution of different minerals is random and uniform, the percentage of contact area of a mineral that is in contact with any other mineral should be proportional to the modal percentage of the latter in the rock. In this situation it can be assumed that the former mineral did not affect the development of neighboring

grains. They observed that potassium feldspar-potassium feldspar and plagioclase-plagioclase contacts were less frequent than expected in a random type of distribution, and concluded that the growth of one feldpar probably prevented the nucleation of a similar crystal. An alternative interpretation is that a growing potassium feldspar grain causes rapid nucleation of the other feldspar lattices in its neighborhood and simply incorporates these into its own structure rather than permit their formation as separate grains (Rogers, 1961). The information they used was in terms of "geometric means of the ratio percentage of contact length of a mineral A in contact with mineral B / modal percentage of mineral B". The modal data were obtained by point counting traverses and the number of times each possible contact was crossed. The value of this ratio for the potassium felspar-potassium feldspar contacts in the granites that they analyzed was 0.45.

Mahan and Rogers (1968) used the same method in a study of grain contacts in some high-grade metamorphic rocks. They computed a ratio of 0.83 for potassium feldspar-potassium feldspar contacts. The relatively high ratio in metamorphic rocks was interpreted as indicative of crystallization of the potassium feldspar in a comparatively solid medium in which a growing grain would probably have less effect on its environment and on nucleation in its neighbor-

hood than it would have in a melt.

Whitefield et al (1959) established definite relationships among textural properties and modal compositions of some granitic rocks. De Vore (1949) proposed a model in which relative grain sizes, grain distribution, extent of various grain associations, and nature of grain contacts are interpreted as an expression of a minimum interfacial free energy of the mineral assemblage. It is a nucleation-crystal growth model with a significant influence of the interfacial free energy on the crystallization of grain assemblages. According to the model there seems to be a definite and valid free-energy relationship, that, if permitted to operate could determine grain distribution and place an upper limit on the modal composition of the phases in the system. Thus these macroscopic features of grain assemblages could be effectively treated in terms of termodynamic equilibria.

Kretz (1966a) succesfully applied a quantitative approach to the study of rock textures, and derived equations for the rate of nucleation from information on crystal size distributions. The study yielded information concerning the growth processes of the minerals and the processes of migration of their compohent elements through the rocks in which they occur. In another contribution published during the same year (Kretz, 1966b) he developed a line of

based on the interfacial angles at the contact between several grains and shapes of individual grains. He succeeded in demonstrating solid-state growth in metamorphic rocks describing that triple points in metamorphic rocks were in positions for theoretical minimum surface energy. The conclusion was that several aspects of the shape of mineral grains in metamorphic rocks can be attributed to a local reduction or minimization of interfacial free energy.

Hobbs (1966) observed that the microstructure of some Australian tectonites that he analyzed by axial distribution analysis (AVA) was consistent with adjustment of grain boundaries under the influence of interfacial tension. The rules which govern the relationships between grains have been carefully developed by metallurgists and follow into two related categories: (1) topological rules which govern the ways in which the parts of an aggregate must be geometrically related to one another, and (2) rules involving the configuration which grains in an aggregate must adopt in order to be in equilibrium under the influence of the interfacial tension of grains. In a single phase aggregate the free energy associated with grain boundaries must tend to a minimum for equilibrium and so grain shapes and boundary relationships must alter to make this possible. In polyphase aggregates the same condition holds but adjustment may take place in order to produce different phases

which have a lower free energy.

Vance and Gilreath (1967) used the same ratio used by Roger and Bogy (1958) in a study of phenocrysts distribution pattern in some porphyritic igneous rocks. The contact relations between the phenocryst minerals studied reveal a moderate to strong general tendency for preferential synneusis of crystals of like minerals which is balanced by an antipathetic relation between unlike minerals in the same rocks. Specific minerals seem to exhibit consistent patterns.

Kretz (1969) examined in detail the distribution of crystal and crystal boundaries in a thin section of pyroxene-scapolite-sphene granulite. The rock was found to be homogeneous and the crystals of pyroxene, scapolite, and sphene appeared to be randomly distributed. He carried out several different statistical tests for homogeneity and randomness in the spatial distribution of the crystals. Different types of measurements were performed and different data were collected and analyzed from one single thin section. In particular the results of the application of one method, called "line-transect method", also used by Vistelius (1966), led to the conclusion that the nucleation site of any crystal in the rock was independent of any other crystal in the neighborhood.

Similar statistical tests applied by Flinn (1969) on

different rocks show that grains in gneisses, instead of being distributed at random are specially arranged so that grains of the same phase tend not to occur in contact with each other. This arrangement was interpreted to arise from grain boundary migration leading to the insertion of grains of one phase between pairs of like grains of other phases. The process was thought to be due to the fact that the interfacial energies of contact between like phases were greater than those between unlike phases. According to Flinn, in metamorphic rocks unlike contacts are statistically favoured over like contacts at high level of significance.

Erlich et al (1972) observed that surface free energy, which is a function of surface area and grain neighborhoods, may be a dominant factor in petrogenesis. Textural variables such as grain shape and surface area of phase contacts per unit volume can provide information concerning reaction pathways and kinetics. In a study of the response of textural variables to metamorphic grade they found progressive increase in the proportion of unlike grain-to-grain contact with incresing grade. This was interpreted as decresing the surface free energy. Similarly an increase in average size of grains, by reducing surface area, should also result in a decrease of surface energy. They concluded that a rock of a given composition affected by increasing

metamorphism, can only conserve or decrease its surface free energy by textural readjustment over a limited range. When this range is exceeded, chemical readjustment is probably triggered, producing new stable assemblages. It then appears that surface free energy may play a fundamental role in the development of these stable assemblages. Both shape and surface area of plagioclase grains appear more effective in defining the gradient than are standard compositional variables.

According to Byerly and Vogel (1973), who studied grain boundary processes and development of metamorphic plagioclase, the only explanations for Flinn's (1969) observations are: (1) the increased effect of impurities on lowering the surface energy for unlike boundaries, and (2) higher activation energy for unlike boundaries due to differences in crystal structures and chemical composition, whereas like boundaries have low activation energies with the source material for diffusion being available in the immediate vicinity of the boundary. In other words the low-energy like boundaries are more mobile than the high-energy unlike boundaries due to the differences in activation energies. Surface energy is a major factor in controlling the processes involved and is itself a function of the geometrical properties, the distribution of phases and the distribution of impurities within the rock aggregate. According to them

grain boundary migration and impurity segregation are two related processes which occur with annealing of any crystalline aggregate; they can explain a major part of the variation of the plagioclases found in metamorphic rocks.

Jen (1975) considered the spatial distribution of crystals in charnockitic granulites as a function of interfacial free energy. The spatial distribution of crystals may give information on nucleation sites and on the role of interfacial free energy. He found that all three major fundamental types of spatial distributions may occur in a rock: clustered, regular and random (also intermediate types such as antiregular and anticlustered). Since this occurs frequently, although in most of the rocks there are two instead of all three types, such mixing mode of spatial distribution would be expected to be the usual case rather than the exception. This suggests that an ideal case of either random, regular or clustered distribution of crystals in natural rocks is rare, and that total equilibrium is rarely achieved. Jen used point-sample and line-transect methods (Kretz, 1969) in his study, and measured an average of 769 transitions per section. The analyses of the transitions were made by computer programming and were based on chi square tests.

During the past twenty years grain boundaries have constantly been a studied problem. The most recent collec-

tion of papers describing the state of the art in this field is in Chadwick and Smith (1976). There the grain boundaries are described and attempts are made to explain their properties. According to one of the definitions in the book, a grain boundary is not simply a collection of dangling lattice sites, but rather a defect structure that may have some degree of regularity. Atomic arrangements at grain boundaries are investigated, and also are the chemical properties. Much work is being done on computer simulation of grain boundaries and on the methods of characterization of grain boundaries in terms of structuring elements.

Whitten et al (1975) and also Whitten and Dacey (1975) studied sequences of mineral grain-transitions along linear traverses across mutually perpendicular sets of serial sections of the same Grenville calc-silicate granulite studied by Kretz (1969) and also in this chapter. Rather exhaustive tests that they performed proved that the granulite possesses the Markov property (Vistelius, 1966, 1972, Vistelius and Faas, 1972, and Vistelius and Romanova, 1972). This property they describe as a property in which observed mineral grains are controlled by the composition of adjacent grains in a rock. Such property seems to reflect petrogenetically important but unidentified factors. They concluded that in the granulite under study major constituents observed in traverses normal to the weak mineralogical

banding show a distinct non random distribution which implies that contacts between grains of the same major mineral are always less abundant than would be expected if the grains were randomly distributed. In the case of the calc-silicate granulite, which is a metasedimentary rock, the Markovian properties must be due to a mineralogy produced by high grade neocrystallization in the solid state. This conclusion is in contrast with a model used by Vistelius and coworkers which imply that the same Markovian properties should be typical of "ideal" granites, representing primary crystallization produced by a melt.

Wadsworth (1975) used grain-transition probabilities among mineral phases to analyse variation in grain sequence among sixty samples distributed throughout the zoned Cornelia pluton in southwestern Arizona. He concluded that variations in the patterns of grain sequences that he recognized among the units of the pluton justified a completely new petrologic understanding of the Cornelia stock. In his study, Wadsworth structured grain-transition data according to the model of "embedded" Markov chains, which avoids the necessity of recognizing grain contacts among like species.

Vernon (1976) emphasized the importance of studying grain boundaries in both mono-phase and poly-phases crystalline aggregates. Their characteristics can be related to the

structural deformation and to the recrystallization which commonly overlap in metamorphic processes.

To complete this review, mention should be made of few particular applications to a very practical problem, that of ore dressing, and of digital and optical analysis of rock textures.

Petruk (1975) applied quantitative mineralogical analysis of ores to ore dressing. He used size distributions of minerals of economic value to predict the optimum grind for liberating the minerals and the degree of liberation that would be obtained at this grind. He observed that measurements of the properties of free and locked mineral grains in mill products show a good correlation between predicted and actual liberation, therefore, demonstrating the advantage of using an image analyzer (a Quantimet 720) in mineral beneficiation research.

Serra (1966) and Agterberg (1967) were among the first to analyze thin sections of rocks by coding the occurrence of the different grain profiles by overlying regular grids on microphotographs. Their statistical analyses of the coded arrays of data was to illustrate new methods of studying spatial relationships between minerals or mineral groups and possibly contribute to petrological interpretations. Serra's study consisted in the analysis of a thin section of Lorraine oolitic iron ore, by comparing experimental vario-

qrams computed in different directions for three minerals. Agterberg worked instead on thin sections of a gabbro from the Muskox layered intrusion, District of MacKenzie, Canada. He computed the two-dimensional covariance function and a two-dimensional power spectrum of the thin section coded data.

While the latter two studies were based essentially on digital data, a method proposed by Preston and Davies (1976) uses Fourier optics and optical data processing for a new approach to the analysis of porous material. The material studied by them consisted of photomicrographs of sandstones of units forming petroleum reservoirs.

8.6 Concluding remarks

The two applications presented in this chapter are by no means exhaustive usage of the software programmed nor complete studies of the two thin sections. The purpose of the work is in attempting to illustrate a method of study by using "real life" samples which require large size images (the largest size for which GIAPP was designed is 1024 x 1024 pixels). In so doing: (a) several geological and stereological concepts are formulated in computer processable terms, (b) a number of possible solutions are pointed out, and (c) the efficiency of the computer approach is compared with that of special instrumentations for image analysis.

A review of geological studies on rock textures is also made because it represents both a supporting background for the applications, and because it suggests that other applications can be considered which go beyond the imagination of a single specialist.

Some limitations of the method here proposed have also been pointed out. The software based approach is very general but not necessarily the most convenient for routine repetitive production work. When special purpose computers, such as the "pipeline processors" will be easily available,

then the gap existing between the software based approach and the hardware based approach will disappear.

9. Towards pattern recognition

9.1 Introduction

Image or picture processing is the computer analysis of data in picture form. In image processing "pattern recognition" generally means the automatic extraction and classification by computers of features from digital pictures. Computers transform the images into other images, i.e. new images are produced which are more informative and from which a variety of measures or features may be extracted. Digital pictures are in explicit picture form or raster format: a matrix or regular array of numbers in point-to-point correspondence with points (very small subareas, also called pixels) on the original material. The numbers can be gray level (film density) values from a scanner, labels identifying objects or groups of objects, colors, or simply 1's and 0's, identifying black and white pixels in "binary images". Picture processing, in general, does not deal with hierarchically structured data as is done in computer graphics (e.g. Bouille, 1976).

Some geological data sets such as maps (Agterberg and Fabbri, 1978 a), photographs, geological sketches (Agterberg

and Fabbri, 1978 b), microscopic images of rocks (Fabbri and Masounave, 1980), and systematic samples, can be digitized and processed by computers as images. On these pictorial data sets the "qualitative pattern recognition" is performed by the geologist who uses his prior knowledge and his vision. For "quantitative recognition", specialized methods and the assistance of a computer are required, because in this our visual system generally fails.

We have been considering applications to geological or geophysical maps and to microscopic images of thin sections of rocks or polished sections of minerals, we can classify those applications in terms of different degrees of uncertainties on what to measure from the material to be analyzed. A greater uncertainty is attached to geological boundaries and to geophysical map contours, than to grain profile boundaries as seen under the microscope.

In the application which follows, we have a lesser degree of uncertainty on what to measure from a negative film of alpha-particle tracks, in order to count the tracks. To the human visual system the problem seems very simple and such trivial pattern recognition tasks are taken for granted. For a computer, this task, as we will see, may require considerable computation, since every single little detail requires its own particular attention, procedures and computer programs.

Part of the content of the following application goes beyond the scope of GIAPP, the computer package programmed for this thesis project. The study was done as a joint collaboration, and was presented by the junior author to the Eighth Annual Automatic Imagery Pattern Recognition Symposium, held during April 3-4, 1978, at the National Bureau of Standards in Gaithersburg, Maryland. The contribution was published on the proceedings of the symposium (Kasvand and Fabbri, 1978). The following section is essentially the text of the published manuscript with a short addition of remarks in Section 9.2.8. The junior author obtained the original information from S. Kaiman and W. Petruk who provided the problem and the sample of alpha-particle tracks. Most of the computer programs used for the experiments were already available at N. R. C. with the senior author. At the time when the study was developed, GIAPP was in its early stages of development. The junior author is responsible for the interpretation of the results, the digitization of the image analyzed and the interactive processing.

9.2 Automatic counting of alpha-tracks from autoradiographs of radioactive minerals

9.2.1 Abstract

An image processing approach is introduced for the automatic separation and counting of randomly distributed segments from binary images of autoradiographs of the alpha particle tracks emitted by radioactive minerals. The computer algorithms presented in this paper provide an alternative to cumbersome and tedious visual counting for statistical estimation. The computing strategy is structured to allow the computer programs to be adapted to a relatively small machine, i.e., a "minicomputer". This requirement puts certain constraints onto the structure of the programs and the amount of picture data that can be kept in the memory of the machine. The method described may be further developed for the automatic counting of overlapping fibers in general, such as asbestos fiber in air samples for pollution studies or fibers in pulp for paper manufacturing. It can also be used for the quantification of linear features from geological maps or aerial photographs. The output of the algorithm provides tables of labeled components which can be used for statistical analysis of the segments.

Keywords: Alpha particle track counting; scene analysis; image processing; counting; alpha particle tracks; scene

segmentation; separation of line segments.

9.2.2 Introduction

The paper introduces an image processing approach for the automatic separation and counting of randomly distributed segments from binary images of autoradiographs of the alpha particle tracks emitted by radioactive minerals.

Uranium-, or thorium-bearing minerals emit alpha particles, beta particles and gamma rays at rates which are proportional to the amount of U^{238}, U^{235} and Th^{232} that they contain.

A method for estimating the amount of radioactivity of those minerals consists of counting the number of alpha particles emitted by crystals which are located at the surface of polished sections or in thin sections. This is done by placing a film coated with alpha particle sensitive emulsion (5 to 200 microns in thickness) in contact with the surface of the section for a given length of time. The appropriate time in each case must be empirically determined in order to produce a large enough number of tracks for the estimation, but not so many as to hinder visual separation and counting. For the present application a polished section with crystals of torbernite, a hydrated phosphate of

copper and hexavalent uranium, has been used. Exposure times range between one hour and three hours. For a given exposure time, the ratio (total number of alpha tracks) / (total exposed crystal surface area) is related to the surface alpha activity of the crystal which in turn is a quantitative measure of uranium content.

Quantitative aspects of alpha particle patterns have been treated in the past by Yagoda (1949) and more recently by Rogers (1973).

The image analyzed in this paper is a Kodak Contrast Process Ortho 4154 negative of a 130X enlargement of a portion of the cloud of tracks emitted by one crystal of torbernite in three hours. A positive print of the image is shown in Figure 9.1a. Most tracks appear as straight disjoint segments of different lengths and orientations. The darkness of the tracks varies irregularly along their length. Few tracks intersect and partly overlap in areas of higher density. Some tracks appear as darker rounded blobs of diameters up to twice the width of the linear tracks. The smaller and lighter dots are emulsion grains of the film. Larger blobs are grains of dust. This image represents a general case, encountered during routine visual counting; the density of tracks in the image is considered satisfactory for both visual and statistical estimates (S. Kaiman, personal communication). In the framed area of

Figure 9.1a, 102 acceptable tracks and 3 unclassifiable blobs can be distinguished.

The task of counting the number of objects in a field, which appear relatively simple to the human eye, is in reality quite complex for a machine if a correct count is desired for an infinite variety of shapes, orientations and overlaps.

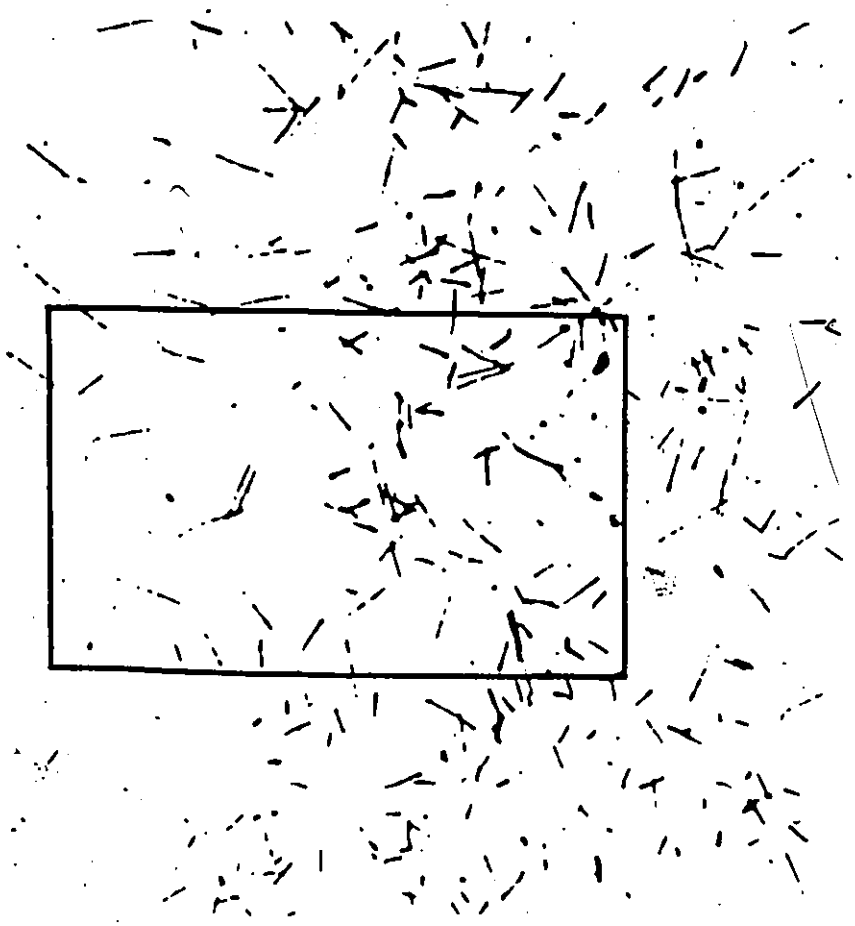

Figure 9.1a: An enlarged positive print of a portion of alpha particle tracks emitted by one crystal of torbernite. The framed area has been scanned and processed digitally.

In several applications, the overlapping individuals are removed from the field of analysis in order to eliminate the bias due to crossings (Cruttwell, 1974) or manual interactions with image analyzers are used, such as light pen probes for isolating or eliminating specific particles from the screen of TV monitors (Jones, 1975).

The problem of separating and counting partly overlapping individuals from an image, for which the human eye and brain are so well suited, has not yet seen much progress. Recent tests made for counting asbestos fibers in air samples (Pavlidis and Steiglitz, 1976) and pulp fibers for paper manufactoring (Graminski and Kirsh, 1977) clearly exemplify both the difficulties and the need of this task. In the present paper experiments towards complete automation are attempted.

9.2.3 Alternate approaches to the alpha particle track problem

The experiments are carried out on a relatively small general purpose computer with 64K of memory, 16 bit word, two 1 M word disks and two 800 bpi tapes. The I/O consits of a card reader, dot matrix printer, teletype, on-line

randomly addressable flying spot scanner and a memory type CRT with a special operator console. The equipment is intended for general research on picture processing rather than specifically for the alpha particle track problem.

The equipment allows several possible approaches.

1) Since the on-line flying spot scanner is randomly addressable, the film transparency of the tracks could be used directly as a nearly homogeneous (to within the resolution of the DA converters of 13 bits) read-only memory to the computer. This approach has been used quite successfully on other problems (Kasvand et al, 1975, and Kasvand, 1972). However, a randomly addressable flying spot scanner is not a generally available computer accessory.

2) There is a certain resemblance between the alpha particle tracks and bubble chamber photographs, i.e. both contain streaks (McIlwain, 1976). Consequently, some of the methods used in analysis of bubble-chamber photographs could be used here, even if the specialized hardware is not available. From results so far obtained it appears that similar line enhancement algorithms may be required.

3) The least specialized and reasonably inexpensive picture scanning device is a TV camera interfaced to some mass storage device (tape, disk) usually via the computer. Thus a raster scanned line-by-line image is captured for further computer processing. This method was selected. The film

transparency was scanned line-by-line and the resultant gray levels stored on tape as a logical record per scan line. This results in an image that is far too large for a minicomputer memory.

The conflicting requirements of a large image size and small computer memory put certain constraints on the program structure. The use of "windows" or small areas of picture data in memory was considered difficult since a conglomeration of criss-crossing tracks could cover an arbitrary size area. There thus is no guarantee that the image of even one set of criss-crossing tracks could be wholly contained in the memory. Instead, the image is processed line-by-line, where only one or a few lines are in the memory at a time. This, of course, means that a track is practically never "wholly visible" to the computer.

9.2.4 The present processing sequence

The fundamental choice to be made is whether to direct the programming effort specifically towards the alpha particle track problem or to use a more generalized approach where the tracks are only a special case. The generalized approach is, of course, far more attractive from the research point of view, even though it results in rather

extensive computations and is slower than an efficient specialized alternative. The danger in the specialized approach is the lack of appreciation of all the difficulties that will be encountered which, if they cannot be resolved, will be blamed on poor picture quality.

In a research environment devoted to picture processing a fair set of applicable programs is already available, frequently accompanied by a picture processing philosophy. Consequently, the path of least resistance is to use whatever programs and methodologies are applicable, and to add new ones as required until a processing sequence has been established for pilot runs. Based on the experience gained and results obtained the practical realization of a production setup can now be evaluated.

Opinions differ as to the actual algorithms to be used (Pavlidis and Steiglitz, 1976, and McIlwain, 1976). It is unlikely that one unique best method exists for solving a reasonably complicated picture processing problem. The merit of a processing method is in its results. In our case the following sequence of processing steps has been tried, and their successes and failures illustrated.

1) An enlarged film transparency (35 mm) is scanned in a region where a characteristic set of tracks can be seen. An example is shown in Figure 9.1a. The scanned pixels are written as one logical record per scan line: 161 records of

256 pixels in the present case.

2) The scanned gray level image is high pass filtered to remove some scanner shading (Figure 9.1b) and the result thresholded to obtain a black and white or binary image (Figure 9.2a).

3) For every pixel on a track the distance to its closest contour is computed in order to estimate the average thickness of each track.

4) The binary image is thinned to one element thick lines (Figure 9.2b) by using a 8-neighbour rule. The thinning simplifies slope computations but is mainly carried out to facilitate the location of junctions between crossing line elements and the listing of their connectivity.

The black and white conversion and subsequent thinning results in some information loss. However, it is believed that this loss is outweighed by the resultantm simplification of the problem. Specialized track sharpening at the gray level stage will be required since some of the tracks tend to breack.

5) The junction points between crossing tracks are detected and numbered sequentially. This segments all crossing lines at the junctions. The resultant line elements will be called segments. A segment may thus have:

a) No junction, in which case it is a free standing line consisting of one or more alpha particle tracks.

Figure 9.1b: The scanned and high pass filtered image of the framed area in Figure 9.1a. The image contains 161 rows of 256 picture elements.

Figure 9.2a: Binary representation of the scanned image in Figure 9.1b. This black and white representation has been obtained by simple thresholding.

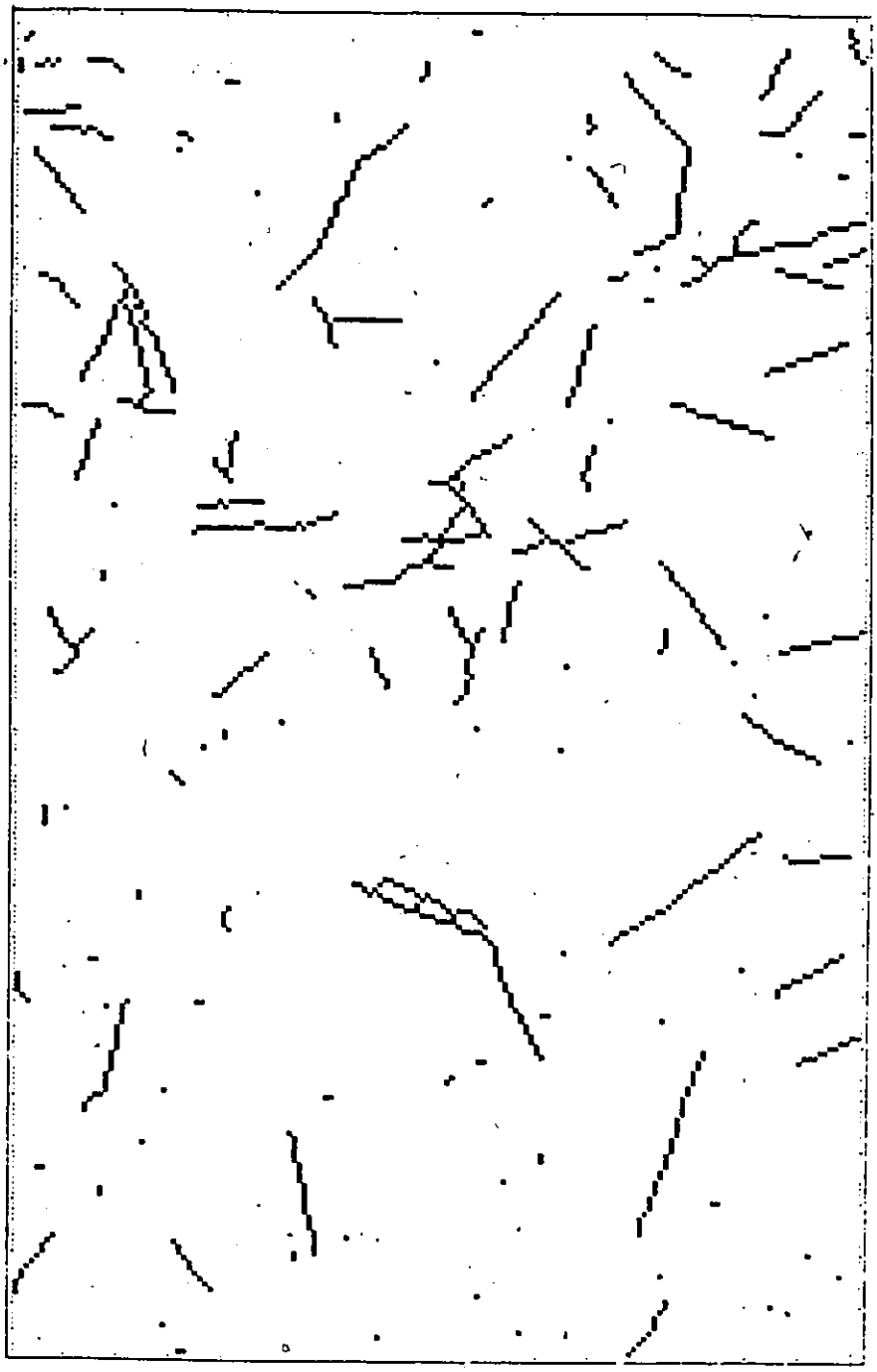

Figure 9.2b: The thinned binary image obtained by thinning Figure 9.2a using an 8-neighbour rule. Computer analysis of the alpha particle tracks is based on this image.

b) A single junction point.

c) Two junction points.

A segment in cases (b) and (c) may consist of a single track connected at ends, a line consisting of multiple tracks joined end-to-end or a part of a track. Basically all combinations are possible.

6) Since the machine "sees" only one or a few scan lines at once, i.e. only a few scan lines are in computer memory, each segment is given a unique label (serial number). At this point in the processing, the binary picture contains serially numbered junctions and serially numbered segments, illustrated in Figures 9.3a, 9.3b. Due to the unequal character and line spacing on a printer, all these pictures are stretched vertically. The letters symbolize segment numbers and the numerals junction numbers. The dots represent the background. The segments can be tabulated individually and their connectivity at a junction can be determined uniquely.

7) Compute the local slopes of the line segments and smooth these values once or twice.

8) Based on the local slopes, it was initially expected that either a slope histogram or a point-to-line transformation (Duda and Hart, 1973) per segment could be used to partition a segment if it consisted of several tracks.

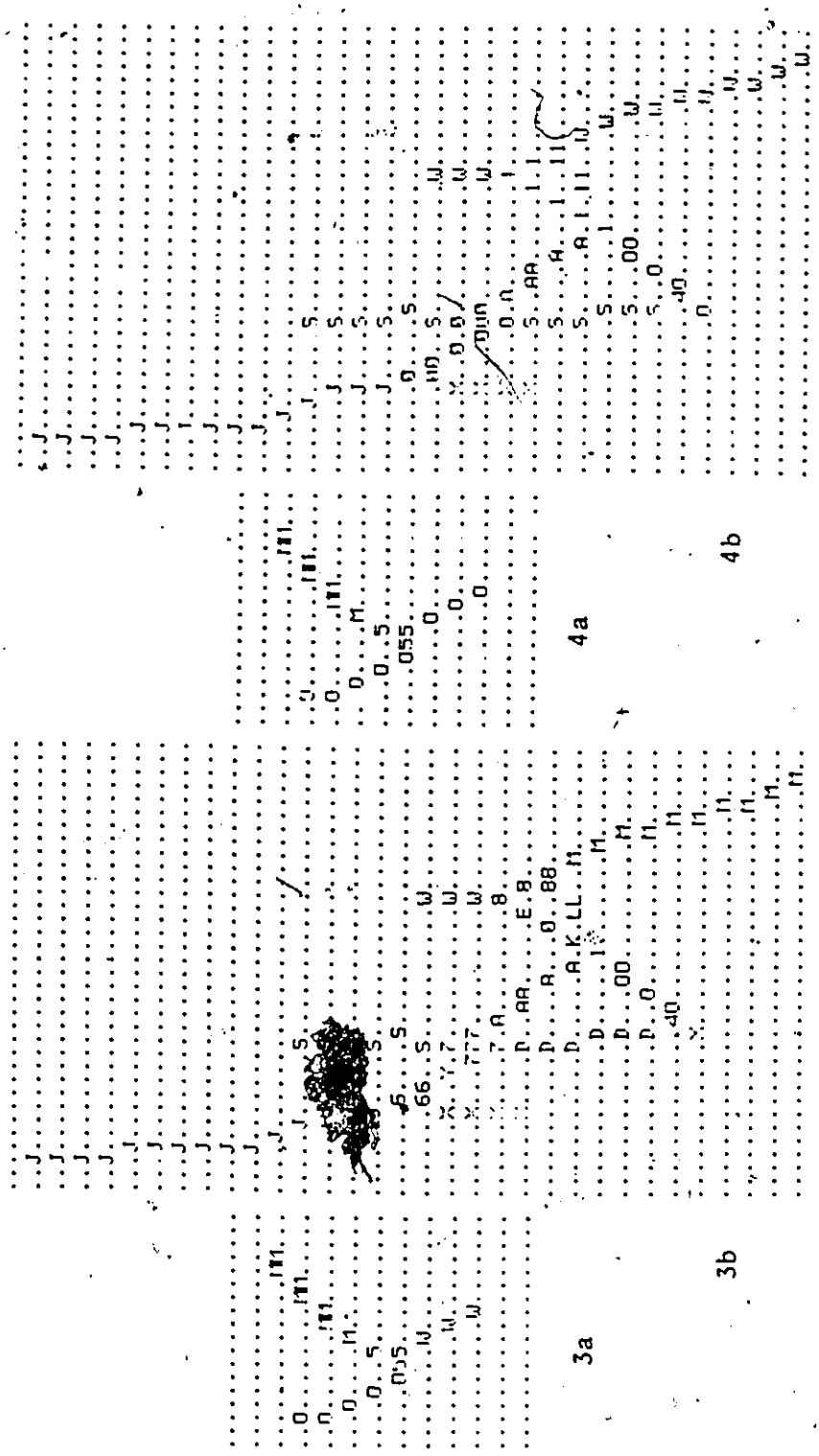

Figure 9.3a: A simple T junction between two tracks.
Figure 9.3b: A more complex track cluster.
Figure 9.4a: Track cluster in Figure 9.3a after processing, giving two identified tracks labelled O and M.
Figure 9.4b: Track cluster in Figure 9.3b after processing.

However, too many counter-examples have been found. Straight line fitting algorithms are now also under development. When these experiments are complete, and no new complications arise, each segment which is not straight will be broken at the "kinks", by introducing new junctions. For simplicity, all segments will be relabelled resulting in a picture of junctions and straight line segments.

At the moment this computation stage is bypassed. Since most of the joining segments are reasonably straight, the connectivity algorithms can be tested irrespective of the missing processing step. The overall track count, however, cannot be used, but the results of machine counting of individual track clusters can be checked.

9) The individual segments meeting at every junction are checked to determine whether they can be connected. If a reasonably straight composite segment can be formed of two segments meeting at a junction, this connection is made, and the segment and junction tables are updated. This process is iterated until no further segment joining is possible.

10) As usual, a whole series of unexpected problems arose. The complicated junctions frequently consist of several neighbouring junctions separated by segments which are only one or few pixels long. A typical case is shown in Figure 9.3b. The solution adopted at the moment is to amalgamate doubly connected short segments (i.e., segments connected at

each end) and junctions. This makes the neighbouring junctions merge, resulting in larger junction regions but allows the connectivity algorithms (in step 9) to proceed past such imperfect junctions. The pixels forming the junction are added to the composite segments to obtain a reasonably accurate measure of track length.

11) Processing steps 9 and 10 are iterated until no further segment connectivity takes place. In most of the cases the resultant connectivity is quite comparable to human performance, given the somewhat degraded thinned binary image as a starting point. Several separated track clusters are shown in Figures 9.4a, b, c, and d. Of course, somewhat comical results may also occur, (Figure 9.4e) while the count may still be correct.

12) Except for certain problem areas to be discussed separately, the computational aspects of this problem are now no longer in the picture processing realm. A table of results is available which contains:

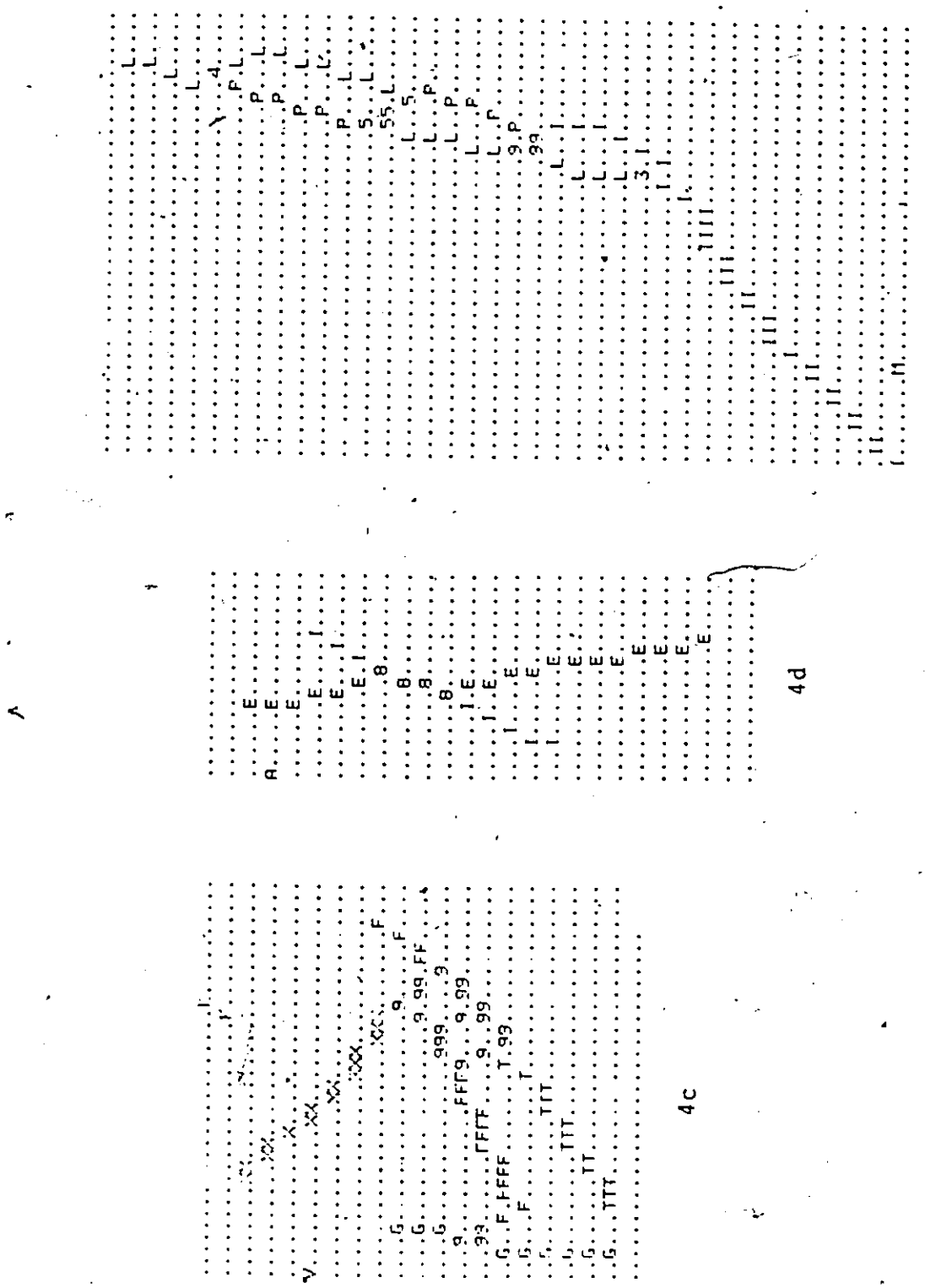

Figure 9.4c: Another resolved track cluster.
Figure 9.4d: Two tracks crossing at about 60 degrees.
Figure 9.4e: Example of two close parallel tracks intersecting a third track at high angle.

a) The track number, i.e. the final serial number assigned to the joined segments.

b) Junction number(s) to which the track may still be connected but further amalgamation cannot take place.

c) The average slope of the track.

d) The length of the track, i.e. its pixel count.

e) The average track thickness.

f) The average gray level along the thinned track (if wanted).

g) The x-y coordinates of the track center.

Additional information on track linearity, its "stringiness" (length/width ratio), average gray level, etc. is or can be made available to form a decision space for recognizing tracks from other artifacts. Furthermore, the basis of an interactive display and verification stage now exists.

9.2.5 Some remaining problem areas

As already mentioned, the gray level image needs further filtering to prevent fragmentation of weak tracks in the binary image. At the same time, however, close parallel tracks or tracks crossing at a very shallow angle should be converted to a proper image to allow the

thinning algorithm to work properly. Figure 9.4e illustrates one such case. Two parallel and touching tracks may only be distinguishable by their nearly double widths.

Another problem is a track in the picture plane crossed by another track nearly vertical to the picture plane. In this case the track contains a dot. Given proper film the gray level density at the crossing point can be higher than along the rest of the track. However, the gray level density alone cannot be used since similar density values occur at two crossing tracks.

Two colinear tracks joined at their ends will form a track with higher density at the junction point. In appearance the resultant track would be very similar to a long track crossed at nearly right angle to the picture plane by another track. Thus the track count is likely to be correct but the interpretation will be incorrect.

The large blobs of black and the very small points are relatively easy to distinguish based on the distance to closest contour and density measures.

9.2.6 Conclusions

A rather lengthy sequence of processing algorithms is described and illustrated to solve the alpha particle

track counting problem. From the practical point of view, the present solution may be too research oriented and lengthy to be of direct practical use. However, considerable simplification of programs is possible, and many processing steps can be collected into a single program.

Due to some unexpected problem areas, the string of algorithms is not yet complete, but the major problems, it is believed, have been solved. The programs allow overlapping curved tracks to be studied, connected, measured and counted. The constraint of straightness, posed by the alpha particle tracks is only used in two places, namely at the segment joining stage where additional decision parameters have been zeroed, and at the segment linearity checking stage, which for the moment is incomplete.

Even though overall counting comparisons between man and machine are not available, the problem of track-clusters, which poses one of the major difficulties for automatic counting is basically solved. The complexity of the required mechanized solution illustrates the variety of procedures available to the human when solving similar problems. To "understand" a picture we ourselves apply a variety of methods to the problem, both with ease and without necessarily even being aware of all the complications. Obviously, if a machine is to rival human performance, each and every processing step has to be described

logically.

The approach presented in this paper can be applied to other types of images in which straight or curved line patterns occur, as was done by Kasvand (1978 and 1979), for paper pulp fibers and for Chinese ideograms. One of its advantages is that the output of these algorithms provide tables of labelled components which can be used for statistical analysis of individual segments. The method represents an alternative to optical processing for quantification and selective extraction of linear features from maps or photographs in fracture trace analysis (Norman, Price and Peters, 1977, and Harnett and Barnett, 1977).

9.2.7 Acknowledgement

Gratitude is is expressed to Mr. S. Kaiman, Canada Centre for Mineral and Energy Technology, for suggesting the problem and provoding useful assistance.

9.2.8 Additional remarks

Later developments of this study has completed the sequence of algorithms by introducing an additional pro-

cessing step between steps (5) and (6) of Subsection 9.2.4. In this step, all places on the lines where major changes of direction occur ("kinks") are located and the pixel at the kink is removed in order to break the lines (Fabbri and Kasvand, 1980). The introduction of this step, allows satisfactory overall counting correspondence between man and machine.

10. Epilogue

This thesis work spans through three different aspects of geological image processing: the philosophical approach of image processing in geology, the programming of the image processing software, and also several applications to geological problems including one pattern recognition experiment. Any undertaking which covers all the three aspects, is certain to be a heavy committment. This thesis resulted in a work which was of necessity much underestimated both in time and labour, and most of all in the complexity of the problems met during the study.

It was important to experience concretely the consequences of the suggested approach with applications of the dimensions and the chracter of conventional geological studies. For this reason the analysis of considerably large (1000 pixels x 1000 pixels) images was performed at some depth for either geological map patterns or microscopic images from thin sections of rocks.

It is of interest that such applications were not started at the completion of the computer programming, i.e., in the order of the chapters of the thesis. On the contrary, the applications started almost immediately. The problems encountered in those applications, and the

solutions required, were the best guidance for building the necessary software. It was the continuous feedback during the applications which helped in correcting both the philosophical side of the approach, and the type of processing.

This exercise made the author aware of how difficult it is to convey novel ideas and methods to the other geologist colleagues, without taking personally part in the practical applications, i.e., there, where the real problems manifest themselves.

Let us now make a "summing up" of the present study and then conclude with some outlook on the possible developments of image processing in geology at least within the framework of this thesis.

A general statement on geological images and how they can be useful is made first in Chapter 1. Chapter 2 describes a small computer dedicated to general image processing. Chapter 3 introduces the software package GIAPP which enables the geologist to perform the processing himself. Mention of the structure of the package and some of the more relevant algorithms in GIAPP is made in Chapter 4. Chapter 5 justifies, from a programmer's point of view, the particular kind of processing proposed. Parallel processing and processors, stereology, mathematical morphology and image analysis are the fields from

which support for the analysis of geological data by image processing methods is sought. Simple examples of the processing of binary geological images are illustrated in Chapter 6. It is only in Chapter 7 that a case history application to the study of regional mineral resources is made. In that application a set of large images in registration with one another is used. The description of the experiments is preceeded by a detailed account of the required digitization and preprocessig steps. Chapter 8 describes the scanning of line drawings from thin sections of rocks and the preprocessing related to this type of digitization. Two applications are made in the chapter to a previously studied granulite in search for a pattern, and to an amphibolite for comparing the performance of an image analyzer (hardware based approach) with that of the software programmed on a minicomputer (software based approach). In Chapter 9, which is entitled "Towards pattern recognition", a first experiment is made of truly automatic processing. Chapter 10, this chapter, is a "summing up" of the work done. Appendices follow the chapters, containing: the list of references cited, Appendix A; GIAPP's user's guide, Appendix B; and the organizational flowcharts of the programs and routines in the package, Appendix C. As mentioned earlier in Chapter 2, the source listings of the Fortran programs and

routines, and those of the machine routines, in GIAPP will be available as a separate technical report (Fabbri, 1981).

What are the consequences of this study? Is image processing really usable in geology? Should we expect more in future, or should we consider this experiment as an isolated peculiar venture, destined to remain in the records of the methods which are searching for an application?

Of course a complete answer to such questions cannot be provided by this work. However, the applications performed, suggest that many geological problems can be formulated with models and can be presented in forms which are very similar to image processing problems. The capability of a computer to complement human vision in some quantitative tasks, and to perform as an interactive helper is being currently exploited by many geologists. New powerful techniques for the definition and subsequent recognition of desirable "environments" in economic geology are needed because of the demands for resources estimation.

As the automobile represents an extension of our senses - we can actually feel a boulder under the wheel of our car almost as if we touched it - or as the microscope gives us the opportunity to penetrate the microcosmos -

where our eyes cannot see by themselves - so computer processing can tell us something about the properties of crystalline fabrics. It can also quantitatively characterize those properties in a systematic manner which is often entirely beyond our physical means. A machine can detect a foliation that we cannot see but we suspect that exists. The machine can tell us how much is a set of crystal profiles more strongly oriented than another set; it can also count objects, faithfully and persistently, relieving us of tedious and error prone mechanical tasks in which we would not like to be involved. Of course this machine does require our guidance in order to perform with any intelligence.

The applications made here, have a main purpose. A geologist should not be afraid to use a novel technology, because as soon as the suspiciousness for the machine and for its rules has been overcome, he has a faithful assistant for expanding his work in many conventional studies but also in some new systematic aspects of his research work.

While the applications have the main purpose of enriching the software of algorithms which could not be imagined without practice, they also want to familiarize the geologist with the image processing approach by way of example. It is the author's hope, that this heavy

committment has produced at least a modest contribution in communicating with the geological community.

10.1 Publications

Several papers have been produced from the material of this thesis, and are either published or under submission.

The content of the pubblications, however, not always corresponds to that of the thesis, since much of it is still entirely unpublished, and also because some of the papers represent applications beyond the purpose of the thesis. They are as follows.

(1) "Automatic counting of alpha-particle tracks from autoradiographs of radioactive minerals" (Kasvand and Fabbri, 1978), described in Chapter 9.

(2) "Spatial correlation of stratigraphic units quantified from geological maps" (Agterberg and Fabbri, 1978a), described in Chapter 6.

(3) "Statistical treatment of tectonic and mineral deposit data" (Agterberg and Fabbri, 1978b), partly related to this thesis.

(4) "Picture processing of geological images" (Fabbri and Kasvand, 1978), described partly in Chapter 5.

(5) "Implementation of an interactive system for comput-

er processing of geological images" (Fabbri, Kasvand, and Stray, 1978), described in Chapter 2.

(6) "GIAPP: geological image analysis program package for estimating geometrical probabilities" (Fabbri, 1980), partly described in Chapters 5 and 6.

(7) "A picture processing approach to stereological problems" (Fabbri and Kasvand, 1980e, partly related to this thesis.

(8) "Experiments on the characterization of metamorphic textures from a micrograph of an amphibolite" (Fabbri and Masounave, 1980), described in Chapter 8.

(9) "Applications at the interface between pattern recognition and geology" (Fabbri and Kasvand, 1981), described in Chapters 7,8, and 9.

(10) "Digitization and processing of large regional geological maps" (Kasvand, Fabbri, and Nel, 1981), partly related to the content of Chapter 7.

(11) "Preliminary geomathematical analysis of geological, mineral occurrence and geophysical data, Southethern District of Keewatin, Northwest Territories" (Agterberg et al, 1981), partly related to the content of Chapter 7.

Appendix A

List of references cited

List of references cited

A.G.I., 1957, Dictionary of geological terms: Prepared under the direction of the American Geological Institute, Garden City, New York, Dolphin Books Doubleday & Company Inc., 575 p.

Agterberg, F. P., 1967, Computer techniques in geology: Earth Sci. Rev., v. 3, p. 47-77.

Agterberg, F. P., 1974, Geomathematics: Amsterdam, Elsevier Scientific Publishing Company, 596 p.

Agterberg, F. P., 1977, Quantification and statistical analysis of geological variables for mineral resource evaluation: Procs. Goguel Colloquium on Earth Sciences and Management, Orléans, France, in Sciences de le Terre et Mesures, Mémoir du B.R.G.M., nº. 91, 1978, p. 399-406.

Agterberg, F. P., 1978, Analysis of spatial patterns in the Earth Science: in Merriam, D. F., Ed., Geomathematics, past, present, and prospects: Syracuse University, Geology Contribution 5, p. 7-18.

Agterberg, F. P., 1979, Algorithm to estimate the frequency values of rose diagrams for boundaries of map features: Computers and Geosciences, v. 5, p. 215-230.

Agterberg, F. P., Chung, C. F., Divi, S. R., Eade, K.

E., and Fabbri, A. G., 1980, Preliminary geomathematical analysis of geological, mineral occurrence, and geophysical data, Southern District of Keewatin, Northwest Territories: Geol. Surv. Canada, Open File 718 (in press).

Agterberg, F. P., Chung, C. F., Fabbri, A. G., Kelly, A. M., and Springer, J. S., 1972, Geomathematical evaluation of copper and zinc potential of the Abitibi area, Ontario and Quebec: Geol. Surv. Canada Paper 71-41, 55 p.

Agterberg, F. P., and Fabbri, A. G., 1978a, Spatial correlation of stratigraphic units quantified from geological maps: Computers and Geosciences, v. 4, p. 285-294.

Agterberg, F. P., and Fabbri, A. G., 1978b, Statistical treatment of tectonic and mineral deposit data: Global Tectonics and Metallogeny, v.1, p. 16-28.

Andrews, H C., 1970, Computer techniques in image processing: New York, Academic Press, 187 p.

Anuta, P. E., Hauska, H., and Levandowski, D. W., 1976, Analysis of geophysical remote sensing data using multivariate pattern recognition techniques: Proceedings of Symposium on Machine Processing of Remotely Sensed Data, June 25-July 1, 1976, Purdue Univ., West Lafayette, Indiana, Inst. Electr. Electron. Eng.,

Inc. Catalog No. 76ch1103 MPRSD, p. 1B-11, 1B-14.

Bernroider, G., 1978, The foundation of computational geometry: theory and application of the point-lattice-concept within modern structure analysis: in Miles, R. L., and Serra, J., Eds., Geometrical probability and biological structure: Buffon's 200th anniversary: New York, Springer-Verlag, 338 p., p. 153-170.

Bouille, F., 1976, Graph theory and digitization of geological maps: Jour. Int. Assoc. Math. Geol., v. 8, p. 375-393.

Byerly, G. R., and Vogel, T. A., 1973, Grain boundary processes and development of metamorphic plagioclase: Lithos, v. 6, p. 183-202.

Chadwick, A., and Smith, D. A., Eds., 1976, Grain boundary structure and properties: New York, Academic Press, 388 p.

Chen, C. H., 1976, Theory and applications of imagery pattern recognition: National Bureau of Standards Special Pubblication 431, Procs. of the 4th Int. Cong. for Stereology, Gaithersburg, Md., Sept. 4-9, 1975, p. 113-116.

Cheng, G. C., 1976, What can pattern recognition do for stereology: National Bureau of Standards Special Pubblication 431, Procs. of the 4th Int. Cong. for Stereology, Gaithersburg, Md., Sept. 4-9, 1975, p.

107-112.

Chermant, J. L., and Coster, M., 1978: Fractal object in image analysis, in International Symposium on Quantitative Metallography: Symposium Papers, Florence, Nov. 21-23, 1978, Associazione Italiana di Metallurgia, Eds., p. 125-138.

Chung, C. F., 1979, A system of interactive graphic programs for multivariate statistical analysis for geological data: Procs. 12th Symp. on Interface of Computer Sciences and Statistics, Univ. of Waterloo, p. 452-456.

Cole, M., 1971, Instrument errors in quantitative image analysis: Microscope, v. 19, p. 87-103.

Cooker, N. B., 1976, Geochemical follow-up studies, Northwestern Manitoba: Geol. Surv. Canada, Paper 76-1C, p. 263-267.

Cruttwell, I. A., 1974, Pattern recognition by automatic image analysis: Microscope, v. 22, p. 27-37.

Delesse, M. A., 1848, Procédé mécanique pour déterminer la composition des roches: Ann. Mines, v. 13, p. 379-388.

De Vore, G. W., 1959, Role of minimum interfacial free energy in determining the macroscopic features of mineral assemblages: I. The model: Jour. of Geology, v. 67, p. 211-227.

Duda, R O., and Hart, P E., 1973, Pattern Classification and Scene Analysis: New York, John Wiley & Sons, 482 p., (pages 335 and 373).

Erlich, R., Vogel, T. A., Weinberg, B., Kamilli, D. C., Byerly, G, and Richter, H., 1972, Textural variations in petrogenetic analyses: Geol. Soc. Am. Bull., v. 83, p. 665-676.

Fabbri, A. G., 1975, Design and structure of geological data banks for regional mineral potential evaluation: Can. Inst. Mining Metall. Bull., v. 68, p. 91-98.

Fabbri, A. G., 1980, GIAPP: geological image analysis program package for esimating geometrical probabilities: Computers and Geosciences, v. 6, p. 153-161.

Fabbri, A. G., 1981, Source listings for the geological image program package GIAPP, operational on a Modcomp II computer: Nat. Res. Council Canada, Elec. Eng. Division, ERB Report (in press).

Fabbri, A. G., Divi, S. R., and Wong, A. J., 1975, A data base for mineral potential estimation in the Appalachian Region of Canada: in Report of Activities, Part C, Geol. Surv. Can., Paper 75-1C, p. 123-132.

Fabbri, A. G., and Kasvand, T, 1978, Picture processing of geological images: in Current Research, Part B, Geol. Surv. Can., Paper 78-1B, p. 169-174.

Fabbri, A. G., and Kasvand, T., 1980, A picture processing

approach to stereological problems: Procs. 5th Int. Cong. for Stereology, Salzburg, Austria, Sept. 4-8, 1979, Microscopica Acta (in press).

Fabbri, A. G., and Kasvand, T., 1981, Applications at the interface between pattern recognition and geology: Sciences de la Terre (in press).

Fabbri, A. G., Kasvand, T., and Stray, J. H., 1978: Implementation of an interactive system for computer processing of geological images: in Current Research, Part C, Geol. Surv. Can., Paper 78-1C, p. 123-124.

Fabbri, A. G., and Masounave, J., 1980, Experiments on the characterization of metamorphic textures from a microphotograph of an amphibolite: 5th International Congress for Stereology, Salzburg, Austria, Sept. 4-8, 1979, Journal of Microscopy (in press).

Flinn, D., 1969, Grain contacts in crystalline rocks: Lithos, v. 3, p. 361-370.

Gibb, R. A., and McConnell, R. K., 1969,The gravity anomaly field in Northern Manitoba and Northeastern Saskatchewan with maps No. 68 to 76: Gravity Map Series of the Dominion Observatory, Ottawa, Canada 28 p.

Gillies, A. W., 1978, An image processing computer which learns by example: in Nevatia, R., Ed., Image understanding systems and industrial applications: Proc.

of the Soc. of Photo-Optical Instrumentation Engineers, SPPIE, Aug. 30-31, 1978, Sandiego, California, v. 155, p. 120-126.

Goetcherian, V., 1980, From binary to grey tone image processing using fuzzy logic concepts: Pattern Recognition, v. 12, p. 7-15.

Golay, M. J. E., 1969, Hexagonal parallel pattern transformations: IEEE Transactions on computers, v. C-18, p. 733-740.

Graminski, E. L., and Kirsh, R. A., 1977, Image analysis in paper manufacturing: Procs. of the IEEE Computer Society Conference on Pattern Recognition and Image Processing, June 6-8, 1977, Troy, New York, v. 77CH1208-9C, p. 137-143.

G. S. C., 1975, Airborne gamma-ray spectrometric survey: Resources Geophysics and Geochemistry Division, Geol. Surv. Canada, Open Files 317 and 318.

Haralick, R. M., 1979, Statistical and structural approaches to texture: Procs. of the IEEE Society, v. 67, p. 786-804.

Harnett, P. R., and Barnett, M. E., 1977, Optical rose diagrams for lineament analysis: Trans. Instn. Min. Metall. (Sect. B: Appl. earth sci.), v. 86, p. B102-B106.

Hobbs, B. E., 1966, Microfabric of tectonites from the

Wyangala Dam Area, New South Wales: Geol. Soc. Am. Bull., v. 77, p. 685-706.

Hougardy, H. P., 1975, Automatic image analysing instruments today: Proc. 4th Int. Cong. for Stereology, Gaithersburg, Maryland, NBS Special Publication 431, p. 141-148.

Jen, L. S., 1975, Spacial distribution of crystals and phase equilibria in charnockitic granulites from the Adirondack Mountains, New York: University of Ottawa, unpublished Ph. D. thesis.

Jesse, A., 1971, Quantitative image analysis in microscopy - a review: Microscope, v. 19, p. 21-30.

Johnston, e. g., 1970, The PAX II picture processing system: in Lipkin, B. S., and Rosenfeld, A., Eds., Picture processing and psychopictorics: New York,- London, Academic Press, 526 p., p. 427-512.

Jones, E. J., 1975, Practical aspects of counting asbestos on the Millipore . MC: Microscope, v. 23, p. 93-101.

Kasvand, T., 1972, Experiments with an online picture language, in Watanabe, S., Ed., Frontiers of Pattern Recognition: New York, Academic Press, 602 p., p. 223-264.

Kasvand, T., 1978, Experiments on automatic extraction of paper pulp fibers: Proc. of the 4th Joint Conf. on Pattern Recognition, Kyoto, Japan, Nov. 7-10, 1978.,

p. 958-960.

Kasvand, T., 1979, Ideogram segmentation and recognition: Procs. of the Int. Conf. on Cybernetics and Society, Oct. 1979, I. E. E. E., v. CH1424-1/79/0000-0674, p. 674-678.

Kasvand, T., and Fabbri, A. G., 1978, Automatic counting of alpha-particle tracks from autoradiographs of radioactive minerals: Procs. Eighth Annual Automatic Imagery Pattern Recognition Symposium, April 3-4, 1978, National Bureau of Standards, Gaithersburg, Maryland, Kirsch, R. A., and Nagel, R. N., Eds., p. 11-26.

Kasvand, T., Fabbri, A. G., and Nel, L. D., 1981, Digitization and processing of large regional geological maps: Nat. Res. Council Canada, Elec. Eng. Division, ERB Report (in press).

Kasvand, T., Hamill, P., Bora, K C., and Douglas, G, 1975, Experimental online karyotyping at the National Research Council of Canada: In Mendelson, M. L.,Ed., Automation of Cytogenetics: Asilomar Workshop, Pacific Grove, California, Nov. 30-Dec. 2, 1975, p. 96-109.

Kirsh, R. A., 1957, Processing pictorial information with digital computers: Am. Inst. Elecrical Engineers, v. CP-57-878.

Kirsh, R. A., Cahn, L., Ray, C., and Urban, G. H., 1957, Experiments in processing pictorial information with a

digital computer: Procs. Eastern Joint Computer Conf., 221 p., p.221-229.

Klein, J. C., and Serra, J., 1972, The texture analyser: Jour. of Microscopy, v. 95, p. 349-356.

Kovasznay, L. S. G., and Joseph, H. M., 1955, Image processing: Procs. of IRE, v. 43, p. 560-670.

Kretz, R., 1966a, Grain size distribution for certain metamorphic minerals in relation to nucleation and growth: Jour. of Geol., v. 74, p. 147-173.

Kretz, R., 1966b, Interpretation of the shape of mineral grains in metamorphic rocks: Jour. of Petrology, v. 7, p. 68-94.

Kretz, R., 1969, On the spatial distribution of crystals in rocks: Lithos, v. 2, p. 39-65.

Kretz, R., 1978, Distribution of Mg, Fe^{2+} and Mn in some calcic pyroxene-hornblende-biotite-garnet gneisses and amphibolites from the Grenville Province: Jour. Geology, v. 86, p. 599-619.

Leech, G. B., 1975, Project Appalachia: Geol. Surv. Can. Paper 75-1, Part C, p. 121-122 (introduces 8 reports in ibidem, p. 123-173).

Mahan, S. M., and Rogers, J. J. W., 1968, A study of grain contacts in some high grade metamorphic rocks: Am. Mineralogist, v. 53, p. 323-327.

Matheron, G., 1972, Elements pour une theorie des milieux

poreux: Paris, Masson & Cie. Eds., 166 p.

Matheron, G., 1975, Random sets and integral geometry: John Wiley & Sons, New York, 261 p.

McCormick, B. H., 1963, The Illinois pattern recognition computer- ILLIAC III: IEEE Trans. Electronic Computers, v. EC-12, p. 791-813.

McIlwain, R. L., Jr., 1976, Image processing in High Energy Physics: in: Topics in Applied Physics, Volume 11, Rosenfeld, A., Ed., Digital Picture Analysis: New York, Springer-Verlag, 1976, 351 p., p. 151-207.

Merriam, D. F., 1981, The roots of quantitative geology: manuscript in preparation (personal communication).

Moore, A. G., 1968, Automatic scanning and computer processes for the quantitative analysis of micrographs and equivalent subjects: in Cheng, G. C., Ledley, R. S., Pollock, D. K., and Rosenfeld, A., Eds.: Pictorial pattern recognition: Washington D. C., Thompson Book Co., 521 p.

Muller, W., 1974, The LEITZ-Texture-Analysing-System (LEITZ - T.A.S.): Leitz Scientific and Technical Information, Suppl. 1,v. 4, p. 101,116.

Norman, J. W., Price, N. J., and Peters, E. R., 1977, Photogeological fracture trace study of controls of kimberlite intrusion in Lesotho basalts: Trans. Intn. Min. Metall. (Sect. B: Appl. earth sci.), v. 86.

p. B78-B90.

Pavel, M., 1976, Projectors in pattern recognition categories: National Bureau of Standards Special Pubblication 431, Procs. of the 4th Int. Cong. for Stereology, Gaithersburg, Md., Sept. 4-9, 1975, p. 133-138.

Pavlidis, T., and Steiglitz, K, 1976, The automatic counting of asbestos fibers in air samples: Procs. of the IEEE Computer Society, The Third Joint Conference on Pattern Recognition, Nov. 8-11, 1976, Coronado, California, v. 76CH1140-3C, p. 789-792.

Petruk, W., 1976, The application of quantitative mineralogical analysis of ores to ore dressing: Can. Inst. Min. Metal. Bul., v. 69, p. 146-153.

Preston, F. W., and Davis, J. C., 1976, Sedimentary porous materials as a realization of stochastic processes, in Merriam, D. F., Ed., Random processes in geology: Springer-Verlag, New York, p. 63-86.

Preston, K., Jr., 1971, Use of the Golay logic processor in pattern-recognition studies using hexagonal neighborhood logic: in Fox, J., Ed., Computers and Automata: New York, Polytechnic Press, p. 609-623.

Preston, K. Jr., Duff, M. J. B., Levialdi, S., Norgren, P. E., and Toriwaki, J-i., 1979, Basics of cellular logic with some applications in medical image processing: Procs. of the IEEE, v. 67, p. 826-858.

Rink, M., 1976a, A new, fast and storage-saving image analysis procedure for investigating individuals by a digital computer:National Bureau of Standards Special Pubblication 431, Procs. of the 4th Int. Cong. for Stereology, Gaithersburg, Md., Sept. 4-9, 1975, p. 117-120.

Rink, M., 1976b,A computerized image process for isolating individuals in an originally netted pattern: National Bureau of Standards Special Pubblication 431, Procs. of the 4th Int. Cong. for Stereology, Gaithersburg, Md., Sept. 4-9, 1975, p. 155-158.

Roberts, F., and Young, J. Z., 1952, The flying-spot microscope: Proc. Inst. Elec. Engrs., v. 99, p. 747-757.

Rogers, A. W., 1973, Techniques of autoradiography: Amsterdam, Elsevier Scientific Pub. Co., 372 p.

Rogers, J. J. W., 1961, Origin of albite in granitic rocks: Amer. Jour. of Sci., v. 259, p. 186-193.

Rogers, J. J. W., and Bogy, D. B., 1958, A study of grain contacts in granitic rocks: Science, v. 127, p. 470-471.

Rosenfeld, A., and Kak, A. C., 1976, Digital picture processing: New York, Academic Press, 457 p.

Schledewitz, D. C. P., 1978, Patterns of regional metamorphism in the Churchill Province of Manitoba (North of

58°):in Metamorphism in the Canadian Shield, Geol. Surv. Can., Paper 78-10, p. 179-190.

Serra, J., 1966, Remarques sur une lame mince de minerai lorrain: Bull. B.R.G.M., v. 6, p. 1-36.

Serra, J., 1967, Buts et réalization de l'analyseur de textures: Revue de l'Industrie Minérale, v. 49, 9 p.

Serra, J., 1970, Device for logical analysis of textures. Inventor: J. Serra.- Assignesss: Association pour la Recherche et le Développement de Processus Industriels (A. R. M. I. N. E. S.), and J. Serra. First application in France, No. 70 21 322, June 10, 1970. (Patented in Austria, Canada, England, Germany, U. S. A.- Application in Japan).

Serra, J., 1974, Theoretical bases of the LEITZ-Texture-Analysing-System: Leitz Scientific and Technical Information, Suppl. 1,v. 4, p. 125-136.

Serra, J, 1975, "Automatic scanning device for analyzing textures". Inventor: J. Serra.- Assignee: Institute de Recherches de la Sidérurgie Francaise (I. R. S. I. D.) First application in France. No. 1.449.059, July 2, 1965. (Patented in Belgium, Canada, England, Germany, Japan, Sweden, U. S. A.).

Serra, J., 1975, 15 Fascicules de morphologie mathmatique, Fontainebleau, France, Jan. 1975 (papers by Chauwe, P. H., Serra, J., Digabel, H., Klein, J. C., Lorrain, M.,

and Naert, B.), 151 p.

Serra, J., 1976, Lectures on image analysis by methematical morphology: Centre de Morphologie Mathématique, Fontainebleau, France, Cahier N-475, July 1976, 225 p.

Serra, J., 1978, One, two, three,... infinity: in Miles, R. L., and Serra, J., Eds., Geometrical probability and biological structure: Buffon's 200th anniversary: New York, Springer-Verlag, 338 p., p. 137-152.

Serra, J., and Muller, W., 1974, In quantitative image analysis. The problem of resolution errors caused by measuring logic: Leitz Scientific and Technical Information, Suppl. 1,4, p. 101,116. Leitz Scientific and Technical Information, Suppl. 1, v. 4, p. 117-124.

Skinner, R., 1974, Geology of the Tetagouche Lakes, Bathurst, and Nepisiguit Falls Map-areas, New Brunswick: Geol. Surv. Canada Memoir 371, 133 p.

Sternberg, S. R., 1978, Cytocomputer real-time pattern recognition (abst.), in 8th Ann. Automatic Imagery Pattern Recognition Symposium Proceedings on "Emerging Pattern in AIPR": National Bureau of Standards, Gaithersburg, Maryland, p. 205.

Soonawala, N. M., Garber, R. J., and Whitworth, R. A, 1979, Follow-up of the uranium reconnaissance program in northwest Manitoba: Can. Inst. of Min. and Metal. Bull., v.72, p. 83-94.

Switzer, P., 1976, Applications of random process models to the description of spatial distributions of qualitative geologic variables: in Merriam, D. F., Ed., Random processes in geology: New York, Springer-Verlag, p. 124-134.

Tamura, H., 1975, Further considerations on line thinning schemes: Assoc. Electr. Comm., Japan, Prof. Note 66, p. 49-56 (in Japanese).

Underwood, E. E., 1970, Quantitative Stereology: Reading, Massachussetts, Addison-Wesley Publ. Co., 274 p.

Unger, S. H., 1958, A computer oriented toward spatial problems: Procs. of IRE, v. 46, p. 1744-1750.

Unger, S. H., 1959, Pattern detection and recognition: Procs. of IRE, v. 47, p. 1737-1752.

Vance, J. A., and Gilreath, J. P., 1967, The effect of synneusis on phenocryst distribution patterns in some porphyritic igneus rocks: The American Mineralogist, v. 52, p. 529-536.

Vernon, R. H., 1976, Metamorphic Processes: Reactions and Microstructure Development:: London, George Allen & Unwin Ltd., and New York, John Wiley, 247 p.

Vistelius, A. B., 1966, Genesis of the Mt. Belaya Granodiorite, Kamchatka (an experiment in stochastic modeling): Acad. Sci. USSR Proc., v. 167, p. 48-50 (Akad. Nauk. SSSR Doklady, v. 167, p. 1115-1118).

Vistelius, A. B., 1969, Preface: Jour. of the Int. Ass. for Math. Geol., v. 1, p. 1-2.

Vistelius, A. B., 1972, Ideal granite and its properties: I. The stochastic model: Internat. Assoc. Math. Geology Jour., v. 4, p. 89-102.

Vistelius, A. B., and Faas, A. A., 1971, The probability properties of sequences of grains of quartz, potassium feldspar, and plagioclase in magmagranites: Acad. Sci. USSR Proc., v. 198, p. 170-172 (Akad. Nauk SSSR Doklady, v. 198, p. 925-928).

Vistelius, A. B., and Romanova, M., 1972, The concept of ideal granites and its use in petrographical survey and search tasks (on material from the Mesozoic granitoids of northeast Asia), in Vistelius, A. B., Ed., Ideal Granites - Issue I (in Russian): Leningrad, Nauka Press, Lab. Math. Geol., Acad. Sci., p. 4-47.

Wadsworth, W. B., 1975, Petrogenetic significance of grain-transition probabilities, Cornelia Pluton, Ajo, Arizona: Geol. Soc. of Am. Memoir 142, p. 257-282.

Watson, G. C., 1975, Texture analysis: Geol. Soc. America Mem. 142, p. 367-391.

Weber, W., Schledewitz, D. C. P., Lamb, C. F., and Thomas, K. A., 1975, Geology of the Kasmere Lake-Whiskey Jack Lake (North Half) Area (Kasmere project): Manitoba Department of Mines, Resources and Environ-

mental Management, Mineral Resources Division, Geological Services Branch, Publication 74-2, 163 p.

Whitfield, J. M., Rogers, J. J. W., and McEwen, M. C., 1959, Relationships among textural properties and modal compositions of some granulitic rocks: Geochim. Cosmochim. Acta, v. 17, p. 272-285.

Whitten, E. H. T., and Dacey, M. F., 1975, On the significance of certain Markovian features of granite textures: Jour. Petrology, v. 16, p. 429-453.

Whitten, E. H. T., Dacey, M. F., and Thompson, K., 1975, Markovian grain relationships of a Grenville granulite: Am. J. Sci., v. 275, p. 1164-1182.

Yagoda, H., 1949, Radioactive measurements with nuclear emulsions: New York, John Wiley & Sons, 356 p.

Appendix B

User's guide for GIAPP.

User's guide for GIAPP.

This user's guide is intended as a set of instructions to interactive processing sessions in GIAPP. It also illustrates in detail the capability of the software and the simplicity with which the system can be run.

The procedures, represented in Appendix C as operational flowcharts, are not necessarily the only working solutions possible: much of GIAPP's versatility lies in the possibility for the user to assemble alternative solutions to processing paths.

The generality of the various routines, called by name in a Fortran-like call in the guide, allows the user to readily allocate storage devices (magnetic tapes or disks), to choose from several I/O devices for input and output of image data, to use several display devices, and to activate a variety of processing algorithms. It then becomes a relatively simple exercise to construct a solution to a given processing task via a preferred sequence of calls to appropriate routines.

/The user's guide gives a short description of each routine, followed by a CALL ROUTINE NAME statement. This contains a list of mnemonic codes, for the calling parameters and the associated addresses, for interactive substitu-

tion of their present values with the new values for a succesfull run. The information is followed by a list of the mnemonic parameter codes, a description of their meaning and the values that they are allowed to assume. When required, some notes to clarify the usage of the routines are also added.

Each description is enclosed in a rectangular box, preceeded by the calling number by which the corresponding routine is activated. The user simply checks that the parameter values are satisfactory and calls the routines by number. In general, after the parameter defaults have been read in, only a few need to be reset for each call (e. g., particular I/O data set, DS, numbers).

As exemplified in Figure 3.4, in running GIAPP any routine can be called after the system prompt "IGOO5:I2" is given, by entering its calling number (05 in the system prompt refers to MASTER 05). The routine name and the values for the parameters are echoed, providing checking and record for future reference (see Figure 3.4). After the routine is run, the system prompt is again given and the next routine can be called. This provides a simple conversation and allows the user to interact at each major step during a session.

In general erroneous conditions for the call or during running af a routine, are detected by the routine, an error

message is generated and the routine is exited after printing on the terminal its name, an error number corresponding to a specific position within the routine, and a list of relevant parameter values which will help to identify the error condition. The control returns to the user who then identifies the cause of error, modifies the parameter values, and proceeds by calling the routine again.

It is advisable to draw a flowchart of the processing prior or during a session in order to facilitate the interpretation of previous runs. The terminal listing, the printer (Versatec) listings and plots, and the photographs of the television (Tektronix) plots will provide complete documentation of the work done.

N O T E

SUPERMASTER I is an "unlabeled system". This means that (1) it does not have automatic file management capabilities, and (2) digital image files do not contain a header, which describes image type and dimensions, nor a commentary, which records the history of processing. The image file consists simply of the pixel values, arranged in records of N pixels (computer words) times M rows. An end-of-file mark is written at the end of each image file.

The image dimensions, the image sequence and its identification should be known in advance to the user because of careful manual bookkeeping. In order to reach the desired file on a magnetic tape, use of calls is required for advancing one end-of-file mark (AVFILE), or for going back past one end-of-file mark (BKFILE), on a given tape mounted on one of the two tape drives available on the computer. The supervision of the subsequent behaviour of the magnetic tape must be exercised.

File elimination is achieved by overwriting its records with another file. Because of the dimensions of the images processed (1024 pixels x 1024 pixels maximum) which can exceed one million computer words, only three input/output, I/O, units are available: the two tape drives and two disks restructured as one single I/O device. Only one image file is allowed to reside on the disks. I/O device numbers allowed are 11, 12, and 17, for MT11, MT12 and the disks, respectively.

A linkage to the labeled systems of image data management in SUPERMASTERS II to V, is obtained by some algorithms which optionally can create labeled image data sets, DS's, on one of the two magnetic tape devices.

Running jobs in automatic mode is possible, within SUPERMASTER I, by entering "04" soon after the prompting message "IGOM:I2". The program control will be switched to the card reader which will expect commands in the format and the sequence prompted on the teletype at the entry of the automatic mode. Instructions from cards will be executed like during an interactive session. However, if an error condition is detected by a program, the control will automatically return to the user on the teletype. This is also achieved by setting SENSW 1 on the computer.

S U P E R M A S T E R I

"SUPERMASTER I" in GIAPP: scanning, thresholding and processing of grey level images.

SUPERMASTER	MASTER	FUNCTIONS
I	01	Scanning on a Flying Spot Scanner, display of the results of the scans, creation of grey level images, study and display of grey levels, thresholding of grey level images, and creation of binary compressed images as labeled data sets for subsequent processing
	02	Selection of subpictures from large original images, point operations on pixels for grey level images

M A S T E R 0 1

01

Read integer and floating point defaults from cards

```
CALL READCM
```

02

Copy picture data from device to device

```
CALL COPY2H(   MTR,   MTW, IDIMP, JDIMP,...)
               467    468    469    470
```

MTR,MTW: input, output picture devices (11, 12, or 17); copy from MTR to MTW.
IDIMP,JDIMP: x,y picture dimensions.

NOTE: magnetic tapes must be positioned correctly before copying starts.

03

Set pincushion correction constant

```
CALL INLIT(0)
```

04

Zero F S Scanner DACS (digital to analog converters)

```
K = LITGRY(0,0,0)
```

05

Select area in picture for scanning and processing

```
CALL SELAR1
```

NOTE: all parameter values are transfered via COMMON; communication via special command console and Tektronix 611 displays with menu and plots.

06

Test F S Scanner and display results of scans on Tektronix 611; also print grey levels on Versatec

```
CALL SETBEA
```

NOTE: all parameter values are transfered via COMMON; communication via special command console and Tektronix 611 displays with menu and plots.

07

Print table of default values

```
CALL TYPIDM(ILPV)
```

08

Enter integer data

```
CALL EINDAT

"EINDAT:ENTER I,J:I4,I6"
(address and value: if address is neg. print value)
```

09

Enter floating point data

```
CALL EDATIN

"EDATIN:ENTER I,J:I4,F15.6"
(address and value: if address is neg. print value)
```

10

Go to master

```
"G I A P P : SM I"

"IGOM:I2"
```

11

Go forward over one end-of-file mark on device MT11

```
CALL AVFILE(IUFT1)
```

12

```
Go forward over one end-of-file mark on device MT12

CALL AVFILE(IUFT2)
```

13

```
Go back one end-of-file mark on device MT11

CALL BKFILE(IUFT1)
```

14

```
Go back one end-of-file mark on device MT12

CALL BKFILE(IUFT2)
```

15

```
Initialize magnetic tape on MT11 for labeled system
DS's

IF(IPODEM(0,-1,...))
```

16

```
Go through magnetic tape on MT11, read all headers
and comments, and create occupancy table for labeled
DS's on MT11

IF(IPODEM(0,0,...))
```

17

```
Rub last DS on magnetic tape on MT11

IF(IPODEM(   KDS,3,...))
```

18

Scan, on the Flying Spot Scanner, picture in square raster or in hexagonal raster scanning configuration and write grey level picture either as labeled DS or as unlabeled picture data file

```
CALL SCANS2(   MTX, ICFIX, JCFIX,.....,.....,MAXDIM,
                433    113    114                 438

            IRUNTP, IDISP, MAXGR, MINGR,NGRAYS, IBLWH,
               435    437    430    431    123    257

            IPULSE,IPULST, NREAD,ITAPES,IGRIDS,  LEVB,
               10     152    458    477    362    478

            IWAIT1,IWAIT2,ISQHEX,...)
               480    481    361
```

MTX : magnetic tape drive; 11 or 12 for MT11 or MT12.

ICFIX,JCFIX: center of reading and display, fixed and in one-to-one correspondence.

IMAXDIM: maximum desired dimension of picture on tape; less or equal to 1024.

IRUNTP: 1=write on tape; 2=only test and display; 3=print B and W picture on Versatec.

IDISP : neg.=for no display; 0=for point display; pos.=for grey level display on Tektronix.

MAXGR,MINGR: max. and min. grey level values at IUP and ILO in percent.

NGRAY : number of grey levels in display on Tektronix (u to 7).

IBLWH : pos. for black on white; neg. for white on black.

IPULSE,IPULST: pulse line (dummy), pulse strength (0 to 7).

NREAD : number of grey level readings from same x,y point; neg. for square root, 0 for LITTON, pos. for LITTAV.

ITAPES: 1=for labeled system; 2=for non-standard tape with header; 3=for non-standard tape without header, and 4=for BCD formatted tape for outside computer.

IGRIDS: neg. or 0 for no grid printing on Versatec plotter; pos. for grid printing.

LEVB : last B/W bias (scanal normally).

```
      IWAIT1,IWAIT2: delay loops between printing of
              lines on Versatec for contrast, and
              after printing, respectively.
      ISQHEX: 1 or 2= square raster, 3= hexagonal
              raster scanning.

NOTE1: need MAXGR, MINGR, NGRAY if IDISP = 1.
NOTE2: if ITAPE = 2,3, then MAXDIM can go to 1024.
NOTE3: set SENSW 7 to cut run. If tape is written,
       the file will not be complete but end-of-file
       mark will be written.
NOTE4: if SENSW 2 is set, row being done is typed.
```

19

Print selected window of picture as digital printout on Versatec

```
CALL PICTOH(IUND(1),  (2),   (3),IFORM(1), (2),   (3),
              300     301    302    303     304    305

            IDIMP, JDIMP, IAREA,  ITOP,  JTOP,  IBOT,
              469    470    310    306    307    308

             JBOT, NEWPO,...)
              309    299

    IUND(.): first, second and third input devices
             for input pictures (11, 12 and 17).
   IFORM(.): fist, second and third picture
             printing formats; neg., 0= (25I5),
             pos. = (25(1XZ4)).
  IDIMP,JDIMP: x,y picture dimensions.
    IAREA : area selection; neg., 0 = print
             entire picture, pos. = print only area
             defined by (ITOP,JTOP) (IBOT,JBOT).
    NEWPO : 1= for change page between picture
             stripes, 2 = for no change.
    ITOP,JTOP,IBOT,JBOT: top left and bottom
             right corners of printed area in
             picture coordinates.

NOTE: SENSW 7 set cuts printing.
```

20

Read trajectory data from magnetic tape

```
CALL RTRAJ1(   MTR,...)
               467
```

MTR : input device for input file;
tape only = 11 or 12.

21

Write trajectory data on magnetic tape

```
CALL WTRAJ1(   MTW,...)
               468
```

MTW : output device for output file;
tape only = 11 or 12.

22

Plot trajectory (+ data) on Tektronix 611 or on F S Scanner

```
CALL TRAJD3( IDIMP, JDIMP,ISCOPE, ICENT, JCENT,  IDXY,
               469    470    246    248    249    250

           NPULB,IFLIPX,IFLIPY,  LXYD,LINCIR, LINTP,
             253    266    267    207    333    334

          LINSTP,    I1,    J1,    I2,    J2,  SCAL,
             335    201    202    203    204    174

             LLS,   LLX,   LLY,  LCOS,  LSIN,...)
             ---    ---    ---    ---    ---
```

IDIMP,JDIMP: x,y picture dimensions.
ISCOPE : neg.,0= Tekrtonix 611; pos.= F S Scanner.
ICENT,JCENT: picture center coordinates on scanner, (0,0) normally.
IDXY : spacing between pixels (square raster).
NPULB : number of pulses-point for binary picture; 2 < NPULB < 4160.
IFLIPX: pos. = for do flip the x axis of picture; neg., 0= for do not.
IFLIPY: pos. = for do flip the y axis of picture; neg., 0= for do not.
LXYD : number of points on trajectory; ≤ 650.
LINCIR: 1= for linear trajectory from (I1,J1) to (I2,J2); 2= for circular trajectory, center at (I2,J2), start at (I1,J1); 3= for special trajectory, constant cos beta.
LINTP : neg. or 0 = for plot trajectory only; pos. = for plot trajectory and print data (LLS(.)*SCAL.
LINSTP: line step size for data.
I1,J1 : start point of trajectory.
I2,J2 : end point of trajectory.
SCAL : scale for data; plotted line = (LLS(.)*SCAL).

NOTE1: need LLX(.), LLY(.), i. e., x,y coordinates of points; need also LCOS(.), LSIN(.) if plot data for LINCIR.
NOTE2: SENSW 7 set cuts display.

23

Plot box around picture on Tektronix 611, grid and cross

```
CALL BXGRP1( IDIMP, JDIMP,ISCOPE, ICENT, JCENT,  IDXY,
               469    470    246    248    249    250

             NPULB,IFLIPX,IFLIPY,  IBGP, LNSTP, IGRID,
               253    266    267    336    335    337

             JGRID,    IP,    JP,...)
               338    339    340
```

IDIMP,JDIMP: x,y picture dimensions.
ISCOPE: 0= Tektronix 611; pos.= F S Scanner camera; neg.= for binary output on Versatec and Tektronix 611.
ICENT,JCENT: picture center coordinates on scanner, (0,0) normally.
IDXY : spacing between pixels (square raster).
NPULB : number pf pulses•oint for binary picture; 2 < NPULB < 4160.
IFLIPX: pos. = for do flip the x axis of picture; neg., 0= for do not.
IFLIPY: pos. = for do flip the y axis of picture; neg., 0= for do not.
IBGP : neg. = for plot box around picture; 0 = for plot grid on picture; pos. = for plot cross at IP,JP, IBGP = 100 suggested value.
LINSTP: line step size for data.
IGRID,JGRID: x,y grid spacings in matrix coordinates.
IP,JP : x,y in matrix coordinates where cross of size 2*IBGP is plotted.

NOTE: SENSW 2 set types readings.

24

Find maximum and minimum grey level values in picture

```
CALL MAMI3H(   MTR, IDIMP, JDIMP,.....,   MAX,   MIN,
               467   469    470           263    264
          ~ ...)
```

MTR : input device for input file;
(11, 12 or 17).
IDIMP,JDIMP: x,y picture dimensions.
MAX,MIN: maximum and minimum values obtained, delivered by the MAMI3H.

NOTE: set SENSW 1 before running if tape is used.

25

Compute row histogram of picture data

```
CALL RAW3H(    MTR, IDIMP, JDIMP,   MPH,   MAX,   MIN,
               467   469    470    217    264

          ...)
```

MTR : input device for input file;
(11, 12 or 17).
IDIMP,JDIMP: x,y picture dimensions.
MPH : number of histogram slots (≤ 256).
MAX,MIN: maximum and minimum values obtained, delivered by MAMI3H.

NOTE: set SENSW 1 before running if tape is used.

26

Compute lower and upper data bounds in histogram

```
CALL LOUP1 (  LHIS,    MPH,    ILO,    IUP,    MAX,    MIN,
                       217     110     111     263     264

           ......, MAXGR, MINGR,...)
                    430     431
```

MPH : number of histogram slots (≤ 256).
ILO,IUP: percentage of histogram area rejected at lower and upper data end, respectively.
MAX,MIN: maximum and minimum values obtained, delivered by MAMI3H.
MAXGR,MINGR: maximum and minimum grey level values corresponding to IUP and ILO (result).

NOTE: set SENSW 1 before running if tape is used.

27

Write histogram onto tape

```
CALL WTRAJ4(   MTW,...)
               468
```

MTW : output tape (11 or 12).

28

Read histogram from tape

```
CALL RTRAJ4(   MTR,...)
               467
```

MTR : input tape (11 or 12).

29

Plot histogram in normal scale on Versatec

```
SCALE=INDATA(214)/100.00
CALL TRAJD2(......, JFORM,ISOLID,   MPH, IGIDT,IGRIDZ,
                    210    211    217    212    213

            IWAIT,......., SCALE,...)
              215           214
```

JFORM : output form; 1= for graph, 2= for numbers, 3= for both.
ISOLID: neg., 0= for graph; pos.= for filled graph.
MPH : number of histogram slots (≤ 256).
IGRIDT: grid spacing along trajectory, 0= no grid.
IGRIDZ: grid spacing for grey levels, 0= no grid.
IWAIT : delay constant for equal black painting on Versatec.
SCALE : multiplicative scale factor for grey level data (SCALE=INDATA(214)/100.00).

30

Expand histogram base by 2

```
      MPH2=MPH*2
      DO 308 K=1,MPH
      LLR(2*K-1)=LHIS(K)
      LLR(2*K  )=LHIS(K)
  308 CONTINUE
```

31

Plot expanded histogram on Versatec

```
SCALE=INDATA(214)/100.00
MPH2=MPH*2
CALL TRAJD2(......, JFORM,ISOLID,   MPH, IGIDT,IGRIDZ,
                      210    211    217    212    213

            IWAIT,.....,  SCALE,...)
              215          214
```

NOTE: see TRAJD2 at (29) for parameters.

32

Clip histogram

```
MAXH=INDATA(216)
IF(LHIS(K)-MAXH.LE.0)
LHIS(K)=MAXH
```

33

Define linear trajectory in picture

```
CALL TRAJS1(    I1,    J1,    I2,    J2, ICENT, JCENT,
                201    202    203    204    205    206

              IDIMP, JDIMP,  LXYD,...)
                469    470    207
```

I1,J1 : first point on trajectory in picture coordinates.
I2,J2 : last point on trajectory in picture coordinates.
ICENT,JCENT: center of picture (any value inside picture is OK).
IDIMP,JDIMP: x,y picture dimensions.
LXYD : number of points on trajectory (≤ 650).

34

Plot trajectory picture on Versatec

```
CALL TRAJP1( IDIMP, JDIMP,IJGRID, ICENT, JCENT,  LXYD,
               469    470    209    205    206    207

                ...)
```

IDIMP,JDIMP: x,y picture dimensions.
IJGRID: grid spacing in picture coordinates.
ICENT,JCENT: center of picture (any value inside picture is OK).
LXYD : number of points on trajectory (≤ 650).

35

Read data from tape or disk for trajectory

```
CALL TRAJR1(  MTR,......., IDIMP, JDIMP,  LXYD, LRDIM,
               467          469    470    207    208

           ...)
```

MTR : input device for input data (11, 12 for tape, 17 for disk).
IDIMP,JDIMP: x,y picture dimensions.
LXYD : number of points on trajectory (≤ 650).
LRDIM : magnetic tape reading array = 1024.

NOTE: magnetic tape must be positioned correctly in all cases, just after the end-of-file mark.

36

Plot data on trajectory on Versatec plotter

```
SCALE=INDATA(214)*100.00
CALL TRAJD2(......., JFORM,ISOLID,   MPH, IGIDT,IGRIDZ,
                      210    211    217    212    213

              IWAIT,......., SCALE,...)
                215          214
```

NOTE: see TRAJD2 at (29) for parameters.

37

Thresholding of grey level picture as: grey level slice or as grey level slice into binary compressed; and/or display on Tektronix 611, Flying Spot Scanner or Versatec, of thresholded picture; creates either a labeled DS or an unlabeled picture file

```
CALL.PICTD(     MTR,   MTW, IDIMP, JDIMP,ISCOPE, IMODE,
                 467    468   469    470    246    247

              ICENT, JCENT,  IGRL,  IGRS, NPULB,  IFRA,
                248    249   251    252    253    254

               LINS, NGRAY,   MAX,   MIN, IBLWH,IFLIPX,
                255    256   263    264    257    266

             IFLIPY,ISQHEX,.......,  DXYI,...)
                267    361          215
```

MTR : input device (tape = 11,12, disk = 17. MTR = 0 for grey test pattern; MTR = neg. for binary test pattern.

MTW : output device for output picture. If MTW neg. write binary compressed DS for labeled system.

IDIMP,JDIMP: x,y picture dimensions.

ISCOPE: 0= Tekrtonix 611; pos.= F S Scanner camera; neg. for binary output on Versatec and Tektronix 611.

IMODE : neg.= for grey level slice to binary (if mingr. ≤ grey level ≤ maxgr, grey level is set to binary 1); 0= for binary display (thresholded grey level is 1, remainder of data is 0); pos.= for grey level display.

```
ICENT,JCENT: picture center on Tektronix 611
        or on F S Scanner (Tekt. 611 ACS
        = 12 bits, F S Sc. DAS = 13 bits).
IGRL  : pos.= for linear grey level distribution;
        0= otherwise.
IGRS  : pos.= fors quare grey level distribution;
        0= otherwise.
NPULB : number pf pulses-point for binary
        picture; 2 < NPULB < 4160.
IFRA  : neg., 0 = for no frame; pos. = for
        frame around picture (uses NPULB).
LINS  : line step length for frame;0, neg. = not.
NGRAY : number of grey levels wanted; 1 to 64 for
        F S Scanner, 1 to 8 for Tektronix 611.
MAX,MIN: max. and min. data values in picture
        (must be given).
IBLWH : 1= black on white; 2= white on black.
IFLIPX,IFLIPY: pos.= do flip x,y coordinates
        of picture being plotted on Tektronix 611
        and/or Versatec. Also flip x coordinate in
        output picture (for flipping y coordinate
        FLIPY should be used instead of PICTD).
        neg. or 0= do not flip.
ISQHEX: 1 or 2 = square raster display; 3 =
        hexagonal.
DXYI  : spacing between pixels in display on
        Tektronix 611.

NOTE1: IMODE and MTR must be negative when
       writing out a picture.
NOTE2: data written on magnetic tape and displayed
       Versatec correctly for IFLIPX only,
       not for IFLIPY.
NOTE3: SENSW 7 set, cuts picture writing
       and plotting.
NOTE4: SENSW 2 set, prints row number being done.
```

01

Select subpictures from a larger one, compute function on local arrays

```
CALL MTMOD5(   MTR,   MTW, IDIMP, JDIMP,ISTART,JSTART,
                467    468    469    470    471    472

              IEND,  JEND,  IDIM,  JDIM, NAVAR,IJSTEP,
               483    484    473    474    475    476

             IMODE,......., FMULT,.,.)
               247            173
```

MTR : input device, disk only, for input picture (large, one pixel per word). MTR=17 only.

MTW : output device for smaller output picture. If output is for labeled system MTW must be 11, otherwise can be 11 or 12.

IDIMP,JDIMP: x,y dimensions for larger picture (at one word per pixel).

ISTART,JSTART: x,y starting point in larger picture.

IEND,JEND: x,y endpoint in larger picture.

IDIM,JDIM: x,y dimensions of smaller picture at one word per pixel.

NAVAR : cell size for local averaging of input picture (can be 1, 2,..., 51).

IJSTEP: step length or compression of input picture (can be 1, 2,..., 20).

IMODE : type of function on local array. 1= for local average; 2=for local maximum value; 3=for local minimum value; 4=for local standard deviation; 5=for local skewness; 6=for local kurtosis; and 7=for local (center value-average)/standard deviation.

FMULT : multiplier for all results.

NOTE1: (ISTART,JSTART), (IEND,JEND) = data area in larger picture.

NOTE2: SENSW 2 set types row being done.

02

Copy picture data from device to device

```
CALL COPY2H(   MTR,   MTW, IDIMP, JDIMP,...)
               467    468    469    470
```

MTR,MTW: input, output picture devices (11, 12, or 17); copy from MTR to MTW.
IDIMP,JDIMP: x,y picture dimensions.

NOTE: magnetic tapes must be positioned correctly before copying starts.

03

Read grey level values in picture and set all values lower than a given value to another given value and copy result as new picture on another device

```
CALL MTMOD8(   MTR,   MTW, IDIMP, JDIMP,   MAX,   MIN,
               467    468    469    470    263    264

             LBIAS,...)
               353
```

MTR,MTW: input, output picture devices (11, 12, or 17).
IDIMP,JDIMP: x,y picture dimensions.
MAX,MIN: maximum, minimum grey level values for setting new value to LBIAS.
LBIAS : new value to substitute if pixel grey level value is less than MIN.

NOTE: magnetic tapes must be positioned correctly.

04

Compute point operations on pixels between two pictures and create a third picture

```
CALL MTMOD6(   MT1,   MT2,   MTW, IOPER, IDIMP, JDIMP,
               467    351    468    352    469    470

            LBIAS,......, FMULT,...)
              353           198
```

MT1,MT2: input picture devices, 11, 12 or 17.
MT2 can be 0.
MTW : output picture device, 11, 12 or 17.
IOPER : operation mode between the pixels of the two input pictures.
1= for (MT1+MT2)*FMULT+LBIAS=MTW.
2= for (MT1-MT2)*FMULT+LBIAS=MTW.
3= for (MT1*MT2)*FMULT+LBIAS=MTW.
4= for (MT1/MT2)*FMULT+LBIAS=MTW.
IDIMP,JDIMP: x,y picture dimensions.
LBIAS : bias for data (constant).
FMULT : multiplier of results (constant).

NOTE: SENSW 7 set cuts picture processing.

05

Print selected window of picture as digital printout on Versatec

```
CALL PICTOH(IUND(1),  (2),   (3),IFORM(1), (2),   (3),
              300     301    302    303     304    305

            IDIMP, JDIMP, IAREA,  ITOP,  JTOP,  IBOT,
              469    470    310    306    307    308

             JBOT, NEWPO,...)
              309    299
```

IUND(.): first, second and third input devices for input pictures (11, 12 and 17).
IFORM(.): fist, second and third picture printing formats; neg., 0= (25I5), pos. = (25(1XZ4)).
IDIMP,JDIMP: x,y picture dimensions.
IAREA : area selection; neg., 0 = print entire picture, pos. = print only area defined by (ITOP,JTOP) (IBOT,JBOT).
NEWPO : 1= for change page between picture stripes, 2 = for no change.
ITOP,JTOP,IBOT,JBOT: top left and bottom right corners of printed area in picture coordinates.

NOTE: SENSW 7 set cuts printing.

06

Flip input picture upside down and copy data to output picture from last to first row.

```
CALL FLIPY(    MTR,   MTW, IDIMP, JDIMP,...)
               467    468   469    470
```

MTR : input device for input picture (11, 12 or 17).
MTW : output device for output picture (11, 12 or 17).
IDIMP,JDIMP: x,y picture dimensions.

NOTE: magnetic tapes must be positioned correctly before copying started.

08

Enter integer data

```
CALL EINDAT

"EINDAT:ENTER I,J:I4,I6"
(address and value: if address is neg. print value)
```

09

Enter floating point data

```
CALL EDATIN

"EDATIN:ENTER I,J:I4,F15.6"
(address and value: if address is neg. print value)
```

10

Go to master

```
"G I A P P : SM I"

"IGOM:I2"
```

N O T E

The following SUPERMASTERS represent "labeled systems" of image data management and processing. Image data sets, DS's, with proper header, describing image dimensions and type, and commentary, recording the history of processing, are necessary part of the image, DS's, and precede the image data sensu strictu. A description of header and commentary structures for an image DS in the labeled systems is made in Figure 3.3.

File searching is automatic in either magnetic tapes or disks. Five I/O unis are available for binary compressed images (two tapes and three disk partitions). They can be called by three digit DS numbers as follows: 100's for MT11, 200's for MT12, 300's, 400's, and 500's for the three disk partitions, respectively. For uncompressed images, in SUPERMASTER III, only one disk I/O unit is available (DS number 500 only) due to the large image dimensions (1024 pixels x 1024 pixels).

A linkage with the unlabeled system of SUPERMASTER I is obtained through SUPERMASTER V.

For SUPERMASTER's III and IV, automatic mode is obtained in a manner identical to the one described for SUPERMASTER I (see NOTE). Such automatic mode is not a useful feature in SUPERMASTER's II and V.

S U P E R M A S T E R I I

"SUPERMASTER II" of GIAPP: graphic tablet subroutines for digitizing line drawings, editing and assemblage of mosaics of binary compressed images.

SUPERMASTER	MASTER	FUNCTIONS
II	03	Graphic tablet programs for digitizing line drawings, creation of files of vectors from a graphic tablet, transformation of vectors into binary images, assemblage of subpictures (384 pixels x 384 pixels maximum) into large mosaics of binary compressed images of line drawings
	04	Assemblage of subpictures (512 pixels x 512 pixels maximum) into large mosaics of binary compressed images of line drawings
	05	Editing, via graphical displays, of binary compressed images

M A S T E R 0 3

01

"COOL START" procedure for two magnetic tapes on devices MT11 and MT12

```
READC (yes/no)
SLLIO (M1,M2,I,J,K)
PREPD (0,0,13,14,17)
RLIO1 (11)
RLIO1 (12)
```

Number of entries of physical	devices
M1: INDAC(254)	11
M2: INDAC(255)	12
I : INDAC(256)	13
J : INDAC(257)	14
K : INDAC(258)	17

NOTE: M1+M2+I+J+K=51
(length of data is 54 on Modcomp)

02

Manual copy of binary compressed DS from one I/O device to another

```
CALL COPY1(IUN,JUN)

"GIVE IUN,JUN:2I3"
```

03

Manual rub of last DS on an I/O device

```
K=IPODS(IUN,3,0)

"RUB IUN:I3"
```

04

Read default values from cards

```
CALL READC

     (Read INDAC and DACIN from cards)
```

05

Type default value table

```
CALL TYPID
```

06

Plot binary compressed picture on Versatec plotter; one dot per pixel (fast plot)

```
CALL VPIX3(    JUN, ITEXT, IWAIT,IWAIT2,...)
               174   116   117   151

     JUN   : input picture DS.
     ITEXT : text of header and comments printed before
             the plot. 1= yes; 0= no.
     IWAIT : delay constant during plotting of picture.
     IWAIT2: delay constant after plotting before
             feeding paper.
```

07

Plot binary compressed picture on Versatec plotter as arrays of n x m dots per pixel; square and pseudo-hexagonal raster plots. Also select area to plot.

```
CALL PICTOV(IUND(1),  (2),  (3),  (4),  (5), IAREA,
              64      65    66    67    68    272

            ITOP,  JTOP,  IBOT,  JBOT, NEWPO,ISQHEX,
            273    274    275    276    54    167

            NPX,   NPY, IWAIT,IWAIT2,  MODE,...)
            228    229   117   151    289
```

IUND(.): input unit DS's.
IAREA : neg. or 0= no area selection; pos.= area selection: ITOP, JTOP, IBOT, JBOT.
ITOP,JTOP: coordinates of top left corner of selected area in picture.
IBOT,JBOT: coordinates of bottom left corner.
NEWPO : 1= change page after each print page; 2= no page change.
ISQHEX: type of plot, 1 or 2= square, 3= pseudo-hexagonal display.
NPX,NPY: nos. of dots per pixel in x,y directions.
IWAIT : delay constant during plotting of picture.
IWAIT2: delay constant after plotting before feeding paper.
MODE : 1= slow, 2= fast but uneven plotting.

NOTE1: 1 to 5 DS's can be plotted with alternating rows.
NOTE2: SENSW 7 set cuts plotting.

08

Enter integer data

```
CALL EINDA

"EINDA:ENTER I,J:I4,I6"
(address and value: if address is neg. print value)
```

09

Enter floating point data

```
CALL EDATI

"EDATI:ENTER I,J:I4,F15.6"
(address and value: if address is neg. print value)
```

10

Go to master

```
"G I A P P : SM II"

"IGOM:I2"
```

11

Establish the four corners of submap to be digitized on tablet and the scale interval in map units; provide rectangularity test and slope angle of upper horizontal map edge

```
CALL TABLT6(    K1,     K2,    NAV,    NFL, IDISP, NPULP,
                14      15      5       6     4      83

              NPULC, ICIRC,  IRAD, LINES,    NP,  IMES,
                84     55     60     85     97      7

               JMES, MESIZ,  JDEL,LPULCH,  SCAL, CHORD,
                 8     13     9      10     42     27

                ...)
```

K1,K2 : pointed location range.
NAV : number of averagings per one point.
NFL : 1= for using pen contact "ON", 2= for using pen contact "OFF" for reading.
IDISP : message device. 1= teletype terminal, 2= Tektronix 611 unit, 3= both.
NPULP : line intensity on Tektronix 611 if pen in proximity.
NPULC : line intensity on Tektronix 611 if pen in contact.
ICIRC : pos.= for drawing circle at vector break points.
IRAD : radius of circle at vector break points.
LINES : step length when drawing a line on Tektronix 611.
NP : line intensity (1 to 7).
IMES, JMES, MESIZ: x,y coordinates and size of message on Tektronix screen.
JDEL : spacing between entered message and prompting message.
LPULCH: pulse strength during character writing.
SCAL : scale for Tektronix 611.
CHORD : circle chord length.

NOTE : SENSW 7 set cuts operation.

12

Establish the number of pixels over the map distance pointed out on the tablet, and suggest dimensions of binary image to be computed (rotate or not decision)

```
CALL TABLT7(NPIXEL, MINAV,  SINT,...)
              11    12     44
```

NPIXEL: number of pixels on the scaling interval.
MINAV : 1= for minimum corners, 2= for average corners.
SINT : scaling interval length.

13

Digitize on the graphic tablet up to 1300 vectors in one run; display vectors on Tektronix 611, eliminate vectors in backward order starting from the last by pushbutton command on the special operator console for online editing

```
CALL TABLT1(    MA,......., ICIRC,.......,  IRAD, NPULP,
                  92            55             60     83

              NPULC, LINES,......., CHORD, DELIN, DELOP,
                84     85             27     39     40

                ANG,   SCAL,...)
                 41     42
```

MA	:	last filled entry in vector table.
ICIRC	:	pos.= for drawing circle at vector break points.
IRAD	:	radius of circle at vector break points.
NPULP	:	line intensity on Tektronix 611 if pen in proximity.
NPULC	:	line intensity on Tektronix 611 if pen in contact.
LINES	:	step length when drawing a line on Tektronix 611.
CHORD	:	circle chord length.
DELIN	:	spacing tolerance between first and second point.
DELOP	:	spacing tolerance between second and all subsequent points.
ANG	:	angle tolerance between consecutive vectors.
SCAL	:	scale for Tektronix 611.

NOTE: if MA is greater than 0, points are added to the vector data array; if MA is neg. or 0, vector data array is zeroed.

14

Create binary picture in core from vector table and optionally plot picture on Versatec. Pictures can be accumulated in core. Optionally zero array for binary picture in core (384 pixels x 384 pixels maximum size)

```
CALL HPR52(     MA,IDIMBX,JDIMBX,    ITL,    JTL,    IBR,
                92    180    182     56      57      58

               JBR,.......,  STEP,...)
                59           43
```

MA : last filled entry in vector table. If MA is set negative, array for binary image in core is zeroed.

IDIMBX,JDIMBX: desired image dimensions in core. Max. dimensions is 384 x 384.

ITL,JTL,IBR,JBR: top, bottom, left and right coordinates of active tablet area. If these are changed a different area is selected for picture generation.

STEP : step size along vectors, in tablet units, for the construction of binary image.

15

Same as in (14) above, but after correction for rotation of map on tablet as computed by (11) above (384 pixels x 384 pixels maximum

```
CALL HPR52A(    MA,IDIMBX,JDIMBX,.......,   XTL,    YTL,
                92    180    182            45      46

               XBR,    YBR,    CO,    SI,  STEP,...)
                47      48     49     50     43
```

MA : last filled entry in vector table. If MA is set negative, array for binary image in core is zeroed.

IDIMBX,JDIMBX: desired image dimension in core. Max. dimensions is 384 x 384.

XTL,YTL,XBR,YBR: top, bottom, left and right coordinates of corners of frame.

CO,SI : cos, sin for the rotation of tablet coordinates.

STEP : step size along vectors, in tablet units, for the construction of binary image.

16

Create DS with tablet vector table in core

```
CALL GEST3M(.....,   JUN,...)
                     174
```

JUN : DS for output of the vector table.

17

Read to core DS with tablet vector table

```
CALL GEST3L(   IUN,...)
               172
```

IUN : input DS with tablet vector table.

18

Create DS with binary compressed image stored in core

```
CALL HPR78B(   JUN,IDIMBX,JDIMBX,.....,   ITL,   JTL,
               174   180    182            56    57

               IBR,   JBR,...)
               58     59
```

JUN : output DS.
IDIMBX,JDIMBX: picture dimensions(no. of binary pixels per row and no. of rows).
ITL,JTL,IBR,JBR: top, bottom, left and right coordinates of active tablet area.

19

Read to core binary compressed image DS (maximum dimensions 384 pixels x 384 pixels)

```
CALL HPR78A(   IUN,...)
               172
```

IUN : input DS.

20

Combine composite binary image from DS and subimage stored in core (384 pixels x 384 pixels maximum) to create DS of combined binary compressed images

```
CALL HPR85A(   IUN,   JUN,    I1,    I2,    J1,    J2
               172    174     16     17     18     19

           IDIMBX,JDIMBX,...)
             180    182
```

IUN,JUN: input, output DS's; if IUN = 0, initialize composite binary compressed picture (i. e., to create a first composite binary image DS.
I1,I2 : compressed binary picture range in x (location of patch).
J1,J2 : compressed binary picture range in y (location of patch).
IDIMBX: number of pixels per row in window (columns) in the patch.
JDIMBX: number of rows of pixels in window in the patch.

21

Take a binary compressed image DS, logically "OR" a subimage DS into it(row by row, data in core) and store the resulting composite image into another DS

```
CALL HPR85B(   IUN,  IUNP,   JUN,    I1,    I2,    J1,
               172    173    174     16     17     18

            J2,...)
            19
```

IUN : input DS; = 0 the first time.
IUNP : input DS with patch.
JUN : output DS.
I1,I2 : compressed binary picture range in x (location of patch).
J1,J2 : compressed binary picture range in y (location of patch).

```
22
    Initialize magnetic tape on device MT11

    CALL PREPD(11,0,0,0,0)

23
    Initialize magnetic tape on device MT12

    CALL PREPD(0,12,0,0,0)

24
    Initialize file occupancy table

    F = SLLIO(30,14,2,2,3).

25
    Type file occupancy table

    CALL TLLIO
```

01

Read to core DS with tablet vector table

```
CALL GEST3L(   IUN,...)
               172
```

IUN : input DS with tablet vector table.

02

Manual copy of binary compressed DS from one I/O device to another

```
CALL COPY1(IUN,JUN)

"GIVE IUN,JUN:2I3"
```

03

Manual rub of last DS on an I/O device

```
K=IPODS(IUN,3,0)

"RUB IUN:I3"
```

04

Establish the number of pixels over the map distance pointed out on the tablet, and suggest dimensions of binary image to be computed (rotate or not decision)

```
CALL TABLT7(NPIXEL, MINAV,  SINT,...)
                11     12     44
```

NPIXEL: number of pixels on the scaling interval.
MINAV : 1= for minimum corners, 2= for average corners.
SINT : scaling interval length.

05

Create binary picture in core from vector table and optionally plot picture on Versatec. Pictures can be accumulated in core. Optionally zero array for binary picture in core (512 pixels x 512 pixels maximum size)

```
CALL HPR52(     MA,IDIMBX,JDIMBX,   ITL,   JTL,   IBR,
                92   180    182     56     57     58

               JBR,.....,  STEP,...)
                59          43
```

MA : last filled entry in vector table. If MA is set negative, array for binary image in core is zeroed.

IDIMBX,JDIMBX: desired image dimensions in core. Max. dimensions is 512 x 512.

ITL,JTL,IBR,JBR: top, bottom, left and right coordinates of active tablet area. If these are changed a different area is selected for picture generation.

STEP : step size along vectors, in tablet units, for the construction of binary image.

06

Plot binary compressed picture on Versatec plotter; one dot per pixel (fast plot)

```
CALL VPIX3(   JUN, ITEXT, IWAIT,IWAIT2,...)
              174   116    117    151
```

JUN : input picture DS.

ITEXT : text of header and comments printed before the plot. 1= yes; 0= no.

IWAIT : delay constant during plotting of picture.

IWAIT2: delay constant after plotting before feeding paper.

07

Plot binary compressed picture on Versatec plotter as arrays of n x m dots per pixel; square and pseudo-hexagonal raster plots. Also select area to plot.

```
CALL PICTOV(IUND(1),  (2),   (3),   (4),   (5), IAREA,
              64      65     66     67     68     272

            ITOP,  JTOP,  IBOT,  JBOT, NEWPO,ISQHEX,
             273    274    275    276     54     167

             NPX,   NPY, IWAIT,IWAIT2,  MODE,...)
             228    229    117    151    289
```

IUND(.): input unit DS's.
IAREA : neg. or 0= no area selection; pos.= area selection: ITOP, JTOP, IBOT, JBOT.
ITOP,JTOP: coordinates of top left corner of selected area in picture.
IBOT,JBOT: coordinates of bottom left corner.
NEWPO : 1= change page after each print page; 2= no page change.
ISQHEX: type of plot, 1 or 2= square, 3= pseudo-hexagonal display.
NPX,NPY: nos. of dots per pixel in x,y directions.
IWAIT : delay constant during plotting of picture.
IWAIT2: delay constant after plotting before feeding paper.
MODE : 1= slow, 2= fast but uneven plotting.

NOTE1: 1 to 5 DS's can be plotted with alternating rows.
NOTE2: SENSW 7 set cuts plotting.

08

Enter integer data

```
CALL EINDA

"EINDA:ENTER I,J:I4,I6"
(address and value: if address is neg. print value)
```

09

Enter floating point data

```
CALL EDATI

"EDATI:ENTER I,J:I4,F15.6"
(address and value: if address is neg. print value)
```

10

Go to master

```
"G I A P P : SM II"

"IGOM:I2"
```

11

Same as in (05) above, but after correction for rotation of map on tablet as computed by (11) above (512 x 512 pixels maximum

```
CALL HPR52A(    MA,IDIMBX,JDIMBX,.....,    XTL,  YTL,
                92    180    182            45    46

              XBR,   YBR,    CO,    SI,  STEP,...)
               47     48     49     50    43
```

MA : last filled entry in vector table. If MA is set negative, array for binary image in core is zeroed.

IDIMBX,JDIMBX: desired image dimension in core. Max. dimensions is 512 x 512.

XTL,YTL,XBR,YBR: top, bottom, left and right coordinates of corners of frame.

CO,SI : cos, sin for the rotation of tablet coordinates.

STEP : step size along vectors, in tablet units, for the construction of binary image in core.

12

Take a binary compressed image DS, logically "OR" a subimage DS into it(row by row, data in core) and store the resulting composite image into another DS

```
CALL HPR85B(   IUN,  IUNP,   JUN,   I1,   I2,   J1,
               172   173    174    16    17    18

               J2,...)
               19
```

IUN : input DS; = 0 the first time.

IUNP : input DS with patch.

JUN : output DS.

I1,I2 : compressed binary picture range in x (location of patch).

J1,J2 : compressed binary picture range in y (location of patch).

01

Interactive editing of binary compressed image (1024 pixels x 1024 pixels maximum) via Tektronix 611 and Versatec displays and commands via a special operator console

```
CALL FIXPX1(   IUN,   JUN,   KUN,   LUN,.....,  IDXY,
               172    174    171    173           359

             JDXY,...)
              364
```

IUN : input DS for image to be edited.
JUN : output DS for edited image.
KUN,LUN: intermediate DS's used during editing; should be on disk (300 and 400).
IDXY,JDXY: spacing between the dots on the Tektronix 611 screen representing the black pixels (suggested value is 30).

NOTE: a menu of instructions and options appears on the Tektronix 611 screen.

02

Manual copy of binary compressed DS from one I/O device to another

```
CALL COPY1(IUN,JUN)

"GIVE IUN,JUN:2I3"
```

03

Manual rub of last DS on an I/O device

```
K=IPODS(IUN,3,0)

"RUB IUN:I3"
```

04

Call for editing another image

```
IFIRST = 0
```

06

Plot binary compressed picture on Versatec plotter; one dot per pixel (fast plot)

```
CALL VPIX3(    JUN, ITEXT, IWAIT,IWAIT2,...)
               174    116    117    151
```

JUN : input picture DS.
ITEXT : text of header and comments printed before the plot. 1= yes; 0= no.
IWAIT : delay constant during plotting of picture.
IWAIT2: delay constant after plotting before feeding paper.

07

Plot binary compressed picture on Versatec plotter as arrays of n x m dots per pixel; square and pseudo-hexagonal raster plots. Also select area to plot.

```
CALL PICTOV(IUND(1),  (2),   (3),   (4),   (5), IAREA,
              64      65     66     67     68     272

            ITOP,  JTOP,  IBOT,  JBOT, NEWPO,ISQHEX,
             273    274    275    276    54     167

             NPX,   NPY, IWAIT,IWAIT2,  MODE,...)
             228    229    117    151    289
```

IUND(.): input unit DS's.
IAREA : neg. or 0= no area selection; pos.= area selection: ITOP, JTOP, IBOT, JBOT.
ITOP,JTOP: coordinates of top left corner of selected area in picture.
IBOT,JBOT: coordinates of bottom left corner.
NEWPO : 1= change page after each print page; 2= no page change.
ISQHEX: type of plot, 1 or 2= square, 3= pseudo-hexagonal display.
NPX,NPY: nos. of dots per pixel in x,y directions.
IWAIT : delay constant during plotting of picture.
IWAIT2: delay constant after plotting before feeding paper.
MODE : 1= slow, 2= fast but uneven plotting.

NOTE1: 1 to 5 DS's can be plotted with alternating rows.
NOTE2: \SENSW 7 set cuts plotting.

08

Enter integer data

```
CALL EINDA

"EINDA:ENTER I,J:I4,I6"
(address and value: if address is neg. print value)
```

09

Enter floating point data

```
CALL EDATI

"EDATI:ENTER I,J:I4,F15.6"
(address and value: if address is neg. print value)
```

10

Go to master

```
"G I A P P : SM II"

"IGOM:I2"
```

S U P E R M A S T E R I I I

"SUPERMASTER III" of GIAPP: line thinning of binary expanded images, component labeling of areas and of lines, phase labeling, and extraction of binary compressed and of phase-labeled images from component-labeled images.

SUPERMASTER	MASTER	FUNCTIONS
III	06	Line thinning of binary expanded images, component labeling of lines, junctions or areas within contours
	07	Pase labeling via interactive displays, creation of phase-labeled images, extraction of binary compressed images of each phase

M A S T E R 0 6

01

"COOL START" procedure for two magnetic tapes on devices MT11 and MT12

```
READC (yes/no)
SLLIO (M1,M2,0,0,K)
PREPD (0,0,0,0,17)
RLIO1 (11)
RLIO1 (12)
```

Number of entries of physical devices	
M1: INDAC(254)	11
M2: INDAC(255)	12
K : INDAC(258)	17

NOTE: M1+M2+K=51
(length of data is 54 on Modcomp)

02

Manual copy of non - compressed DS from one I/O device to another

```
CALL COPY1F(IUN,JUN)

"GIVE IUN,JUN:2I3"
```

03

Manual rub of last DS on an I/O device

```
K=IPODS(IUN,3,0)

"RUB IUN:I3"
```

04

Read default values from cards

```
CALL READC
```

(Read INDAC and DACIN from cards)

05

Type default value table

```
CALL TYPID
```

06

Plot binary compressed picture on Versatec plotter:
one dot per pixel (fast plot)

```
CALL VPIX3(    JUN, ITEXT, IWAIT,IWAIT2,...)
                174    116    117    151

      JUN    : input picture DS.
      ITEXT  : text of header and comments printed before
               the plot. 1= yes; 0= no.
      IWAIT  : delay constant during plotting of picture.
      IWAIT2 : delay constant after plotting before
               feeding paper.
```

07

Plot binary compressed picture on Versatec plotter as arrays of n x m dots per pixel; square and pseudo-hexagonal raster plots. Also select area to plot

```
CALL PICTOV(IUND(1), (2), (3), (4), (5), IAREA,
                64     65     66     67     68    272

            ITOP,  JTOP,  IBOT,  JBOT, NEWPO,ISQHEX,
             273    274    275    276     54    167

             NPX,   NPY, IWAIT,IWAIT2,  MODE,...)
             228    229    117    151    289
```

IUND(.): input unit DS's.
IAREA : neg. or 0= no area selection; pos.= area selection: ITOP, JTOP, IBOT, JBOT.
ITOP,JTOP: coordinates of top left corner of selected area in picture.
IBOT,JBOT: coordinates of bottom left corner.
NEWPO : 1= change page after each print page; 2= no page change.
ISQHEX: type of plot, 1 or 2= square, 3= pseudo-hexagonal display.
NPX,NPY: nos. of dots per pixel in x,y directions.
IWAIT : delay constant during plotting of picture.
IWAIT2: delay constant after plotting before feeding paper.
MODE : 1= slow, 2= fast but univen plotting.

NOTE1: 1 to 5 DS's can be plotted with alternating rows.
NOTE2: SENSW 7 set cuts plotting.

08

Enter integer data

```
CALL EINDA

"EINDA:ENTER I,J:I4,I6"
(address and value: if address is neg. print value)
```

09

Enter floating point data

```
CALL EDATI

"EDATI:ENTER I,J:I4,F15.6"
(address and value: if address is neg. print value)
```

10

Go to master

```
"G I A P P : SM  III"

"IGOM:I2"
```

11

Print uncompressed pictures in DS's IUND(1) to IUND(5) using formats (25I5) or (25(1X,Z4)) on Versatec printer

```
CALL PICTOF(IUND(1),  (2),   (3),   (4),   (5),
              262     263    264    265    266

            IFORM(1), (2),   (3),   (4),   (5), IAREA,
              267     268    269    270    271    272

             ITOP,  JTOP,  IBOT,  JBOT, NEWPO,...)
              273    274   275    276    54

     IUND(.): input unit DS's.
     IFORM(.): 1= (25I5), 2= (25(1X,Z4)) formats.
     IAREA : neg. or 0= no area selection; pos.= area
             selection: ITOP, JTOP, IBOT, JBOT.
     ITOP,JTOP: coordinates of top left corner of
             selected area in picture.
     IBOT,JBOT: coordinates of bottom left corner.
     NEWPO : 1= change page after each print page;
             2= no page change.

NOTE1: 1 to 5 DS's can be printed with alternating
       rows.
NOTE2: SENSW 7 set cuts printing.
```

12

Manual copy of binary compressed DS from one I/O device to another

```
CALL COPY1(IUN,JUN)

"GIVE IUN,JUN:2I3"
```

13

Compress binary expanded picture

```
CALL CMPB1F(  IUN,   JUN,...)
              172    174
```

IUN,JUN: input and output DS's.

14

Expand binary compressed picture

```
CALL EXPB2F(  IUN,   JUN,   )
              172    174
```

IUN,JUN: input and output DS's.

15

Print selected window of non-compressed picture in various forms as one character per pixel

```
CALL PICT2F(   IUN,  IUNM, IMAGT, NGRAY,   MAX,   MIN,
                11    200    42    44     51     52

             IBLWH,IBLWHM, NPICP, NEWPG, ITEXT,...)
               49     43     45    50    116
```

- IUN : input picture DS.
- IUNM : binary mask input SS.
- IMAGT : image type. 1= grey level, 2= binary expanded, 3= hexagonal, 4= (0 to 31) 5= binary+junctions+lines, 6= slopes, 7= curvatures of lines, 8= component-(phase-) labeled pictures.
- NGRAY : number of grey levels desired.
- MAX,MIN: maximum, minimum data value in picture.
- IBLWH : 1= black on white, 2= white on black.
- IBLWHM: 1= normal mask, 2= inverse mask.
- NPICP : number of picture points on one horizontal line of print.
- NEWPG : 1= change page after each print page, 2=no change of page.
- ITEXT : neg. or 0= print no text, skip over comments; pos.= text on seperate page.

NOTE: SENSW 7 set cuts printing.

16

Line thinning of binary expanded image

```
CALL THIN3F(   IUN,   JUN,   KUN,ISQHEX, NCYCL,...)
                11     12     13    167     14
```

- IUN : input DS.
- JUN : output DS.
- KUN : temporary DS (rubbed after run).
- ISQHEX: 1,2= square raster, 3= hexagonal.
- NCYCL : maximum number of thinning iterations.

17

Postprocessing after thinning to retain binary data; elimination of negative iteration labels

```
CALL HILDI4(   IUN,   JUN,...)
                11     12
```

IUN : input DS.
JUN : output DS.

18

Component labeling of areas (zero's) enclosed within contours (one's)

```
CALL ENUM4A(   IUN,   KUN,ISQHEX,...)
                11     13    167
```

IUN : input DS.
KUN : output DS.
ISQHEX: 1,2= square raster, 3= hexagonal.

19

Relabeling of image labeled by ENUM4A (18) to eliminate redundant labels

```
CALL ENUM5(   IUN,ISQHEX,   JUN,...)
               11    167     12
```

IUN : input DS.
JUN : output DS.
ISQHEX: 1,2= square raster, 3= hexagonal.
JUN : output DS.

20

Find junctions, line segments, and line ends on binary uncompressed image of thin lines

```
CALL JUNC1F(   IUN,  IUNM,   JUN, JTYPE,  IPAD, IPADV,
                11    200    12     18    290    291

          ITHIN,...)
             15
```

IUN : input DS (thinned binary image of contours or lines).
IUNM : input DS for mask (binary).
JUN :JUN : output DS with junctions marked.
JTYPE : 1= junctions marked negative, 2= junctions zeroed, 3= line ends numbered.
IPAD : neg.= no padding of picture frame, 0= pad with neighbors as before, pos.= pad picture frame with IPADV value.
IPADV : padding value if used.
ITHIN : 1= retain lonely points, 2= remove them.

NOTE1: if mask is used, then entries outside mask are zeroed.

NOTE2: IJTYPE=3 works only on pictures with junctions marked negetive or on pictures of separate line segments. Junctions code word is negative.

NOTE3: JTYPE=1 and =2 do not produce exactly the same junctions.

NOTE4: the running sequence is as follows. (1)JTYPE=1 for junctions, (2)JTYPE=3 for line ends on (1).

21

Label line segments of binary expanded image after junction detection and elimination of junctions if so desired

```
CALL ENUM2F(   IUN,   IUNM,   JUN,    KUN,...)
                11     200     12      13
```

IUN : input DS of binary separate line segments (with junctions numbers also).
IUNM : input DS for mask (=0 if not used).
JUN : output DS of labeled line segments.
KUN : temporary DS, rubbed after use.

NOTE: IUN is binary separate thin line segments (disconnected) or with line junctions marked negative; JUN consists of labeled line segments without junction numbers (negative).

22

Relabel junctions and line segments that touch (redundant labels) after ENUM2F in (21)

```
CALL ENUM3F(   IUN,   IUNM,   JUN,    KUN, JULIN,...)
                11     200     12      13     78
```

IUN : input DS of binary separate line segments (with junction numbers also)
IUNM : input DS for mask (0= no mask).
JUN : output DS of labeled line segments.
KUN : temporary DS, rubbed after use.
JULIN : 1=label junctions, 2= label line segments,

NOTE: IUN is the output of ENUM2F or JUNC1F, i.e., junctions+line segments (binary or labeled); JUN consists of relabeled junctions+ line segments (binary or labeled).

23

List labels, coordinates of center of gravity and number of pixels for each label

```
CALL ENUM7(   IUN,   MIN,...)
               11     52
```

IUN : input DS, labeled image (positive labels).
MIN : minimum label value desired from picture =2 or greater.

24

Initialize magnetic tape on device MT11

```
CALL PREPD(11,0,0,0,0)
```

25

Initialize magnetic tape on device MT12

```
CALL PREPD(0,12,0,0,0)
```

26

Initialize file occupancy table

```
F = SLLIO(30,14,2,2,3)
```

26

Type file occupancy table

```
CALL TLLIO
```

27

Type file occupancy table

```
CALL TLLIO
```

M A S T E R 0 7

01

```
Manual copy of non - compressed DS from one I/O
device to another

CALL COPY1F(IUN,JUN)

"GIVE IUN,JUN:2I3"
```

02

```
Manual copy of binary compressed DS from one I/O
device to another

CALL COPY1(IUN,JUN)

"GIVE IUN,JUN:2I3"
```

03

```
Manual rub of last DS on an I/O device

K=IPODS(IUN,3,0)

"RUB IUN:I3"
```

04

Read component-labeled image DS and create in core table of labels

```
CALL HPR86(    IUN, LABS,...)
               167   363
```

IUN : input DS of labeled components (areas).
LABS : starting label number if too many labels.

05

Create DS of table of labels stored in core

```
CALL GEST3M(  IUNL,  JUNL,...)
               168     12
```

IUNL : input DS for adding commentary to JUNL.
JUNL : output DS for table of labels.

06

Read to core label table from table DS

```
CALL GEST3L(  IUNL,...)
               168
```

IUNL : input DS with table of labels.

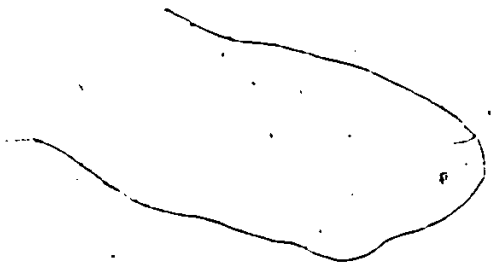

07

Interactive selection of labels via special operator console and Tektronix 611 displays of binary compressed images of boundaries; creates DS of updated table of labels for phase labeling

```
CALL FIXPX2(   IUN,   IUNL,    KUN,   JUNL,MSGCON,....,
               167     168      11      12     367

             IDXY,   JDXY,.......,  XRAT,  YRAT,...)
              359     360           57     58
```

IUN : input DS of binary compressed image of boundaries.
IUNL : input DS of table of labels.
KUN : intermediate DS into which IUN is copied for plotting on Tektronix.
JUNL : output DS for partly or fully edited table of labels of components and phases.
MSGCON: spacing in screen coordinates of phase label to appear on screen (suggested value is 50).
IDXY : horizontal spacing between pixels in screen coordinates (suggested val.: 30).
IDXY : vertical spacing between pixels in screen coordinates (suggested val.: 30).
XRAT, YRAT: percentage of overlap between adjacent successive frames if automatic mode for scanning the entire image is chosen during interaction.

NOTE: an instruction menu will appear on the screen during interaction.

08

Enter integer data

```
CALL EINDA

"EINDA:ENTER I,J:I4,I6"
(address and value: if address is neg. print value)
```

09

Enter floating point data

```
CALL EDATI

"EDATI:ENTER I,J:I4,F15.6"
(address and value: if address is neg. print value)
```

10

Go to master

```
"G I A P P : SM III"

"IGOM:I2"
```

11

Find area (component) labels that correspond to pointed out pixel coordinates during interaction with FIXPX2 (07)

```
CALL HPR87(    IUN,  LABS,.......,LADSEQ,   LAD,...)
               167    363           365     364
```

IUN : input DS of labeled components (areas).
LABS : subtractor from label number (set to 2).
LADSEQ: last filled entry address for sequential search.
LAD : last filled entry in table.

NOTE1: LABS, LADSEQ and LAD are automatically set when a table is read to core by GEST3L either within FIXPX2 or separately after using it.

NOTE2: set SENSW 2 to print unmarked label on Versatec printer; data on duplicate labels are always printed if encountered.

12

Select pointed-out labels and convert the component-labeled image to binary compressed image or to phase-labeled image

```
CALL HPR88(    IUN,   JUN, JTYPE, LTYPE,  LABS,.....,
               167    168   366    374    363

               LAD,LADSEQ,...)
               364    365
```

IUN : input DS of labeled components (areas).
JUN : output DS: binary compressed image or phase-labeled image of selected labels.
JTYPE : neg. or 0= for binary compressed output; pos.= for phase-labeled image (uncompressed).
LTYPE : pointing symbol in table of labels, i. e., the area type wanted as binary 1 (black).
LABS : starting label if too many labels.
LAD : last filled entry in table.
LADSEQ: last filled entry address for sequential search.

13

List the tables of labels in core on Versatec printer

```
CALL TYPLTC
```

14

Plot binary compressed picture on Versatec plotter; one dot per pixel (fast plot)

```
VALL VPIX3(    JUN, ITEXT, IWAIT,IWAIT2,...)
                174   116   117    151
```

JUN : input picture DS.
ITEXT : text of header and comments printed before the plot. 1= yes; 0= no.
IWAIT : delay constant during plotting of picture.
IWAIT2: delay constant after plotting before feeding paper.

15

Call for interactive session with FIXPX2 (7) with another image

```
IFIRST = 0
```

S U P E R M A S T E R "V"

"SUPERMASTER IV" of GIAPP: processing of binary compressed images.

SUPERMASTER	MASTER	FUNCTIONS
IV	08	Logical operations on or between binary compressed images, Minkowski operations or transformations by means of programmable structuring elements, displays of binary compressed images
	09	Auto- and cross-correlation of binary compressed images in two dimensions creation of correlation images

M A S T E R 0 8

01

"COOL.START" procedure for two magnetic tapes on devices MT11 and MT12

```
READC (yes/no)
SLLIO (M1,M2,I,J,K)
PREPD (0,0,13,14,17)
RLIO1 (11)
RLIO1 (12)
```

Number of entries of physical	devices
M1: INDAC(254)	11
M2: INDAC(255)	12
I : INDAC(256)	13
J : INDAC(257)	14
K : INDAC(258)	17

NOTE: M1+M2+I+J+K=51
(length of data is 54 on Modcomp)

02

Manual copy of binary compressed DS from one I/O device to another

```
CALL COPY1(IUN,JUN)

"GIVE IUN,JUN:2I3"
```

03

Manual rub of last DS on an I/O device

```
K=IPODS(IUN,3,0)

"RUB IUN:I3"
```

04

Read default values from cards

```
CALL READC
```

(Read INDAC and DACIN from cards)

05

Type default value table

```
CALL TYPID
```

06

Plot binary compressed picture on Versatec plotter;
one dot per pixel (fast plot)

```
CALL VPIX3(    JUN, ITEXT, IWAIT,IWAIT2,...)
               174    116    117    151
```

JUN : input picture DS.
ITEXT : text of header and comments printed before the plot. 1= yes; 0= no.
IWAIT : delay constant during plotting of picture.
IWAIT2: delay constant after plotting before feeding paper.

07

Plot binary compressed picture on Versatec plotter as arrays of n x m dots per pixel: square and pseudo-hexagonal raster plots. Also select area to plot.

```
CALL PICTOV(IUND(1),  (2),   (3),   (4),   (5), IAREA,
              64      65     66     67     68     272

            ITOP,  JTOP,  IBOT,  JBOT, NEWPO,ISQHEX,
             273    274    275    276     54     167

             NPX,   NPY, IWAIT,IWAIT2,  MODE,...)
             228    229    117    151    289
```

IUND(.): input unit DS's.
IAREA : neg. or 0= no area selection; pos.= area selection: ITOP, JTOP, IBOT, JBOT.
ITOP,JTOP: coordinates of top left corner of selected area in picture.
IBOT,JBOT: coordinates of bottom left corner.
NEWPO : 1= change page after each print page; 2= no page change.
ISQHEX: type of plot, 1 or 2= square, 3= pseudo-hexagonal display.
NPX,NPY: nos. of dots per pixel in x,y directions.
IWAIT : delay constant during plotting of picture.
IWAIT2: delay constant after plotting before feeding paper.
MODE : 1= slow, 2= fast but uneven plotting.

NOTE1: 1 to 5 DS's can be plotted with alternating rows.
NOTE2: SENSW 7 set cuts plotting.

08

Enter integer data

```
CALL EINDA

"EINDA:ENTER I,J:I4,I6"
(address and value: if address is neg. print value)
```

09

Enter floating point data

```
CALL EDATI

"EDATI:ENTER I,J:I4,F15.6"
(address and value: if address is neg. print value)
```

10

Go to master

```
"G I A P P : SM IV"

"IGOM:I2"
```

11

Display binary compressed picture on Tektronix 611

```
CALL PICTC(    JUN,   ICOR,   JCOR,    DXY,   IBWD,ISQHEX,
               174    177    178     179     29     167

                NP,...)
               180

     JUN    : input DS.
     ICOR,JCOR: screen coordinates of top left corner
              of picture.
     DXY    : spacing between the pixels.
     IBWD   : 1= B on W; 2= W on B.
     ISQHEX: 1 or 2= square plot; 3= hexagonal plot.
     NP     : intensity of dots (1 to 7).

NOTE: SENSW 7 set cuts plotting.
```

12

Create images either from cards or from terminal

```
CALL HPR50( IDIMBN,  IDIM,  JDIM, IGRTP,    IO,    JO,
              80      81     82    214     224    225

             ID,    JD,   NPX,   NPY,...)
            226    227    229    230
```

IDIMBN: number of binary pixels per row.
IDIM : number of 16 bit words per row.
JDIM : number of rows.
IGRTP : 1=card input for whole picture; 2= grid from cards; 3=grid computed; 4=points from cards; 5=points from terminal; 6= midpoints of rectangular arrays (max. 64) from cards; 7=like 6 from terminal.
NPX,NPY: number of points in x & y directions.
IO,JO : starting point of grid picture coordinates.
ID,JD : step size in x & y directions in picture coordinates.

13

Create structuring element or mask DS's as binary expanded images

```
CALL HPR49(   IDIM,  JDIM,  MODE,...)
               81     82     289
```

IDIM : number of words in one row of picture.
JDIM : number of rows on picture.
MODE : 1=structuring element input; 2=mask input.

NOTE : IDIM,JDIM odd numbers between 3 and 15.

14

Create in core structuring element window or mask window of binary dimensions to coincide with those of the image to be processed. Windows created for either square raster images or for odd and even rows of hexagonal raster images

```
CALL HPR92(    IUN,ISQHEX,IDIMBN, MODE, IXDIM, JYDIM,
               172    167     80   289     83    84

             KXDIM,...)
               85
```

IUN : input DS (structuring element or mask).
ISQHEX: 1,2= for square raster image; 3= for hexagonal raster image.
IDIMBN: binary dimension (bits per row) of the binary compressed image to be processed by either MINK1 or MINK2.
MODE : 1= load structuring element window; 2= load mask window.
IXDIM : number of words in one row of structuring element image.
JYDIM : number of rows in both structuring element image and structuring element window.
KXDIM : number of words in one row of structuring element window.

15

Compute Minkowski type transformation (erosion or dilatation by structuring element) of binary compressed image; only coinciding black pixels are considered in the transformation

```
CALL MINK1(   IUNA,  IUNB,   JUN, IOPER,ISQHEX,...)
               172    173    174    169    167
```

IUNA : input DS for image to be processed.
IUNB : input DS for structuring element used for adding comments to processed image.
JUN : output DS for transformed image.
IOPER : type of transformation. 1= dilatation; 2= erosion.
ISQHEX: 1= square, 2=hexagonal raster image.

16.

Compute Minkowski type transformation (erosion or dilatation by structuring element) of binary compressed image; both black and white pixels are considered in the transformation

```
CALL MINK2(   IUNA,  IUNB,   JUN, IOPER,ISQHEX,...)
               172    173    174    169    167
```

IUNA : input DS for image to be processed.
IUNB : input DS for structuring element used for adding comments to processed image.
JUN : output DS for transformed image.
IOPER : type of transformation. 1= dilatation; 2= erosion.
ISQHEX: 1= square, 2=hexagonal raster image.

17

Logical operation between (or on) compressed images

```
CALL LOGO3(   IUNA,  IUNB,   JUN, LOGOP,...)
               172    173    174    175
```

IUNA,IUNB: input picture DS's.
JUN : output picture DS.
(JUN=IUNA.LOGOP.IUNB)
or
(JUN= complement of IUNA).

NOTE : "(+)" = .EXOR.; "•" = .AND.,
"+" = .OR., and "NOT" = .NOT. (complement).

LOGOP : 1= A•B; 2= A+B; 3= A(+)B; 4= NOT(A);
5= NOT(A•B); 6= NOT(A+B); 7= NOT(A(+)B);
8= A•NOT(B); 9= A+NOT(B); 10= A(+)NOT(B).

Output messages are numbers of black pixels in: IUNA, IUNB, and JUN.

22

```
Initialize magnetic tape on device MT11
CALL PREPD(11,0,0,0,0)
```

23

```
Initialize magnetic tape on device MT12
CALL PREPD(0,12,0,0,0)
```

24

```
Initialize file occupancy table
F = SLLIO(30,14,2,2,3)
```

25

```
Type file occupancy table
CALL TLLIO
```

M A S T E R 0 9

01

Auto- and cross-correlation between two binary compressed pictures

```
CALL CORRLN( IUNA,  IUNB, NSHXL, NSHXR, NSHYL, NSHYR,
              172    173    194    195    196    197

             KSTEPX,KSTEPY,...)
               198    199
```

IUNA,IUNB: first and second DS':
IUNA is shifted.
NSHXL,NSHXR,KSTEPX: do correlation matrix from x= NSHXL, to x=NSHXR in steps of KSTEPX.
NSHYL,NSHYR,KSTEPY: do correlation matrix from y= NSHYL, to y=NSHYR in steps of KSTEPY.
KSTEPX,KSTEPY: steps along x and y (=1,2,3,...n).

NOTE1: coordinates for correlation go from - to + in left-to-right direction, and in down-to-up direction.
NOTE2: SENSW 7 set cuts processing.

02

Manual copy of binary compressed DS from one I/O device to another

```
CALL COPY1(IUN,JUN)

"GIVE IUN,JUN:2I3"
```

03

Manual rub of last DS on an I/O device

```
K=IPODS(IUN,3,0)

"RUB IUN:I3"
```

04

Create DS of correlation array (64 x 64 values)

```
CALL HPR51(   IUNA,  IUNB,   JUN,   ..., FMULT,...)
               172    173    174           52
```

IUNA,IUNB: input DS's.
JUN : output DS.
FMULT : multiplication factor for scaling of correlation values to be stored as integers.

05

Manual copy of non - compressed DS from one I/O device to another

```
CALL COPY1F(IUN,JUN)

"GIVE IUN,JUN:2I3"
```

06

Plot binary compressed picture on Versatec plotter; one dot per pixel (fast plot)

```
CALL VPIX3(    JUN, ITEXT, IWAIT,IWAIT2,...)
               174    116   117    151
```

JUN : input picture DS.
ITEXT : text of header and comments printed before the plot. 1= yes; 0= no.
IWAIT : delay constant during plotting of picture.
IWAIT2: delay constant after plotting before feeding paper.

07

Print uncompressed pictures in DS's IUND(1) to IUND(5) using formats (25I5) or (25(1X,Z4)) on Versatec printer

```
CALL PICTOF(IUND(1),  (2),   (3),   (4),   (5),
              262     263    264    265    266

          IFORM(1), (2),   (3),   (4),   (5), IAREA,
             267    268    269    270    271    272

            ITOP,  JTOP,  IBOT,  JBOT, NEWPO,...)
             273    274    275    276     54
```

IUND(.): input unit DS's.
IFORM(.): 1= (25I5), 2= (25(1X,Z4)) formats.
IAREA : neg. or 0= no area selection; pos.= area selection: ITOP, JTOP, IBOT, JBOT.
ITOP,JTOP: coordinates of top left corner of selected area in picture.
IBOT,JBOT: coordinates of bottom left corner.
NEWPO : 1= change page after each print page; 2= no page change.

NOTE1: 1 to 5 DS's can be printed with alternating rows.
NOTE2: SENSW 7 set cuts printing.

08

Enter integer data

```
CALL EINDA

"EINDA:ENTER I,J:I4,I6"
(address and value: if address is neg. print value)
```

09

Enter floating point data

```
CALL EDATI

"EDATI:ENTER I,J:I4,F15.6"
(address and value: if address is neg. print value)
```

10

Go to master

```
"G I A P P : SM IV"

"IGOM:I2"
```

11

Compress binary expanded picture

```
CALL CMPB1F(   IUN,   JUN,...)
               172    174

     IUN,JUN: input and output DS's.
```

12

Expand binary compressed picture

```
CALL EXPB2F(   IUN,   JUN,   )
               172    174

     IUN,JUN: input and output DS's.
```

S U P E R M A S T E R V

"SUPERMASTER V" of GIAPP: output of image files in Binary Coded Decimal formats for transfering of data to other computing devices.

SUPERMASTER	MASTER	FUNCTIONS
V	10	Output of binary expanded images, labeled images and grey level images for transfer in different BCD formats

01

"COOL START" procedure for magnetic tape in device MT11

```
.READC (yes/no)
SLLIO (M1,0,0,0,K)
PREPD (0,0,0,0,17)
RLIO1 (11)
```

Number of entries of physical devices	
M1: INDAC(254)	11
K : INDAC(258)	17

NOTE: M1+K=51.
(length of data is 54 on Modcomp)

02

Read labeled uncompressed data set from magnetic tape on device MT11 and write on magnetic tape on device MT12 an unlabeled file in a selection of different formats with or without header and comments records (for image transfer to a different computer)

```
CALL HPR91W(   IUN,  MTIN, MTOUT,  MODE, KFORM, LFORM,)
               172    89     90     87     91     92
```

IUN : input DS for labeled system.
MTIN : input device for input DS (must be 11).
MTOUT : output device for formatted DS to transfer.
MODE : set to 1 for running this routine.
KFORM : format od image data for printing on Versatec printer.
1= for (80I1); 2= for (40I2); 3= for (13I6); and 4= for (13(Z5,1X)).
LFORM : format of output picture data.
1= for binary picture in (80I1).
2= for phase-labeled picture in format (40I2).
3= for grey level or component-labeled picture in format (13I6).
4= for not writing on MTOUT, only printing on Versatec for testing.
5= for binary or non-binary picture in Modcomp II internal format.

03

Go back one end-of-file mark on device MT12

```
CALL BKFILE(IUFT2)
```

04

Go forward over one end-of-file mark on device MT12

```
CALL AVFILE(IUFT2)
```

08

Enter integer data

```
CALL EINDA

"EINDA:ENTER I,J:I4,I6"
(address and value: if address is neg. print value)
```

09

Enter floating point data

```
CALL EDATI

"EDATI:ENTER I,J:I4,F15.6"
(address and value: if address is neg. print value)
```

Appendix C

Operational flowcharts for GIAPP

Operational flowcharts for GIAPP

The programming philosophy is described in the form of generalized flow charts. The software developed takes into consideration various alternative paths for obtaining digitized submaps, creation of the mosaics, editing, thinning, producing phase-labeled images, extraction of binary compressed images corresponding to given phase labels, digitization of photographic transparencies by a flying spot scanner, processing of grey level images, and processing and display of binary compressed images.

The following block diagrams correspond to hierarchically ordered logical tasks, as follows:

(1) Digitize and save the vectors in a submap.

(2) Create a binary submap from previously stored vector data.

(3) Alternate procedure for digitization and binary submap creation.

(4) Patch binary submap into a mosaic.

(5) Patching of binary submap data sets into binary mosaic data set without loading the patch into computer memory.

(6) Printing of binary mosaic visual verification and online editing.

(7) Contour thinning and automatic area labeling.

(8) Interactive phase labeling and extraction of binary compressed images.

(9) Scanning procedures with flying spot scanner.

(10) Display of grey level histograms and trajectories.

(11) File handling features in unlabeled system.

(12) Preparatory processing for generating a binary compressed image.

(13) Logical operations between (or on) binary compressed images.

(14) Correlation between two binary compressed images.

(15) Minkowski type transformations of binary compressed images (only coincident black pixels).

(16) Minkowski type transformations of binary compressed images (both white and black coincident pixels).

(17) File handling and other features in labeled system.

A source listing documentation for the entire GIAPP system will be available as a separate technical report (Fabbri, 1981).

DIGITIZATION AND SAVING OF VECTORS IN A SUBMAP
(conservative procedure, i.e., all
partial results are saved)

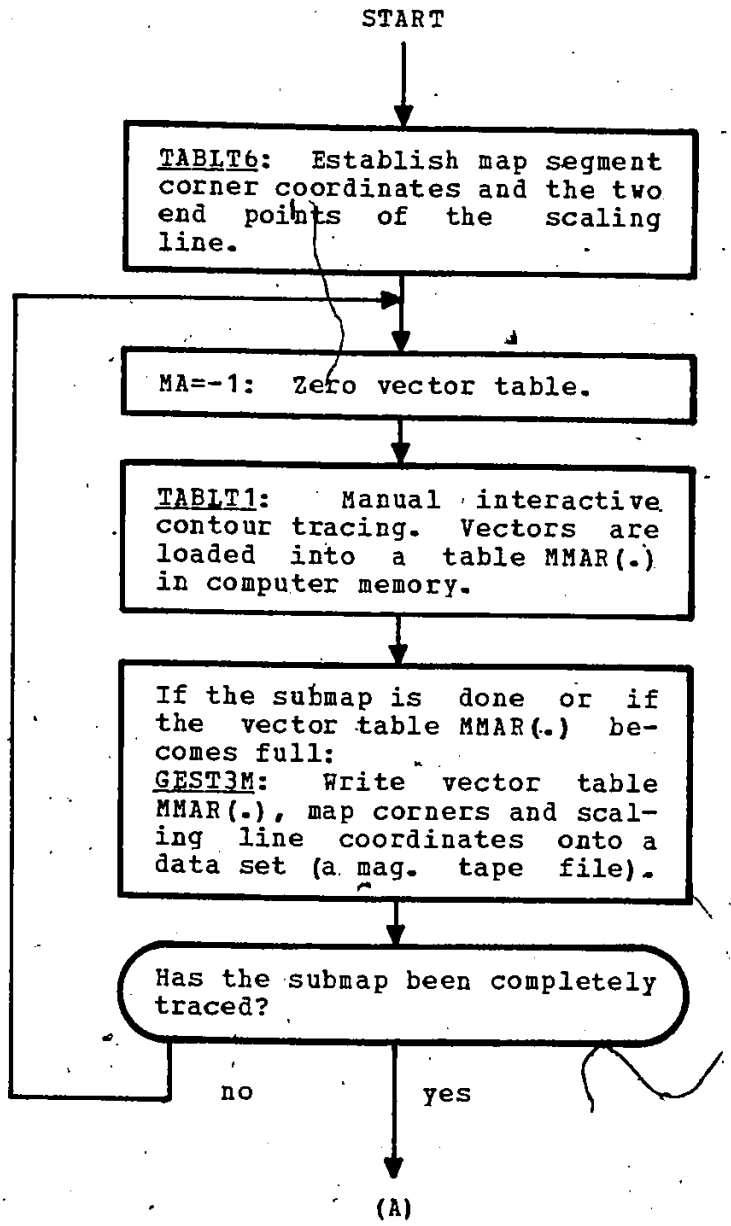

CREATE A BINARY SUBMAP FROM PREVIOUSLY STORED VECTOR DATA
(conservative procedure, i.e., all partial results are saved)

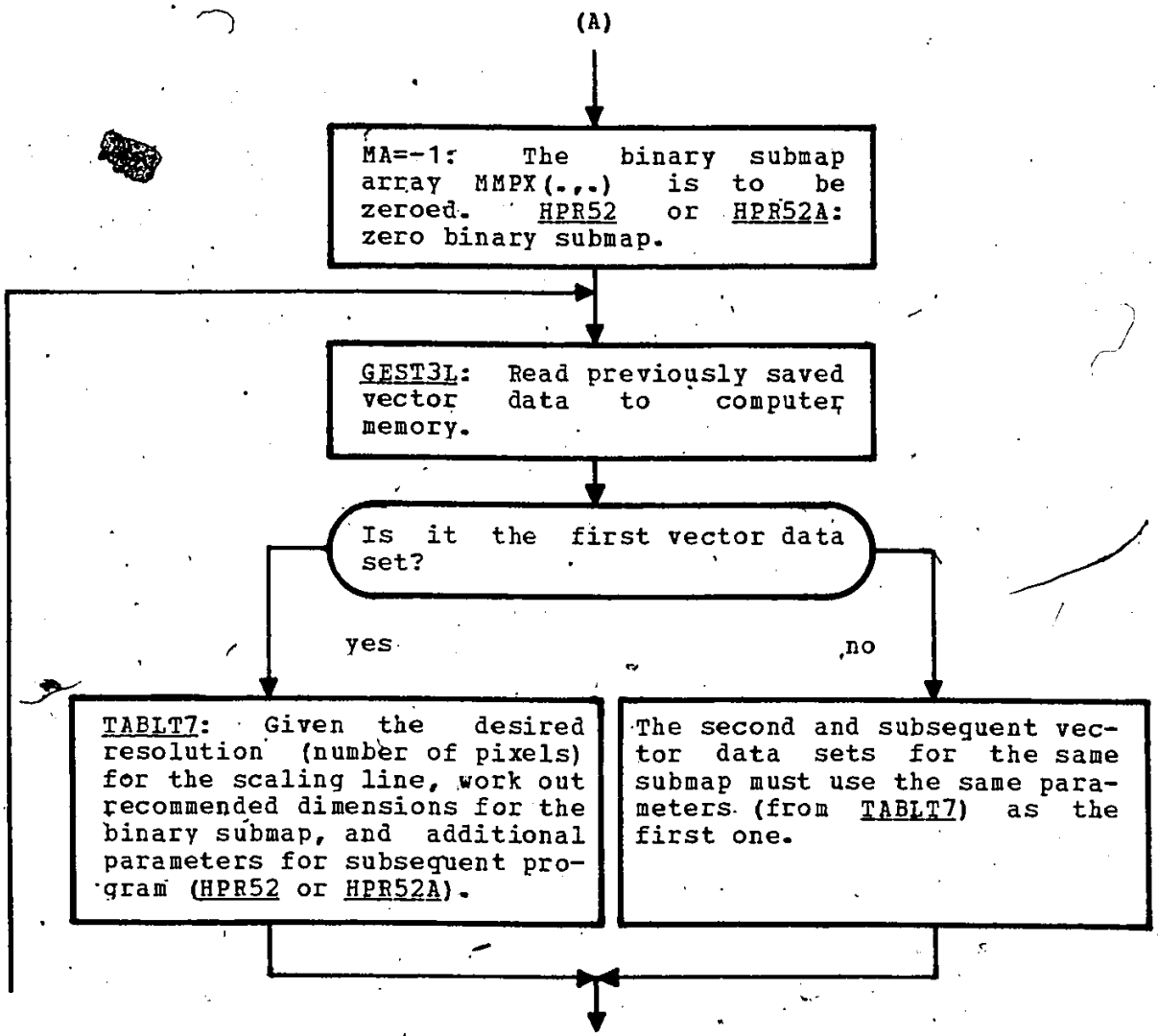

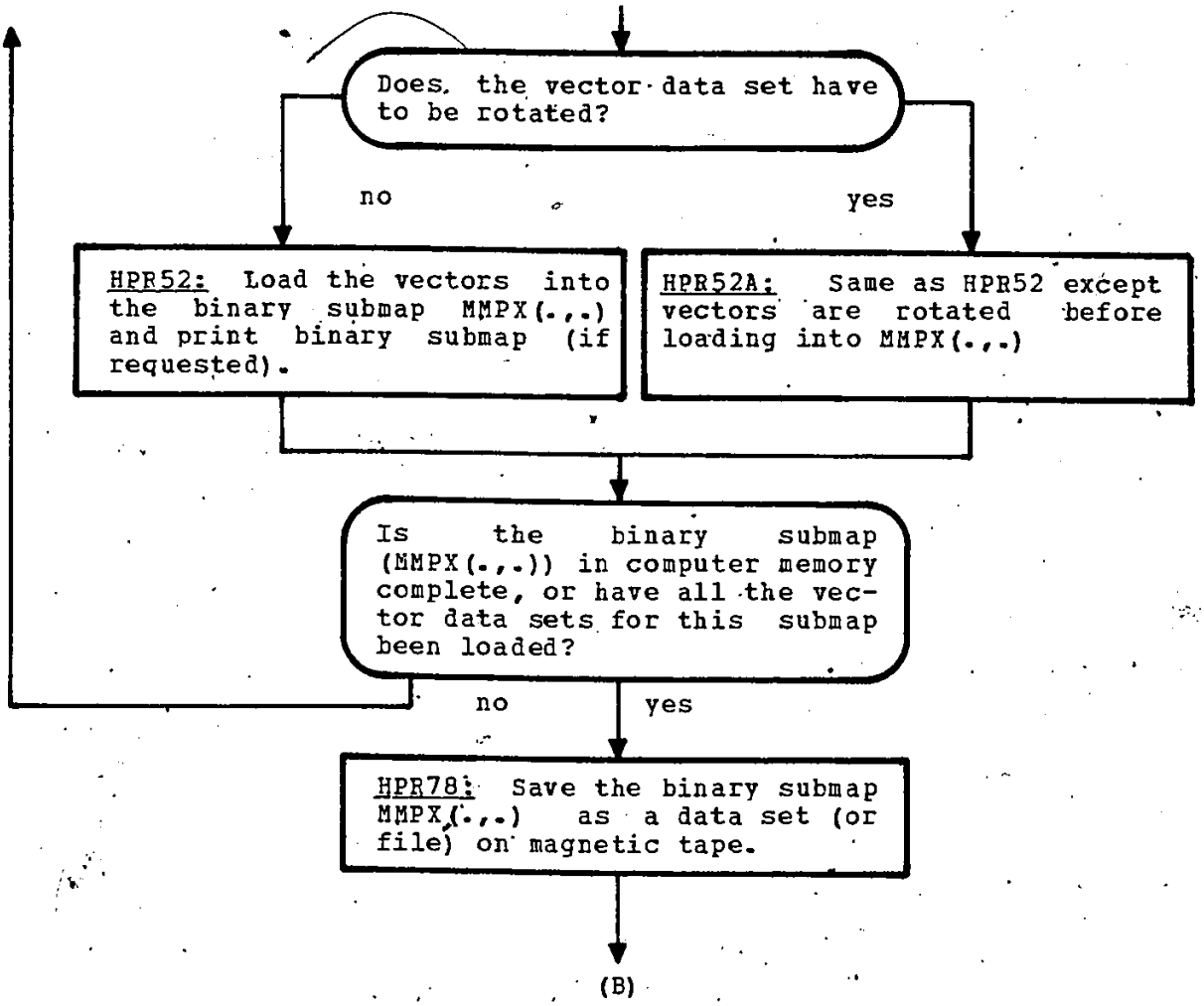
Does the vector data set have to be rotated?
no
yes
HPR52: Load the vectors into the binary submap MMPX(.,.) and print binary submap (if requested).
HPR52A: Same as HPR52 except vectors are rotated before loading into MMPX(.,.)
Is the binary submap (MMPX(.,.)) in computer memory complete, or have all the vector data sets for this submap been loaded?
no
yes
HPR78: Save the binary submap MMPX(.,.) as a data set (or file) on magnetic tape.
(B)

ALTERNATE PROCEDURE FOR DIGITIZATION AND
BINARY SUBMAP CREATION
(vector data and binary submap are saved;
see prior diagrams for details)

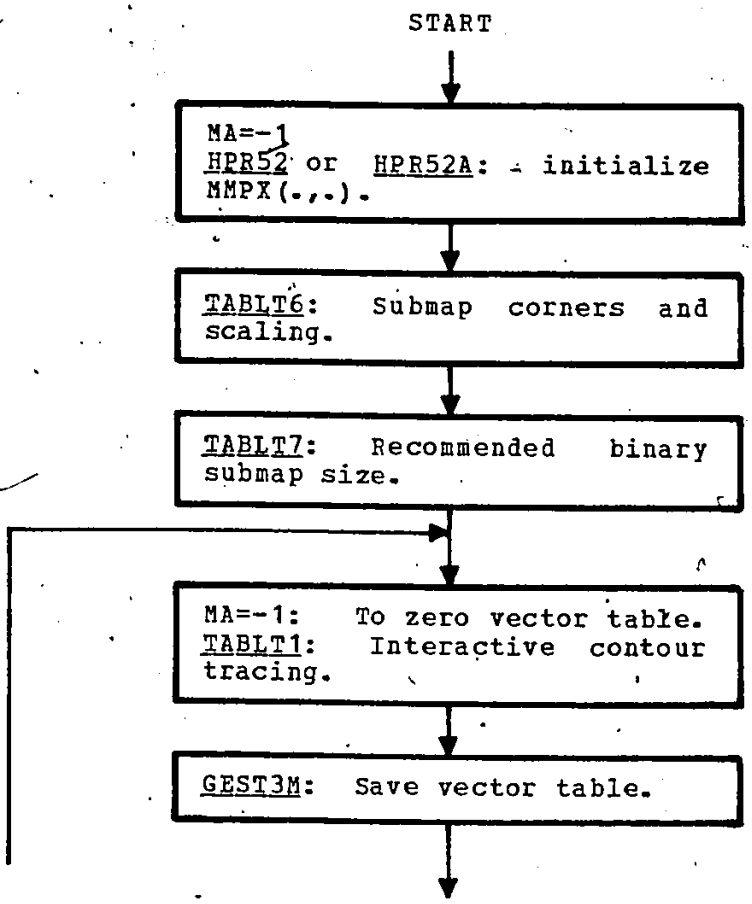

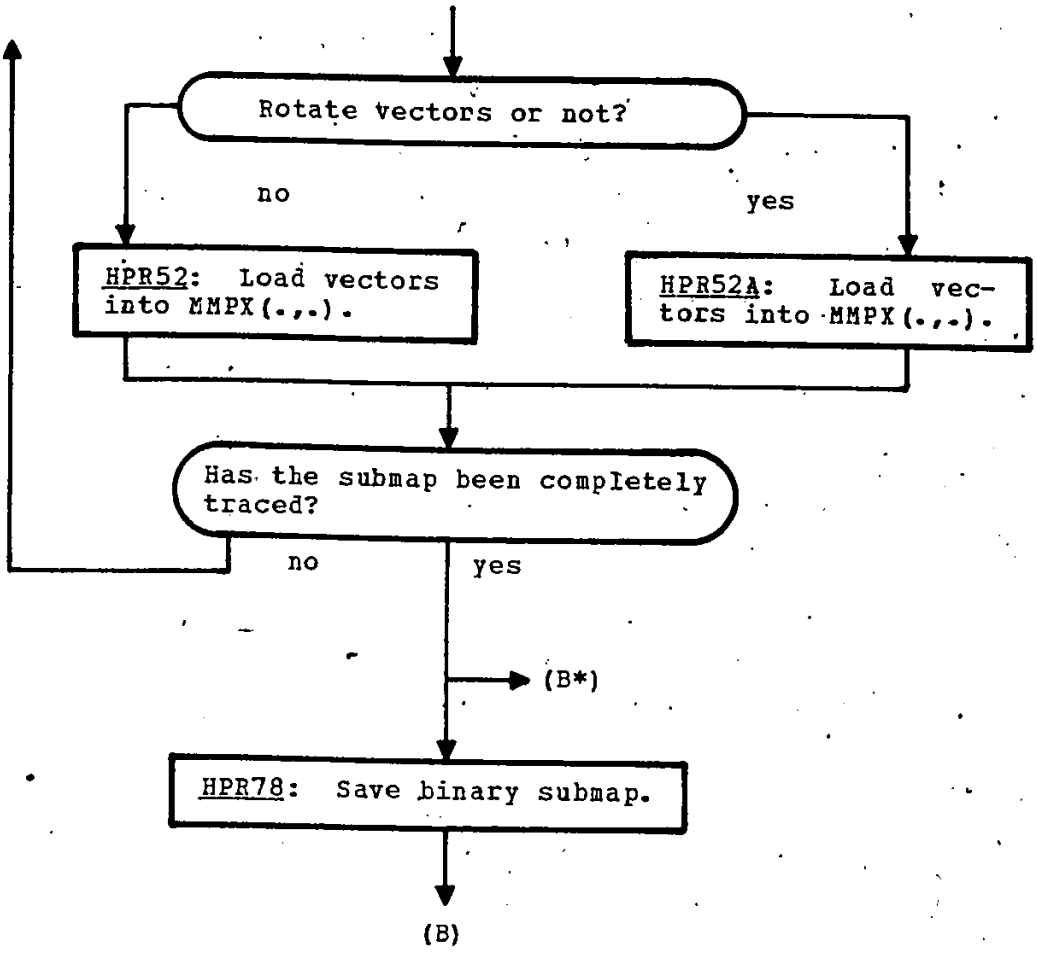
Rotate vectors or not?
no
yes
HPR52: Load vectors into MMPX(.,.).
HPR52A: Load vectors into MMPX(.,.).
Has the submap been completely traced?
no
yes
(B*)
HPR78: Save binary submap.
(B)

PATCH BINARY SUBMAP INTO A MOSAIC
(i.e., create and save the large
binary map)

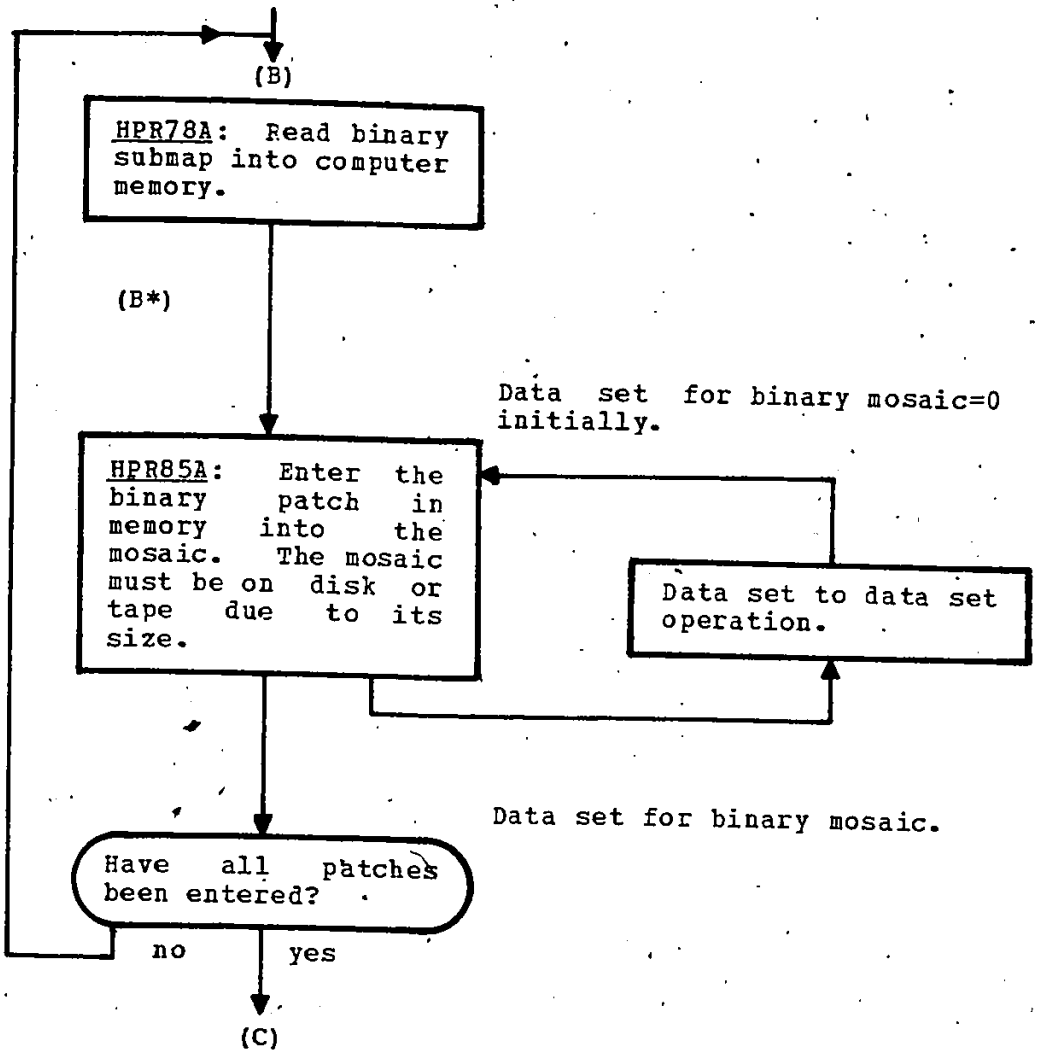

The mosaic is already on a data set due to the data set to data set operation in HPR85A.
Note: If the binary patch is already in memory, HPR78A may be bypassed, see B*; return to "START" for more than one patch.

PATCHING OF BINARY SUBMAP DATA SETS INTO
BINARY MOSAIC DATA SET WITHOUT LOADING
THE PATCH INTO COMPUTER MEMORY

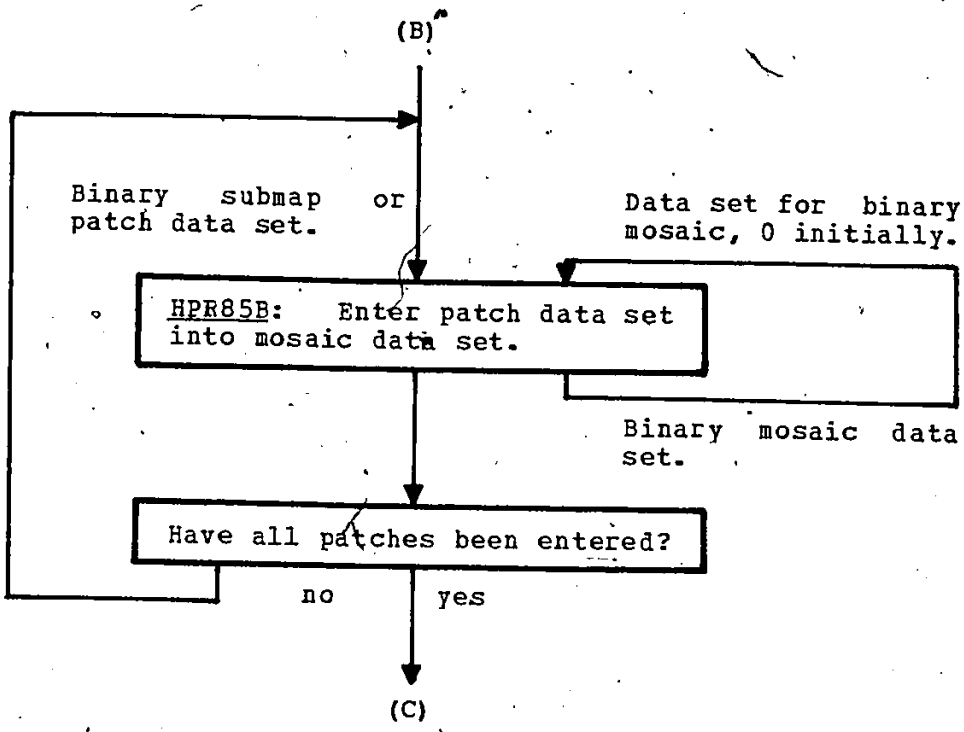

The mosaic is already on a data set due to the data set to data set operation in HPR85B.

PRINTING OF BINARY MOSAIC, VISUAL VERIFICATION and online editing

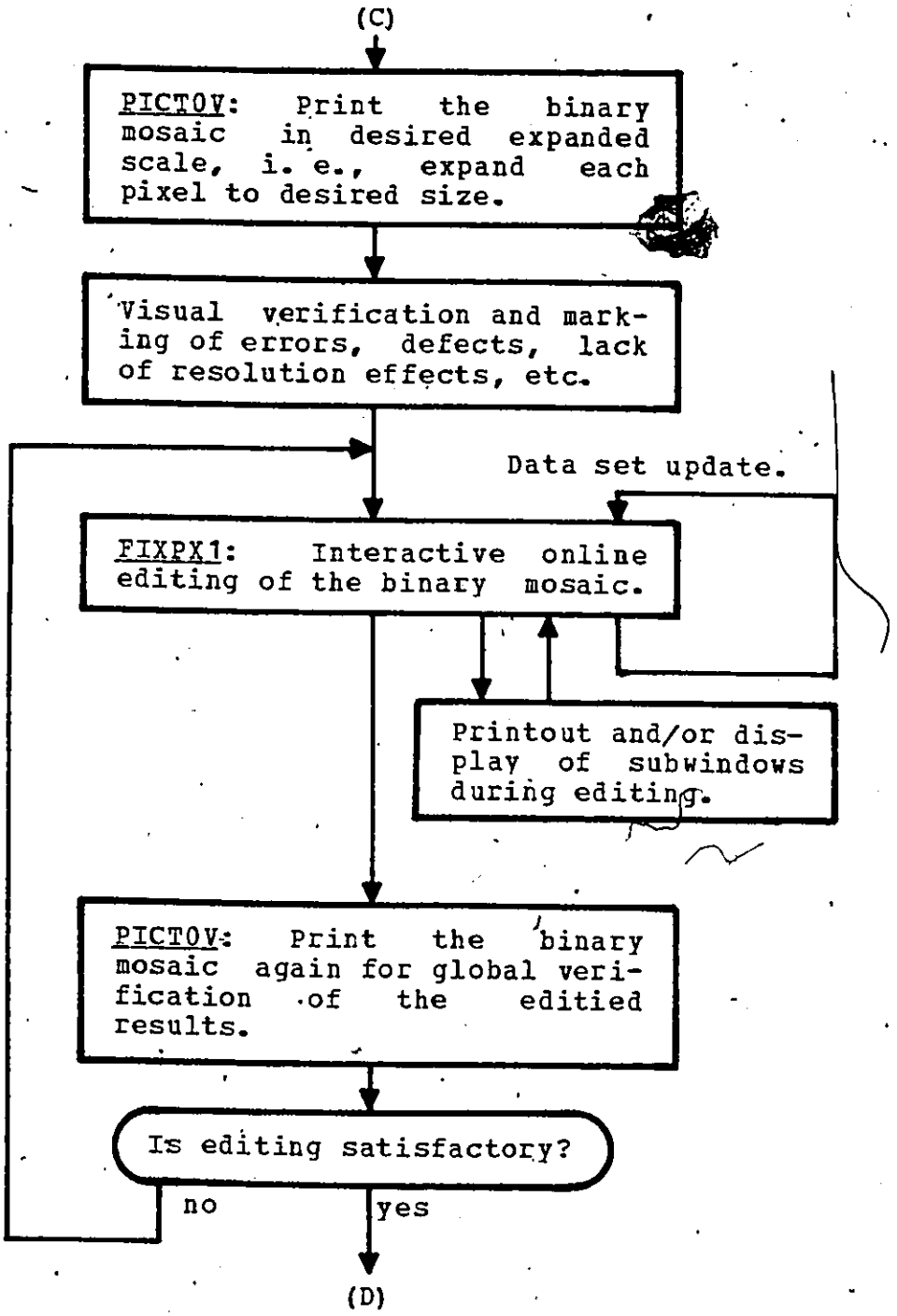

CONTOUR THINNING, AND AUTOMATIC AREA LABELING,
(from edited binary mosaic)

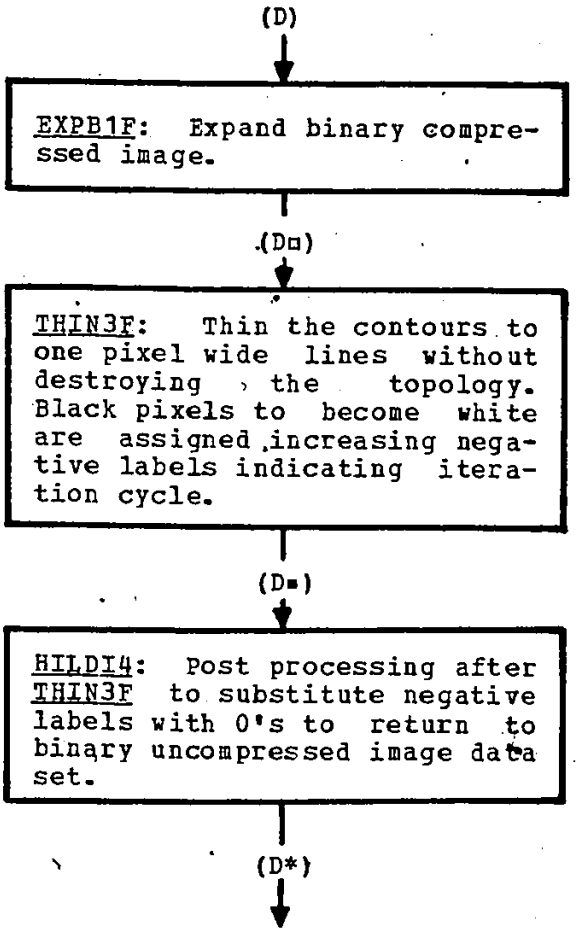

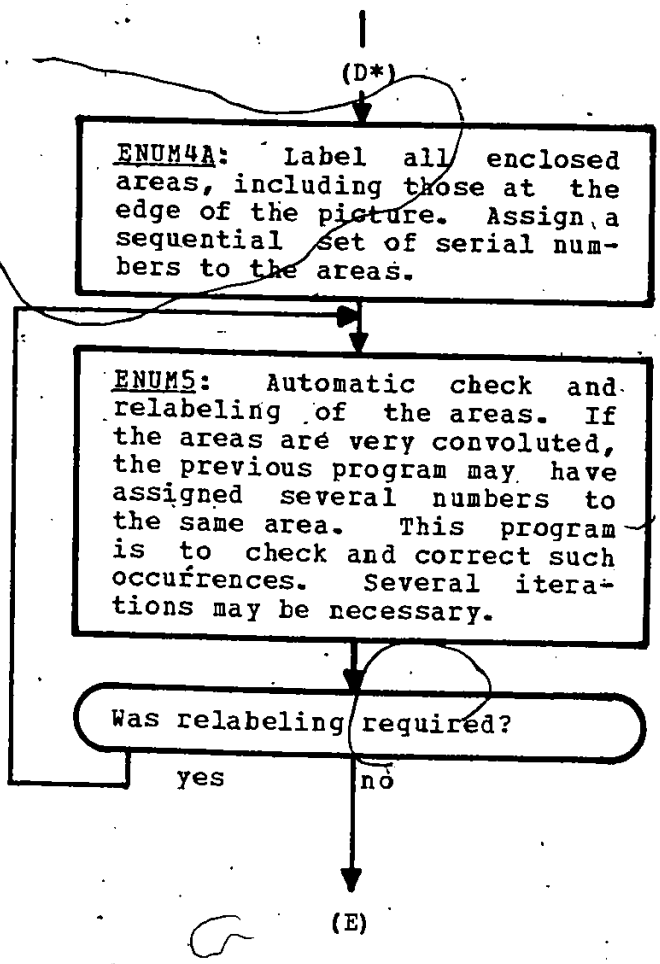

Automatically area labeled picture.

INTERACTIVE PHASE LABELING AND EXTRACTION OF BINARY COMPRESSED IMAGES
(from area labeled picture and edited binary mosaic)

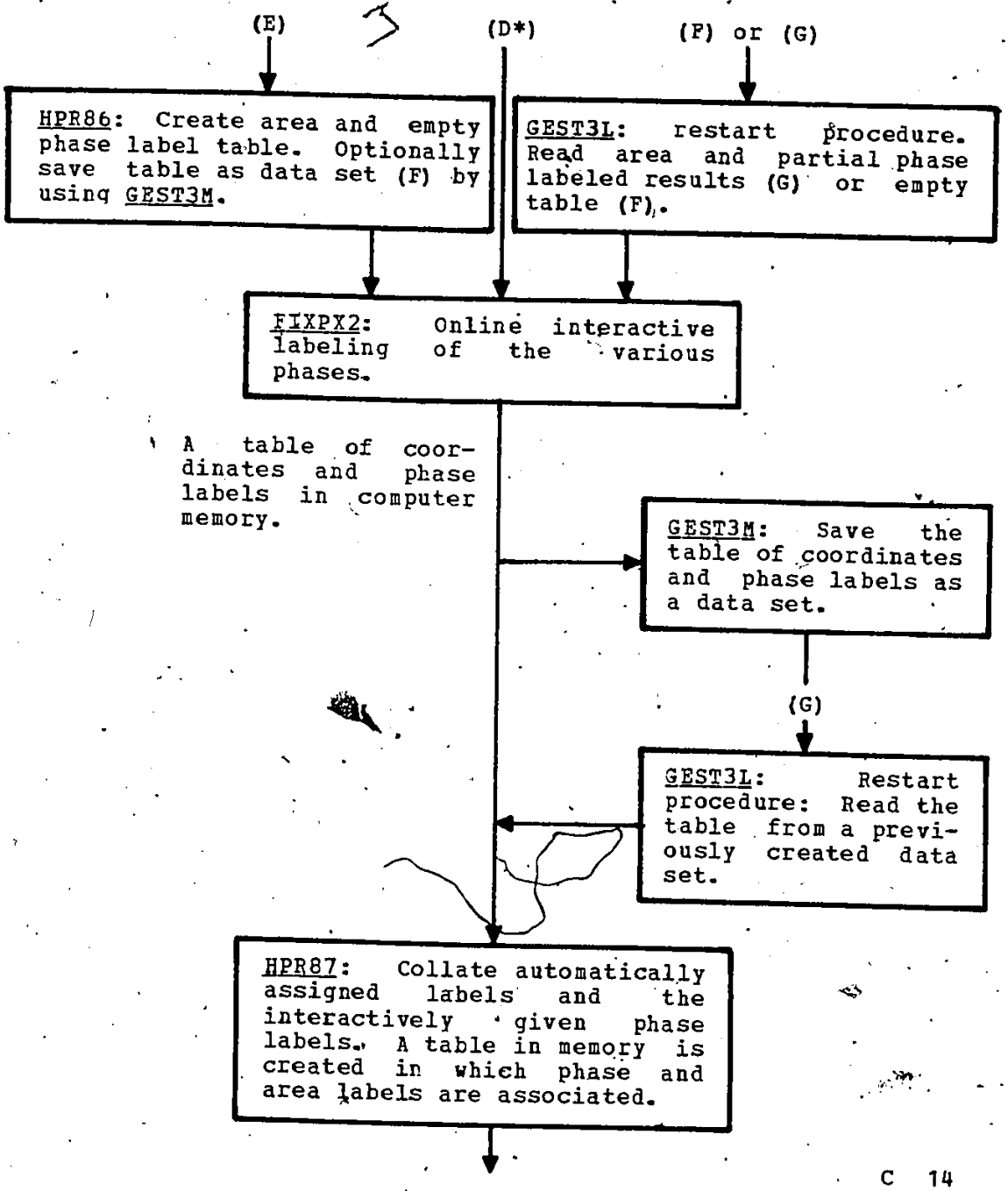

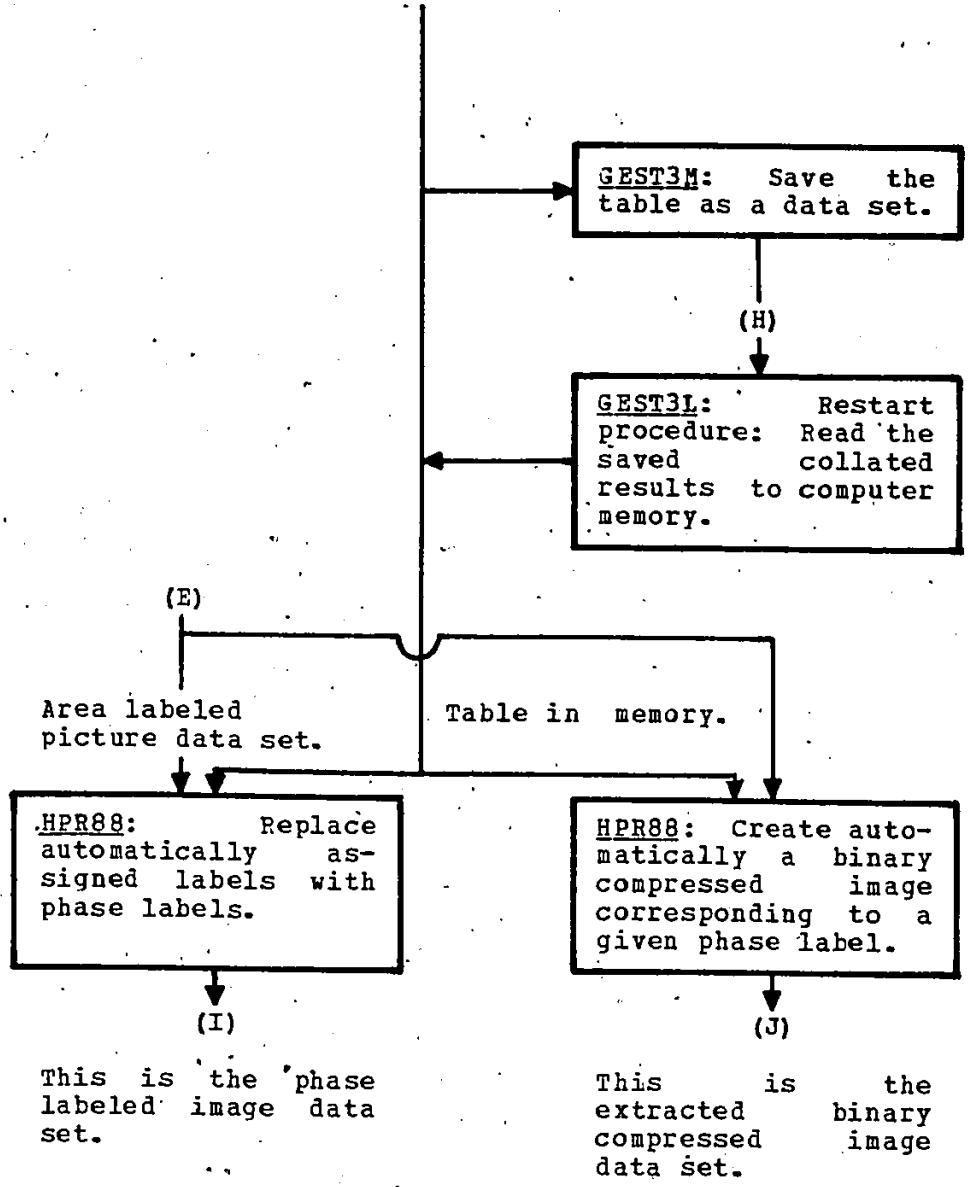
GEST3M: Save the table as a data set.
(H)
GEST3L: Restart procedure: Read the saved collated results to computer memory.
(E)
Area labeled picture data set.
Table in memory.
HPR88: Replace automatically assigned labels with phase labels.
HPR88: Create automatically a binary compressed image corresponding to a given phase label.
(I)
(J)
This is the phase labeled image data set.
This is the extracted binary compressed image data set.

SCANNING PROCEDURES WITH FLYING SPOT SCANNER
(for a 35 mm transparency in scanner)

35 mm picture transparency in scanner

(P)

Turn on scanner and initialize scanning procedures with the assistance of a technician.

SELAR1: Select area in picture for processing, display the transparency in scanner with automatic grey level scaling to generate best visible contrast. This produces a display which is in one-to-one correspondence with the transparency in the scanner. In order to select the area interactively, move a pointer on the Tektronix 611 screen and get the scanner coordinates for that point. Generate a movable and adjustable (but not rotatable) box for selecting suitable area in the picture for subsequent scanning, display or, on demand, display histogram of grey level readings within the selected area.

SETBEA: Look at signal level and resolution along a set of straight line trajectories in the picture, selected interactively via pushbuttons on special command console. Establish grey level (resolution) range for a grey level profile, drawn along a straight line between two points selected interactively.

SCANS2: Scan picture according to a square or a hexagonal raster configuration with the selected resolution within the area of the box defined interactively; write digital image on magnetic tape, for labeled system, unlabeled system or in BCD format (binary coded decimal) for outside magnetic tape.

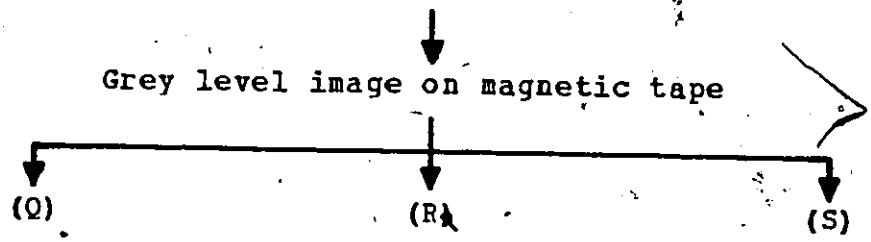

Labeled or unlabeled data set in BCD format.

Unlabeled data set for unlabeled system.

Labeled data set for labeled system.

Programs in labeled system for handling grey level images.

PICTOF: Digital display program for Versatec printer.
or
COPY1F: Copy uncompressed image from one storage (I/O) device to another.
or
HPR91W: Read labeled uncompressed image data set from magnetic tape and write the data in BCD with selected format on another magnetic tape for transfer to another computer.

DISPLAY OF GREY LEVEL HISTOGRAMS AND TRAJECTORIES
(for studying grey level pictures)

(R)

Grey level picture unlabeled data set on magnetic tape.

Histograms

MAMI3H: Read digitized image to find maximum and minimum grey levels. The grey level range of pixel values is ±2048 (AD converter resolution = 13 bits).

RAW3H: Read digitized tape in order to compute a histogram between the max. min. values computed from the previous program. Maximum size of histogram is 256 values.

WTRAJ4: Save histogram from core on magnetic tape.

(T)[1]

RTRAJ4: Read histogram to core from magnetic tape.

LOUP1: Remove tails of histogram to display the majority of the pixels within the dynamic range of the display device (e. g., 5% from either end).

Trajectories

TRAJS1: Define linear trajectory by selecting two endpoints across the picture and the number of points across the trajectory (max. 650).

TRAJP1: Plot trajectory on Versatec plotter.

TRAJR1: Read picture data from tape or disc for values on trajectory.

TRAJD2: Plot data on trajectory on Versatec plotter.

TRAJD3: Plot data on trajectory on Tektronix 611 storage display unit.

WTRAJ1: Save trajectory data in core on magnetic tape.

(T)[2]

RTRAJ1: Read trajectory data to core from magnetic tape.

FILE HANDLING FEATURES IN UNLABELED SYSTEM

(R)

Grey level picture unlabeled data set for unlabeled system.

↓

COPY2H: Read image from tape or disk and copy it to tape or disk.

PICTOH: List grey level values within a selected area in the picture.

BKFILE: Go back one end-of-file mark on the selected magnetic tape.

AVFILE: Go forward one end-of-file mark on the selected magnetic tape.

(D)

Binary compressed image data set for labeled system.

↓

Prepare (initialize with beginning-of-data record and end-of-data record) magnetic tape on device MT11 for storing images in labeled system.

Rub last file (data set) on magnetic tape on MT11 (i. e., overwrite with end-of-data record).

Read data on magnetic tape on MT11, if initialized for labeled system, and create in core a file occupancy table for MT11.

PREPARATORY PROCESSING FOR GENERATING A BINARY COMPRESSED IMAGE

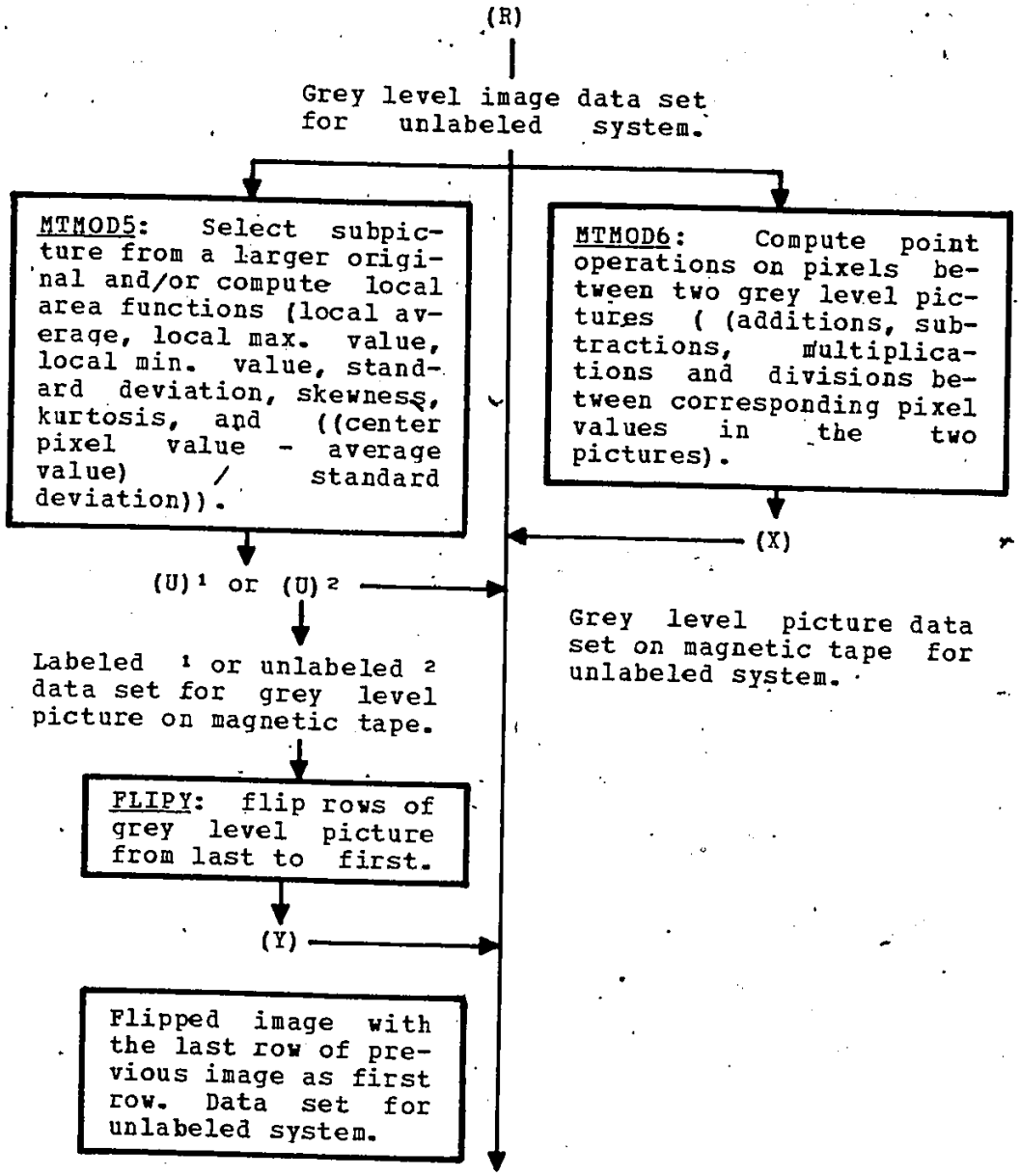

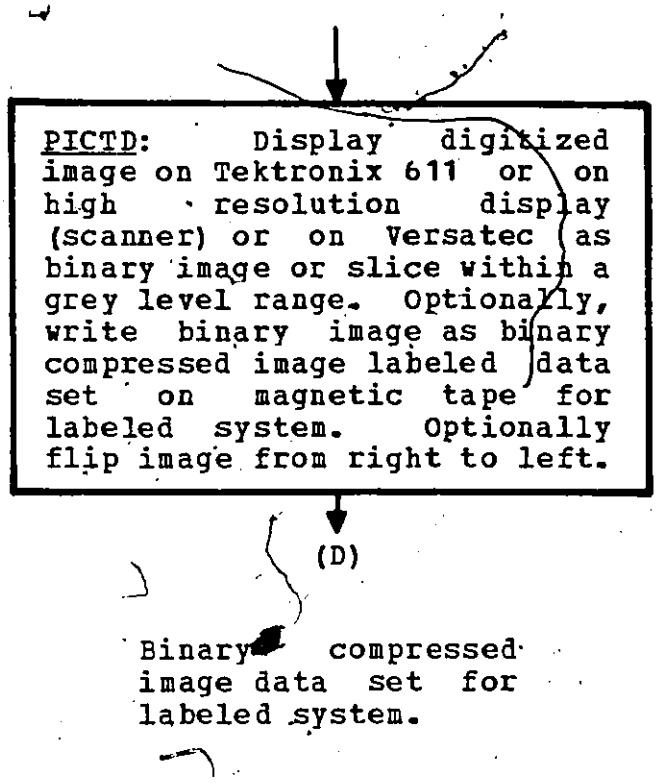
PICTD: Display digitized image on Tektronix 611 or on high resolution display (scanner) or on Versatec as binary image or slice within a grey level range. Optionally, write binary image as binary compressed image labeled data set on magnetic tape for labeled system. Optionally flip image from right to left.
(D)
Binary compressed image data set for labeled system.

LOGICAL OPERATIONS BETWEEN (OR ON) BINARY COMPRESSED IMAGES

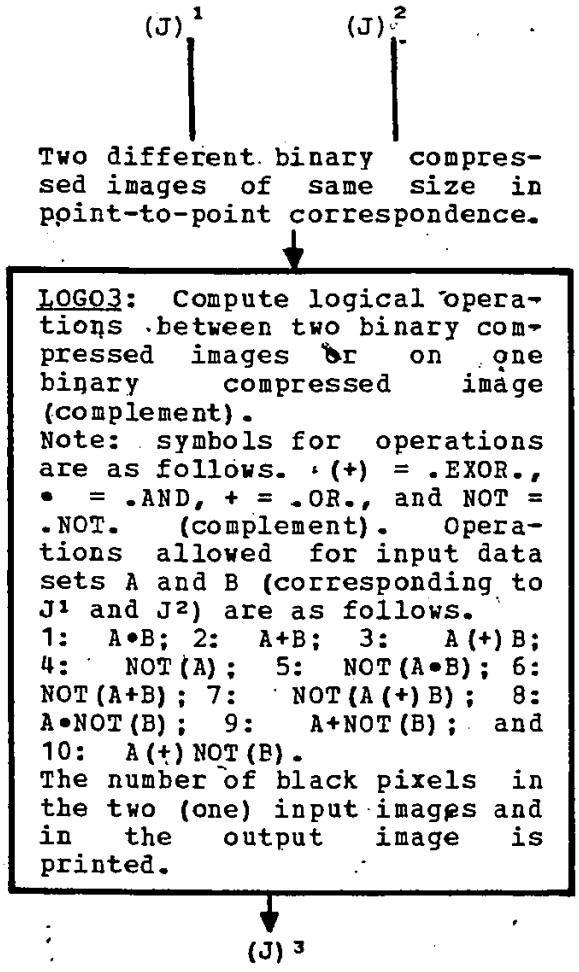

CORRELATION BETWEEN TWO BINARY COMPRESSED IMAGES (auto-correlation and cross-correlation)

(J) 4 (J) 5

Two identical binary compressed images for computing auto-correlation; two different binary compressed images for computing cross-correlation.

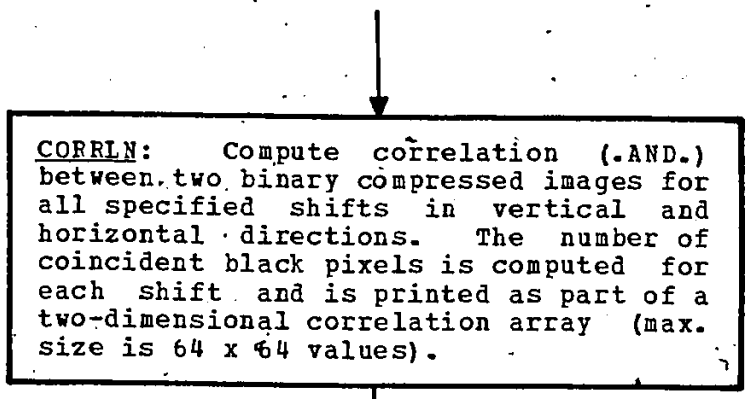

Correlation array stored in core.

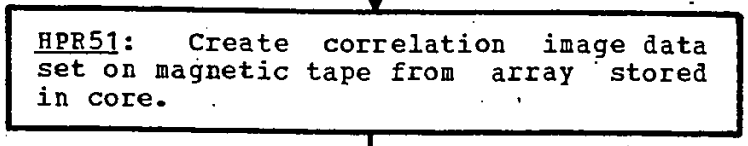

(K)

Correlation image data set: grey level image of maximum size 64 x 64 pixels. It can be displayed on the Versatec printer by PICTOF.

MINKOWSKI TYPE TRANSFORMATIONS OF BINARY COMPRESSED IMAGES
(Erosions and dilatations by structuring elements:
only coincident black pixels considered)

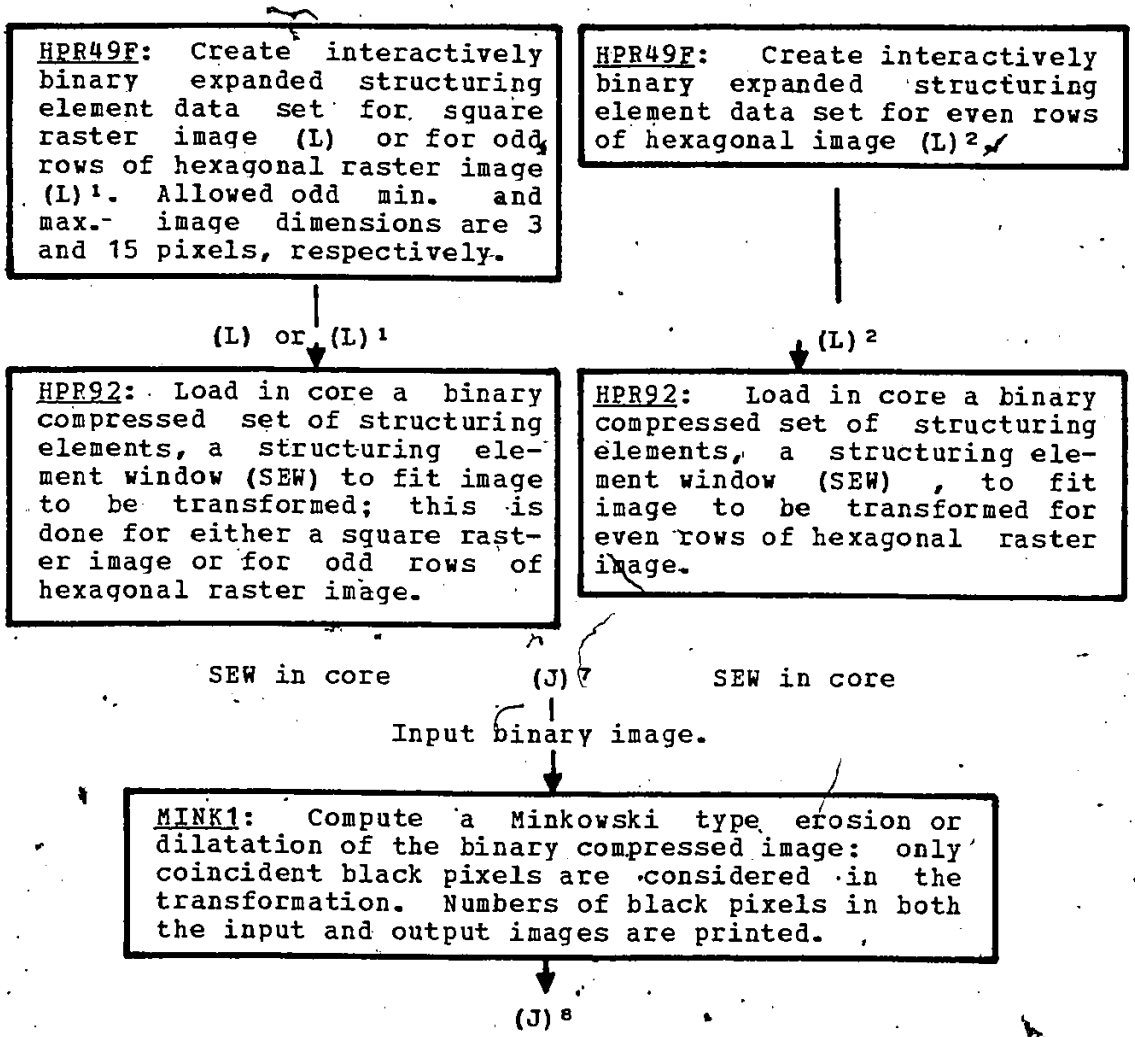

Binary compressed image data set transformed by the structuring element in (L) or in (L)¹ and (L)². It can be displayed on the Versatec by VPIX3 and PICTOV, and on the Tektronix 611 by PICTC.

MINKOWSKI TYPE TRANSFORMATIONS OF BINARY COMPRESSED IMAGES
(Erosions and dilatations by structuring elements:
both white and black coincident pixels considered)

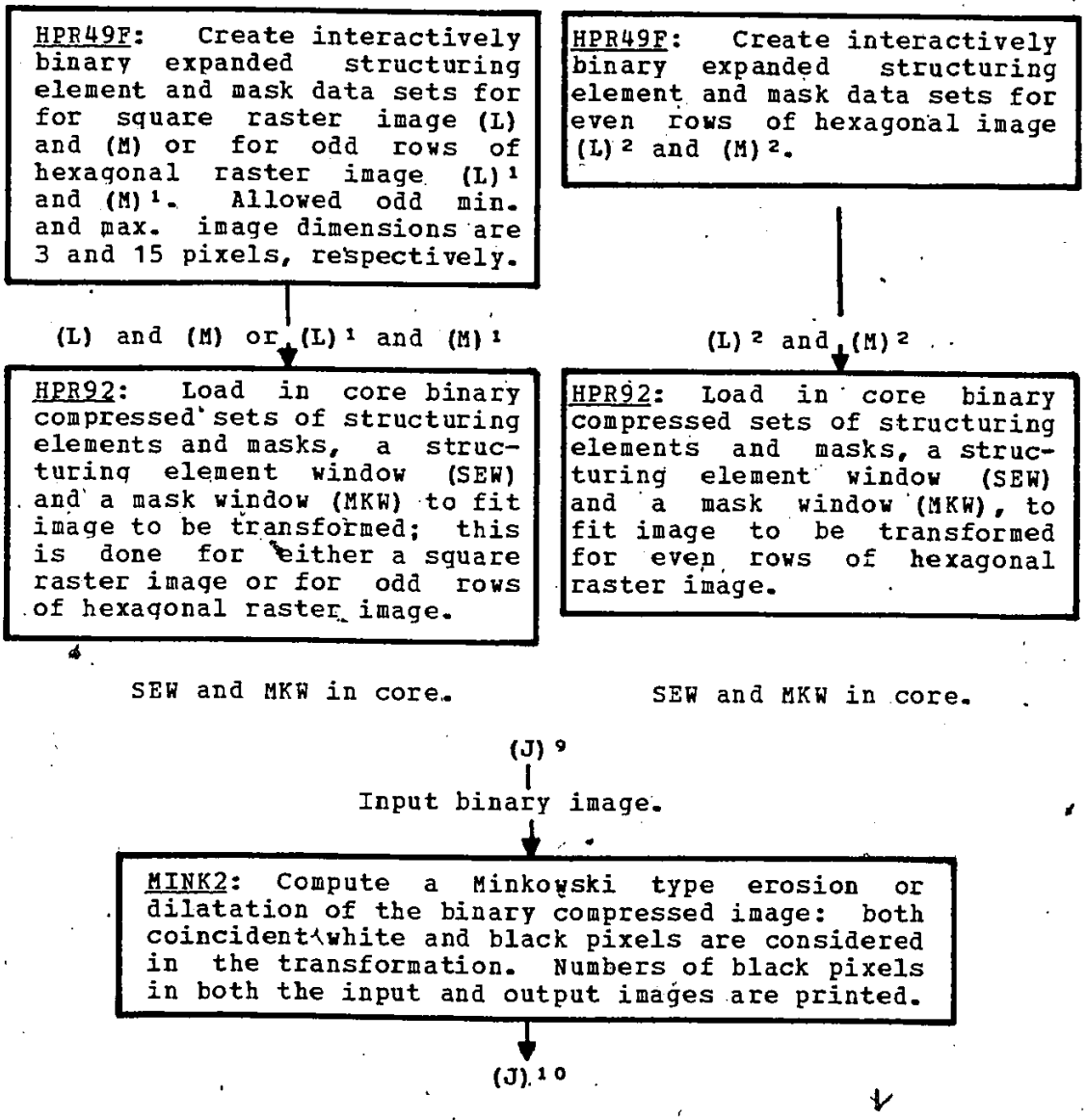

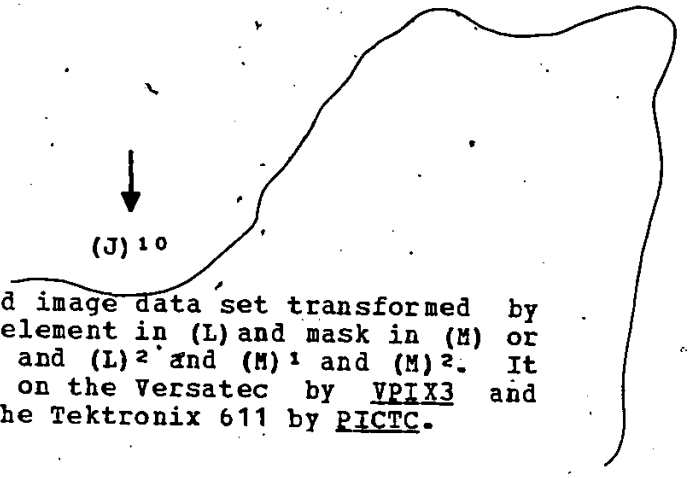

(J)^{10}

Binary compressed image data set transformed by the structuring element in (L) and mask in (M) or those in (L)^1 and (L)^2 and (M)^1 and (M)^2. It can be displayed on the Versatec by VPIX3 and PICTOV, and on the Tektronix 611 by PICTC.

FILE HANDLING AND OTHER FEATURES IN LABELED SYSTEM

COPY1: Copy binary compressed image data set from one I/O device to another.

Manual rub: Overwrite last data set on a given I/O device with end-of-data record.

COPY1F: Copy uncompressed image data set from one I/O device to another.

CMPB1F: Compress binary expanded image data set from one I/O device to another (from one word per pixel to one bit per pixel).

EXPB2F: Expand binary compressed image data set from one I/O device to another (from one bit per pixel to one word per pixel).

VPIX3: Plot binary compressed image on Versatec plotter (one dot per pixel).

PICT0V: Plot binary compressed image on Versatec plotter (n x m dots per pixel). Both square and pseudo-hexagonal displays are available.

PICTC: Plot binary compressed image on Tektronix 611 (one dot per pixel at selected spacing). Both square and hexagonal raster displays are available.

PICT0F: Print on Versatec printer the pixel values within a selected rectangular area of uncompressed image data set.

HPR50: Create binary compressed image data set from cards or by interactive commands from teletype. Images of regular grids, arbitrary grids, and images of sets of black rectangles of different dimensions can also be created to be used as masks or as test images.

HPR91W: Read uncompressed image data set from magnetic tape on MT11 and write data set on magnetic tape on MT12, with or without header and commentary records, in one of several BCD formats, or in Modcomp II internal binary format.